POLITECNICO DI TORINO

Ph.D. in Mechanic, XXV cycle

PhD Thesis

Study and Development of New Passive Micromixers Based on Split and Recombination Principle

Tutor :

Prof. Vladimir Viktorov

Coordinator:

Prof. Luigi Garibaldi

Candidate:

Mohammad Nimafar

February 2013

‘’To my dear Father and Mother’’

Index

Table of Contents

Index i

Abstract 1

Chapter 1

1.1 Introduction 3
1.2 Micro mixers and Mixing 4
1.2.1 Surface to Volume Ratio 5
1.3 Classification of Micro mixers 5
1.4 Characterization of Mixing Quality 5
1.5 Various Principle of Passive Micro mixers 6
1.6 Transport Phenomena 6
1.6.1 Molecular Level based on the Chapman- Enskog Theory 6
1.6.2 Continuum Level 9
1.6.2.1 Conservation of Mass 9
1.6.2.2 Conservation of Momentum 9
1.6.2.3 Conservation of Energy 10
1.7 Molecular Diffusion 10
1.7.1 Brownian Motion 10
1.7.2 Stoke-Einstein Model of Diffusion 11
1.7.3 Diffusion Coefficient in Liquid 12
1.8 Taylor Dispersion 12
1.9 Chaotic Advection 14
1.9.1 Basic Concept 14
1.9.1.1 Lorentz's Convection Flow 15
1.9.1.2 Dean Flow in Curved Pipe 17
1.10 Flow in Helical Pipe 20
1.11 Scaling laws and fluid flow at the Micro Scale 22
1.12 Summary and motivation 24

1.13 Objectives 24
References 26

Chapter 2

2.1 Introduction 30
2.2 Review of Passive Micro mixing 30
2.2.1 SAR Process 31
2.2.2 Injection 32
2.2.3 Droplet 33
2.2.4 Rotation 34
2.3 Experimental equipment 35
2.3.1 Syringe pump 36
2.3.2 Microscope 37
2.4 Test bench 38
2.5 Flow visualization and mixing characterization 39
2.5.1 Top-view imaging 39
2.5.2 Cross-sectional imaging 40
2.6 Image sensors 41
2.7 Digital images 43
2.8 Gray scale image 44
2.9 Experimental procedure 46
References 48

Chapter 3

3.1 Introduction 52
3.2 Measurement of concentration field by fluorescent dye 54
3.3 Qualification methods for micro mixers 55
3.3.1 Indirect methods 55
3.3.2 Direct statistical methods 56
3.4 Details of Experiments 61
3.5 T- micro mixer 62
3.6 O- micro mixer 63
3.7 Tear-drop micro mixer 63
3.7.1 Sequential lamination 66
3.8 H- micro mixer 67

3.9 Chain- micro mixer 69
3.9.1 Chain 1- micro mixer 70
3.9.1.1 Theoretical background of Chain 1- micro mixer 70
3.9.2 Chain 2- micro mixer 72
3.9.3 Chain 3- micro mixer 72
3.9.4 Chain 4- micro mixer 73
3.10 Focusing of mixing stream 74
3.10.1 Streams with the same viscosity 75
3.10.2 Streams with the different viscosities 77
References 81

Chapter 4

4.1 Introduction 85
4.2 Brief statement of experimental analysis 85
4.3 T-micro mixer analyse 87
4.4 O-micro mixer analyse 90
4.5 Tear-drop micro mixer analyse 94
4.5.1 Comparison of Tear-drop micro mixer with T- and O-micro mixers ... 98
4.6 H-micro mixer analyse 100
4.6.1 Comparison of H- micro mixer with T- and O-micro mixers 104
4.7 Chain micro mixers 106
4.7.1 Chain 1-micromixer analyse 106
4.7.2 Chain 2-micromixer analyse 110
4.7.3 Chain 3-micromixer analyse 114
4.7.4 Chain 4-micromixer analyse 118
4.8 Comparison of Chain micro mixers 122
References 125

Chapter 5

5.1 Introduction 127
5.2 Mathematical Model 128
5.3 Numerical simulation 129
5.4 T-micro mixer analyse 131
5.5 O-micro mixer analyse 133
5.6 Tear-drop micro mixer analyse 135

5.7 H-micro mixer analyse 137
5.8 Chain micro mixer analyse 139
5.8.1 Chain 1- micro mixer analyse 139
5.8.2 Chain 2- micro mixer analyse 141
5.8.3 Chain 3- micro mixer analyse 143
5.8.4 Chain 4- micro mixer analyse 145
5.9 Comparison of micro mixers 148
References 152

Conclusions 154

Nomenclature

C	Species concentration
C^*	Colored water normalized concentration along Microchannel
$\vec{C^*}$	Expected normalized concentration
d	Hydraulic diameter
D	Diffusion coefficient of the species
H	Height of the microchannel
i	Counter from 1 up to N
L	Length of the microchannel
N	Number of the points defined by the probability distribution function in terms of concentration
P	Pressure
Q_m	Mass flow rate
Q_v	Volume flow rate
Re	Reynolds number
V	Average velocity
$\vec{V}$	Average velocity
W	Width of the microchannel
MEMS	Micro Electro Mechanical System
MI	Mixing Index
PDF	Probability Distribution Function
σ	Standard deviation of the concentration
η	Mixing efficiency
μ	Viscosity
τ	Shear stress
ρ	Density

Abstract

Micromixers have been a major topic of research in the past decade and progress on recent development of micromixers has been reviewed by many researchers. Developing devices for microfluidic technology has been a major concern for industry and microfluidic devices offer many advantages over conventional techniques. Compared to conventional macroscopic methods, microfluidic devices have the advantages of reduced solvent, reagent and cell consumption, shorter reaction times, portability, low cost and low power consumption. Also, micromixers are key elements in microfluidic technology and have been addressed by a large body of research.

Interestingly, the historical development of microfluidics and its preoccupation with micromixing are the main fields of microtechnology. Micromixers have a wide variety of potential applications in industry. In modern technology, micromixers are applied in microtechnologies such as biological systems, as microreactors for chemical reactions, and as MEMS and lab-on-a-chip devices. This means that the community of engineers and scientist now engaged in microfluidic devices and also mixing process in micro scales. Indeed, they have entered the field from a variety of different backgrounds and they would have been confronted by the problems of mixing processing and mass transport at the micro scales.

According to the survey carried out in my research, the main driving forces for this investigation are applications in incompressible mixing processing at low Reynolds number range, $0.08<Re<4.16$. As far as we know, the technology and science of microfluidics cover a wide spectrum ranging from fundamental studies to real applications in laboratories and industries. This research focuses on an important subject of microfluidics, namely mixing processing at the microscale. The science of such mixing has carried out on newly fabricated micro scale devices on an extensive collection of established knowledge. Due to its applied nature, my research discuss practical outcome in the design and characterization of micromixers.

Abstract

In this thesis, first and foremost, I describe the method that I've used for analyzing the experimental data. The laminar flow regime (0.08<Re<4.16) was considered during tests and image-based techniques are used to evaluate mixing efficiency.

This study propose a novel generation of 3D splitting and recombination passive micromixers. Mixing characteristics of two species are elucidated via experimental and numerical studies associated with microchannels with various inlet flow rates (velocities) and results compared with the previous well-known micromixers. It was found that mixing performance is significantly affected by the split and recombination (SAR) flows and depends on Reynolds number (inlet velocities). As well as the efficiencies of my proposed mixer are almost quite the same with the well-known basic mixers at each desired region, the required pressure drop is approximately two times less than previous mixers. This is a good particular result that with higher efficiency the required pressure drop decreases. Hence, this new geometries satisfies both of targets in micromixer design which are higher mixing efficiency and lower pressure drop in comparison with previous well-known mixers. These results open the new operating windows for rapid mixing in the microchannel to overcome the fluid mixing which strongly limited to laminar regime with lower required pressure drop.

Chapter 1

Introduction to Mixing Process in Micromixers

1.1 Introduction

The research reported in this thesis investigates the microfluidic devices for mixing process. Effective mixing is a crucial process in microfluidic systems and the potential applications of micromixers are widespread in the industries. Microscale devices have become widely applied in biological systems, medical diagnostic, microreactors for chemical reactions, genetic sequencing, environmental monitoring, MEMS and lab-on-a-chip devices [1, 2].

Indeed, microscale devices propose fundamental advantages compared with conventional macroscale systems because of their small characteristic dimensions [3]. Microfluidic devices offer many advantages including low energy requirements, faster analysis, reduced reagent and cell consumption, rapid mixing, low cost, rapid heat and mass transfer and portability [4, 5, 6].

In microfluidic systems, viscosity dominates flow [7, 8] and mixing is limited to molecular diffusion due to the laminar nature of microflows [9, 10, 11]),and the flows tend to form a laminate structure instead of a uniform mixture due to the small Reynolds number [12]. Therefore, vortex generator are required to enhance the mixing performance because mixing by only molecular diffusion is very slow [13]. Hence, the focus on this field of research is to propose a device itself and to optimization of the geometry to enhance fluid mixing within the microchannel [14, 15, 16].
Kim et al. [17] studied on the shape optimization of a micromixer with staggered herringbone grooves (SHGs) at both the bottom and top walls has been performed using 3D Navier-Stokes analysis and a surrogate model for maximizing the degree of mixing. They found the micromixer with SHGs patterned at both the bottom and top walls shows higher mixing performance when compared to the reference micromixer with SHGs at a single wall. Also, Yang et al. [18] developed a passive micromixer with combination of a square-wave structure and periodic cubic grooves. They found that square-wave structure caused laminar recirculation, and the cubic grooves induced flow stretching. These characteristics jointly contributed to the 3D periodic perturbation, resulting in significantly enhanced mixing over a wide range of the Reynolds number.

As mentioned above, several experimental and numerical investigations have been carried out for different passive micromixers. In the present study, some new types of micromixers were designed and investigated experimentally to find out the efficiency and numerically to detect the pressure drop, and results compared with the mixing performance of known basic micromixers. Two colored water solutions (blue and yellow) are used for mixing. For visualization the flow, blue and yellow food dyes are diluted in water as the mixing flow in experimental tests. In all cases microchannel dimensions are as follows: W=0.4 mm, H=0.4 mm. The aspect ratio of the channel cross-section is unity (*W/H=1*).

1.2 Micromixers and Mixing

This study discusses the design and characterization of micromixers, which are defined as miniaturized mixing devices for at least two different liquid phases. The structure of a micromixer are fabricated partially or wholly using microtechnology or precision engineering. The characteristic channel size of micromixers is in the submillimeter range. Common channel width and height are on the order of 100 to 500 μm, while the channel length could be a few millimeters or more [19]. Also the overall volume defined by a micromixer is from microliters to milliliters.

Mixing is a transport process for species and phases to reduce inhomogeneity. Mixing leads to secondary effect such as reaction and change in properties. There are three mixing techniques in macroscale that reported in the literature: macromixing, mesomixing and micromixing [19]. Macromixing refers to mixing governed by the largest scale of fluid motion. For example, the scale of macromixing corresponds to the diameter of the mixing tank. Micromixing is mixing at the smallest scale of fluid motion and molecular motion. In conventional macroscale mixing, the smallest scale of fluid motion is the size of turbulent eddies, also called the Kolmogorov scale. Messomixing is in the scale between macromixing and micromixing. There are many different ways to provide mixing in the macroscale such as molecular diffusion, eddy diffusion, advection and Taylor dispersion [19].Eddy diffusion is the transport of large group of species and requires a turbulent flow. Because of the dominant viscous effect at the microscale, turbulent is not possible in micromixers. Mixing based on eddy diffusion is not relevant for micromixers. Therefore, the main transport phenomena in micromixers are molecular diffusion, advection and Taylor dispersion. Molecular diffusion is caused by the random motion of molecules and this mechanism is characterized by the molecular diffusion coefficient. Advection is the transport phenomena caused by fluid motion. A simple Eulerian velocity can lead to a chaotic distribution of the mixed species. A stable and laminar flow can also lead to chaotic advection. Taylor dispersion is advection caused by a velocity gradient.

According to the mentioned knowledge, designing micromixers for efficient mixing is a crucial problem, because existing designs in macroscale can not simply be scaled down for microscale application.

1.2.1 Surface to Volume Ratio

In micromixers, one of the main challenges related to miniaturization is the dominance of surface effects over volume effects. The dominant surface phenomena at the microscale also affect mixing processes with immiscible interfaces. The large surface to volume ratio at the micro scale is an advantage for the dissolving process. In immiscible liquids, additional energy is needed to overcome interfacial tension. On the one hand, dispersion the immiscible phases is a hard process and on the other hand, surface tension breaks the stretched fluid into segments and forms micro droplets [19]. The advantage of the microscale is that the formation process can be controlled down to each individual droplet. Hence, emulsion with a homogenous droplet size can be achieved in micromixers.

1.3 Classification of Micromixers

Micromixers reported in the literature can be classified as either active and passive fluid mixer [20-23], depending on how they manipulate the fluid to be mixed. Active micromixer require external forces, such as periodical variation of pumping capacity, electrokinetic instabilities, acoustically induced vibration, electrowetting-induced merging of droplets, magneto-hydrodynamic action, small impellers, piezoelectrically vibrating membrane or integrated micro valves and pumps [24-26]). By contrast with active mixers, a passive type requires no external energy and agitation except that associated with producing the pressure drop for flow. For practical reasons, Passive micromixers are preferred from active micromixers [27]. Since high electric field, mechanical shearing, or generation of heat involved the active mixing, the active techniques are not suitable to employ in applications involving sensitive species (e.g. biological system). To avoid the above problems, passive micromixing are exploited.

1.4 Characterization of Mixing Quality

The mixing quality in microscale devices can be characterized using a number of different approaches: a)direct methods of measurement which are usually experimental essence, flow visualization and mixing performance techniques such as acid-base neutralization with an indicator, radioactive tracer and different optical analytical techniques; b)indirect approaches from which the

degree of mixing can be quantified include Poincare section analysis, residence time distribution and numerical particle tracking method [28].

1.5 Various Principle of Passive Micromixers

Over the past decade passive micromixers based on various principles have been designed and investigated. The mixing of microfluids in a passive device is founded on some main principles: a) flow lamination which is used in basic T-mixers and Y-mixers [29-31]), in mixers with different geometries: zig-zag, square-wave, rhombic and similar [32], in serial multi-stage and multi-layer mixers [33]; b) chaotic mixing by eddy formation, stretching and folding [34]; c) split-and-recombine concepts (SAR) [35-36]).

The mixing mechanism of the mixer [36] is based on split and recombination (SAR) with chaotic advection principles is best suited to mixing the fluids with relatively high Reynolds numbers.

1.6 Transport Phenomena

Transport process in microfluidic device can be explained theoretically a two levels: 1) molecular level and 2) continuum level. Continuum model can be describe most transport process in micromixers. At continuum level, the fluid is considered as a continuum. Fluid properties are defined continuously throughout the space. At this level, fluid properties, such as density, conductivity and viscosity , are considered as material properties. Transport phenomena can be described by a set of conservation equations for mass, momentum and energy. These equations are partial differential equations, which can be solved for physical fields in a micromixer, such as concentration and velocity.

1.6.1 Molecular Level based on the Chapman-Enskog Theory

At molecular level, the simplest description of transport phenomena is based on the kinetic theory of diluted monatomic gases which is called Chapman-Enskog theory. The interaction between nonpolar molecules is represented by the Lennard-Jones potential which based on experimental form of :

$$\emptyset_{ij}(r) = 4\varepsilon\left[c_{ij}(\frac{\sigma}{r})^{12} - d_{ij}\left(\frac{\sigma}{r}\right)^{6}\right] \qquad (1.1)$$

Where:

σ is the characteristic diameter of the molecule,

r is the distance between the two molecules, and

ε is the characteristic energy which is the maximum energy of attraction between the molecules.

Table 1.1 Lennard-Jones Characteristic Energies [19].

Gas	Characteristic energy (ε/k_B)	Characteristic diameter σ (nm)
Air	97.0	0.362
N_2	91.5	0.368
CO_2	190.0	0.400
O_2	113.0	0.343
Ar	124.0	0.342

In equation (1.1) the term $(\frac{\sigma}{r})^{12}$ represent the repulsion potential, while the term $(\frac{\sigma}{r})^{6}$ represent the attraction potential between the pairs of molecules.

The coefficient c_{ij} and d_{ij} are determined by molecule types and often assumed to be 1. Table 1.1 lists parameters of some common gases. With the Leonard-Jones potential, the force between the molecules can be derived as :

$$F_{ij} = -\frac{d\emptyset_{ij}(r)}{dr} = \frac{48\varepsilon}{\sigma}\left[c_{ij}(\frac{\sigma}{r})^{13} - d_{ij}\left(\frac{\sigma}{r}\right)^{7}\right] \qquad (1.2)$$

The Lennard-Jones model results in the characteristic time:

$$\tau = \sigma\sqrt{(M/\varepsilon)} \qquad (1.3)$$

Where M is the molecular mass. This characteristic time corresponds to the oscillation period between repulsion and attraction. Also, the model allows the determination of the dynamic viscosity of a pure monatomic gas:

$$\boldsymbol{\mu = \frac{2.68*10^{-26}\sqrt{MT}}{\sigma^2\Omega}} \qquad (1.4)$$

Where the collision integral Ω is a function of the dimensionless temperature $k_B T/\varepsilon$ describing the deviation from rigid sphere behaviour and k_B is the Boltzmann constant.

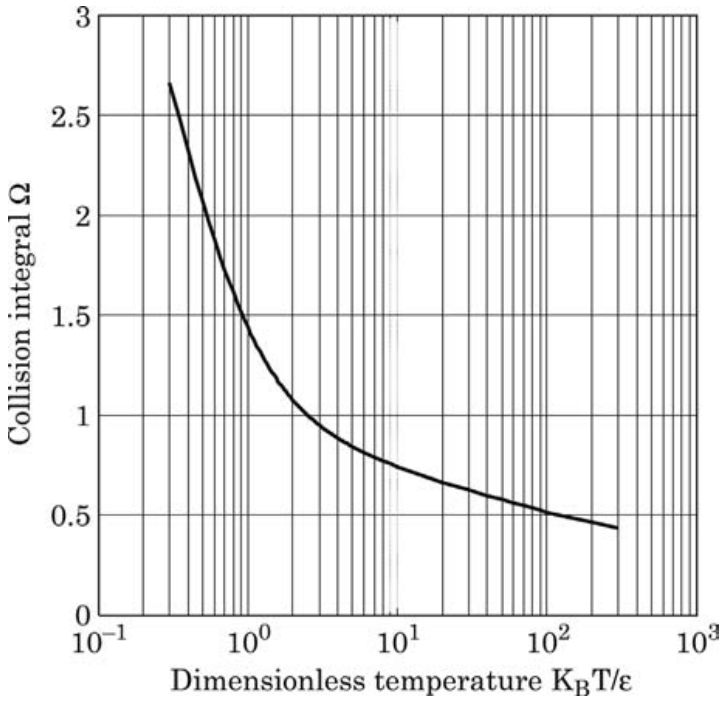

Figure 1.1 Collision integral Ω as a function of dimensionless temperature $k_B T/\varepsilon$ [19]

Fig. 1.1 depicts the function of Ω. The value of the collision integral Ω is of the order of 1. The equation (1.4) allows the determination of Lennard-Jones parameters σ and ε from the measurement of viscosity μ, a macroscopic continuum property.

Kinetic theory can be applied to liquid as well. In this model the motion of liquid molecules is confined within a space limited by its neighboring molecules. Based on this theory, the viscosity of a liquid can be estimated as :

$$\mu = \frac{N_A \bar{h}}{\bar{v}} \exp\left(3.8\, T_b/T\right) \qquad (1.5)$$

Where $N_A = 6.023 * 10^{23}$ is the Avogadro number or the number of the molecules in one mole;

$\bar{h} = 6.626068 * 10^{-34}$ $m^2 kg/s$ is the Plank constant;

$\bar{v}$ is the molar volume;

T_b is the boiling temperature;

and T is the temperature of the liquid.

1.6.2 Continuum Level

At the continuum level, transport phenomena are described with a set of conservation equations. As far as we know, flow regime in micromixer is laminar and we don't need to deal with turbulent flow which is impossible to solve by analytical method. Three conservation equations are :

- Conservation of mass (continuity equation)
- Conservation of momentum (Newton's second law or Navier-Stokes equation)
- Conservation of energy (First law of thermodynamic or energy equation)

1.6.2.1 Conservation of Mass

The continuity equation in the micromixer has the form :

$$\frac{\partial \rho}{\partial t} + \nabla(\rho \overrightarrow{V}) = 0 \qquad (1.6)$$

Where the ∇ is the nabla operator and

$\vec{V}$ is velocity vector :

$$\vec{V} = (u, v, w) \qquad (1.7)$$

For micromixer that transport two incompressible fluid, continuity equation can be further simplified:

$$\nabla . \vec{V} = 0 \qquad (1.8)$$

1.6.2.2 Conservation of Momentum

Conservation of momentum is described by Newton's second law:

$$\frac{\partial \rho \vec{V}}{\partial t} + \nabla(\rho \vec{V}\vec{V}) = -\nabla p + \nabla\left\{\mu\left[(\nabla \vec{V} + \nabla \vec{V}^{T}) - \frac{2}{3}\nabla \vec{V} I\right]\right\} \qquad (1.9)$$

Solving above equations will result in two variables : the velocity *V* and the pressure *P*. These equations are formulized for a solo phase of homogenous composition. In microfluidic device,

fluid convey one or more samples. Hence further equation are needed to explain the transport of species in micromixers.

1.6.2.3 Conservation of Energy (convection- diffusion equation)

$$\frac{\partial C}{\partial t} + \vec{V}.\nabla C = D\nabla C \qquad (1.10)$$

Where C denotes the species concentration and D the diffusion coefficient of the species. Computational fluid dynamics software, ANSYS-Fluent 13.0, was used to solve the governing equations (1.8) and (1.9) in this thesis. The value of the ρ and μ are 998 kg m^{-3} and 0.00089 kg $m^{-1}s^{-1}$ respectively. Also some assumptions such as steady-state flow, no-slip conditions and incompressible fluid are proposed.

1.7 Molecular Diffusion

1.7.1 Brownian Motion

Brownian motion is the presumably random moving of particles suspended in a fluid (liquid or gas) resulting from their bombardment by the fast-moving atoms or molecules in the fluid. A random walk is the path traced by a particle taking successive steps, each in a random direction.

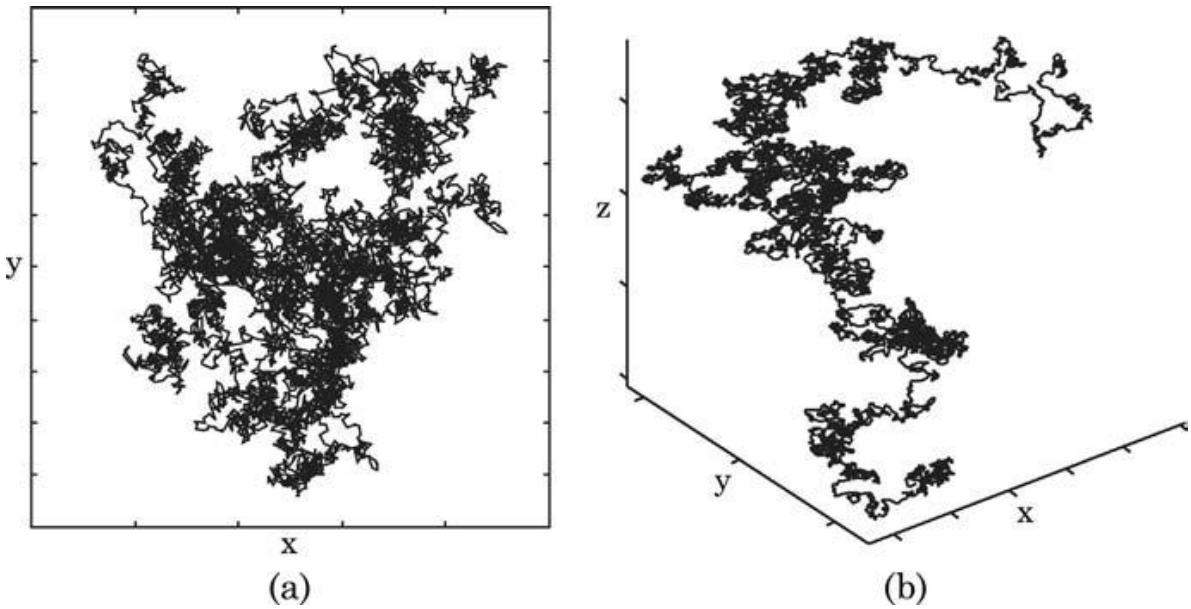

Figure 1.2 Random walk of a particle (a) two-dimensional (b) three-dimensional.[19]

The construction of a random walk follows these rules [19] :

- The particle starts at a predefined points,
- The distance done by each step is equal

- The direction from one point to the next step is random.

Following these assumption, a random walk of particle can be realized with a simple program. Considering a one-dimensional random walk on a line, the particle has a random choice of two directions for each step.

$$x\,(n) = \sum_{i=1}^{n} s_i \qquad (1.11)$$

Where s_i is a random step, and the value of s_i is $+s$ or $-s$. The squared value of the position $x\,(n)$ is :

$$x(n)^2 = \sum_{i=1}^{n} {s_i}^2 = ns^2 \propto D_t \qquad (1.12)$$

The proportionally factor determines how fast the particle walks, which actually is the diffusion coefficient. As mentioned before, Brownian motion is the random walk with very small steps. Figure 1.2 illustrates the random walk of a particle calculated for 10000 steps in two and three dimensions. The Brownian motion of particles in a liquid is due to the instantaneous imbalance in the forces exerted by the small liquid molecules on the particles. Hence, the diffusion coefficient can be derived from the force balance equation.

1.7.2 Stoke-Einstein Model of Diffusion

The time evaluation of the position of the Brownian particle itself can be described approximately by the force balance equation where the random force of the liquid molecules represents one term in the balance equation also called Langevin equation.

$$m\frac{dv}{dt} = \beta v + F(t) \qquad (1.13)$$

Where m is the mass of the particle, β is the friction coefficient and $F(t)$ is the random force of the liquid molecules.

The friction coefficient can be calculated by equation (1.14) on a spherical particle :

$$\beta = 3\pi\mu\sigma_p \qquad (1.14)$$

Where σ_p is the radius of the particle and μ is the viscosity of the liquid.

By solving equation (1.13), the diffusion coefficient can be characterized as :

$$D = \frac{u^2 m}{\beta} \quad (1.15)$$

Where u^2 is the variance of particle velocity.
The kinetic energy of the particle is related to the temperature as :

$$\frac{1}{2}mu^2 = \frac{1}{2}k_B T \quad (1.16)$$

Submitting $u^2 = {k_B T}/{m}$ in (1.15) results in the Stoke-Einstein equation of the diffusion coefficient as follows:

$$D = \frac{k_B T}{3\pi\mu\sigma_p} \quad (1.17)$$

1.7.3 Diffusion Coefficient in Liquid

While diffusion coefficient of the gases are of the order of $10^{-5}\ {m^2}/{sec}$, diffusion coefficient in the liquids are of the order of $10^{-9}\ {m^2}/{sec}$, and for the large molecules can be the order of $10^{-11}\ {m^2}/{sec}$.

Diffusion coefficient of a molecule i in a solute j with a viscosity of μ_j can be estimated with the Stoke-Einstein equation.

$$D_{ij} = \frac{k_B T}{3\pi\mu_j\sigma_i} \quad (1.18)$$

Where σ_i is the diameter of the molecule i .
In the equation of (1.18), numerator term represents the kinetic energy of the molecule and denominator represents the friction force acting on the molecule.

1.8 Taylor Dispersion

Taylor dispersion is an effect in fluid mechanic in which a shear flow can increase the effective diffusivity of a species. Essentially, the shear acts to smear out the concentration distribution in the direction of the flow, enhancing the rate at which it spreads in the direction.

Taylor dispersion is an effective mechanism for mixing of a solute in a distribution velocity field, such as pressure driven flow in a microchannel. This axial effect arises from a coupling between molecular diffusion in the transverse direction and transverse distribution of the flow velocity. Figure 1.3 depicts the difference between molecular diffusion in a plug-like flow and Taylor dispersion in a distributed flow.

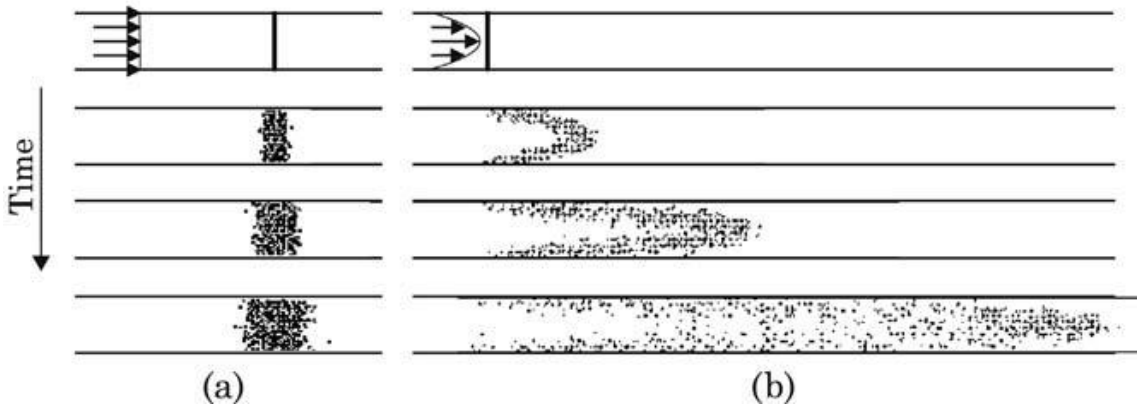

Figure 1.3 Particle distribution in a microchannel: (a) uniform velocity profile, (b) parabolic velocity profile

In a uniform flow field, for instance the plug-like Electroosmotic flow, advection and diffusion are independent. Axial diffusion is the same as molecular diffusion, Figure 1.3 (a). In a distributed flow field, such as the pressure driven flow with a parabolic velocity distribution, the solvent is stretched more in the idle of the channel than near the wall due to the axial convective transport. The resulting concentration gradient between the different fluid layers are then blurred by diffusion in the transverse direction as can shown in Figure 1.3 (b) [19]. As can be seen, the solute appears to be ‘’ diffusing’’ in the axial direction at a rate that is much faster than what would be predicted by ordinary molecular diffusion.

Figure 1.4 illustrates the model for determination of Taylor dispersion in a circular channel. As can be seen , dispersion coefficients are derived by a two-dimensional model involving one axial and one transversal spatial dimension.

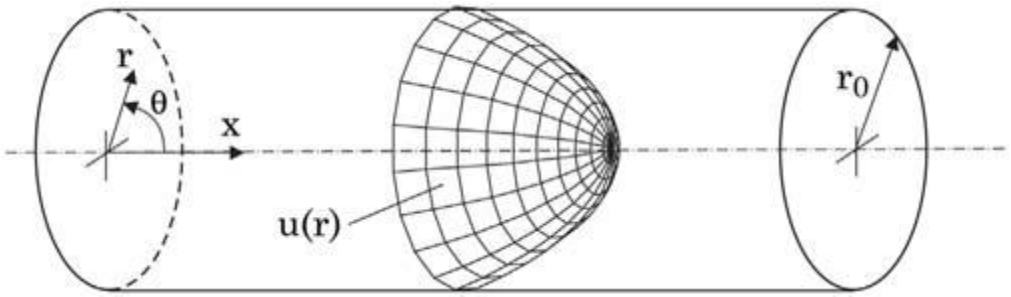

Figure 1.4 Taylor dispersion model in a circular channel.

Taylor was the first to present a working model for the transverse average that managed to capture the influence of both transverse diffusion and the transverse variation of the fluid velocity field. As shown in figure 1.4, Taylor analysis is based on the model of a long cylindrical capillary.

1.9 Chaotic Advection

In chaos theory and fluid mixing, chaotic mixing is a process by which flow tracers develop into complex fractals under the action of a fluid flow. The flow is characterized by an exponential growth of fluid filaments. Two basic mechanisms are responsible for fluid mixing are : diffusion and advection. In liquids, molecular diffusion alone is hardly efficient for mixing. Advection, that is the transport of matter by a flow, is required for better mixing. The fluid flow obeys fundamental equations of fluid dynamics (Conservation of mass and Conservation of momentum). These equations are written for the Eulerian velocity field rather than Lagrangian position of the fluid particles. Lagrangian trajectories are then obtained by integrating the flow.

1.9.1 Basic Concept

The term chaotic advection refers to the phenomena where a simple Eulerian velocity field leads to a chaotic response in the distribution of a Lagrangian indication, such as a tracing particle, and also advection refer to species transport by the flow. A flow field can be chaotic even in the laminar flow. It is important to note that chaotic advection is not turbulence. The streamline of steady chaotic advection flow across each other causing the particles to change their paths. Under chaotic advection, the particles diverge exponentially and enhance mixing between the species. There are few terminologies related to visualization of an Eulerian velocity field. The common terminology is the pathline (also called trajectory) of a fluid particle in the flow field. The particle transport mechanism can be described by the advection equation :

$$\begin{cases} \frac{dx}{dt} = u(x,y,z,t) \\ \frac{dy}{dt} = v(x,y,z,t) \\ \frac{dz}{dt} = w(x,y,z,t) \end{cases} \quad (1.19)$$

Pathlines can be obtained by solving equation (1.19) . In a two dimensional flow, streamlines are given by solution of equation (1.20) .

$$\begin{cases} \frac{dx}{ds} = u(x,y,z,t) \\ \frac{dy}{ds} = v(x,y,z,t) \end{cases} \quad (1.20)$$

Where s is independent variable. In experiments, streamline can be constructed from the two images recorded with particle image velocimetry (PIV). Particle images are recorded at two successive time instances t and $t + \Delta t$. The particle velocities are determined by the record particle displacement and the time delay Δt . The streamlines can be depicted as level sets of the stream function ψ, which is defined as :

$$\begin{cases} \frac{dx}{dt} = u(x,t) = \frac{\partial \psi}{\partial y} \\ \frac{dy}{dt} = v(x,t) = -\frac{\partial \psi}{\partial x} \end{cases} \quad (1.21)$$

Equation 1.19 represents a system of coupled ordinary differential equations (ODEs). Similar dynamic system in engineering and fluid flow have shown a strong chaotic behavior.

The terminologies for chaotic advection can be borrowed from the more established field of dynamical system theory. The advection equation (1.19) can be solved explicitly for the fluid particle position (x, y, z) at a given time t and this solution used for describing the motion of the fluid particles in a specific region, such as a micromixer cross section, and can be called a mapping function. Each transformation is called an advection cycle, which correspond to a mixing element in different micromixer design, such as sequential lamination and etc. As examples of chaotic advection we can cite (a) Lorentz's Convection Flow and (b) Dean Flow in Curved pipes [19].

1.9.1.1 Lorentz's Convection Flow

Lorentz's Convection Flow is described for a three-dimensional system, and the equations (1.19) are more than enough to create a nonintegrable or chaotic dynamic. Lorenz [37] derived a

simplified system of equations for convection rolls in atmosphere :

$$\begin{cases} \frac{dx}{dt} = Pr(y - x) \\ \frac{dy}{dt} = x\left(\frac{Ra}{Ra_c} - z\right) - y \\ \frac{dz}{dt} = xy - \beta z \end{cases} \quad (1.22)$$

Where the variable *x* is proportional to convective intensity, *y* is proportional to the temperature difference between descending and ascending currents, and *z* is proportional to the difference in vertical temperature profile from linearity in this system of equations.

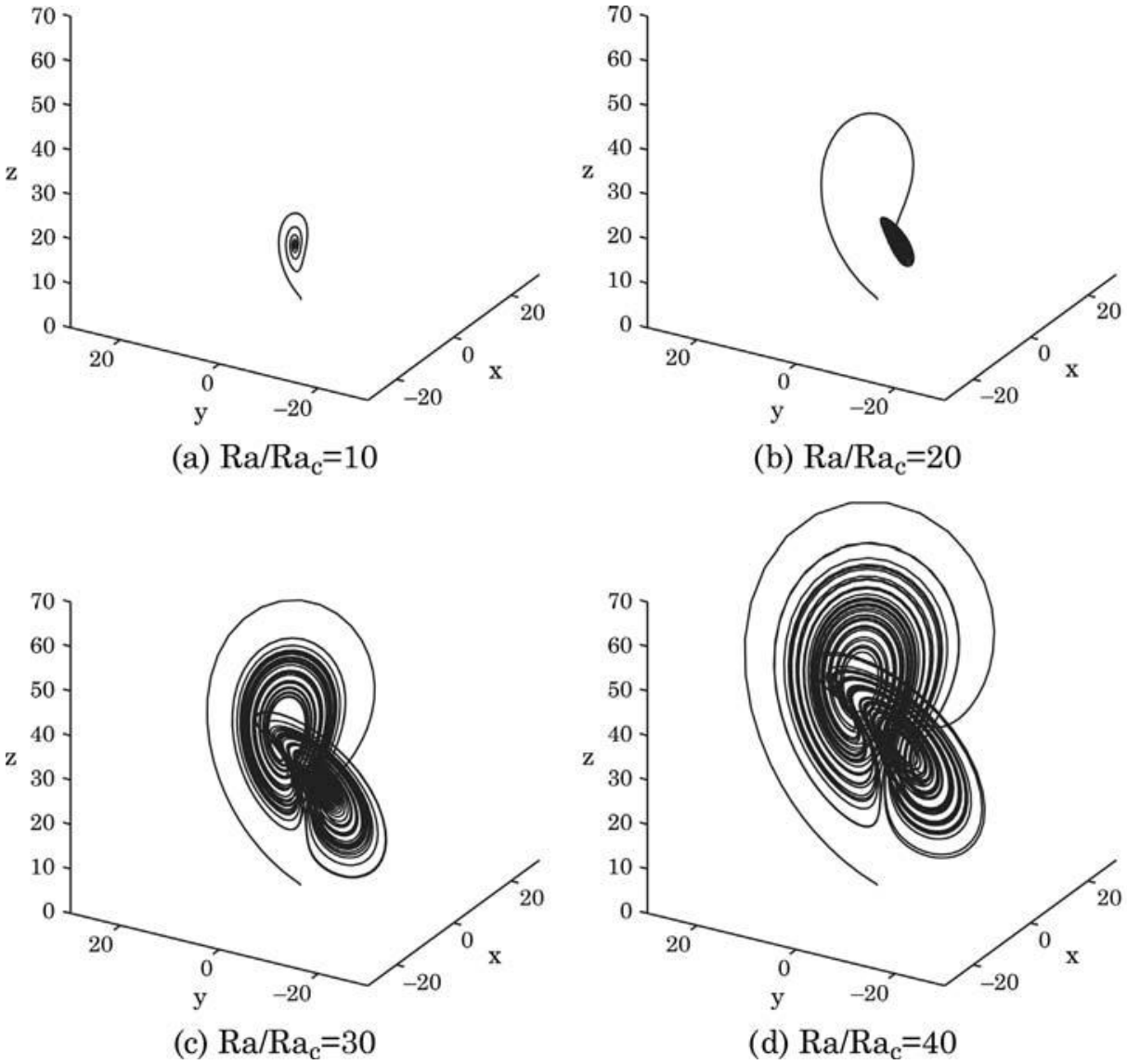

Figure 1.5 Solution of Lorentz's equations for different Rayleigh numbers (Pr=10 and $\beta = 8/3$): (a) $^{Ra}/_{Ra_c} = 10$*; (b)* $^{Ra}/_{Ra_c} = 20$ *; (c)* $^{Ra}/_{Ra_c} = 30$ *; (d)* $^{Ra}/_{Ra_c} = 40$. [37]

(b)

In Figure (1.5), Pr, Ra, Ra_c and β are the Prndtl number, Rayleigh number, critical Rayleigh number and the geometric factor respectively. As shown in Figure (1.5), a small change in Rayleigh number leads to a large change in the solution.

1.9.1.2 Dean Flow in Curved Pipe

The flow field inside a curved pipe was first investigated by Dean [38] . The model for the flow in a toroidal pipe is depicted in Figure 1.6 . The pipe has the form of a toroid of a radius *R* and the pipe diameter is *a*.

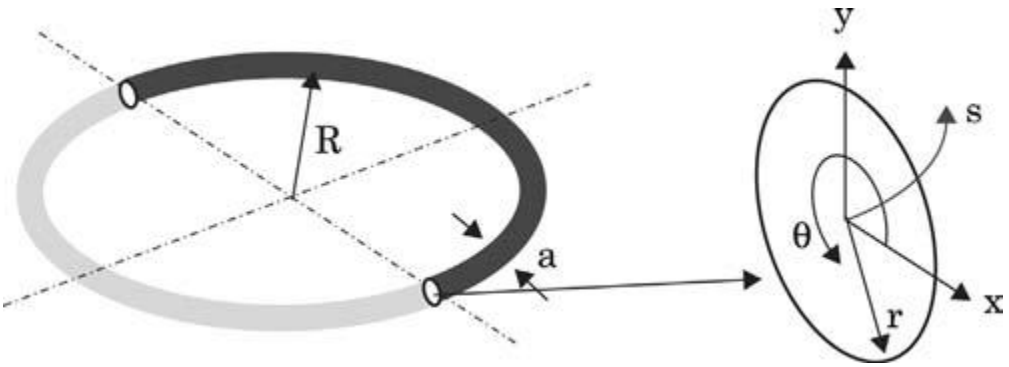

Figure 1.6 Model of Dean flow. [38]

The coordinate system for this model is based on cylindrical coordinates, where s is the coordinate of the toroid's centerline q. The metric of this coordinate system is :

$$(dq)^2 = (1 + \frac{r}{R}\sin\theta)^2\,(ds)^2 + (ds)^2 + r^2(d\theta)^2 \quad (1.23)$$

With the assumption of laminar flow, s is zero. By solving above equation, the dimensionless velocity field of pipe cross section, secondary velocity field and also streamline of velocity field could be calculated and plotted. Figure 1.7 illustrates the dimensionless velocity field graphically in a pipe cross section. As shown in Figure 1.7, the effect of the centrifugal force can be seen clearly.

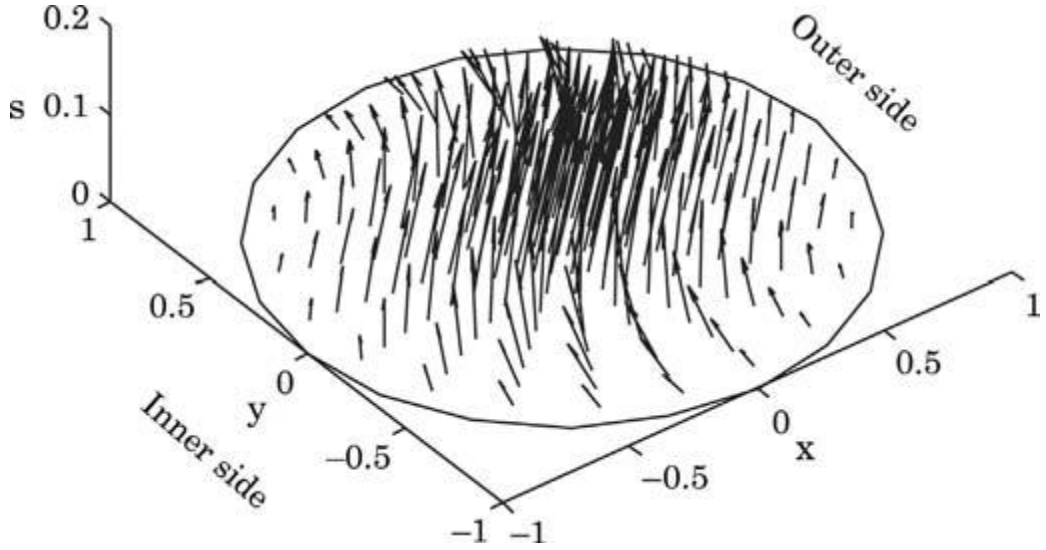

Figure 1.7 Dimensionless velocity field of a pipe cross section.

Figure 1.8 depicts the secondary velocity field of the pipe cross section. Centrifugal force causes the fluid to move outward. Also streamlines illustrated in Figure 1.8 (b) show that two vortices in the lower and upper halves of the pipe.

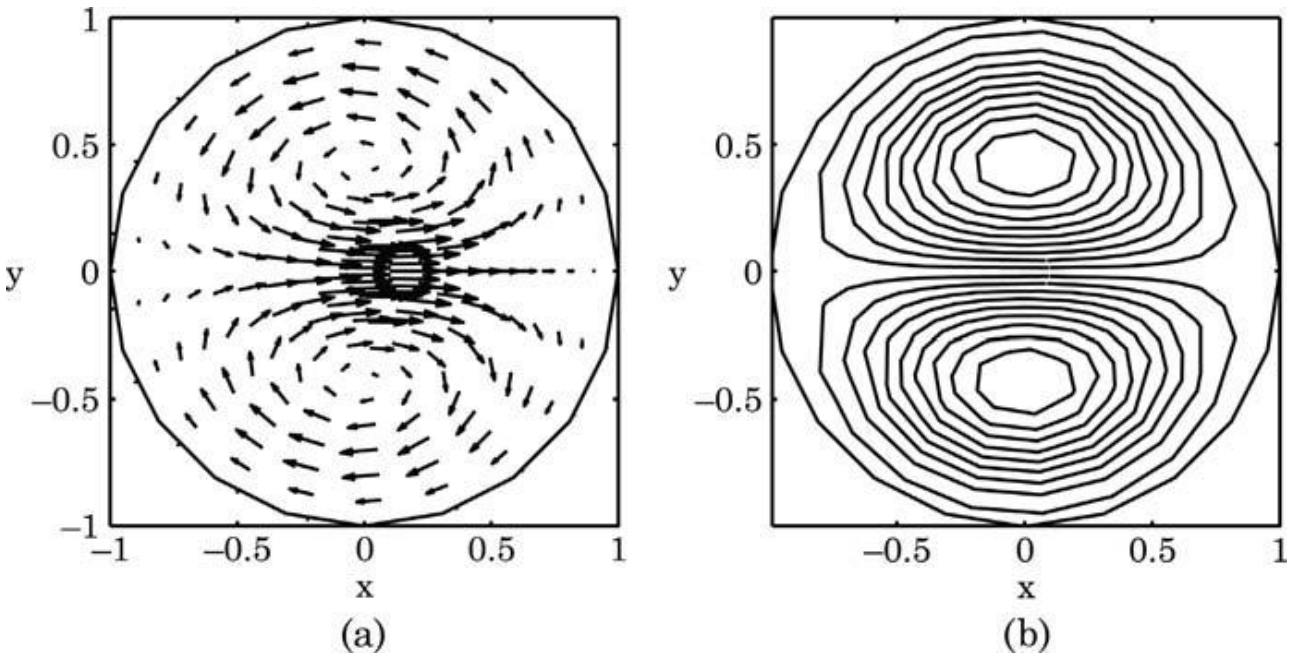

Figure 1.8 Dean vortices: (a) secondary velocity field; (b) streamlines of the secondary velocity field.

Projecting the particle position on a single two-dimensional cross section results in the Poincare section. Figure 1. 9 shows the trajectories and Poincare sections of the Dean flow.

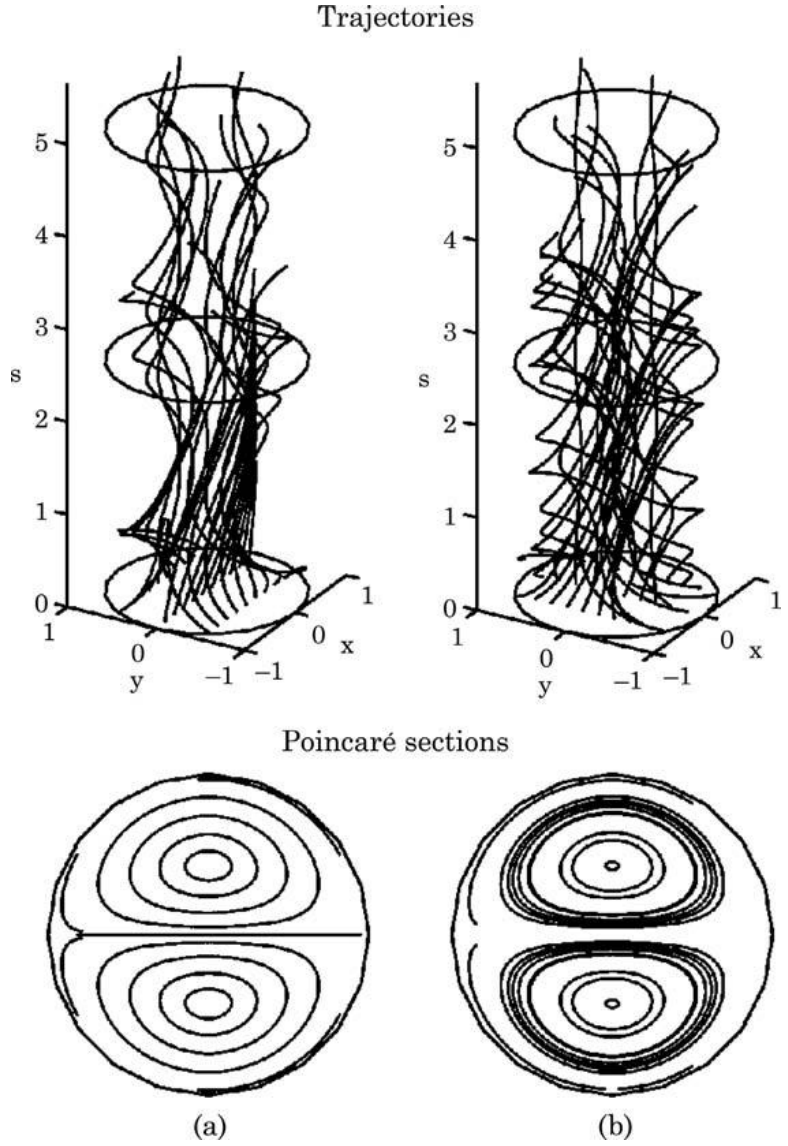

Figure 1.9 Trajectories and Poincare sections for fluid particle in Dean flow; (a) seeding line parallel to the x-axis; (b) seeding line parallel to the y-axis.

The results show that independent of the orientation seeding line, the Poincare section follow the streamlines as illustrated in Figure 1.8 (b). If this fluid is used in a micromixer, the solvent and solute should be introduced on the left and right of the cross section or the outer and inner sides of the curved channel. If the solvent and solute introduced either in the upper and lower halves of the channel, or outer and inner side of the curved channel, advection mixing will not appear. The mentioned analysis assume a small ratio between the pipe diameter and radius of curvature $\alpha/R \ll 1$. For realistic channel design, this ratio can be approximately unity. In this case, the flow is characterized by the Dean number :

$$De = Re\sqrt{\frac{\alpha}{R}} \qquad (1.24)$$

The Dean number represents the ratio between centrifugal force and inertial force. There exists a critical Dean number $De_{cr} = 150$ where the secondary flow pattern changes. For $De < 150$, there is only one pair of counter-rotating vortices as analyzed above. At higher Dean number, $De > 150$, the centrifugal force is dominant leading to the formation of two additional vortices at the outer channel wall.

1.10 Flow in Helical Pipe

In helical pipes, the cross section rotates around the pipe center line q, as shown in Figure 1.10. Assuming a constant torsion of τ, the rotation at s is τs. Further, a constant curvature $k = {d\psi}/{ds}$.

Germano [39] derived the metric equation :

$$(dq)^2 = [(1 - kr\,sin(\theta + \tau s)](ds)^2 + (dr)^2 + r^2(d\theta)^2 \qquad (1.25)$$

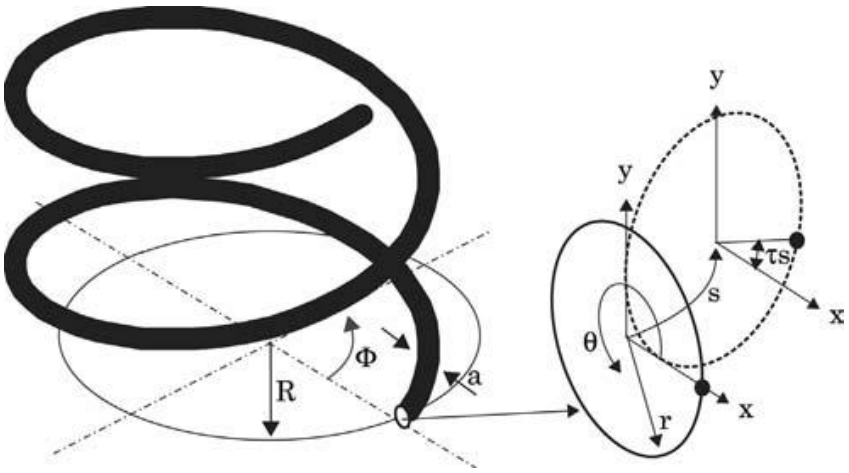

Figure 1.10 Model of the helical pipe.

The stream function of this flow has the form :

$$\psi = \frac{\lambda r^2}{2}\left(\frac{r^2}{2} - 1\right) + \frac{y}{4}(4 - r^2)(1 - r^2)^2 \qquad (1.26)$$

Figure 1.11 illustrates the streamlines calculated using equation 1.26 . The initial positions of the

particles on the depicted trajectories are on a seeding line parallel the *y*-axis. The results show that at increasing torsion, the secondary flow transforms from two counter-rotating vortices into a single vortex [39].

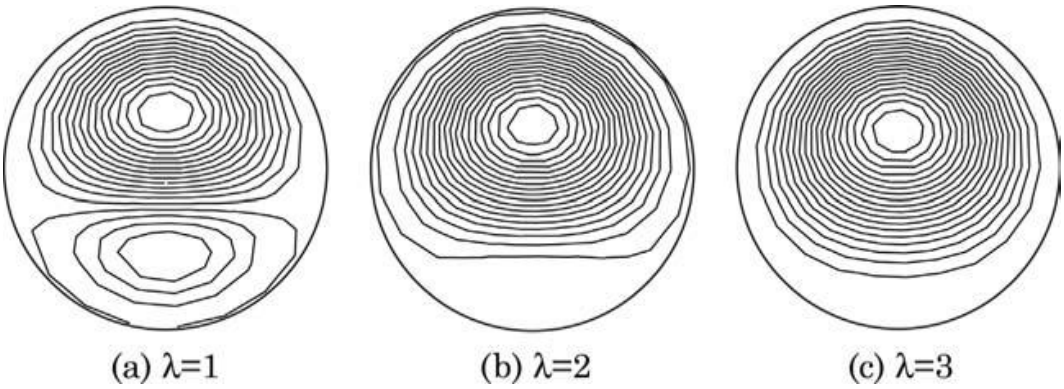

Figure 1.11 Streamlines of the flow inside a helical pipe of different geometry parameters; (a) $\lambda = 1$*; (b)* $\lambda = 2$*; (c)* $\lambda = 3$.

Where the curvature and torsion are combined in the geometry parameter λ :

$$\lambda = \frac{144\nu}{\bar{u}}\frac{\tau}{k} \qquad (1.27)$$

Where the $\bar{u}$ is the mean velocity.

The Poincare sections of the flow in helical pipes with different geometry parameters are depicted in Figure 1.12.The flow is initially sampled with a seeding line parallel to the *y*-axis. At $\lambda = 0$, there is no torsion and the pipe is a torus. The flow is clearly not chaotic, the particles follow the streamlines. At $\lambda > 0$, chaotic advection is apparent.

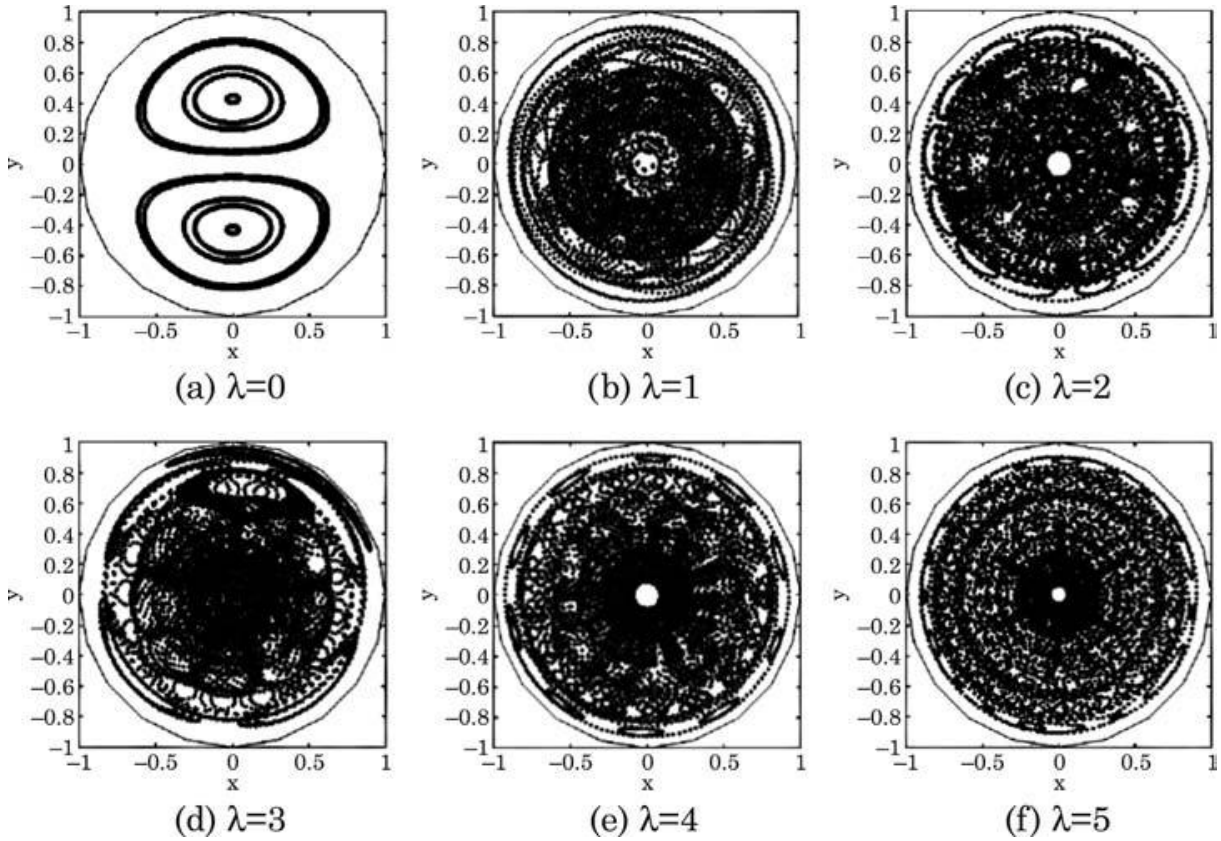

Figure 1.12 Poincare sections with different geometry parameters: (a) $\lambda = 0$; (b) $\lambda = 1$; (c) $\lambda = 2$; (d) $\lambda = 3$; (e) $\lambda = 4$; (f) $\lambda = 5$.

1.11 Scaling laws and fluid flow at the Micro Scale

Transport properties in the fluid flow at the micro scale are : the diffusion coefficient D, the kinematic viscosity ν, and the thermal diffusivity $\alpha = {}^{k}/_{\rho c}$, and all have the same unit of ${}^{m^2}/_{s}$

,where *k*, ρ and *c* are thermal conductivity, density, and specific heat respectively. The ratios between these properties represent a group of dimensionless numbers characteristic for the ratios between the competing transport processes. These dimensionless numbers help to compare molecular diffusion with other transport processes in microfluidics. Some of these dimensionless numbers are as follows: Schmidt number, Lewis number, Reynolds number, Peclet number, and Fourier number.

The Schmidt number is the ration between momentum transport and diffusive mass transport:

$$Sc = \frac{momentum\ transport}{diffusive\ mass\ transport} = \frac{\nu}{D} = \frac{\mu}{\rho D} \qquad (1.28)$$

For most liquids and gases, the Schmidt number is larger than unity, $Sc > 1$.

The Lewis number is the ratio between heat transport and diffusive mass transport :

$$Le = \frac{heat\ transport}{diffusive\ mass\ transport} = \frac{\alpha}{D} = \frac{k}{\rho c D} \qquad (1.29)$$

The ration between advective transport and momentum transport is called the Reynolds number:

$$Re = \frac{advective\ mass\ transport}{momentum\ transport} = \frac{\rho \bar{u} L_{ch}}{\mu} = \frac{\bar{u} L_{ch}}{\nu} \qquad (1.30)$$

Where $\bar{u}$ is the mean velocity in the flow direction and L_{ch} is the characteristic length of the micro channel. In many cases , the hydraulic diameter is taken as the characteristic length. As an example, for typical value of $L_{ch} = 100\,\mu m,\ \bar{u} = 1\,mm/s,\ \nu = 10^{-5}\,cm^2/s,$ the Reynolds number is $Re = 0.01$. This small number means that laminar flow regime exists in almost all microfluidic applications.

The Peclet number is the ratio between advective mass transport and diffusive mass transport:

$$Pe = \frac{advective\ mass\ transport}{diffusive\ mass\ transport} = \frac{\bar{u} L_{ch}}{D} \qquad (1.30)$$

The ratio between the Peclet number and the Reynolds number is actually the ratio between momentum transport and diffusive mass transport, i.e. the Schmidt number. For diffusion coefficient ranging from $10^{-5}\,m^2 s^{-1}$ to $10^{-7}\,m^2 s^{-1}$, the Peclet numbers for the values mentioned above are $100 < Pe < 10000$, which means advective mass transport dominates over diffusive transport in almost all microfluidic applications.

The average diffusion time t_{diff} over the characteristic mixing length L_{ch} , also called the striation thickness, is represented by the Fourier number [40].

$$Fo = \frac{D t_{diff}}{L_{mixing}^2} \qquad (1.31)$$

The Fourier number is usually in ranging between 0.1 and 1.

The mentioned equation reveals that a very compact micromixer can be designed using sequentional lamination or chaotic advection. In general, fast mixing can be achieved with smaller mixing path and larger interfacial area. If the channel geometry is very small, the fluid molecules collide most often with the channel wall and not with other molecules.

1.12 Summary and motivation

In a micromixers designs, degree of mixing is characterized by flowing of two parallel liquids and observing the minimum distance from inlet part over which they become intermixed. Foremost, results of experiments in micromixers are detected visually. In order to characterize the micromixers, in my studies, blue and yellow dyed water are applied and injected to the microchannel by a syringe pump to evaluate the mixing performance. For a well-mixed micromixer, the outlet color of the microchannel is green , while it could be seen two separate color (yellow and blue) at the outlet of the microchannel if the mixing degree is very low or does not occur.

However, the comparison of the mixing colors just visually are unable to provide enough quantitative analysis to evaluate the mixing degree, thus some techniques implemented to analyze the experimental data. Different researchers employ different techniques to determine the efficiency of the micromixers. For instance, some research groups utilized ‘’top view’’ measurement technique, and some researchers employed confocal microscopy at the cross section of the microchannel. The situation becomes more complex when the different experimental characterization techniques is further combined with the use of different fluid and different data analysis regulation. However, in order to develop advanced micromixers, the data precisely needed to be analyzed to satisfy the demands on this field. In this thesis, we employed image-based technique to analyze the experimental data .

As far as we know, the targets in micromixers design are: (a) high mixing efficiency (over 80%) and (b) low pressure drop.

The motivation behind this work is to overcome the fluid mixing in micromixers which strongly limited to laminar regime with lower required pressure drop. Micromixers are in a crucial need of techniques where passive micromixing can be achieved in the shortest possible distance by using simplified microchannels that can be easily constructed. Naturally occurring splitting and recombination (SAR) process that arise in my proposed geometry offer a tremendous occasion of constructing and helping micromixer technology to overcome mentioned expected potentials. This study propose a novel passive micromixers. Mixing characteristics of two species are elucidated via experimental and numerical studies associated with microchannels with various inlet flow rates (velocities) and results compared with the previous well-known micromixers.

1.13 Objectives

While current generation passive micromixing techniques have made useful contribution in microfluidic field of research, many micromixers need channel geometries which utilize complex manufacture techniques. Although patterning surface with complicated geometry is becoming

accurate, the problem appears when two patterned surfaces require to be assembled, aligned, and bonded with precision. Mentioned problem is not only time consuming but also expensive to perform in the laboratories. Considering all these factors, there still exist the need to build micromixers that achieve fine passive micromixing in the shortest possible distance by using simplified microchannels.

The purpose of this investigation is to achieve two targets which are higher mixing efficiency and lower pressure drop in micromixers by exploiting splitting and recombination (SAR) process in microchannels. The following micromixer designs are investigated and characterized:

- T micromixer
- O micromixer
- Tear-drop micromixer
- H micromixer
- Chain 1 micromixer
- Chain 2 micromixer
- Chain 3 micromixer
- Chain 4 micromixer.

References

[1] Bothe D., Lojewski A., Warnecke H.J., 2011. Fully resolved numerical simulation of reactive mixing in a T-shaped micromixer using parabolised species equations, Chemical Engineering Science 66, 6424-6440, doi: 10.1016/j.ces.2011.08.045.

[2] Yang J.T., Wang L., Lyu P.C., 2007. An overlapping crisscross micromixer, J. Chemical Engineering Science 62, 711- 720, doi: 10.1016/j.ces.2006.09.048.

[3] Soleymani A., Yousefi H., Turunen I., 2008. Dimensionless number for identification of flow patterns inside a T- micromixer, Chemical Engineering Science 63, 5291-5297, doi: 10.1016/j.ces.2008.07.002.

[4] Fu L.M., Lin C.H., 2007. A rapid DNA digestion system, Biomed Microdevices 9, 277-286, doi: 10.1007/s 10544-006- 9036-0 .

[5] Sheu T.S., Chen S.J., Chen J.J., 2012. Mixing of a split and recombine micromixer with tapered curved microchannels, Chemical Engineering Science 71, 321-332, doi: 10.1016/j.ces.2011.12.042.

[6] Song K.H., Jung Y.J., Park S.H., Choe J., 2012. Recrystallization of polyethylene submicron particles using a continuous flow micromixer system, Powder Technology 217, 325-329, doi: 10.1016/j.powtec.2011.10.044.

[7] Wang H., Iovenitti P., Harvey E., Masood S., 2003. Numerical investigation of mixing in microchannels with patterned grooves, J. Micromech. Microeng. 13, 801-808.

[8] Yang J.T., Fang W.F., Tung K.Y., 2008. Fluid mixing in devices with connected-groove channels, J. Chemical Engineering Science 63, 1871-1881, doi: 10.1016/j.ces.2007.12.027.

[9] Sinton D., Coleman J.T., 2005. A sequentional injection microfluidic mixing strategy, Microfluidic Nanofluidic Journal 1, 319-327, doi: 10.1007/s10404-005-0034-y.

[10] Hong C.C., Choi J.W, Ahn C.H., 2004. A novel in-plane passive microfluidic mixer with modified Tesla structures, Miniaturization for chem. Biology & Bioeng., Lab Chip 4, 109-113.

[11] Aubin J., Fletcher D.F., Xuereb C., 2005. Design of micromixers using CFD modelling, Chemical Engineering Science 60, 2503-2516, doi: 10.1016/j.ces.2004.11.043.

[12] Wang Y., Zhang K., Guo S., Zhao L., Zhao X., Chan H.L.W., 2011. Realization of planar mixing by chaotic velocity in microfluidics, Microelectronic Engineering 88, 959-963, doi: 10.1016/j.mee.2010.12.029.

[13] Cho H.H, Kim B.S., Kwak B.S., Shin S., Lee S., Kim K.M., Jung H.I., 2011. Optimization of microscale vortex generators in a microchannel using advanced response surface method,

International Journal of Heat and Mass Transfer 54, 118-125, doi:10.1016/j.ijheatmasstransfer.2010.09.061.

[14] Matsuyama K., Mine K., Hideaki K., Aoki N., Mae K., 2010. Optimization methodology of operation of orifice-shaped micromixer based on micro-jet concept, Chemical Engineering Science 65, 5912-5920, doi:10.1016/j.ces.2010.08.013.

[15] Shih T.R., Chung C.K., 2008 .A high-efficiency planar micromixer with convection and diffusion mixing over a wide Reynolds number range, Microfluidic Nanofluidic Journal 5, 175-183, doi:10.1007/s10404-007-0238-4.

[16] Matsuyama K., Mine K., Kubo H., Mae K., 2011. Design of micromixer for emulsification and application to conventional commercial plant for cosmetic, Chemical Engineering Journal 167, 727-733, doi: 10.1016/j.cej.2010.09.085.

[17] Kim K.Y., Hossain S., Husain A., 2010. Shape optimization of a micromixer with staggered-herringbone grooves patterned on opposite walls, Chemical Engineering Journal 162, 730- 737, doi: 10.1016/j.cej.2010.05.056.

[18] Yang J.T., Fang W.F., Tung K.Y., 2008. Fluid mixing in devices with connected-groove channels, J. Chemical Engineering Science 63, 1871-1881, doi: 10.1016/j.ces.2007.12.027.

[19] Nguyen N.T., 2008. Micromixers: Fundamentals, Design and Fabrication. William Andrew, Norwich, NY, USA.

[20] Hessel V., Lowe H., Schonfeld F., 2005. Micromixers-a review on passive and active mixing principles, Chemical Engineering Science 60, 2479-2501.

[21] Mansur E.A., Mingxing Y., Yondong W., Youyuan D., 2008. A State-of-the-art Review of Mixing in Microfluidic Mixers, Chinese Journal of Chemical Engineering 16 (4), 503-516.

[22] Nguyen N.T., Wu Z., 2005. Micromixers- a review, J. Micromech. Microeng. 15, R1-R16.

[23] Bockhorn H., Mewes D., Peukert W., WarneckeH.J., 2010. Micro and Macro Mixing: Analysis, Simulation and Numerical Calculation, Heat and Mass Transfer (Springer), ISBN: 3642045480.

[24] Yang Z. et al., 2001. Ultrasonic micromixerfor microfluidic systems, Sensors and Actuators A 93, 266-272.

[25] Liu R.H. et al., 2003. Hybridization enhancement using cavitation microstraming, Analytical Chemistry 75, 1911-917.

[26] Glasgow I., Aubry N., 2003. Enhancement of microfluidic mixing using time pulsing, Lab on a Chip 3, 114-120.

[27] Serra C.A., Bally F., Hessel V., Hadziioannou G., 2011. Micromixer-assisted polymerization processes, Chemical Enginering Science 66, 1449-1462, doi: 10.1016/j.ces.2010.07.026.

[28] Solliec C., Mouheb N.A., Montillet A., Malsch D., Henkel T., 2012. Numerical and experimental investigations of mixing in T-shaped and cross-shaped micromixers, Chemical Engineering Science 68, 278-289, doi: 10.1016/j.ces.2011.09.036

[29] Kamholz A.E. et al., 1999. Quantiative analysis of molecular interactive in microfluidic channel: the T-sensor, Anal. Chem. 71, 5340-7.

[30] Sullivan S.P. et al., 2007. Simulation of miscible diffusive mixing in microchannels, Sensors and Actuators B 123, 1142-1152.

[31] Swickratha M.J., Burnsa S.D., Wnekb G.E., 2009. Modulating passive micromixing in 2-D microfluidic devices via discontinuities in surface energy, Sensors and Actuators B 140, 656-662.

[32] Hossain S.,Ansari M.A., Kim K.Y., 2009. Evaluation of the mixing performance of three passive micromixers, Chemical Engineering Journal 150, 492-501.

[33] Tofteberg T., Skolimowski M., Andreassen E., Geschke O., 2010. A novel passive micromixer: lamination in a planar channel system, Microfluidic Nanofluidic Volume 8, Number 2, 209-215.

[34] Xua Z., Li C., Vadilloc D., Ruanb X., Fub X., 2011. Numerical simulation on fluid mixing by effects of geometry in staggered oriented ridges micromixers, Sensors and Actuators B 153, 284-292.

[35] Ohkawa K., Nakamotob T., Izukab Y., et al., 2008. Flow and mixing characteristics of σ-type plate static mixer with splitting and inverse recombination, Chemical Engineering research and Design 86, 1447-1453.

[36] Lee S.W., Lee S.S., 2008. Rotation effect in split and recombination micromixing, Sensors and Actuators B 129, 364-371.

[37] Lorenz, E.N., 1963, Deterministic nonperiodic flow. Journal of the Atmospheric Science, Vol. 20, pp, 130-141.

[38] Dean, W.R., 1927. Note on the motion of the fluid in a curved pipe. Philosophy Magazine, Vol. 4, pp. 208-223.

[39] Germano M., 1982. On the effect of torsion on helical pipe flow. Journal of Fluid Mechanics, Vol. 203, pp. 1-8.

[40] Cussler E.L., 1997. Diffusion: Mass Transfer in Fluid System. 2nd edition, Cambridge University Press.

Chapter 2

Experimental Equipments and Procedures

2.1 Introduction

Before to analyze the detail problems and the techniques for the experimental data obtained in microfluidic laboratory, it is suitable to study the experimental procedures and equipments which was used during the micromixing. Thus foremost, to explain the procedures, it is useful to explain the passive micromixing strategies.

To compare our field of study with other investigations, this chapter, also review the current state of knowledge concerning the experiments and techniques that use in common survey of micromixers. Standard investigations in micromixers field of study don't exist at high Reynolds number and there aren't experimental procedure universally accepted by turbulence flow regime. Generally, even for equipments which are used in laboratory, there is the same operating principle, for instance a syringe pump and flow rate during the tests. Flow experiments were carried out using a standard syringe pump and cross-sectional image-based techniques were obtained for analyzing the data. It is possible to find in the literature the constructive solutions that used in different analyzing.

In this section will be discussed the variety of passive mixing and also standard experiment equipments employed for testing the passive micromixers and the experimentation techniques used in this research.

2.2 Review of Passive Micromixing

Micromixing have been a major topic of research in the past decade [1], and progress on recent development of micromixers has been reviewed by Kumar et al. [2]. Micromixers are miniaturized mixing devices used for two or more different substances, which may be either pure liquids or solutes dissolved in a solvent. Mixing in microchannels plays an important role in micro total analysis systems (μ-TAS) and MEMS [3,4]. Micromixers have a wide variety of potential

applications in industry. In modern technology, micromixers are applied in microtechnologies such as biological systems, as microreactors for chemical reactions, and as MEMS and lab-on-a-chip devices [5]. Micromixing process is extremely slow since it is purely dictated by passive molecular diffusions due to the laminar nature of the fluid flow within the microfluidic channels, as a result of the small dimensions of the channels and slow flow rate of the fluids within the channels [6].

For purely diffusive microfluidic mixing, the species need to diffuse across the entire channel to achieve homogenous mixing [7]. In micromixers, splitting reactant fluids into small fluid segments is a method to reduce diffusion length and thus enhance mixing performance [8]. Lee and Choi [9] reported that mixing in the passive micromixer occurs with the diffusion of molecules in the microsystem and the process is very slow. Complex geometry or long microchannels should thus be used for efficient mixing. At high Reynolds numbers (typically > 2400), two fluids can readily be mixed by turbulence. In microchannels with cross-sections less than one millimeter, this becomes difficult to achieve [10,11]. The Reynolds number for liquids flowing in these microchannels is very small (typically <10). At such low Reynolds numbers, turbulent mixing does not occur and homogenization of the solution occurs through diffusion processes alone [12]. In a typical microfluidic device, viscosity dominates flow [13] and microfluidic mixing is limited to diffusion due to the laminar nature of microflows [14,15].

Different mixing principles and micromixer designs have been reported in order to enhance fluid mixing within the microchannel [16,17]).

As mentioned in chapter 1, mixing strategies can be classified as either active or passive, depending on the operational of mechanism. Since high electric field, mechanical shearing, or generation of heat involved the active mixing, the active techniques are not suitable to employ in applications involving sensitive species (e.g. biological system). To avoid the above problems, passive micromixing are exploited. Kim et al. [18] as well as Cortes-Quiroz et al. [19] demonstrated that mixing in a passive micromixer can be improved by modifying the geometry.

In this research passive micromixing are considered that can be broadly sub-classified into designs based on SAR process (lamination), rotation, injection and droplet techniques.

2.2.1 SAR process

Split and recombine (or SAR) process in the micromixers rely on the concept of repeated inter-layering of multiple parallel streams in order to increase the interfacial area of the two species, also called the lamination.

Parallel lamination and sequential (serial) lamination are two established methods used to reduce the mixing path in passive micromixers, as shows in Figure 2.1.

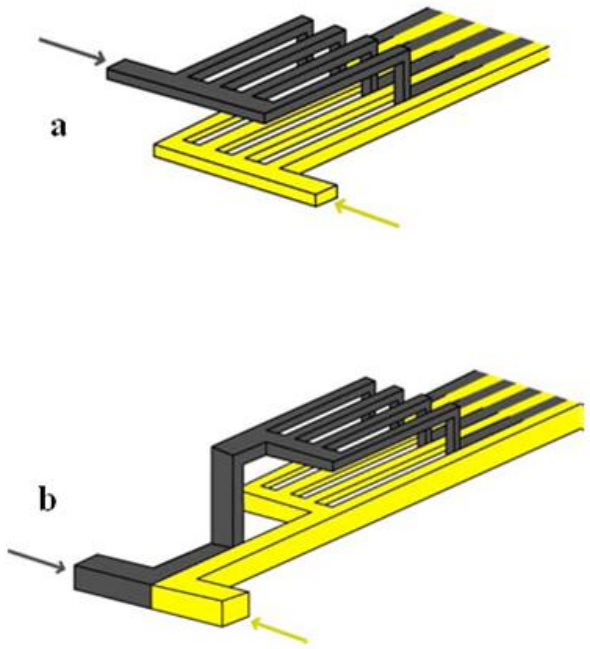

Figure 2.1 SAR process (a) parallel lamination (b)sequential lamination.

Parallel lamination is achieved by splitting the species into sub streams and then joining them in a mixing channel, while sequential lamination is achieved by pushing the fluid through a certain channel geometry. Although molecular diffusion is still the main mixing mechanism.
As indicate in 1.7.3, the diffusion coefficient is a material constant and cannot be improved.

2.2.2 Injection

Injection-type micromixers are similar to parallel lamination, except that only one of the inlet flow is split into multiple layers and then injected into the flowing stream. In fact, arrays of the micro-nozzles are used to inject one fluid on top of the other to increase diffusing mixing.

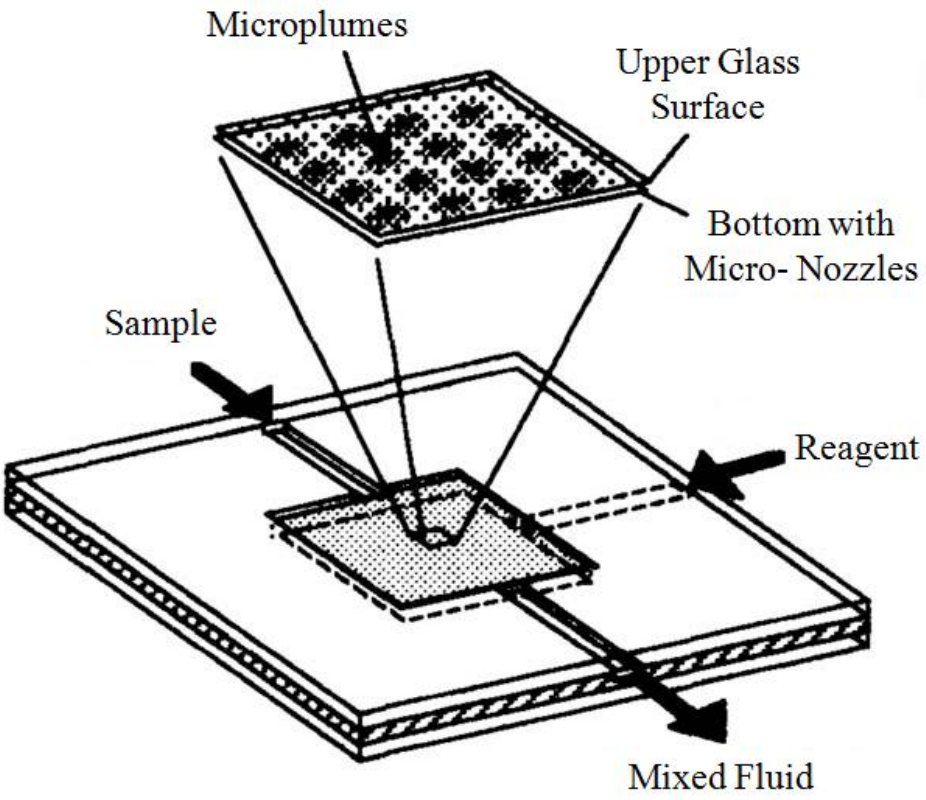

Figure 2.2 Injection-type Micromixer.

The mixing is first filled with one sample and the second fluid is injected directly into the first fluid via micro-nozzles, as shown in Figure 2.2.

2.2.3 Droplet

To overcome complexities associated with fabrication of 3D structure, micromixers based on droplet mixing suggested. Fluid elements trapped in droplets get rapidly intermixed because of the attendance of an internal flow field which is the characteristic of motive droplets.

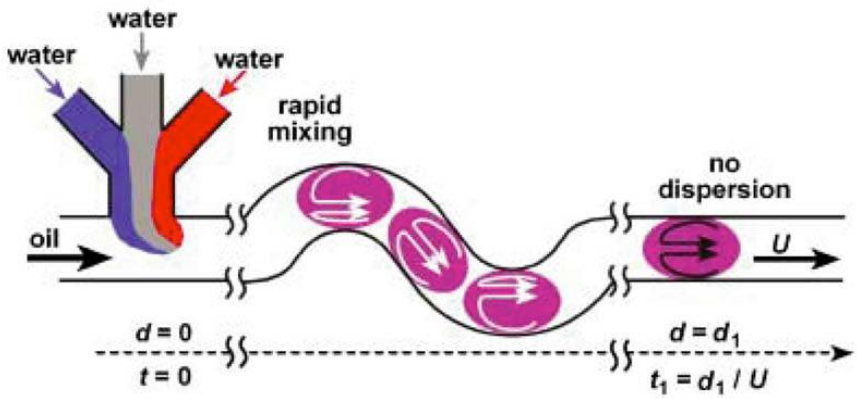

Figure 2.3 Droplet-based Micromixer.

In droplet-based micromixer, furthermore liquids can be mixed by recirculation that is associated with the gas phase that forms a segmented gas-liquid slug flow. An impediment of this technique is that since immiscible liquids are needed to generate droplets, an additional separation step would be required if the mixed elements inside the droplet are to be extracted.

2.2.4 Rotation

Passive rotation mixers are designed to generate transverse flows across the channel cross-section. Grooves, ridges, projections, obstacle and barrier are examples of features that are patterned inside channels to induce disturbances to the flow. As an example of rotation technique, connected groove and staggered herringbone groove micromixers are illustrated.

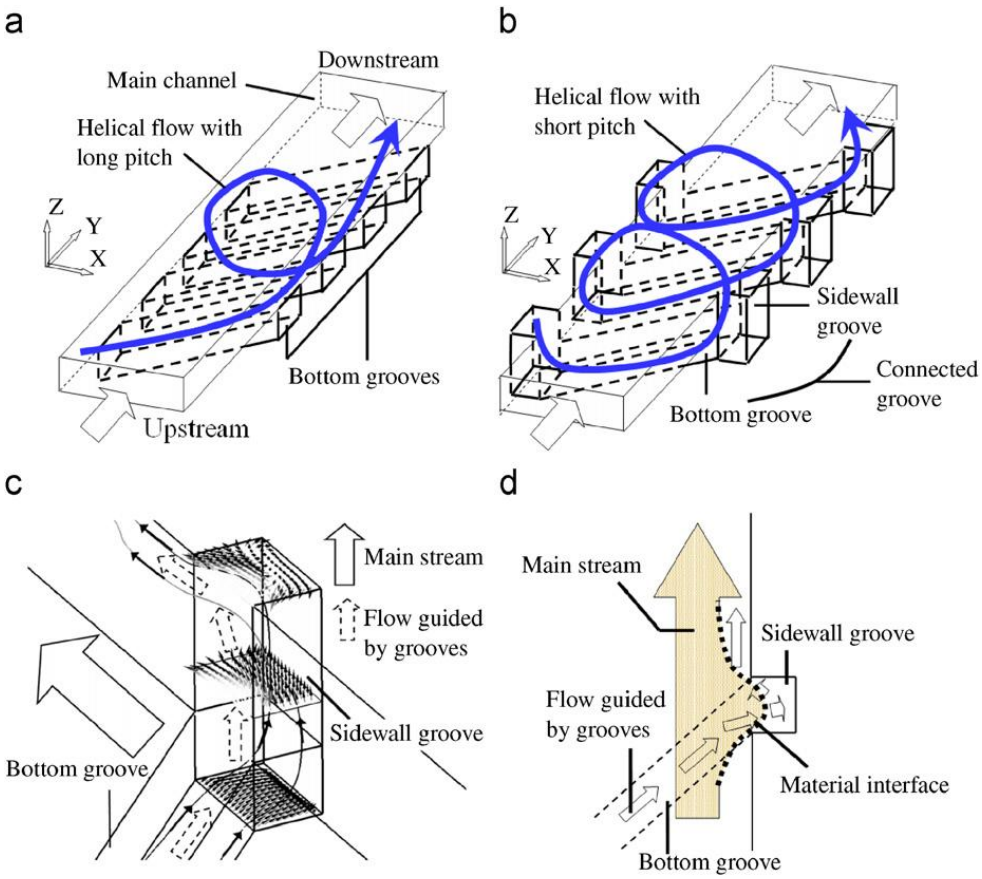

Figure 2.3 Schematic of the connected groove concept.[20]

In general, a patterned-groove micromixer mainly utilizes the grooves on a single side of a channel to generate transverse components and thereby to enlarge the fluidic interface to increase the degree of mixing. Through the aid of the grooves on a single side (for instance, bottom grooves), fluid is

guided to transfer onto the bottom of the main channel and then to undergo a relatively weak helical motion, as depicted in figure 2.3.

Figure 2.4 illustrates the staggered herringbone groove micromixer. As could be seen, the herringbone induces transverse rotation to the flow and repeatedly stretches and folds fluid elements across the cross-section as depicted below the channel schematic figure 2.4. The asymmetric nature of the herringbone varies the centre of transverse rotation.

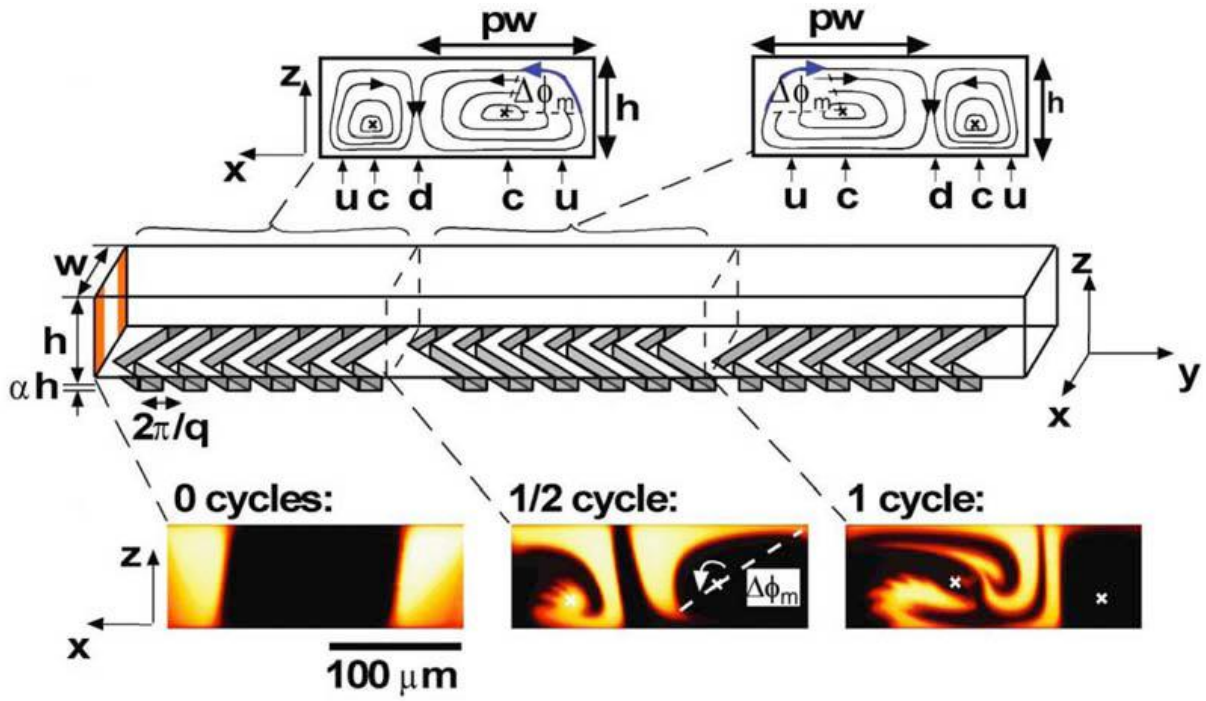

Figure 2.4 Staggered herringbone groove micromixer.

As mentioned above, some techniques of the passive mixing are introduced and examined for enhancing the efficiency of the passive micromixers. In the next sections, experimental equipments and image-based technique are considered which is necessary to obtain the experimental data and analyzing them. In this research the Reynolds number range is $0.083 \leq Re \leq 4.166$.

2.3 Experimental equipments

The experimental equipments used for this investigation are:

1. Syringe Pump
2. Injection Syringe
3. Transparent Tube (inlet and outlet)
4. Microscope
5. Micromixer

These devices and materials are explained and shown separately in this section.

2.3.1 Syringe Pump

The syringe pump used in this study is a KDS 210 series.

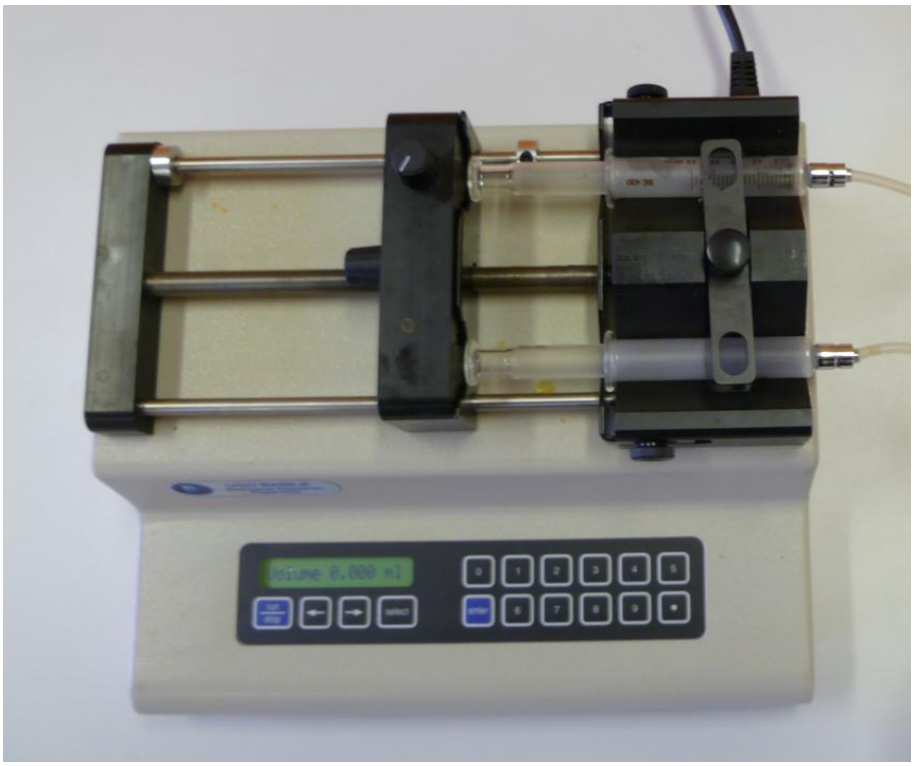

Figure 2.5 Syringe pump KDS 210.

Features for KDS 210 Seri are :

- Holds two syringe
- Backlit LCD display
- Knob locks / unlocks drive block for effortless, drag-free adjustment
- Simple menu-driven setup:
    - select syringe size from display table
    - dispense volume
    - dispense flow rates
- Continuous dispense volume display
- Preset volume control and automatic shut-off
- Setting can be reviewed or changed during operation
- Stall detection

- Choice of unit selection
- Built-in RS232C interface for computer ‘’daisy chaining’’ up to 100 pumps

The flow rate range for this instrument is from 0.1 µl/hr (10µl syringe) to 506 ml/hr (60 ml syringe) with errors less than 1% . In all tests, The mass flow rates of the mixing species are controlled by means of this programmable syringe pump (KDS 210 Series, KD Scientific).

2.3.2 Microscope

The microscope used during the mixing process is a Veho model VMS-004D-400x USB microscope, with 400X magnification, 2 Megapixel Cmos lens (interpolated) and measurement software.

Figure 2.6 Microscope.

The VMS-004D-400x USB microscope provides many uses from laboratory research and comes with integrated snapshot and recording functions. Offering some characteristics such as fine slider adjustment for brightness and hue are too important for analyzing the experimental data.

Features for Veho VMS-004D-400x are :

- Adjustable LEDs for object illumination
- 2Mp CMOS sensor (interpolated)
- Measurement function using enclosed software
- Snapshot and video recording function
- With a base zoom level 20x, the VMS-004 can also magnify 400x

- Fine slider adjustment for brightness, hue, saturation and sharpness, plus a black and white display mode
- The lens can be adjusted to point in any direction using the moveable arm
- Simply install the drivers, plug the microscope into the computer via USB

Due to mentioned characteristics, this model are used in this research.

2.4 Test bench

The test bench layout used for this experimental investigation is shown in figure 2.7.

Device	Description
1	Syringe pump
2	Injection syringe 1
3	Injection syringe 2
4	Transparent tube of syringe 1
5	Transparent tube of syringe 2
6	Micromixer
7	Microscope
8	Outlet tube

Figure 2.7 Test bench layout.

Experimental tests were performed using a microscope with high speed image acquisition. Colored water was used as mixing species in all tests; specifically, blue and yellow solutions were produced by blending 1 gram powder in 0.5 liter water.

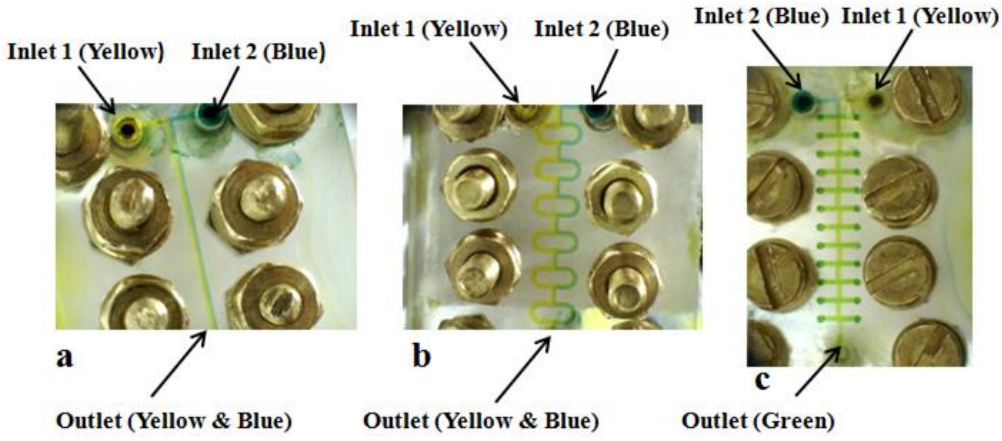

Figure 2.8 colored images during experimental test (a) T-micromixers (b) O-micromixer (c)H-micromixer.

Figure 2.8 illustrated the colored image during the experiments. Within the mixing process, several pictures were taken with the microscope from the entrance area to the end of the channel. This was repeated for all Reynolds numbers used in this study.

2.5 Flow visualization and mixing characterization

All flow and mixing experiments were performed using aqueous system. Two different imaging mechanism exist to analyzing the data : (a) Top-view imaging and (b) Cross-sectional imaging.

2.5.1 Top-view imaging

In the Top-view imaging mechanism, digital images of the flow were obtained using a microscope's Cmos lens provide bit depth of 8 interfaced with a digital camera (Veho model VMS-004D-400x). This technique was used for imaging parallel aqueous streams labelled with blue and yellow dyes. Flow rates were controlled using syringe pump (KDS 210 Series, KD Scientific). The devices were interfaced with the syringe pump and syringes interfaced with the micromixer with transparent tubes. It is very important to ensure a sealed connection in all parts of the test bench.

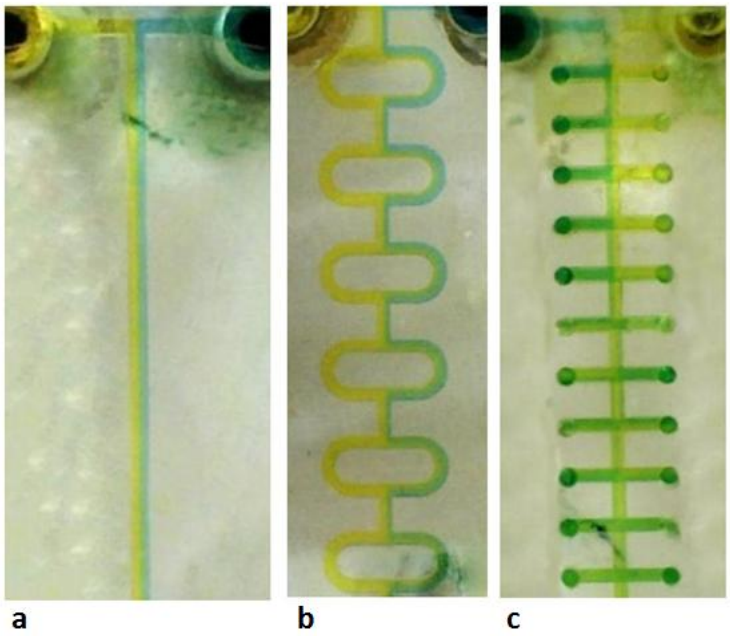

Figure 2.9 Micromixers after filling : (a) T-micromixers (b) O-micromixer (c)H-micromixer.

The extent of mixing in microchannels was determined by the amount of green color which was generated when the blue and yellow streams mixed in the microchannel. The colored images were

imported to Adobe Photoshop 12.0 where the green color was filtered out and the images converted to gray-scale images (figure 2.10) .

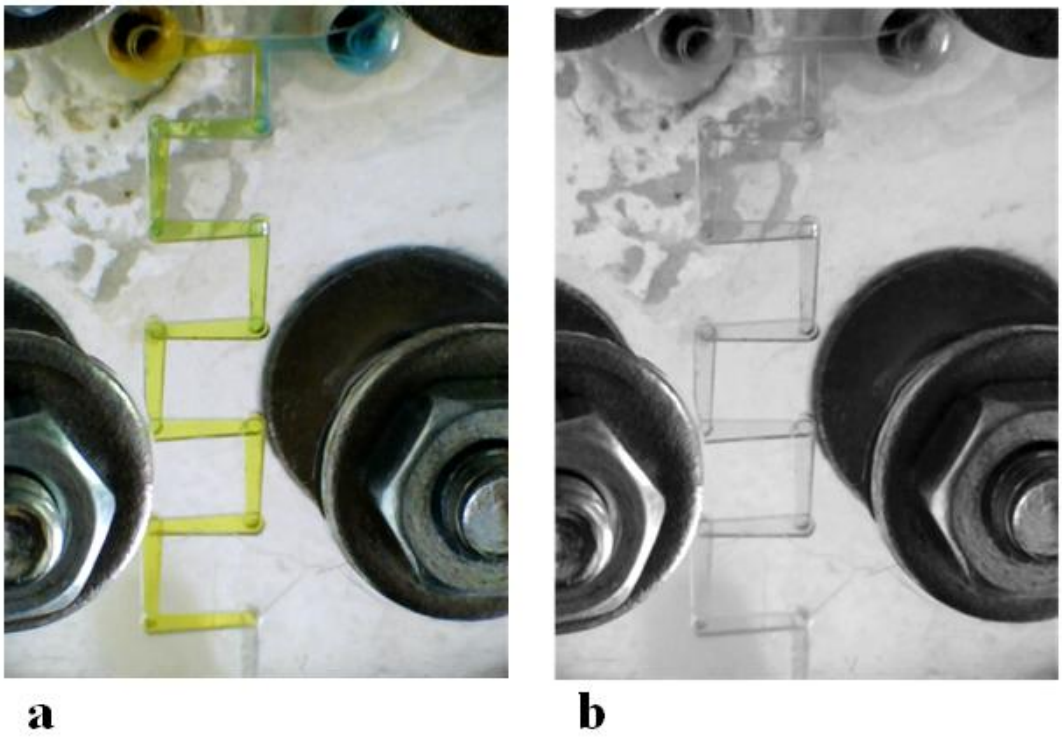

Figure 2.10 Image processing (a) colored image (b) gray-scale image.

Then efficiency of mixing could be calculated that will explain in chapter 3. In this thesis this method are used for analyzing the experimental data.

2.5.2 Cross-sectional imaging

Cross-sectional images of flow in the microchannels were obtained by using a confocal scanning microscopes. Flow images of two aqueous streams, one of which was labelled with fluorescent Rhodamine were obtained.

Mixing efficiency is quantified by computing the standard deviation of the intensity distribution over each images.

$$\sigma = (I - \bar{I})^2 \qquad (2.1)$$

Where I is the grayscale value of each pixel (scaled between 0 and 1) and $\bar{I}$ denotes an average over all the pixels in the image.

Figure 2.11 Cross-sectional Imaging using a confocal microscope.

As was the case with the Top-view imaging, a syringe pump interfaced with the micromixers is used to control the flow rate during the experiments. A typical cross-sectional image from confocal laser scanning is depicted in figure 2.12.

Figure 2.12 Typical Cross-sectional image obtained from confocal laser scanning.

2.6 Image sensors

Characterization of micromixers require accurate measurement of the intensity field, which is equivalent to the concentration field. Furthermore the requirements for the light source and the optical system discussed before, the optical detector should be offer good properties, such as linearity, dynamic range and sensitively.

Currently, two types of high resolution solid state imaging device are available : charged-coupled devices (CCDs) and complementary metal oxide semiconductor (CMOS) image sensors [21]. Both imaging sensors were developed between the early and late 1970s, but CMOS sensors have only gained attention since the early 1990s due to the advances in CMOS technology. Both CCD and CMOS sensors detect light based on the photoelectric effect, where photon interact with silicon to move electrons from the valence band into the conduction band. These electrons are called photoelectrons. The number of photoelectrons generated is a function of the wavelength and the light intensity [21]. Photoelectrons are collected in a potential well until the exposure period is completed. These charges are then either converted into a voltage in CMOS sensors or transferred

to a register in a CCD sensors. The sensors pixel is photodiode. The pixels are typically organized in an orthogonal matrix ranging from 128*128 pixels to a more common 1280*1024 pixels. Both CCD and CMOS sensors are black and white devices, responding a sequential series of red, green and blue filters.

The quantum efficiency η is defined as equation 2.2 .

$$\eta = \frac{N_{pe}}{N_p} \qquad (2.2)$$

Where the N_{pe} is the number of generated photoelectrons and N_p is the number of arriving photons. An ideal detector should have 100% quantum efficiency and zero sensor noise. A CCD sensors has a typical quantum efficiency in the range of 30% to 50%. Special CCD sensors with thinned back illuminated CCD arrays may have a quantum efficiency up to 80%. Figure 2.13 illustrates the schematic concept of a CCD image sensor and its external circuit.

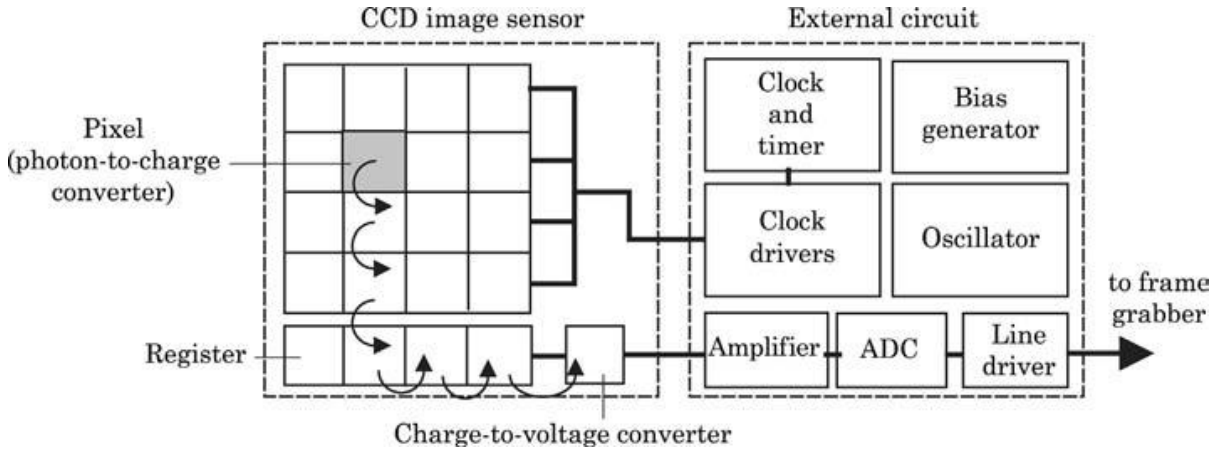

Figure 2.13 Schematic concept of CCD image sensor and the external circuit. [21]

The dark current is caused by thermally-generated electrons. this current leads to noise in the detected signal. Thus, noise will be minimized if the temperature of the sensing material is reduced. Noise level can be significantly decreased using cooling methods such as a liquid nitrogen or thermoelectric cooling. The special resolution of a CCD sensor is determined by the sensor width, height, and its pixel size. All CCD chips have defects, which are regions either with reduced sensitivity or with increased dark current. CCD sensors are graded according to the number of defects. In a CMOS image sensor, each pixel has its own charge-to-voltage conversion. Voltage amplifiers, noise correction, and analog-to-digital converters are integrated in a single chip.

Figure 2.14 shows the schematic concept of a CMOS image sensor and its external circuit

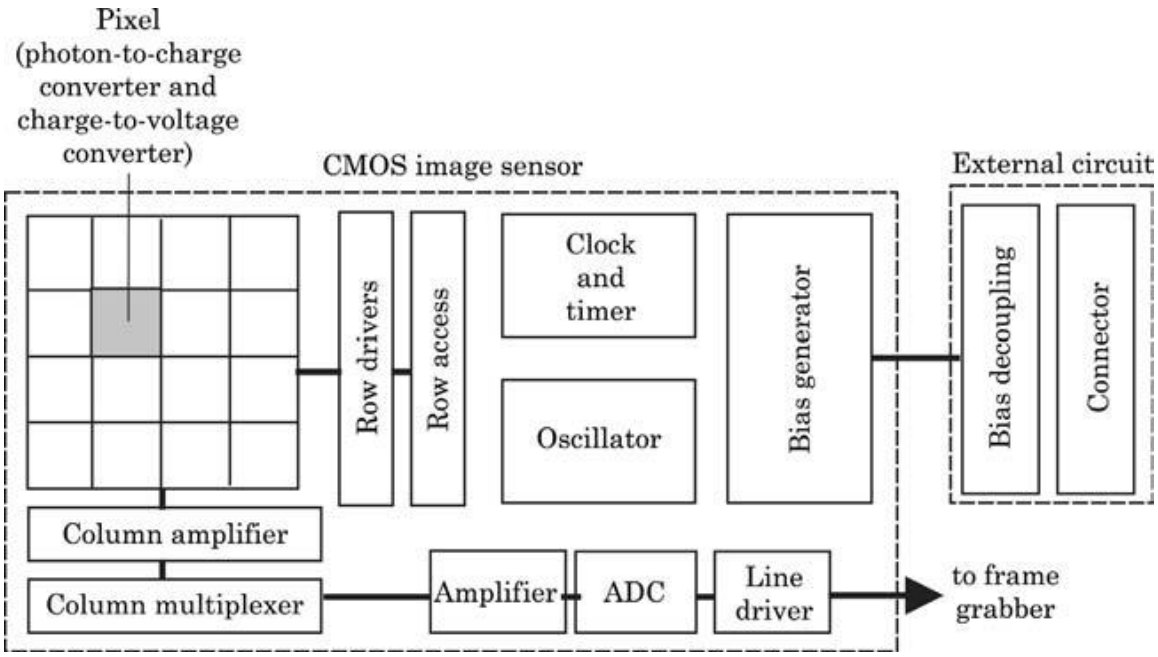

Figure 2.14 Schematic concept of CMOS image sensor and the external circuit. [21]

Because CMOS technologies are available at low cost, CMOS image sensors can be fabricated at a lower cost than a CCD image sensor. The ratio between the sensing surface area and the total pixel area is called the fill factor. The fill factor for a CMOS image sensor ranges from 30% to 80%. Also a CMOS image sensor uses digital signal processing (DSP) to reduce or eliminate the noise.

2.7 Digital images

An image captured with an optical instrument is continuously varying array of shades and color tones. Images capture on films for instance are referred to as continuous –tone because the shade and hues blend together without disruption. Continuous-tone images are captured with analog optical and electronic devices. Optical signals are converted to analog electrical signals or to continuous change of the chemical properties. In the world of digital system, this continuous –tone images need to be converted to digital format and continuous –tones of an analog image are divided into individual intensity value. Similar to the analog-to-digital converting process in electronics, the conversion to a digital image requires two steps : sampling and quantization [21]. With the pixel array, sampling and quantization occur in a CCD or CMOS image sensor automatically. Each pixel contains specific information about intensity and can be described by a specific digital data value in a precise location. Each image pixel is represented by the intensity value and a coordinate-pair with specific *x* and *y* values arranged in a Cartesian coordinate system. In many situation, the *x* location

is referred to as the pixel number, and the *y* location is known as the line number. In the literature the aspect ratio of a digital image defined as the ratio between the width and the height of the image M/N . For instance the recommended NTSC (National Television System Committee) commercial broadcast standard aspect ratio for television and video equipment is $M/N = 4/3$ while for digital high-definition television (HDTV) is $M/N = 16/9$. The image resolution determines the quality of a digital image and referred to as special resolution and gray scale resolution. The special resolution is determined by the number of pixels *M*N* . Within a given physical dimensions, a digital image with a higher number of pixels will have a higher special resolution. The gray scale resolution is directly proportional to the bit depth of the digital device which be described in section 2.8.

2.8 Gray scale image

In photography a gray scale digital image is an image in which the value of each pixel is a single sample that carries only intensity information. Image of this sort, also known as black- and-white, are composed exclusively of shade of gray, varying from black at the weakest and white at the strongest [22].

Gray scale images are distinct from one-bit bi-tonal black-and-white images, which in the context of computer imaging are images with only the two colors black and white also called binary images or monochromatic, denoting the presence of only mono color (chrome). grayscale images are often the result of measuring the intensity of light at each pixel in a single band of the electromagnetic spectrum and can be synthesizes from a full color image. The intensity of a pixel is expressed within a given range between a minimum and maximum (that is applied in the program Matlab code for calibration of the program). This range is represented in an abstract was as a range from 0 (black) and 1 (white), with any fractional in between. Another convention is to employ percentage, so the scale is then from 0% to 100%. This range is used for a more intuitive approach. In computing, although the gray scale can be computed through rational numbers, image pixels are stored in binary, quantized form. Some early gray scale monitors can only show up to 16 (2^4, with a camera with bit depth of 4) shades, but today grayscale images intended for visual display are commonly stored with 8 bit per sampled pixel, which allows 256 (2^8) different intensities. A bit depth of n can generate 2^n different gray scales. Recently, most common CCD and CMOS sensors provide bit depth of 8, 10 or 12 that can describe 256,1024 and 4096 different gray levels respectively. If the image depicted in figure 2.15 has a bit depth of 8, the value of the white pixel (1,1) is 255 , while the value of the black pixel (6,6) is 0. The human eye can better discriminate between different shades of color than between varying shades of gray.

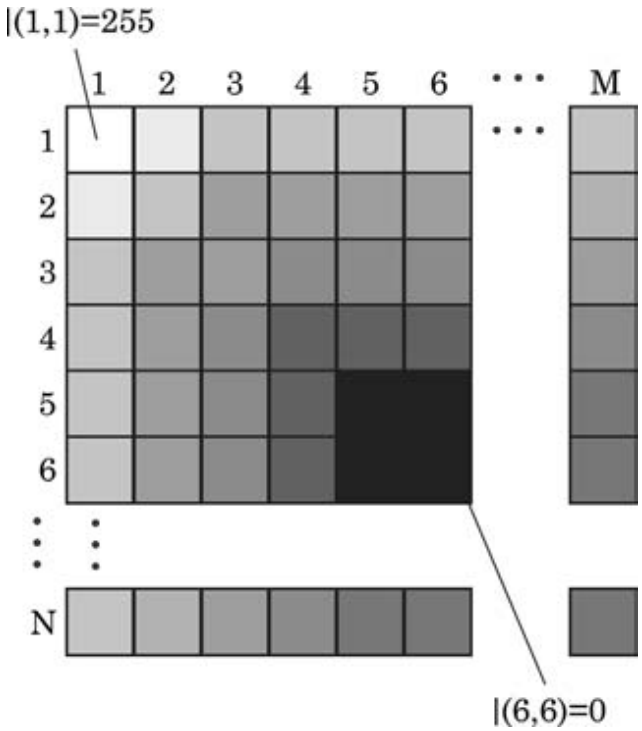

*Figure 2.15 Schematic representation of the intensity array of a M*N digital image.* [21]

Therefore, gray scale images are often rendered in pseudocolor by assigning specific gray level ranges to particular color values. This technique is useful for highlighting regions of interest, especially concentration fields in micromixers [21].

The intensity of the pixels in a digital image can be graphically illustrated in a gray scale histogram, which maps the number of pixels at each gray level present in the image. The histogram can be used directly for evaluating the extent of mixing.

As illustrated in figure 2.16, the histogram of a not mixed concentration field shows two intensity peaks corresponding to the two liquids (figure 2.16 a) while the gray scale histogram of a well-mixed concentration shows a single peak (figure 2.16 b).

A digital image can be stored in a single file. Intensity values are stored in a single vector. Also the horizontal and vertical dimension of an image is stored in a header of the image. Reading the files with known dimension can restore the two-dimensional matrix for further processing. The size of a digital image file depends on the pixel dimension format and bit depth of the image. Uncompressed file format, such as tagged image file format (TIFF) results in the largest file sizes. In this thesis TIFF format are used for analyzing the captured images to import to the Matlab program.

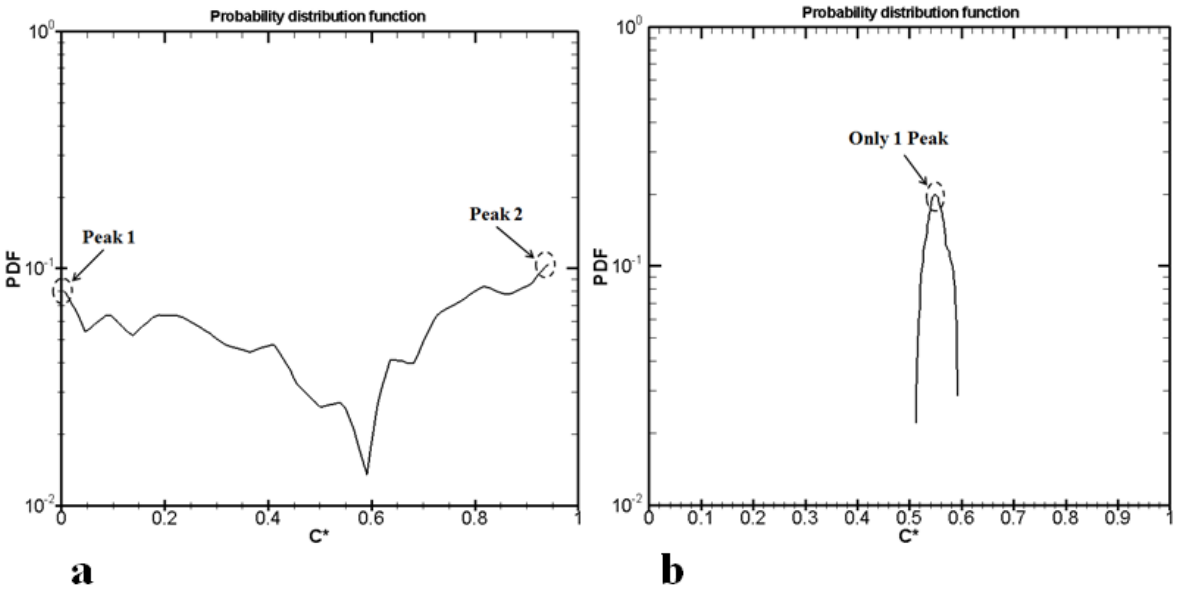

Figure 2.16 Probability distribution function of : (a) a not-mixed region (b) a well-mixed region.

Using compression algorithms, such as the popular joint photographic expert group (JPEG) technique, can reduce the file size significantly, while the image quality is reasonably maintained.

2.9 Experimental procedure

Experimental tests were performed using a microscope with high speed image acquisition. Colored water was used as mixing species in all tests; specifically, blue and yellow solutions were produced by blending 1 gram powder in 0.5 liter water. The mass flow rates of the mixing species are controlled by means of a programmable syringe pump (KDS 210 Series, KD Scientific).

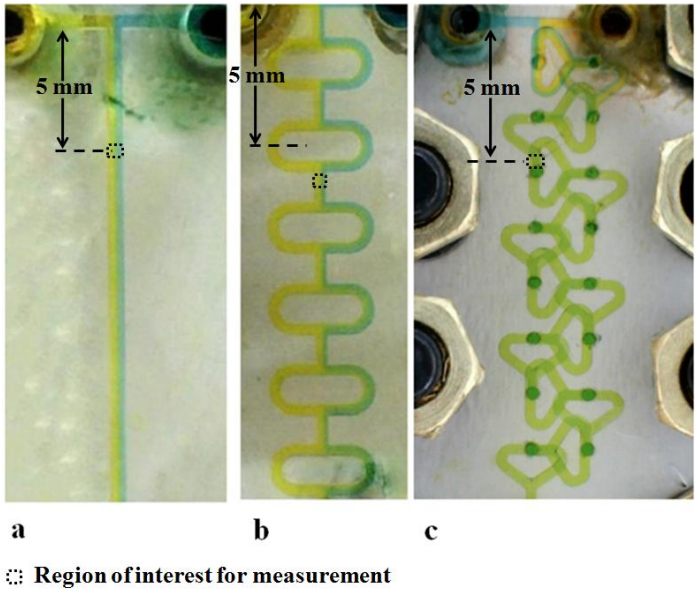

Figure 2.17 Colored image of micromixers after filling: (a) T-micromixer (b) O-micromixer (c) Tear-drop micromixer.

A kind of color image that used in this study are shown in figure 2.17. During the mixing process, several pictures were taken with the microscope from the entrance area to the end of the channel. This was repeated for all Reynolds numbers and also for all mixers which used in this study. The region of interest for analyzing the micromixers studied in this thesis are shown in figure 2-18.

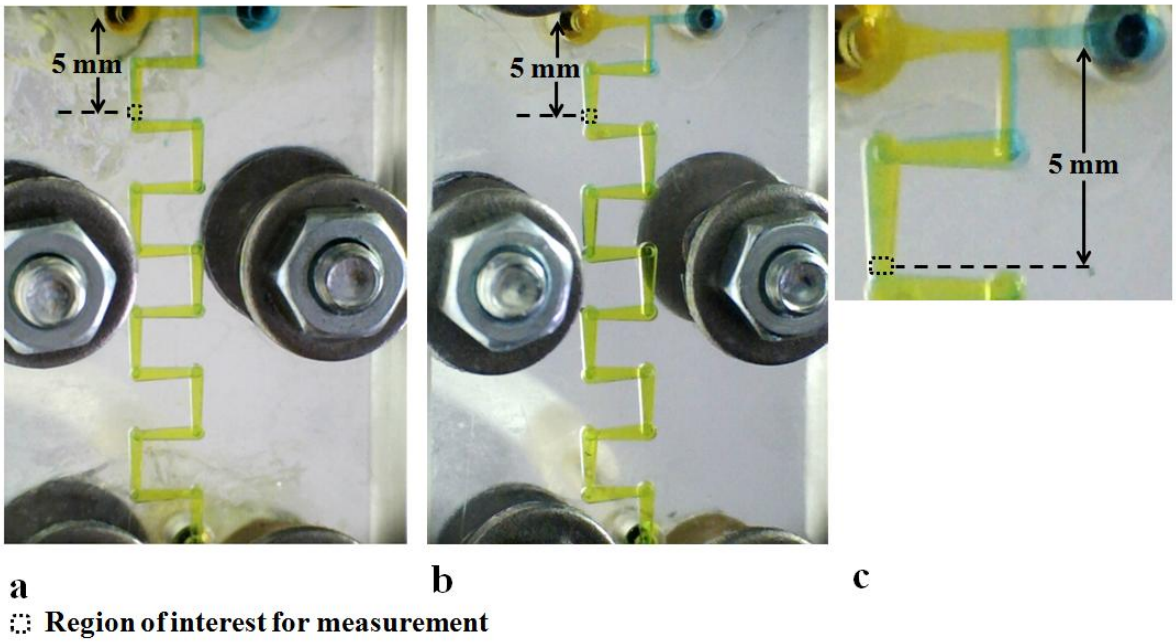

Figure 2.18 Region of interest in Chain Micromixers after filling: (a) Chain 1-micromixer (b) Chain 2-micromixer (c) Chain 2-micromixer, inlet part to 5 mm.

Image-based techniques were used to evaluate the mixing performance of the prototypes, and the gray scale value was applied for post processing. To analyze the image, the captured color images were converted into gray scale images. Conversion of a color image to gray scale is not unique (i.e. writing a program code or using software). To convert any color to gray scale representation of its luminance, first one must obtain the value of its red, green and blue (RGB) primaries in linear intensity encoding. Then add together 30% of the red values, 59% of the green values, and 11% of the blue values. In this study Adobe Photoshop software version 12.0 is applied to convert the colored images to gray-scale images. This technique (gray scale value) is useful for highlighting regions of interest, especially the concentration field in the micromixer [21]. Then post processing of the data are considered that explained in chapter 3.

References

[1] Kim K.W., Hossain S., Ansari M.A., Husain A., 2010. Analysis and optimization of a micromixer with a modified Tesla structure, Chemical Engineering Journal 158, 305-314, doi: 10.1016/j.cej.2010.02.002.

[2] Kumar V., Paraschivoiu M., Nigam K.D.P.,2011. Single-phase flow and mixing in microchannels, Chemical Engineering Science 66, 1329-1373, doi: 10.1016/j.ces.2010.08.016.

[3] Delaure J. A. et. Al, 2007. A novel microfluidic flow-injection analysis device with fluorescence detection for cation sensing. Application to potassium, Anal Bioanal Chem 387, 2627-2632, doi: 10.1007/s00216-007-1132-3.

[4] Chen J.J., Lai Y.R., Tsai R.T., Lin J.D., Wu C.Y., 2011. Crosswise ridge micromixers with split and recombination helical flows, Chemical engineering Science 66, 2164-2176, doi : 10.1016/j.ces.2011.02.022.

[5] Bothe D., Lojewski A., Warnecke H.J., 2011. Fully resolved numerical simulation of reactive mixing in a T-shaped micromixer using parabolised species equations, Chemical Engineering Science,66, 6424-6440, doi: 10.1016/j.ces.2011.08.045.

[6] Zhang Z., Yim C., Lin M., Cao X., 2008. Quantitative characterization of micromixing simulation, Biomicrofluidic 2 034104-1.

[7] Mao X., Juluri B.K., Lapsley M.L., Stratton Z.S., Huang T.J., 2010. Milliseconds microfluidic chaotic bubble mixer, Microfluidic Nanofluidic Journal 8, 139-144, doi:10.1007/s10404-009-0496-4.

[8] Mae K., Aoki N., Umei R., Yoshida A., 2011. Design method for micromixers considering influence of channel confluence and bend on diffusion length, Chemical Engineering Journal 167, 643-650, doi: 10.1016/j.cej.2010.08.084.

[9] Lee S.H., Kang H.J., Choi B., 2009. A study on the novel micromixer with chaotic flows, Microsyst. Technol. 15, 269-277 . doi: 10.1007/s00542-008-0664-6.

[10] Tofteberg T. , Skolimowski M., Andreassen E., Geschke O., 2010. A novel passive micromixer: lamination in a planar channel system, Microfluidic Nanofluidic Journal 8, 209-215. doi:10.1007/s10404-009-0456-z.

[11] Yang J.T., Wang L., Lyu P.C., 2007. An overlapping crisscross micromixer, Chemical Engineering Science 62, 711-720, doi : 10.1016/j.ces.2006.09.048.

[12] Fu L.M., Lin C.H., Chien Y.S., 2004. Microfluidic T-Form Mixer Utilizing Switching Electroosmotic Flow, Analytical Chemistry Journal. 76, 5265-5272, doi:10.1021/ac0494782.

[13] Wang H., Iovenitti P., Harvey E., Masood S., 2003. Numerical investigation of mixing in microchannels with patterned grooves, J. Micromech. Microeng. 13, 801-808.

[14] Sinton D., Coleman J.T., 2005. A sequentional injection microfluidic mixing strategy, Microfluidic Nanofluidic Journal 1, 319-327, doi: 10.1007/s10404-005-0034-y.

[15] Hong C.C., Choi J.W, Ahn C.H., 2004. A novel in-plane passive microfluidic mixer with modified Tesla structures, Miniaturization for chem. Biology & Bioeng., Lab Chip 4, 109-113.

[16] Yang J.T., Haung K.J., Tung K.Y., Hu I.C., Lyu P.C., 2007. A chaotic micromixer modulated by constructive vortex agitation, J. Micromech. Microeng. 17, 2084-2092, doi: 10.1088/0960-1317/17/10/021.

[17] Kwon T.H., Park J.M., Kim D.S., Kang T.G., 2007. Improved serpentine lamination micromixer with enhanced local advection, Microfluidic Nanofluidic Journal, Research Paper, doi :10.1007/s10404-007-0208-x.

[18] Kim K.Y., Hossain S., Ansari M.A., 2009. Evaluation of the mixing performance of three passive micromixers, Chemical Engineering Journal 150, 492-501, doi:10.1016/j.cej.2009.02.033.

[19] Cortes-Quiroz C.A., Zangeneh M., 2008. On multi-objective optimization of geometry of staggered herringbone micromixer, Microfluidic Nanofluidic Journal 7, 29-43, doi:10.1007/s10404-008-0355-8.

[20] Yang J. T., Fang W. F., Tung K. Y., 2008. Fluids mixing in devices with connected-groove channels, Chemical Engineering Science 63, 1871-1881, doi: 10.1016/j.ces.2007.12.027.

[21] Nguyen N.T., 2008. Micromixers: Fundamentals, Design and Fabrication. William Andrew, Norwich, NY, USA.

[22] http://en.wikipedia.org/wiki/Grayscale

Chapter 3

Analyzing Technique and Development of Micromixers

List of symbols

C	Species concentration
C^*	Colored water normalized concentration along Microchannel
$\overline{C^*}$	Expected normalized concentration
d	Hydraulic diameter
D	Diffusion coefficient of the species
H	Height of the microchannel
i	Counter from 1 up to N
L	Length of the microchannel
N	Number of the points defined by the probability distribution function in terms of concentration
P	Pressure
Q_m	Mass flow rate
Q_v	Volume flow rate
Re	Reynolds number
V	Average velocity
$\vec{V}$	Average velocity
W	Width of the microchannel

Greek letters

σ	Standard deviation of the concentration
η	Mixing efficiency
μ	Viscosity
τ	Shear stress
ρ	Density

Abbreviations

MEMS Micro Electro Mechanical System

MI Mixing Index

PDF Probability Distribution Function

3.1 Introduction

Imaging techniques and optical microscopy is the key tool for characterization micromixers. Optical microscopy offers a fine measurement at the micro scale that is useful for analyzing the micromixers. As mentioned before, together with digital cameras and digital image processing, a number of measurements in microchannels can be carried out with optical microscopy. Optical microscopy works with the part of the electromagnetic spectrum which is visible to human eyes. A typical human eyes responds to wavelengths in air from 400 to 700 nm [1]. The corresponding wavelengths in other media are reduced by a factor of refractive index. A human eye has maximum sensitivity about 555 nm, which is the green region.

The understanding of physical phenomena , such as flow behavior and mass transfer of the microfluidic devices is needed in order to develop these microsystems for industrial applications [2]. Different researchers apply various techniques in microscale. Huchet et al. [3] used electrodiffusion technique to measure local value of wall shear rate. While Chen et al. [4] proposed the fluorescent resonant-energy transfer (FRET) to analyze the performance of the microreactors.

As alluded before it is a complicated task to achieve a high level of mixing inside a microchannel because of the flow characterized by low Reynolds number (*Re*) [5,6]. Park et al. [7] introduced serpentine lamination micromixer (SLM) and reported that this F-shape micromixer enhance the mixing performance by combination of splitting/recombination and chaotic advection.

Mixing in microfluidic systems starts almost from regular periodical concentration profiles with steep gradient, which is governed by molecular diffusion proceeding in deformed fluid elements [8] and grows during the microchannel length. In order to quantitatively evaluate the degree of mixing some techniques reported by researchers [9]. For determination of the degree of mixing at different position in the SAR mixer, a photometric technique was used by Hardt et al. [10]. Zolgharni et al. [11] explained that a quantitative criterion to characterize the efficiency of the micromixer is so-called ‘’ discrete intensity of segregation’’ which is extracted from statistical parameters. They reported that intensity of segregation is the variance of the concentration distribution.

Chen and Shie [12] reported that in the design of any micromixer, one of the most important performance parameters is a measure of mixing intensity. They quantified the mixing intensity by calculating the mass concentration distribution and described that the uniformity of mixing at sampled section is assessed by determining the mixing index (MI) .

Cook et al. [13] employed induced fluorescence to obtain quantitative data in terms of concentration distribution within the scaled micromixer channels.

Aoki et al. [14] evaluated mixing performance of the microchannels using parallel-competitive redox and neutralization reactions called the Villermaux/Dushman reaction. The reactions occur by mixing two reactant fluids. One is a solution of diluted strong acid (referred as solution 1), and the other is a buffer solution (mixture of weak acid and strong base) containing KI and KIO_3 (redox reagents). Then, they used the UV light absorbance at 352 nm as a measure of mixing performance. They sampled mixed solutions and measured the absorbance of the solutions with a UV-Vis spectrometer.

Suh et al. [15] expressed that the easiest method for judging the mixing efficiency in micromixer structures is by flow visualization, which is done using dilution-type experiments and also notified that to quantitatively represent the composition uniformity, the coefficient of variation, COV, which is the ratio of the standard deviation of each cross section σ, to the mean of each cross section has used. Also they quantitatively characterized the mixing efficiency of electro-kinetic micromixer by defining the mixing index (MI).

Fang and Yang [16] studied based on a concept encompassing splitting and recombination (SAR) and chaotic advection in a novel microreactor with 3D rotating flow. They used a methods to assess the mixing performance of a micro device involve blending of dye liquors (food dye and fluorescent dye) and the reaction of chemical indicators to approach to the reaction length. They reported that a reaction length assessed based on an analysis of the gray scale intensity of image captured via image processing. They calculated the average intensity of all pixels from a sampling image. The sampling image was determined on trimming the captured images and the average intensity of the sampled images extracted in sequence from upstream to downstream was normalized to get the normalized intensity which expresses the efficiency.

Also Lee et al. [17] studied on rotation effect in split and recombination micromixing and in order to quantify the degree of mixing in micromixers, a standard deviation (Stdev.) of the distribution of intensity values (I) for the image data was calculated, when black is 0 and white is 255. These values were obtained by the image process using 8 bit depth lens.

Jeong et al. [18] reported that the mixing performance could be evaluated by two different methods. The first method was to focus on the upper part to measure how fast the fluorescent dye, which was

initially located at the lower region of the microchannel, disseminated to the upper region. The other was to focus on the lower part to evaluate how fast the fluorescent dye located in the lower region disappeared. They found that the second method more suitable for mixing strategy and therefore adopted it to estimate the mixing performance.

Hardt et al. [19] studied based on passive micromixers for applications in the microreactor and expressed that a typical scenario encountered in μTAS is the mixing of liquid samples at small Reynolds (*Re*) numbers (*Re* <10). Also they reported that analyzing the data using both CFD methods and photometric techniques, allowing to quantify the progress of mixing.

Sheu et al. [20] surveyed the mixing of a split and recombine micromixer with tapered curved microchannels. For evaluating the degree of mixing, they used the standard deviation of the concentration on a cross-section normal to the flow direction and introduced the normalize standard deviation is the average value of the concentration over the sampled section and then reported that the uniformity of mixing at sampled sections is assessed by determining the mixing index of the solute concentration.

As mentioned above, because measurement of intensity distribution is important for quantitative characterization of micromixers, the quality of the illuminating system is important for the microscope setup. The illuminating system of a research grade microscope should fulfill three basic criteria of :

- Allowing maximum resolution and maximum contrast
- Being simple and easy to adjustment
- Having uniform illumination.

The most illumination source of modern microscopes is a laser. The laser light produces an output beams that is both coherent and collimated, which is ideal for illumination purposes.

3.2 Measurement of concentration field by fluorescent dye

The intensity of a fluorescent dye solution is proportional to the concentration of the dye molecules. Thus, the concentration field can be measured indirectly as the intensity field of fluorescent dye. For evaluating the digital image using concentration field of a fluorescent dye, some functions are needed. These functions are available in the Image Processing Toolbox of Matlab (Mathwork, Inc). Then the image can be displayed in the default 256 gray level, and as shown in figure 3.1, there is a high level of noise, especially in the area with high intensity.

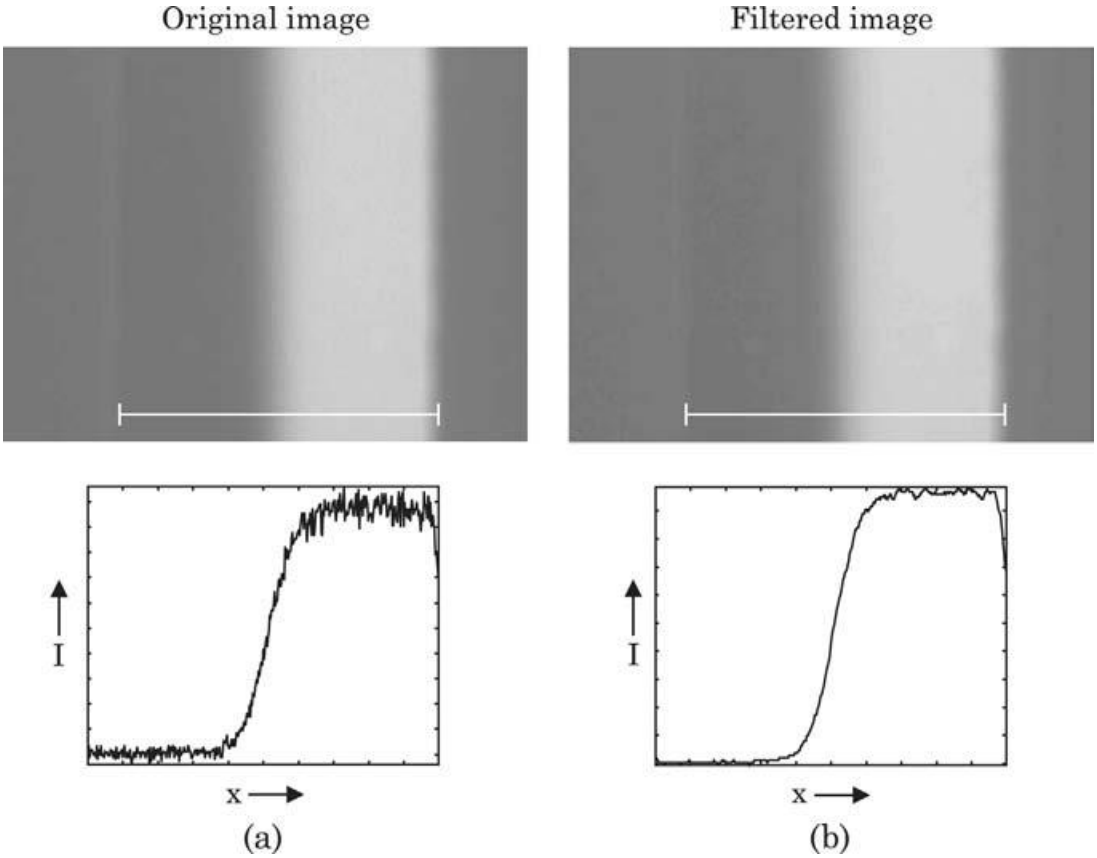

Figure 3.1 Intensity images: (a)original; (b) filtered. [1]

To reduce the noise, spacial filtering can be applied to each point of the intensity array. spacial filtering is implemented in the following step:

- Defining the processed point
- Applying the filtering algorithm to a window around the point
- Repeating the process for all points of the intensity array.

Depending on the kind of the filtering algorithm, linear and nonlinear spacial filtering is available. Matlab provides ‘’imfilter’’ and ‘’fspacial’’ for filtering and selecting he algorithm respectively. For instance, one of the effective noise cancelling filtering algorithm is Wiener filtering [1]. Applying Wiener filtering is useful for the original intensity array (*I*) and a processing window of 5*5 pixels.

3.3 Quantification methods for micromixers

3.3.1 Indirect methods

Indirect methods measure the extent of mixing based on the products of chemical reactions or change in fluorescent dye to a change of PH level in the mixed fluids.

To evaluate the degree of mixing parallel competing reaction can be used. For example, when a mixture of iodate, iodine, sodium hydroxide and boric acid is mixed with sulfuric acid, the so-called Dushman reaction occurs:

$$H^2BO_3^- + H^+ \leftrightarrow H_3BO_3$$
$$5I^- + IO_3^- + 6H^+ \leftrightarrow 3I_2 + 3H_2O \qquad (3.1)$$
$$I^- + I_2 \leftrightarrow I_3^-$$

As alluded in the introduction, the first reaction is a neutralization, which is very fast compared to the second reaction. If mixing is well-done, there is no acid left for the second reaction to form iodine. In fact, the amount of iodine produce depends on the efficiency of mixing process. The concentration of I_3^- in the mixing products indicates the degree of mixing. The concentration of I_3^- in the mixing measured via the absorbance at 353 nm. Using this method , the mixing efficiency can be determined as :

$$\eta_{mixing} = \frac{ABS}{ABS_\infty} \qquad (3.2)$$

Where ABS is the result of the absorbance measurement and ABS_∞ is the absorbance of the fully mixed solution. The disadvantage of this technique is that the absorbance measurement would normally need to be carried out off the chip and also integration of fiber optics for on-chip measurement would be expensive. characterizing of the microchannel is still in challenge due to the two dimensional nature of fluorescent measurement with a camera – microscope system. Using mixing index and PDF are based on statistical evaluation the fluorescent dye and these methods are useful for analyzing the image during the microchannel, as depicted in figure 3.2. For considering the concentration distribution along the microchannel, measurement would only be possible with the more expensive laser scanning confocal system. Munson and Yager [21] suggested a fluorescent detection techniques based on the PH sensitivity of a fluorophore. Two species are mixed with an equal concentration (10 µm) of fluorescein. They only differ in the PH levels. Then they used a equation 3.3 to evaluate the mixing efficiency.

$$\eta = \frac{I - I_0}{I_\infty - I_0} \qquad (3.3)$$

Where the I_0 is the average intensity measured across the both fluids at the inlet, I_∞ the fully mixed solution and I is the averaged intensity of the region of interest.

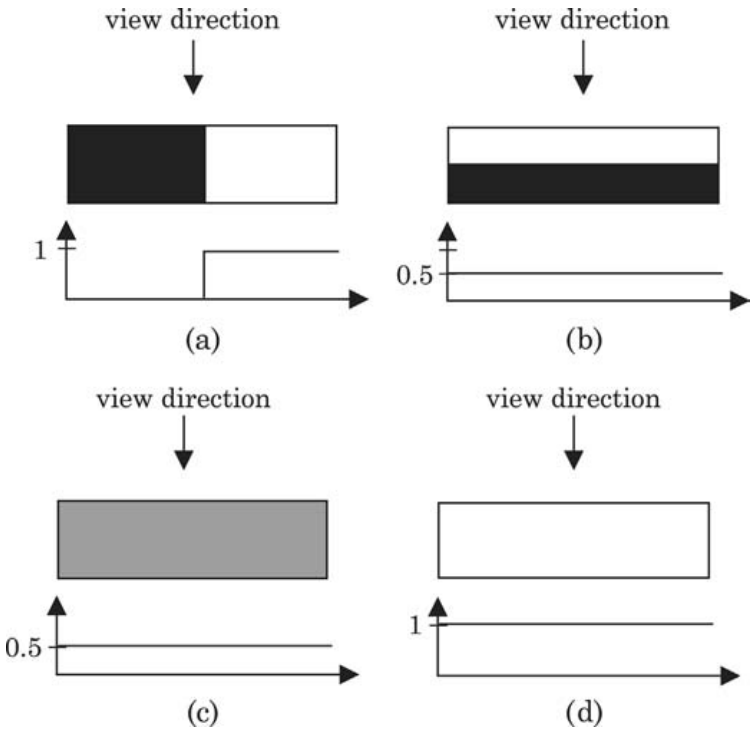

Figure 3.2 Mixing evaluation using fluorescent dye: (a) before mixing, view direction parallel to fluid interface; (b) before mixing, view direction perpendicular to fluid interface; (c) results of mixing, using conventional fluorescent technique; (d) results of mixing, using fluorescent technique based on PH sensitivity.[1]

3.3.2 Direct statistical methods

As far as we know, there are several quantification methods for analyzing the micromixers. In this thesis, direct statistical method is used to analyze the micromixers. Because good mixing is understood as the homogeneity of the mixed result, the distribution of the concentration (or distribution of the intensity) values of an image can be used for evaluating the degree of mixing. The gray scale histogram actually represent the probability distribution function (PDF) of the concentration[1]. The probability values can be obtained by normalizing the pixel number of each concentration value by the total number of the pixels in the evaluated regions.

In this method, the region of interest is selected by a mouse click as a rectangle in the displayed image as shown in figure 3.3 . Subsequently, probabilities for the concentration values are calculated and plotted.

For evaluating the efficiency of mixing, in the first stage it is needed to calculate the standard deviation (variance) of the concentration in the diagram of PDF in terms of concentration using equation 3.4

$$\sigma = \sqrt{\frac{1}{N}\sum_{i=1}^{N}(C_i^* - \bar{C}^*)^2 * PDF_i} \qquad (3.4)$$

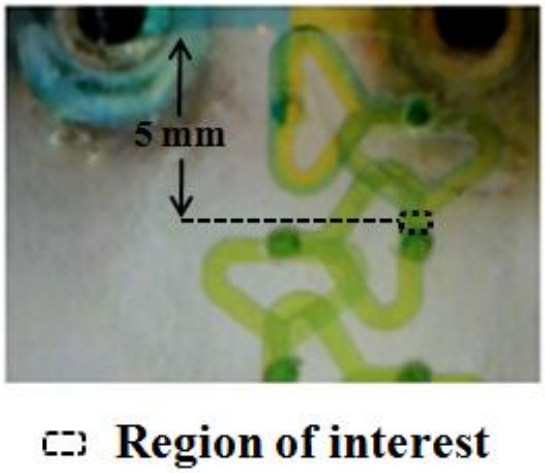

Figure 3.3 Selecting the region of interest for analyzing in Tear-drop micromixer.

As an example, figure 3.4 depicted the probability distribution function in Tear-drop micromixer in two regions, entrance region and end region of the microchannel.

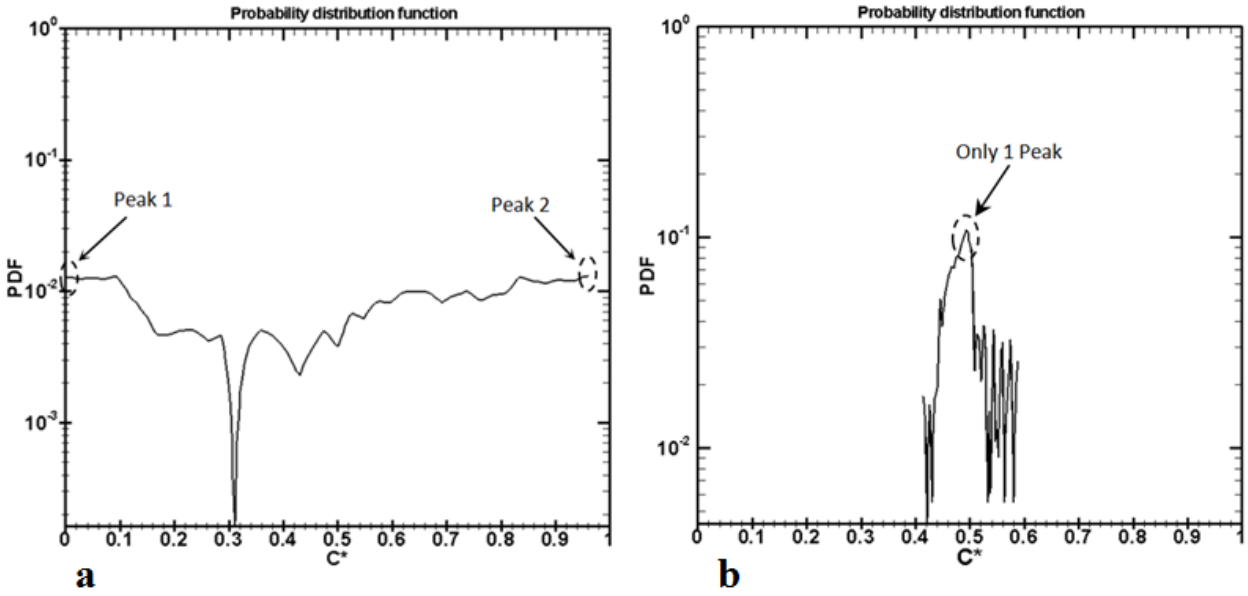

Figure 3.4 PDF in Tear-drop micromixer at Re=1.666: (a) entrance region (b) after 20 mm.

The homogeneity can be expressed as the standard deviation of the concentration and can be calculated using equation 3.4, where C^* is the normalized concentration and $\overline{C^*}$ is the expected normalized concentration.

To evaluate the standard deviation of concentration, mixing index and efficiency of the prototypes, three kinds of Matlab M-file code were written (PDF1, PDF2 and Efficiency). Data was analyzed using the following procedure:

1. Converting the color image to gray scale image
2. Calibrating the program by using PDF 1

   The microscope's Cmos lens provide bit depth of 8 and an 8-bit depth describes 256 (2^8) different gray levels. If the species are black and white, the gray level varies from 0 to 255 respectively and there is no need to calibrate the program which show that concentration varies from 0 to 1 in the PDF diagram . Since the species are yellow and blue, gray level does not vary from 0 to 255 and gray level range reduces (for example: between 45 and 210). Hence, it does need to be calibrate that concentration varies from 0 to 1in the PDF diagram. For this purpose, in the program code we put for example 45 (instead of 0) as a minimum value and 210 (instead of 255) as a maximum value.
3. Evaluating the concentration by using PDF 2 (PDF 2 to evaluate the concentration)
4. Evaluating the standard deviation of concentration
5. Evaluating the Mixing Index (MI)
6. Evaluating the mixing efficiency

The two species are not mixed in the entrance region of the micromixers, where there are two predominant concentration values resulting in two separate peaks as shown in figure 3.4 (a). In a region of well-mixed fluids, there is one predominant concentration that this point depends on the color of the mixing process that can be seen as the best issue , resulting in a single peak as illustrated in figure 3.4 (b).

The standard deviation can be normalized again by the mean concentration to evaluate the mixing index (MI) :

$$MI = \sqrt{\frac{1}{N}\sum_{i=1}^{N}\left(\frac{C_i^* - \bar{C}^*}{\bar{C}^*}\right)^2 * PDF_i} \qquad (3.5)$$

The mixing indexes (*MI*) are 1 and 0 for the unmixed case and well-mixed case, respectively.
Mixing efficiency can be defined through equation 3.6 :

$$\eta = 1 - MI = 1 - \sqrt{\frac{1}{N}\sum_{i=1}^{N}\left(\frac{C_i^* - \bar{C}^*}{\bar{C}^*}\right)^2 * PDF_i} \qquad (3.6)$$

As shown in Figure 3.5, analysis of the experimental data indicates that at the starting point where two fluids join together, the standard deviation is high, mixing index is 1 and efficiency is 0%.

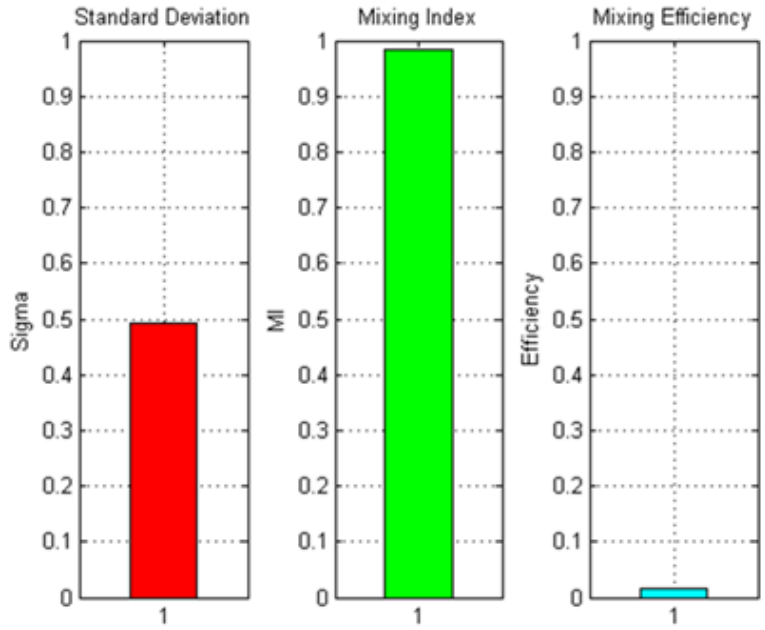

Figure 3.5 ***σ***, ***MI*** *and* ***η*** *in Tear-drop micromixer, Re = 1.666, inlet section.*

The experimental results demonstrate that efficiency is 98% at the end section of the Tear-drop mixer under certain conditions. Figure 3.6 shows σ, MI and η at the same Reynolds number of 1.666, where efficiency is 98%. These processes continue for Reynolds numbers of 0.083, 0.416, 0.832 and 4.166 for the Tear-drop prototype.

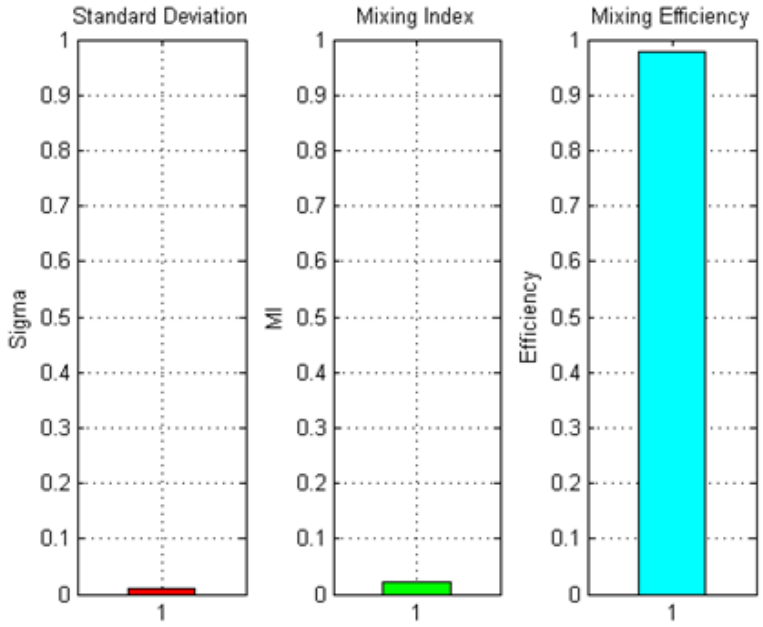

Figure 3.6 ***σ***, ***MI*** *and* ***η*** *in Tear-drop micromixer, Re = 1.666, after 20 mm.*

Referring to equation 3.6, it is found that mixing efficiency is 1 (or 100%) if the two fluids are fully mixed. An efficiency between 80% and 100% is acceptable for mixing process applications [1].
By the knowledge that mentioned above, the flow chart of the post processing for analyzing the micromixer can be plotted :

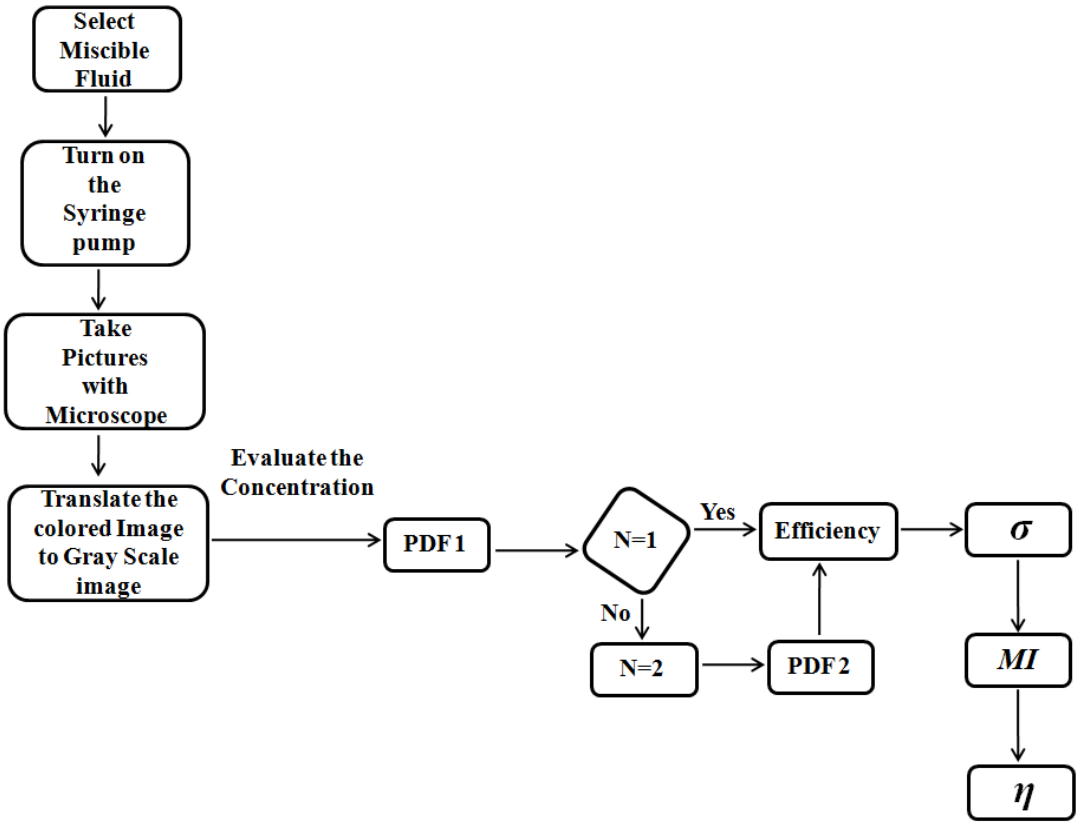

Figure 3.6 Flow chart for experimental analyzing.

In this thesis, this method is used to analyze the concentration along the microchannel.

3.4 Details of Experiments

In this study, the effects of geometry and various Reynolds numbers on flow field and mixing characteristic along the microchannels are examined and mixing efficiencies are compared with previous well-known micromixers. The corresponding flow average velocity and Reynolds numbers that used in this investigations, are shown in table 3.1.

Table 3.1 Flow rate , *Re* and velocity values during experimental investigation.

Q_v (ml/min)	Q_m (kg/s)	V (mm/s)	*Re*
0.001	$1.66*10^{-8}$	0. 1	0.083
0.005	$8.31*10^{-8}$	0. 5	0.416
0.01	$1.66*10^{-7}$	1	0.832
0.02	$3.32*10^{-7}$	2	1.666
0.05	$8.32*10^{-7}$	5.2	4.166

As shown in table 3.1, five different flow rates (ml/min) were considered.

Also, the effects of various Reynolds numbers and geometry on pressure drop were examined numerically using CFD code, ANSYS FLUENT-13.0. Henceforth, numerical results for Chain microchannels are compared with well-known basic microchannels.

3.5 T- micromixer

The T-micromixer is illustrated in figure 3.7 [22]. This kind of micromixer was constructed to compare the mixing efficiency of the new microdevice presented in this study. Figure 3.7 shows the T-micromixers which was designed and fabricated from plexiglas using a computer milling process. The prototypes were fabricated in I.T.D S.n.c. di Depaoli S. & C. (Turin, Italy) using CNC Milling and Engraving Machine P20 S, KUNLMANN (Germany). Geometric characterization was constant for all prototypes. Two species flow into the microchannel by means of two entrances.

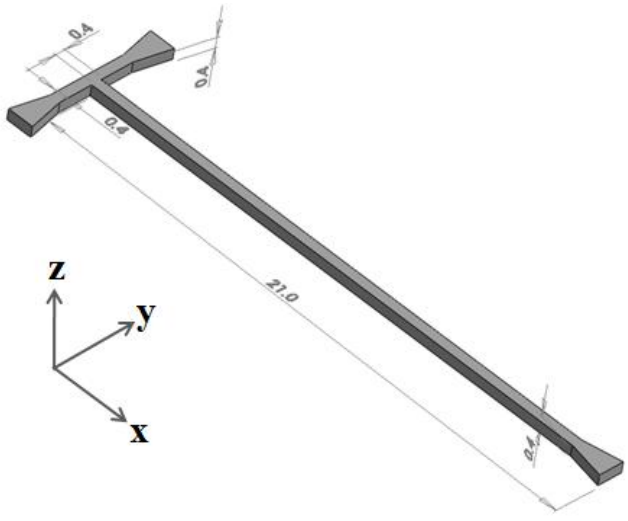

Figure 3.7 Design of T-micromixer.

The T-micromixer is the simplest microfluidic device with rectangular cross section and consists of two inlets with a straight channel. As shown in figure 3.7, there is no special geometry along the microchannel. The geometry consists of a mixing channel with 21 mm length and 0.4 mm width and depth . All results given here refer to a microchannel with mentioned cross section dimensions.

3.6 O- micromixer

Figure 3.8 illustrates the O-mixer [23], whose microchannel is divided into two segments: straight channel and O-segment. Like T-micromixer, O-mixer was designed and fabricated from plexiglas using a computer milling process.

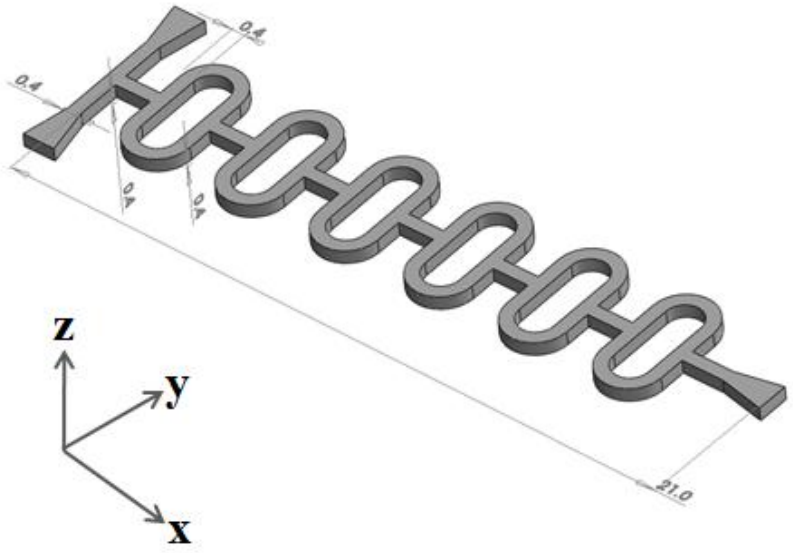

Figure 3.7 Design of O-micromixer.

Two species flow into the microchannel and through the straight section. Subsequently, the stream is divided into two parts and the two streams connect to each other at the end of the O-segment. This splitting and rejoining induce the molecular diffusion effect to enhance mixing efficiency. This process takes place six times along the microchannel.

3.7 Tear-drop micromixer

On the basis of the investigation presented in [24], Tear-drop SAR micromixer was designed and constructed with polycarbonate using a computerized milling process. Tear-drop micromixer design is shown in figure 3.8.

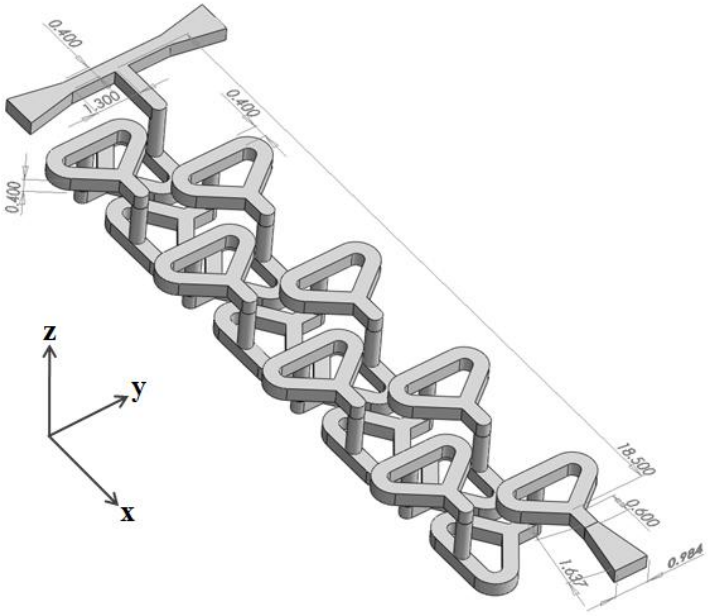

Figure 3.8 Design of Tear-drop micromixer.

Channel width and height are 0.4 mm. As can be seen in figure 3.9, the Tear-drop mixer has a two-layer structure. The modules of the upper layer (yellow color) and lower layer (red color) are connected by simple vertical channels. The inlet to the mixer is designed as a T-junction element (left side of figure).

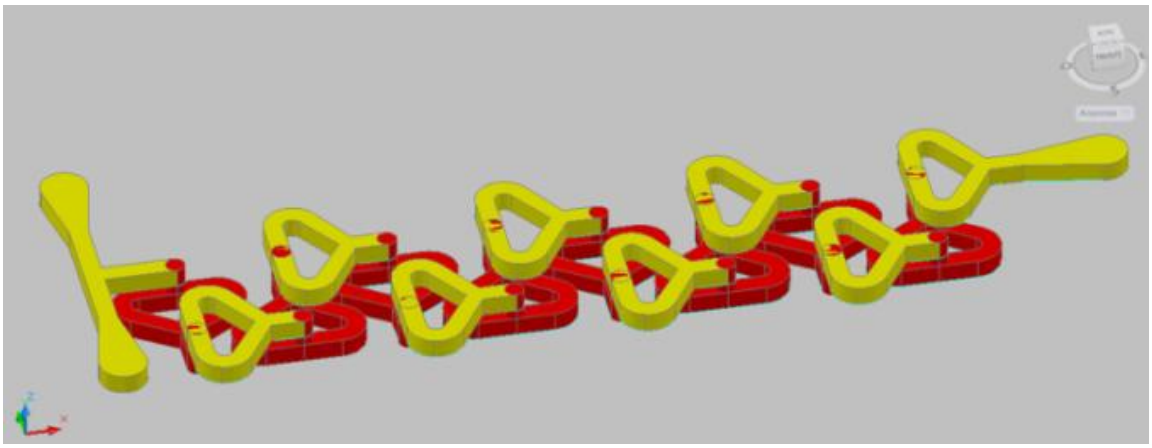

Figure 3.9 Tear-drop micromixer.

Figure 3.10 shows structural details of the Tear-drop micromixer. Two miscible liquids move through the entrance and reach the mixing region of the T-junction element, where they flow along the +X direction. The fluids flow in parallel through the first element. The stream then reaches the

vertical channel (segment 2) and moves in the –Z direction. At the end of the vertical channel, the stream reaches the first Y segment (principal module) and is split into two flows (segment 3).

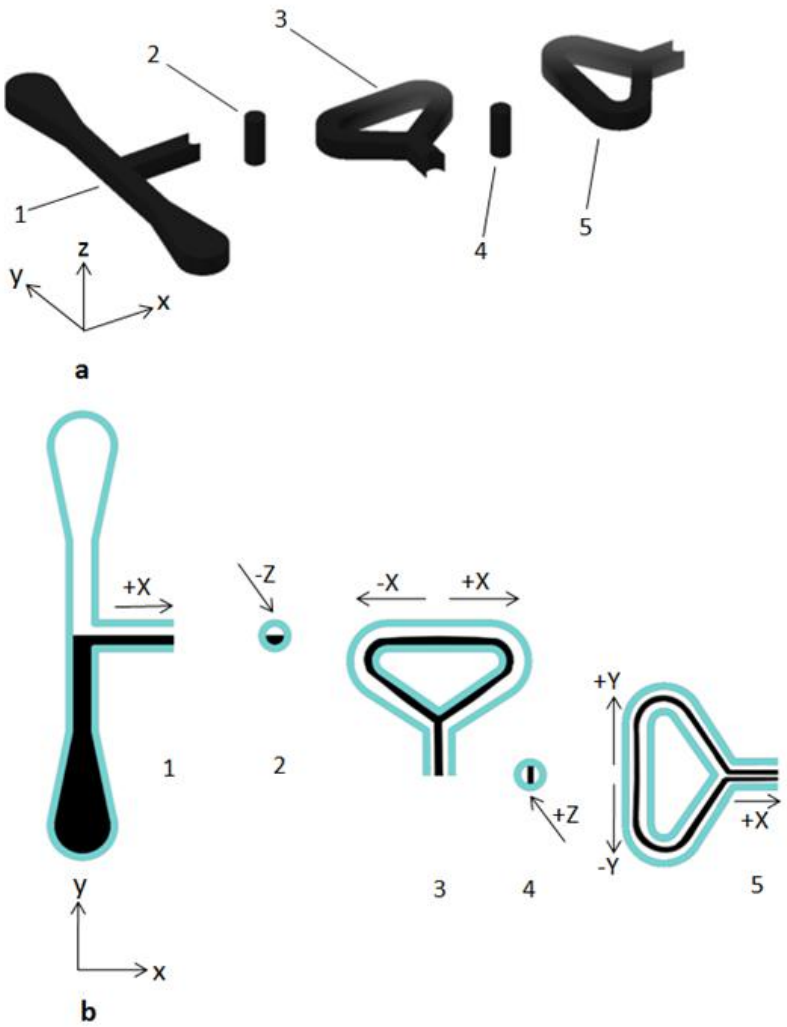

Figure 3.10 Tear-drop structural detail, ; (a) Tear-drop microchannel segments; (b) Sequential lamination of layers.

One stream moves in the +X direction and the other moves in the –X direction. Both flows then cross the Y segment of the principal module, at the end of which they are recombined and move in the –Y direction. Subsequently, the reunited stream reaches the vertical channel and moves in the +Z direction. At the end of the vertical channel, it arrives at the Y segment and is again split into two streams. One stream moves in the +Y direction and the other in the –Y direction, and both then pass through the Y segment. At the end of the Y segment, they are once again recombined and move in the +X direction. This process continues to the end of the mixer microchannels.

Indeed, this method of splitting and recombining the flow provides a way of increasing the number of fluid layers. It is founded that the efficiency of this mixer is high and also the required pressure drop is great.

3.7.1 Sequential lamination

Sequential lamination segregates the joined stream into to channels, and rejoins them at the next transformation stage, figure 3.11.

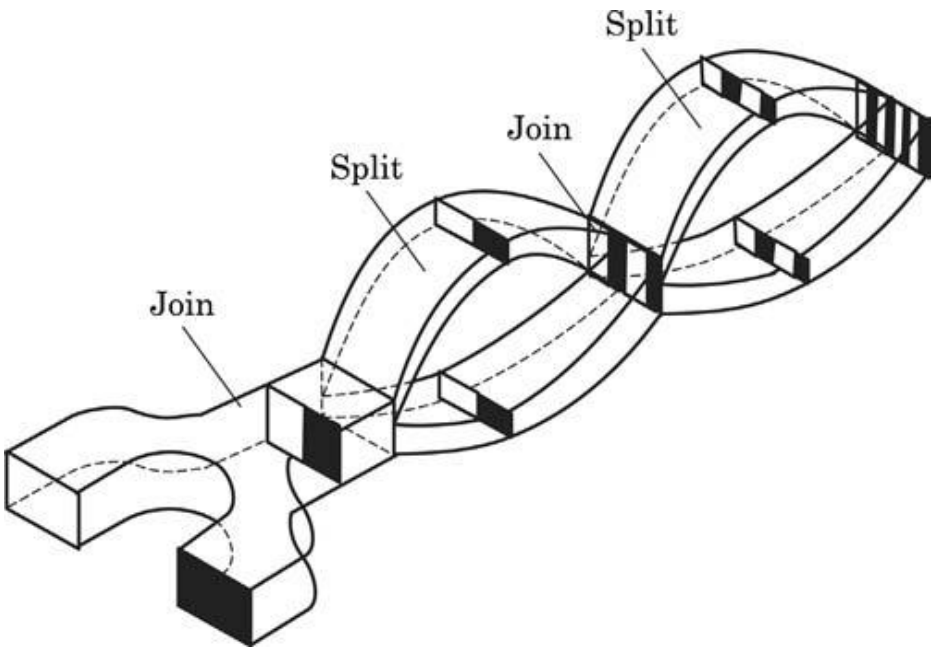

Figure 3.11 concept of sequential lamination.

Because of this characteristic, sequential lamination is called ‘’Split and recombination’’ or ‘’SAR’’ concept. Since SAR process is similar to the stretching and folding of mixing fluids, it is also called the baker’s transformation (or Bernoulli transformation) [1]. The transformation illustrated in figure 3.11 can be achieved either by sequential lamination or by chaotic advection. Sequential lamination can be implemented by forced splitting and recombining or by chaotic advection. Forced splitting and lamination are achieved at low Reynolds numbers with a complex channel design and chaotic advection occurs at a higher Reynolds number. The implementation of the concept depicted in figure 3.11 is referred to as sequential lamination with vertical lamination and horizontal splitting. Similar transformations can be achieved with horizontal lamination and vertical splitting. This mixing concept requires relatively complicate three-dimensional fluidic structures that performed on Chain micromixers (3.9). The sequential lamination concept results in much faster mixing compared to the parallel concept with the same device area. Hence in chain mixer, sequential lamination are used to design and construct a novel generation micromixers.

3.8 H- micromixer

This type of passive micromixer is based on the SAR process meaning that the two fluids to be mixed are split and recombined to optimize the diffusion process. In this case, the H-shape makes it possible to move part of the flow near the wall, in the central zone of the channel along the axial direction and vice versa. The H-micromixer has been designed and constructed from plexiglas using a computer milling process. Design and a photograph of the prototype are shown in figure 3.12.

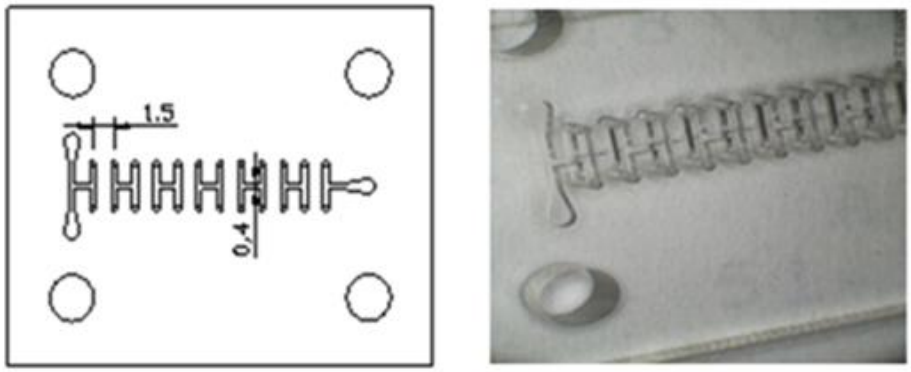

Figure 3.12 H-micromixer.

As illustrated in figure 3.12, the H-micromixer geometry consists of two parts: the straight channel and the H-segment. The flow follows a 3D path. Figure 3.13 shows the 3D path and describes the SAR process: first, two species move in the +X direction, after which the flow reaches the H segment and is split into two flows: one moving in the +Y direction and the other moving in the –Y direction. Both flows then move to –Z. Afterwards, one moves in the +Y direction and the other moves in the –Y direction until the two flows are connected. The reunited flow then moves in the +X direction and the SAR process starts again.

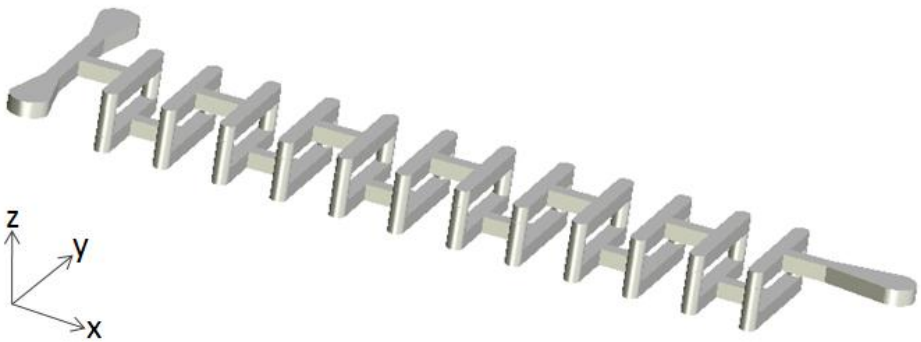

Figure 3.13 H-micromixer design.

This 3D path increases the micromixer's efficiency. In particular, figure 3.14 shows that when the flow is split and recombined, the part of the flow near the wall is moved into the central zone of the channel.

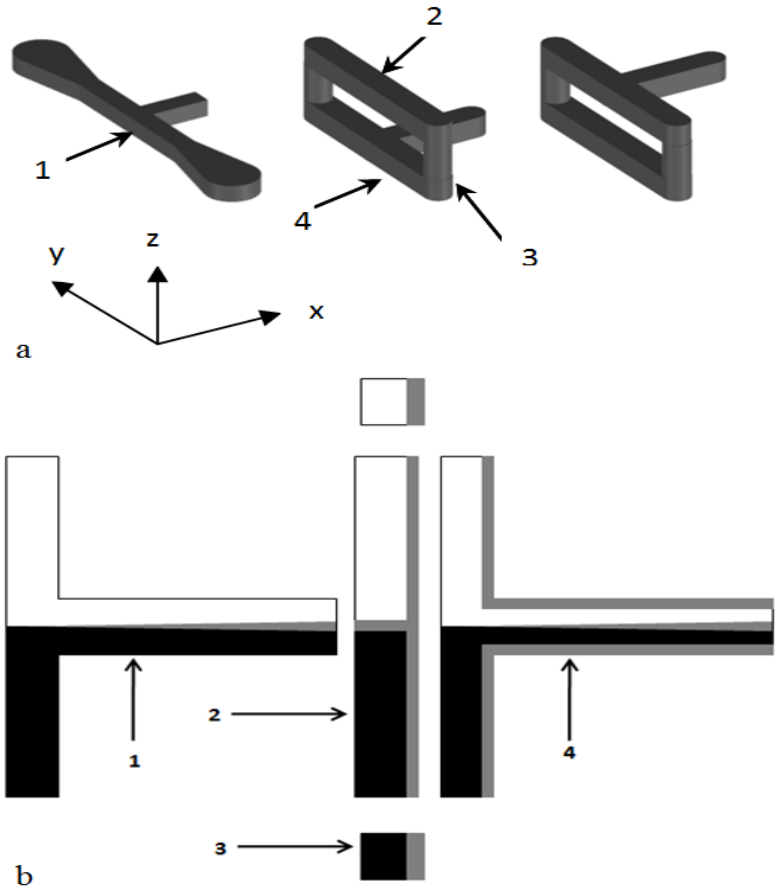

Figure 3.14 Detail of H-micromixer structure: (a) H-microchannel segments, (b) Sequential lamination of layers.

As depicted in segment 1 of figure 3.14, when the two mixing flows (shown in black and white) meet along the entrance microchannel, only the central zone is mixed (shown in grey).

The mixed zone is then moved against a wall and the flow is split into two new flows (one is shown in white and grey and the other is black and grey). The mixed zone (grey) is now near the wall.

When these two flows are recombined again, a new central zone (unmixed) is generated. As occurs in segment 1, the new central zone is then mixed at the end of segment 4.

The stream is thus split into five layers (figure 3.14, part 4) and this process continues to the end of the H-micromixer.

As the SAR process is more effective than molecular diffusion, mixing can be improved significantly. After each splitting and recombining, the number of layers increases.

In this regime (assuming no slip condition, Newtonian fluids and laminar flow), the speed of the flow near the wall is zero and the velocity profile in a channel is approximately parabolic. The shear stress is proportional to the derivative of the velocity profile, and absolute shear stress $\tau = \mu \left|\frac{\partial u}{\partial y}\right|$ is maximum at the wall and zero in the central zone, as shown in figure 3.15.

Because of the SAR process described above, which occurs in every H-segment, the fluid in the central zone with maximum speed (no shear stress) moves to the wall (maximum shear stress) and the speed of this layer drops from maximum to minimum. Conversely, the fluid in the wall zone moves in the central part of the channel. By this means each fluid element of the mixed fluids moves in the mixer channels with a periodically changing velocity and shear stress. In such a situation, the mean velocities of the fluid elements in the mixer are roughly equal. These effects also contribute to increase the mixing efficiency.

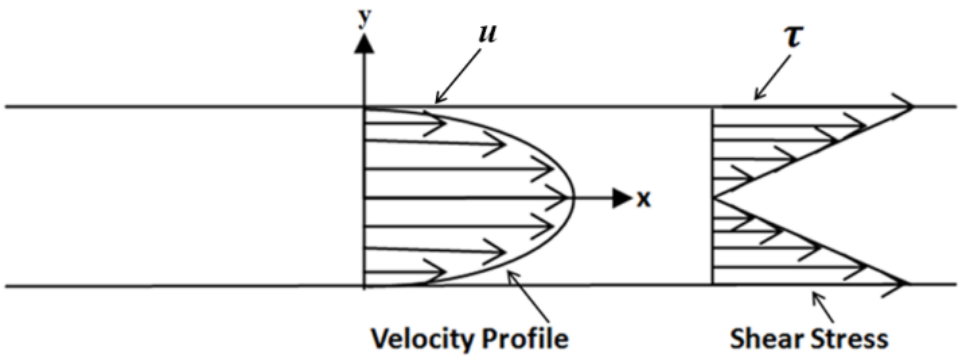

Figure 3.15 Velocity profile and shear stress in laminar flow.

In some cases, the mixed fluid contains particles. It is known that the shear stress gradient turns the particles, which helps increasing mixing efficiency. In the proposed mixer the periodical shifting of the fluid element position assures that fluid elements move through the mixer with a sufficient shear stress gradient.

3.9 Chain micromixer

A novel generation of 3D passive micromixer concept is introduced in this thesis. This type of micromixer called the ‘’Chain micromixer’’ which is based on the SAR process, meaning that the two fluids to be mixed are split and recombined to optimize the diffusion process. The main working principle for this type of microchannel is to make 90º rotation of a flow, folding the stream and then split and recombine the flow to enhance the efficiency of the microchannel. This process is repeated during the microchannel until achieving the desired degree of mixing. In current

study four kind of Chain micromixer were designed, constructed and analyzed and results compared with other micromixers.

3.9.1 Chain 1-micromixer

Chain 1-micromixer was designed and fabricated from plexiglas using a computer milling process. As illustrated in figures 3.16, 3.17, and 3.18, the flow follows a 3D path along the microchannel.

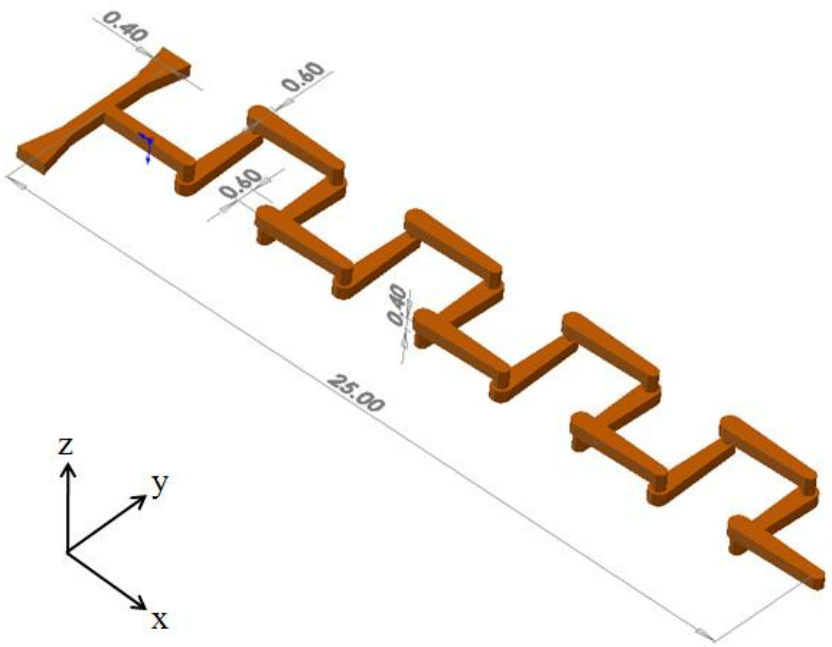

Figure 3.16 design of Chain 1-micromixer.

Figure 3.16 illustrates the Chain 1-micromixer. As shown in figure 3.16, after each vertical part (z direction), the diameter of the new section is 0.6 mm and extended 0.2 mm rather than the outlet of vertical part (0.4 mm).

3.9.1.1 Theoretical background of Chain 1-micromixer

As alluded in previous section (3.9.1), after each vertical part (z direction), the diameter of the new section is 0.6 mm and extended 0.2 mm rather than the outlet of vertical part (0.4 mm). This characteristic of the geometry causes the splitting of the flow in the inlet of new part as depicted in figure 3.17, segments 3,5,7 and 9, and in the central part of the segment the recombination effect takes place. At the outlet of the segment, the diameter is again 0.4 mm like the vertical part (figure

3.17 a, segments 3,5,7 and 9. Indeed, after extension in the inlet, the flow getting constricted while go across these parts and the maximum constriction occurs at the outlet of this section. The maximum width of the microchannel is 0.6 mm and reduces during this part to minimum value of 0.4 mm.

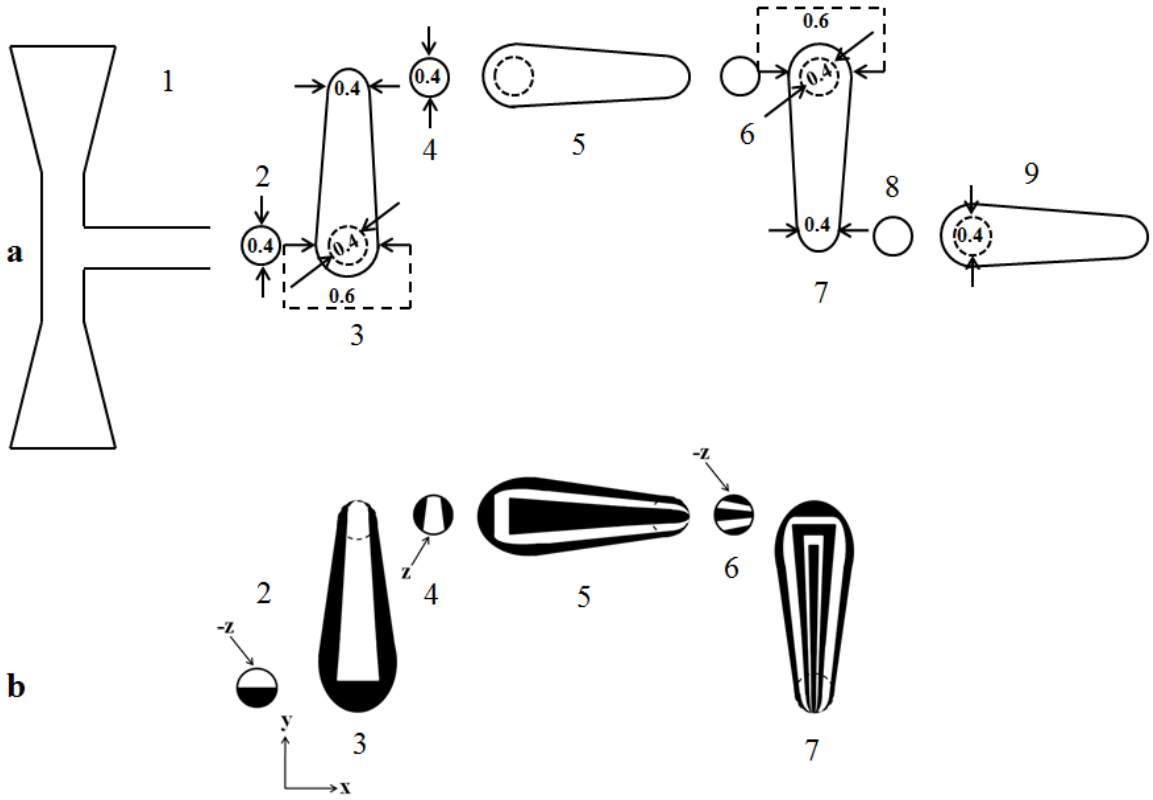

Figure 3.17 structural design of Chain 1-micromixer, ; (a) of Chain 1microchannel segments; (b) Sequential lamination of layers.

As in the case of the Tear-drop micromixer depicted in figure 3.10 b, two mixing flows meet along the entrance microchannel and move along the entrance part until to reach the vertical part. In the vertical part the flow moves in –z direction. At the end of the vertical channel the stream reaches the first chain element.

The black color flow is then moved against a wall and the white color flow is moved to central part of the chain segment (3). In this way the flow is first splitted and then recombined into three layers flow, white and two black flows, as depicted in figure 3.17 b section (4). After reaching to the vertical part, where these layers rotate 90º, in the next mixer segment (5), five layers are created as illustrated in figure 3.17 b part (6). By the same procedure, after segment 7 nine flow layers are formed. This process continues to the end of the Chain-micromixer. In fact, splitting and recombination cause large number of different layers and with increasing the layers, thickness of

the layers will be smaller and the thickness of the poor mixed zone will be shorter and part of this zone moves to other mixed zone and this process proceed. This property enhance the mixing and also result in homogeneity. Therefore with splitting and recombination, mixing can be improved significantly.

3.9.2 Chain 2-micromixer

Figure 3.18 illustrates the Chain 2 mixer which differs only by one parameter from the Chain 1 mixer. As shown in figure 3.18, after each vertical part (z direction), the diameter of the new section is 0.8 mm and extended 0.4 mm rather than the outlet of vertical part (0.4 mm).

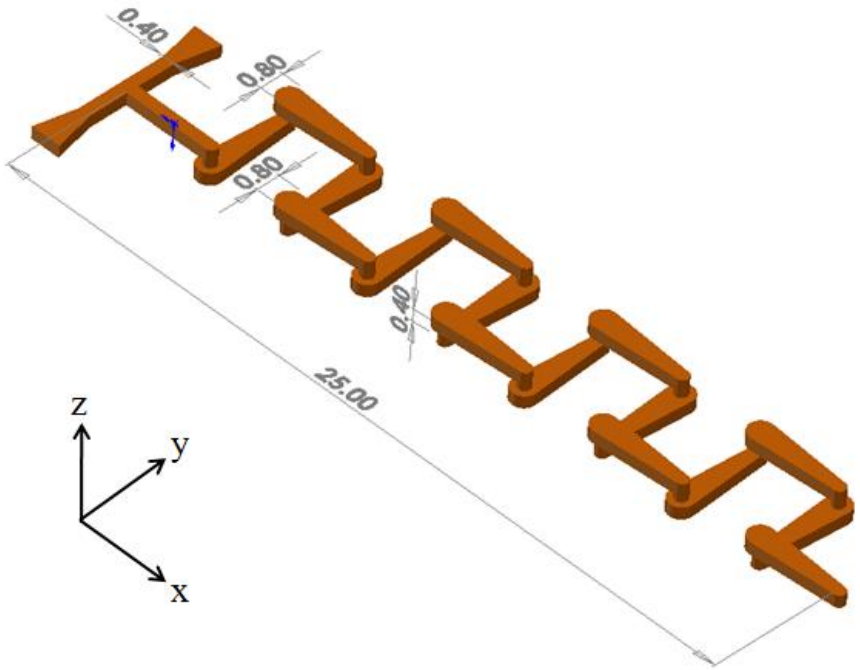

Figure 3.18 Design of Chain 2-micromixer.

The mail goals for designing chain-2 is to find out the effects of the new geometry on efficiency of the mixing and also pressure drop rather than Chain-1 mixer. Hence, experimental examination (in chapter 4) and numerical tests (discussed in chapter 5) are performed to figure out the mixing efficiency and pressure drop respectively.

3.9.3 Chain 3-micromixer

Chain 3-micromixer was designed and fabricated from plexiglas using a computer milling process. As illustrated in figures 3.19, number of elements in this micromixer is twice rather than Chain 1 .

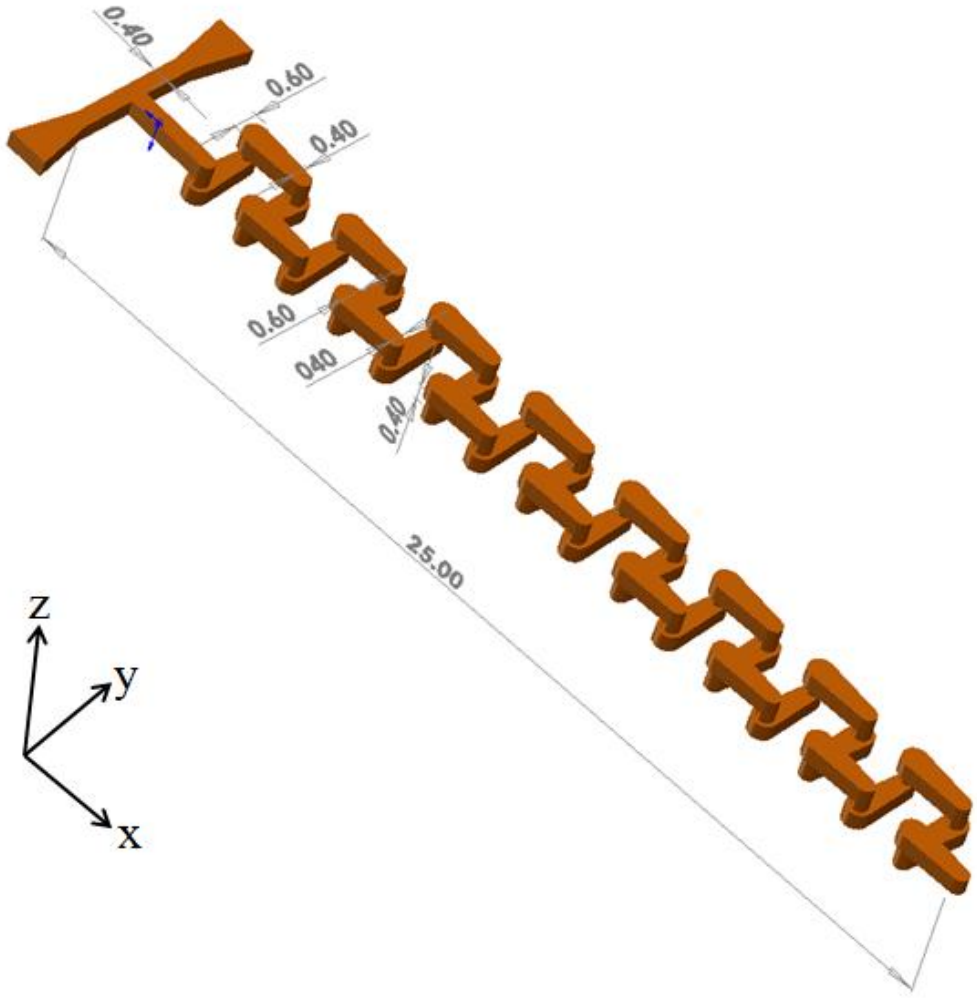

Figure 3.19 Design of Chain 3-micromixer.

Indeed, numbers of the replacement of layers during moving the species in microchannel is twice rather than Chain 1- and Chain 2-micromixers. The purpose to design of chain 3 is that to understand the effect of this property on mixing efficiency and also the effect of new geometry on pressure drop.

3.9.4 Chain 4-micromixer

Like other chain mixers, Chain 4-micromixer was designed and fabricated from plexiglas using a computer milling process. Figure 3.20 illustrates the Chain 4 mixer which differs only by one parameter from the Chain 3 mixer. As shown in figure 3.20, after each vertical part (z direction), the diameter of the new section is 0.8 mm and extended 0.4 mm rather than the outlet of vertical part (0.4 mm).

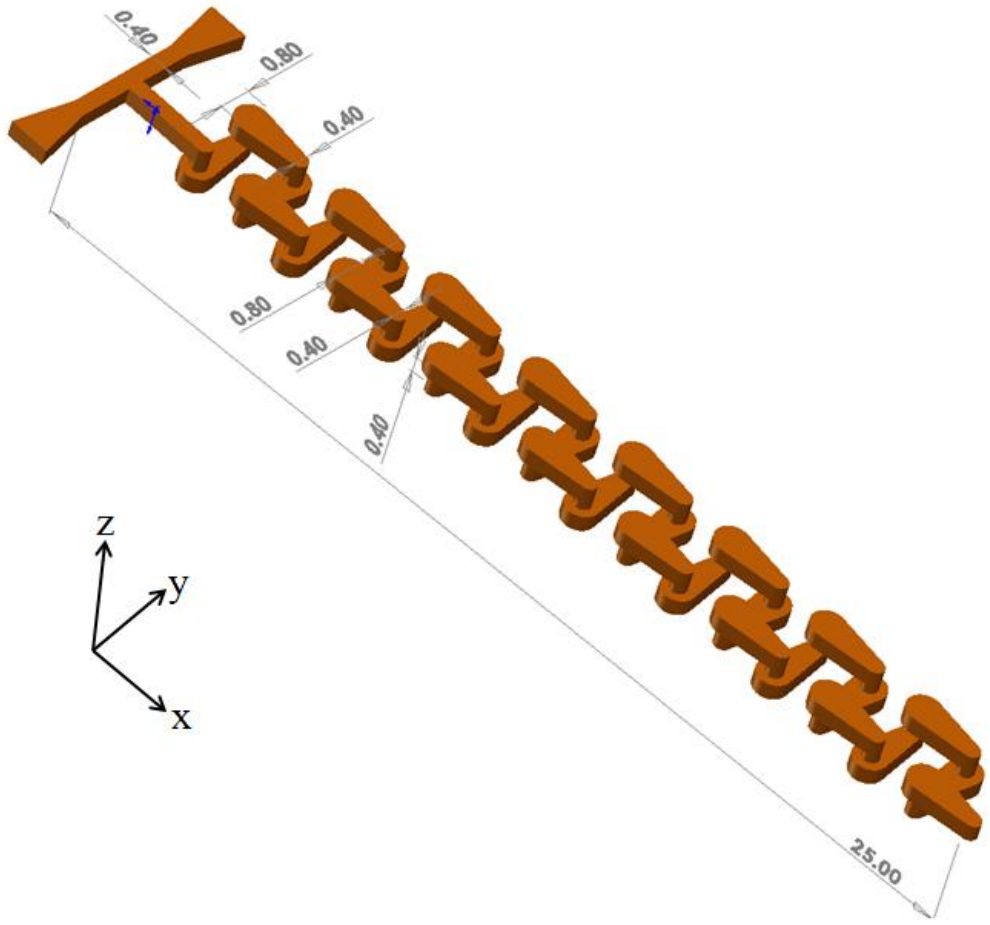

Figure 3.20 Design of Chain 4-micromixer.

In fact, in this type of microchannel it is tried to realize the effect of extending in the inlet part of the elements in degree of mixing and pressure drop. According to the theoretical background alluded in 3.9.1.1, it is expected to reach a good mixing efficiency with low pressure drop in chain micromixers rather than previous well-known micromixers.

Split and recombination mixing in chain mixers involves the generation of multiple lamellae of the fluids to be mixed, thereby creating an increased interfacial area across which diffusive transport can take place. By using this approach, reductions in mixing length are capable of being achieve.

3.10 Focusing of mixing stream

Before analyzing the data, it is useful to explain the mixing stream in two base : (a) steams with the same viscosity, and (b) streams with different viscosity. Because this knowledge helps to

understand the differences between two species that would suppose to be mixed and also variations of the properties during the microchannels.

3.10.1 Streams with the same viscosity

Hydrodynamic focusing reduces the mixing path by decreasing the width of the solute flow. As shown in figure 3.21 (as a good example), two solvent streams work as sheath flows in this concept. Knight et al. [25] Studied detailed experimental results for hydrodynamic focusing.

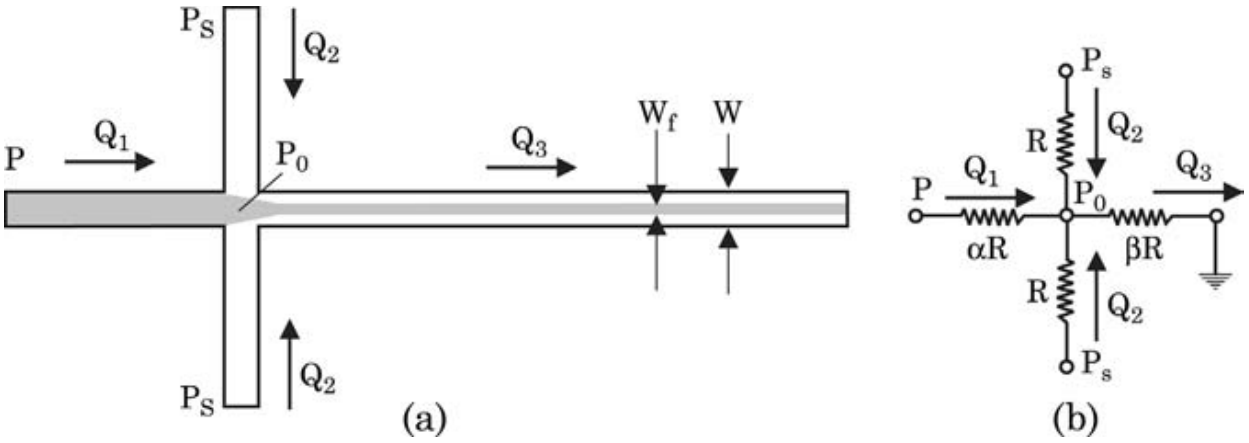

Figure 3.21Focusing concept: (a) geometric focusing (b) hydrodynamic focusing.[1]

However the theoretical model reported in [25] was erroneous. The correct model is presented as follows :

If the sheath streams have the same viscosity as the sample follow and all liquids are incompressible, the effect of hydrodynamic focusing can be represented by a simple network model. Assuming the flow is laminar and the pressure differences across a microchannel is proportional to the velocity (flow rate). Figure 3.21 (b) depicts the network model of hydrodynamic focusing, where microchannels are represented by fluidic resistances. For further simplicity, it is assumed that both sheath microchannels have the same fluidic resistance of *R*, which is defined as the quotient between the applied pressure difference and he flow rate.

$$R = \frac{\Delta P}{Q} \qquad (3.7)$$

The resistance of the inlet microchannel and the mixing microchannel are αR and βR, respectively. The factors of α and β are determined by geometry parameters such as shape and size of channel cross section as well as channel length. Taking the exit pressure as the reference, the relations

between the pressure at simple inlet, sheath flow inlets, and flow rates are given by the equation systems (3.8):

$$\begin{cases} Q_1 + 2Q_2 = Q_3 \\ P - P_0 = \alpha R Q_1 \\ P_s - P_0 = R Q_2 \\ P_0 = \beta R Q_3 \end{cases} \quad (3.8)$$

Where the P, P_s and P_0 are the pressure at the sample inlet, sheath flow inlet and the junction respectively. The flow rates through the fluidic resistance are Q_1, Q_2 and Q_3. Eliminating Q_3 from the equation system leads to :

$$\begin{cases} P = P_1 + \alpha R Q_1 \\ P_s = P_0 + R Q_2 \\ P_0 = \beta R Q_3 \end{cases} \quad (3.9)$$

The ratio between the sheath flow pressure and the sample pressure $r = {}^{P_s}/_{P}$ can be derived as follows:

$$r = \frac{P_s}{P} = \frac{\beta Q_1 + (2\beta + 1) Q_2}{(\beta + \alpha) Q_1 + 2\beta Q_2} \quad (3.10)$$

The maximum and minimum values of the pressure ratio is subsequently determined by setting $Q_1 = 0$ and $Q_2 = 0$, respectively:

$$r_{max} = \frac{2\beta + 1}{2\beta} \quad (3.11)$$

$$r_{min} = \frac{\beta}{\beta + \alpha} \quad (3.12)$$

With the focusing width W_f and the channel width W, the dimensionless focusing width W_f^* can be determined as :

$$W_f^* = \frac{W_f}{W} = \frac{Q_1}{Q_1 + 2Q_2} = \frac{1}{2\,{}^{Q_2}/_{Q_1} + 1} \quad (3.13)$$

The ratio Q_2/Q_1 can be solved as explicit function of α, β and r from systems of equation (3.9) :

$$\frac{Q_2}{Q_1} = \frac{\beta - r(\alpha+\beta)}{2\beta r - 2\beta - 1} \qquad (3.14)$$

And finally leading to :

$$W_f^* = \frac{1+2\beta-2\beta r}{1+2\alpha r} \qquad (3.15)$$

The benefits of these analyzing for micromixer are to found the range of pressure ratio between the sheath flow and sample flow and also required pressure ratio for a focusing width.

3.10.2 streams with the different viscosities

The following model analyzes the effect of hydrodynamic focusing for reducing the width of streams. As shown in figure 3.22, in the model, the sample streams in sandwiched between two identical sheath streams.

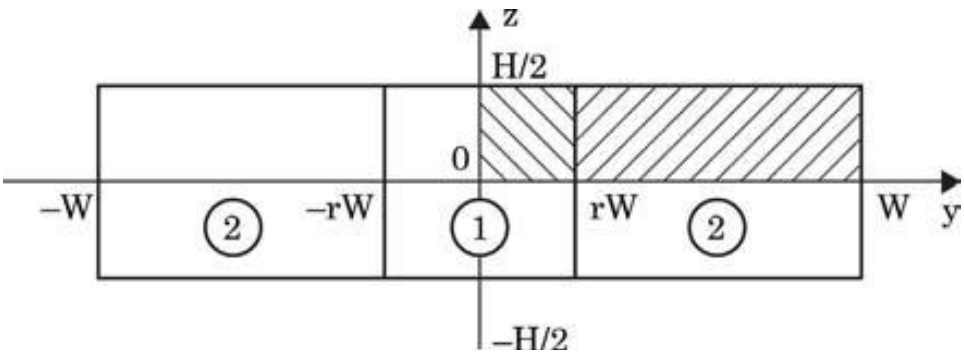

Figure 3.22 Analytical model for two phase modeling.[1]

The sample stream and the sheath stream are assumed to be immiscible. Figure 3.22 shows the geometry of the channel cross section with the above two phases. As can be seen, the channel has a width of 2W and a height of H. The position of the interface is rW. Since the model is symmetrical regarding the y-axis and z-axis, only one-fourth of the cross section needs to be considered.
The velocity distribution u_1 and u_2 in the channel can be described by the Navier-Stokes equations.

$$\begin{cases} \frac{\partial^2 u_1}{\partial y^2} + \frac{\partial^2 u_1}{\partial z^2} = \frac{1}{\mu_1}\frac{\partial p}{\partial x} \\ \frac{\partial^2 u_2}{\partial y^2} + \frac{\partial^2 u_2}{\partial z^2} = \frac{1}{\mu_2}\frac{\partial p}{\partial x} \end{cases} \quad (3.16)$$

Where indices 1 and 2 describe the sample flow and the sheath flow, respectively. In system of equations 3.16 μ_1 and μ_2 are the viscosities of the sample fluid and of the sheath fluid. Normalizing the velocity by a reference velocity u_0, and the coordinates by W, leads to the dimensionless model:

$$\begin{cases} \frac{\partial^2 u_1^*}{\partial y^{*2}} + \frac{\partial^2 u_1^*}{\partial z^{*2}} = P' \\ \frac{\partial^2 u_2^*}{\partial y^{*2}} + \frac{\partial^2 u_2^*}{\partial z^{*2}} = P' \end{cases} \quad (3.17)$$

With $P' = \frac{W}{\mu_1 u_0}\frac{\partial P}{\partial x^*}$, $\beta = \frac{\mu_2}{\mu_1}$, and $\theta = \frac{(2n-1)\pi}{n}$, the solution of 3.17 have the forms ($0 < y^* < 1, 0 < z^* < {}^{h}/_{2}$):

$$\begin{cases} u_1^*(y^*, z^*) = P'\left[\frac{z^{*2} - {h^2}/{4}}{2} + \sum_{n=1}^{\infty} cos\theta z^* (A_1\, cosh\theta y^* + B_1\, sinh\theta y^*)\right] \\ u_2^*(y^*, z^*) = \frac{P'}{\beta}\left[\frac{z^{*2} - {h^2}/{4}}{2} + \sum_{n=1}^{\infty} cos\theta z^* (A_2\, cosh\theta y^* + B_2\, sinh\theta y^*)\right] \end{cases} \quad (3.18)$$

The non slip condition at the wall are :

$$u_2^*(1, z^*) = 0 \quad (3.19)$$

The symmetry condition at the z^*-axis is:

$$\left.\frac{\partial u_1^*}{\partial y^*}\right|_{y^*=0} = 0 \quad (3.20)$$

At the interface between the sample flow and the sheath flow, the velocity and the shear rate are continuous:

$$\begin{cases} u_2^*(r,z^*) = u_1^*(r,z^*) \\ \left.\frac{\partial u_1^*}{\partial y^*}\right|_{y^*=r} = \beta \left.\frac{\partial u_2^*}{\partial y^*}\right|_{y^*=r} \end{cases} \quad (3.21)$$

For a flat channel (h << 1), the position of the interface can be estimated as:

$$r = \frac{1}{1+2\beta k} \quad (3.22)$$

Where $k = {\dot{m}_2}/{\dot{m}_1}$ is the flow rate ratio between the sheath streams and the mixing streams. A Fourier analysis with the above boundary conditions results in the coefficient of equations 3.18 . The theoretical model is depicted with the solid lines in figure 3.23.

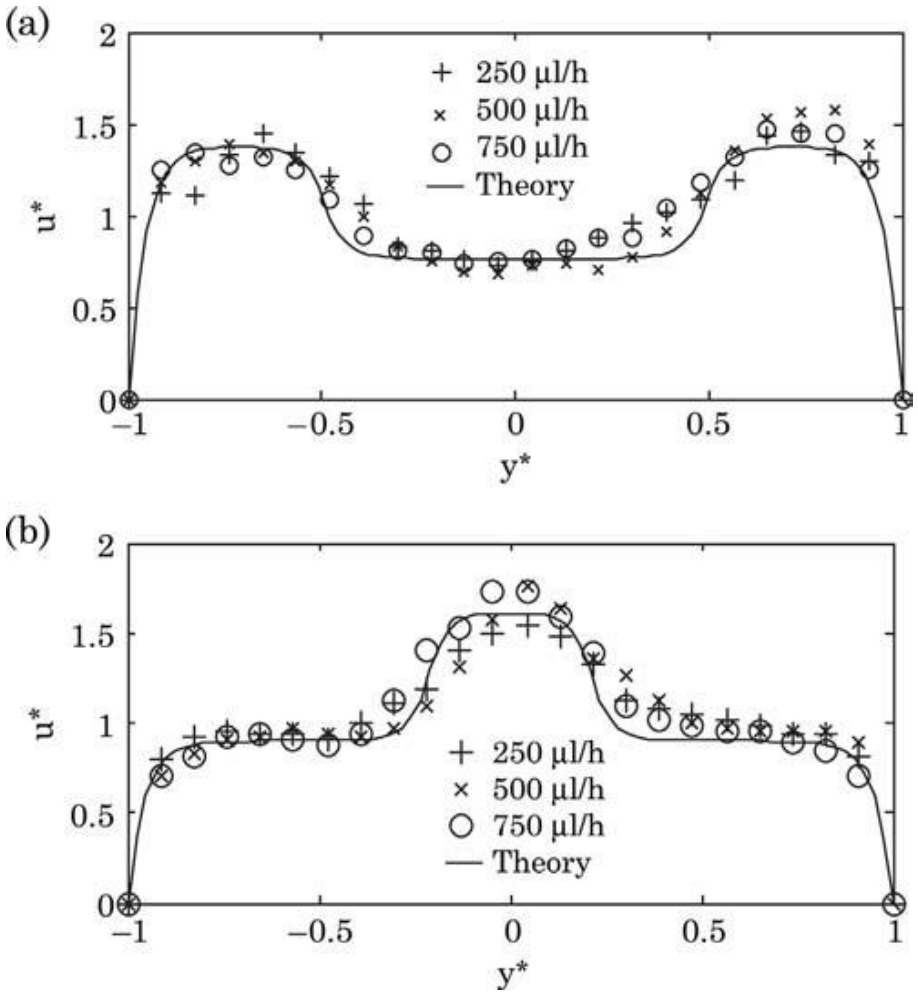

Figure 3.23 The dimensionless velocity profile (h=0.1, k=1): (a)$\beta = {1}/{1.8}$;(b)$\beta = 1.8$. [1]

The velocity of the sample flow is lower if the sample flow is more viscous than the sheath flow ($\beta < 1$), as illustrated in figure 3.23 (a). If the sheath flows are more viscous ($\beta > 1$), the sample flow is faster as shown in figure 3.23(b).

References

[1] Nguyen N.T., 2008. Micromixers: Fundamentals, Design and Fabrication. William Andrew, Norwich, NY, USA.

[2] Zhang Y., Hu and Wu H., 2012. Design and simulation of passive micromixers based on capillary, Microfluidic Nanofluidic, doi: 10.1007/s10404-012-1002y.

[3] Huchet F., Havlica J., Legentilhomme P., Montillet A., Comiti J and Tihon J., 2008. Use of electrochemical microsensors for hydrodynamics study in crossing microchannels, Microfluidic Nanofluidic 5: 55-64, doi: 10.1007/s10404-007-0220-1.

[4] Chen Y.T., Fang W.F. and Liu Y.C., 2011. Analysis of chaos and FRET reaction in split-and-recombine microreactors, Microfluidic Nanofluidic 11: 339-352, doi: 10.1007/s10404-011-0803-8.

[5] Chang C.C. and Yang R.J., 2007. Electrokinetic mixing in microfluidic systems, Microfluidic Nanofluidic 3: 501-525, doi: 10.1007/s10404-007-0178-z.

[6] Malecha k., Golonka L., Baldyga J., Jasinska M. And Sobieszuk P, 2009. Serpantine microfluidic mixer made in LTCC, Sensors and Actuators B: Chemical 143: 400-413, doi: 10.1016/j.snb.2009.08.010.

[7] Park J.M., Kim D.S., Kang T.G. and kwon T.H., 2008. Improved serpentine laminating micromixer with enhanced local advection. Microfluidic Nanofluidic 4: 513-523, doi : 10.1007/s10404-007-0208-x.

[8] Mansur E.A., Mingxing Y.E., Yundong W. and Youyuan D, 2008. A state-of-the-art Review of Mixing in Microfluidic Mixers, Chinese Journal of Chemical Engineering, 16(4) 503-516.

[9] Erickson D., 2005. Toward numerical prototyping of labs-on-chip: modeling for integrated microfluidic devices, Microfluidic Nanofluidic 1: 301-318.

[10] Hardt S., Pennemann H. and Schonfeld F, 2006. Theoretical and experimental characterization of a low-Reynolds number split-and-recombine mixer, Microfluidic Nanofluidic 2: 237-248, doi: 10.1007/s10404-005-0071-6.

[11] Zolgharni M., Azimi S.M., Bahmanyar M.R. and Balachandran W, 2007. A numerical design study of chaotic mixing of magnetic particles in a microfluidic bio-separator, Microfluidic Nanofluidic 3: 677-687, doi: 10.1007//s10404-007-0160-9.

[12] Chen J.J. and Shie Y.S., 2012. Interfacial configurations and mixing performances of fluids in staggered curved-channel micromixers, Microsyst Technol 18: 1823-1833, doi: 10.1007/s00542-012-1489-x.

[13] Cook K.J., Fan Y.F. and Hassan I., 2012. Experimental investigation of a scaled-up passive micromixer with uneven interdigital inlet and teardrop obstruction elements, Exp Fluids 52: 1261-1257, doi: 10.1007/s00348-011-1246-4.

[14] Aoki N., Fukuda T., Maeda N. and Mae K., 2012. Deign of confluence and bend geometry for rapid mixing in microchannels, Chemical engineering Journal, doi: 10.1016/j.cej.2012.03.061.

[15] Suh Y.K., Jayaraj S. And Kang S., 2007. A Review on the Analysis and Experiment of Fluid Flow and Mixing in Micro-Channels, Journal of Mechanical Science and Technology 21: 536~548.

[16] Fang W.F. and Yang J.T., 2009. A novel microreactor with 3D rotating flow to boost fluid reaction and mixing of viscous fluids, Sensors and Actuators B: Chemical 140: 629-642, doi: 10.1016/j.snb.2009.05.007.

[17] Lee S.W. and Lee S.S., 2008. Rotation effect in split and recombination micromixing, Sensors and Actuators B: Chemical 129: 364-371, doi: 10.1016/j.snb.2007.08.038.

[18] Jeong S., Park J., Kim J.M. and Park S., 2011. Microfluidic mixing using periodically induced secondary potential in Electroosmotic flow, Journal of Electrostatics 69: 429-434, doi: 10.1016/j.elstat.2011.06.001.

[19] Hardt S., Drese K.S., Hessel V. And Schonfeld F., 2005. Passive micromixers for applications in the microreactor and μTAS fields, Microfluidic Nanofluidic 1: 108-118, doi: 10.1007/s10404-004-0029-0.

[20] Sheu T.S., Chen S.J. and Chen J.J., 2012. Mixing of a split and recombine micromixer with tapered curved microchannels, Chemical Engineering science 71: 321-332, doi: 10.1016/j.ces.2011.12.042.

[21] Munson M.S. and Yager P., 2004. Simple quantitative optical method for monitoring the extent of mixing applied to a novel microfluidic mixer, Analytica Chimica Acta Vol. 507, pp. 63-71.

[22] Ma Y. et. Al., 2008. An unsteady microfluidic T-form mixer perturbed by hydrodynamic pressure, Journal of Micromechanics and Microengineering 18, 045015, doi: 1088/0960-1317/18/045015.

[23] Garstecki P., Fuerstman M.J., Fischbach M.A., Sia S.K., Whitesides G.M., 2006. Mixing with bubbles: a practical technology for use with portable microfluidic devices, Lab on a Chip 6, 207-212, doi :10.1039/b510843h.

[24] Chen Z., Bown M.R., Sullivan B.O., MacInnes J.M., Allen R.W.K., Mulder M., Blom M., van't Oever R., 2009. Performance analysis of a folding flow micromixer, Microfluid Nanofluid 6:763–774, doi: 10.1007/s10404-008-0351-z.

[25] Knight J.B., Vishwanath A.P., Brody J. and Austin R., 1998. Hydrodynamic focusing on a silicon chip: Mixing nanoliters in microseconds, Physical Review Letters, Vol. 80, pp. 3863-3866.

Chapter 4
Experimental Results

4.1 Introduction

This section will present the experimental results obtained in microfluidic laboratory at different Reynolds numbers in all mentioned micromixers. First of all it will be showed the prototypes of alluded micromixers. After that it will be analyzed the experimental results using Direct Statistical Method (expressed on 3.3.2) to evaluate the efficiency of mixing presented in chapter 3.

4.2 Brief statement of experimental analysis

As mentioned in chapter 3, all prototypes tested in five Reynolds numbers according to table 3.1. Then the data are analyzed and efficiency of mixing evaluated regarding to flowchart 3.6. to the best of our knowledge, to evaluate the performance of micromixers that applied in current study, first and foremost T –micromixer is analyzed and the degree of mixing in other micromixers compared with T- micromixer.

Afterward results of experiments in micromixers are presented and the efficiency detected visually. In order to characterize the mentioned micromixers, blue and yellow dyed water was applied and injected to the microchannel by a syringe pump to evaluate the mixing performance.

However, the comparison of the mixing colors just visually are unable to provide enough quantitative analysis to evaluate the mixing degree, thus image-based technique implemented to analyze the experimental data.

Experimental tests were performed under the microscope (VMS-004D, Veho) with high speed image acquisition. As miscible fluids, colored water (blue and yellow) was used in all tests on the prototypes. Colored water solutions for the tests were produced by blending 1 gram powder in 0.5 liter water. Species flow in the microchannel were controlled by means of a programmable syringe pump. After the mixing process was visualized, mixing efficiencies for all micromixers were calculated and compared.

During the mixing process, several pictures were taken with the microscope from the inlet section to the end of the channel as shown in figure 4.1. This was repeated for all Reynolds numbers used in this study.

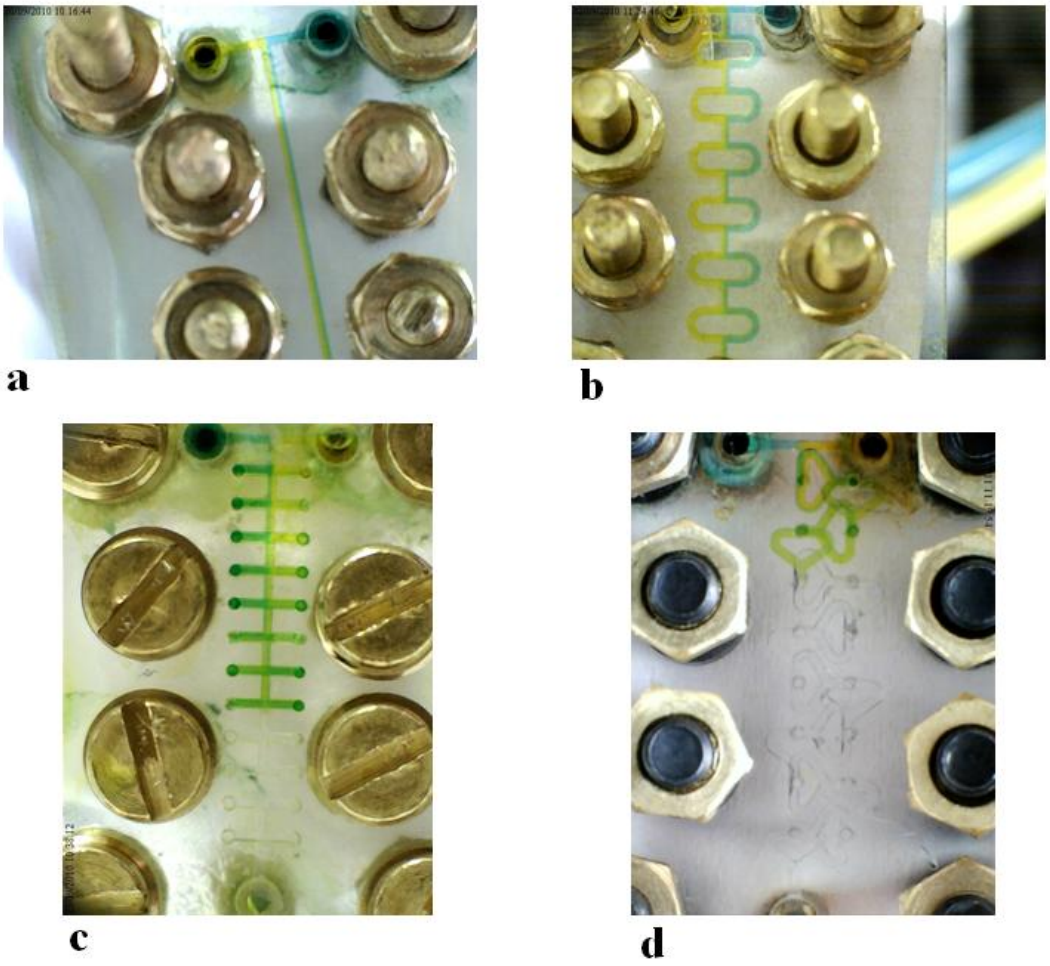

Figure 4.1 Micromixers during the test: (a) T-mixer; (b) O-mixer; (c) H-mixer; (d) Tear-drop mixer.

As alluded before, to investigate the mixing process, experimental tests were performed at five flow rates. Image-based techniques were used to evaluate the mixing performance of the prototypes, and the gray scale value was applied for post processing. To analyze the image, the captured color images were converted into gray scale images. Gray scale images are also called monochromatic, denoting the absence of any chromatic variation (also called bi level or binary images). To convert any color to a gray scale representation of its luminance, the value of its red, green and blue (RGB) primaries must first be obtained in linear intensity encoding, after which 30% of the red values, 59% of the green values, and 11% of the blue values are added together. This technique (gray scale value) is useful for highlighting regions of interest, especially the concentration field in the

micromixer [1]. Then, the efficiency of mixing evaluated regarding to flowchart 3.6 as follows in this chapter for all prototypes.

4.3 T-micromixer analyze

Results of experimental investigation of the T micromixer [2] are presented below.

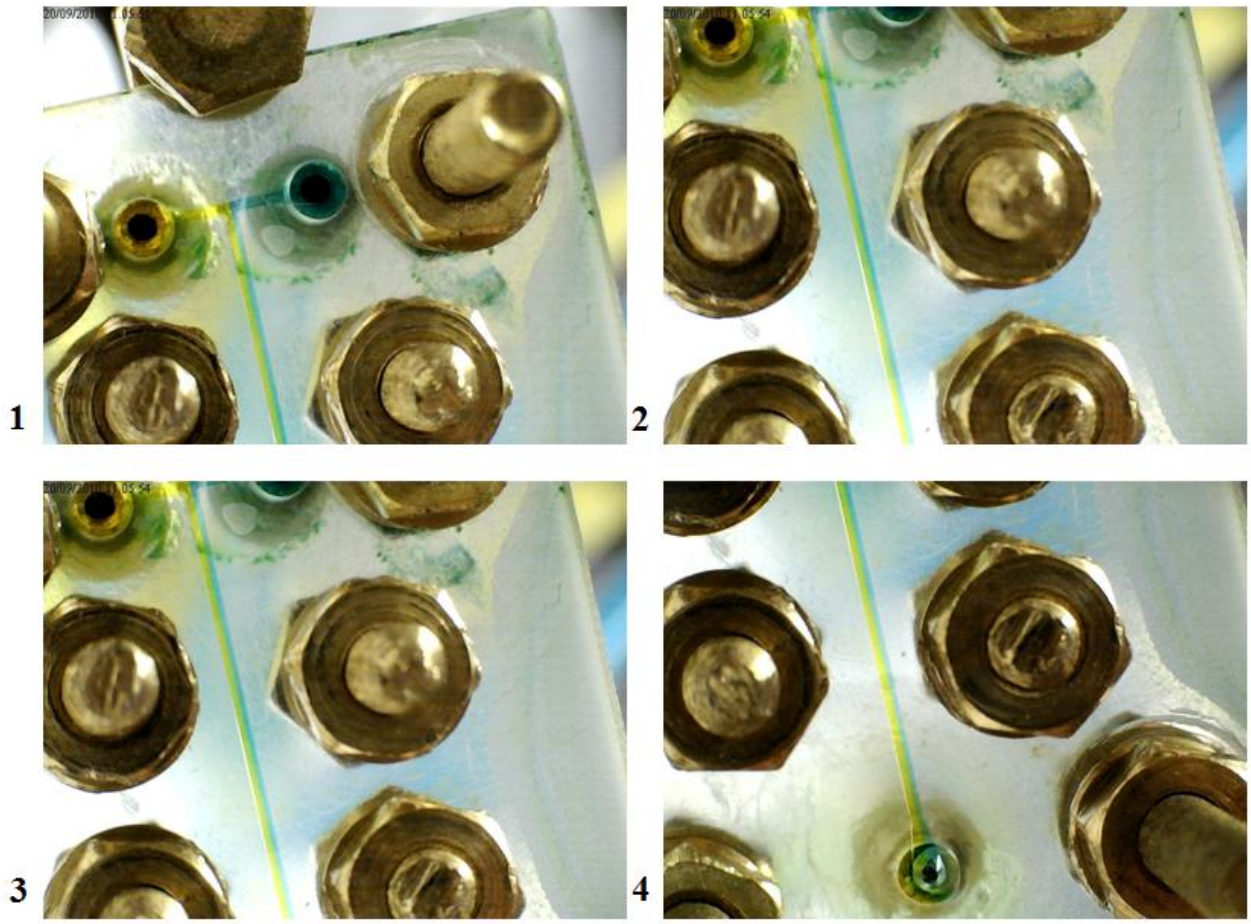

Figure 4.2 T-micromixer during the test.

PDF software and equations 3.4, 3.5 and 3.6 were used to calculate and plot standard deviation σ, mixing index *MI* and efficiency η at different *Re* and along the micromixer. The mixing efficiency is quantified by evaluating the variance of the mixture in a cross-section that is normal to the flow direction by equation (3.4). The variance can be normalized again by the mean concentration to get the Mixing Index by equation (3.5) . Then the efficiency can be defined based on the Mixing Index by equation (3.6).

Experimental tests were performed at five flow rates and Reynolds numbers *Re* as shown in Table 4.1.

Table 4.1 Standard deviation of concentration (σ) during experimental investigation in T-micromixer.

σ	0 mm	5 mm	10 mm	15 mm	20 mm
Q=0.001(ml/min)	0.4	0.0950	0.1974	0.1857	0.1974
Q=0.005	0.1301	0.1184	0.01213	0.1272	0.2061
Q=0.01	0.1711	0.1857	0.1330	0.1096	0.1243
Q=0.02	0.22	0.2452	0.1575	0.1685	0.1755
Q=0.05	0.599	0.1886	0.1096	0.1447	0.1944

Table 4.2 Mixing index (*MI*) during experimental test in T-micromixer.

MI	0 mm	5 mm	10 mm	15 mm	20 mm
Q=0.001(ml/min)	1	0.09956	0.9985	0.9956	0.9956
Q=0.005	0.9956	0.9985	0.9985	0.9956	0.9956
Q=0.01	0.9956	0.9956	0.99	0.9985	0.9985
Q=0.02	0.9562	0.9888	0.9855	0.9952	0.9950
Q=0.05	0.9985	0.9985	0.9956	0.9956	0.9999

Table 4.3 Mixing efficiency in T-micromixer.

η	0 mm	5 mm	10 mm	15 mm	20 mm
Q=0.001(ml/min)	0	0.0005	0.0015	0.0015	0.0044
Q=0.005	0.00	0.0015	0.0044	0.0015	0.0044
Q=0.01	0.0015	0.0044	0.01	0.001	0.0015
Q=0.02	0.0438	0.0112	0.0145	0.0048	0.005
Q=0.05	0.0015	0.0015	0.0044	0.0044	0.0001

Tables 4.1, 4.2 and 4.3 illustrate the standard deviation of concentration σ, Mixing Index (*MI*) and efficiency of mixing (η) respectively.

Figures 4.3 illustrates the probability distribution function in terms of concentration in the entrance region in T-micromixer at Q=0.001 ml/min (Re=0.083). Also figure 4.4 depicts the mixing efficiency in T-micromixer at the same Reynolds number. As can be seen visually in the figure 4.2, in the outlet of the T-micromixer, there are two separate color (yellow and blue). It shows that the mixing does not occur (or very poor). Then analyzing the data show that in the entrance region, where two fluids join together, the standard deviation is 0.04, mixing index is 1 and efficiency is 0%.

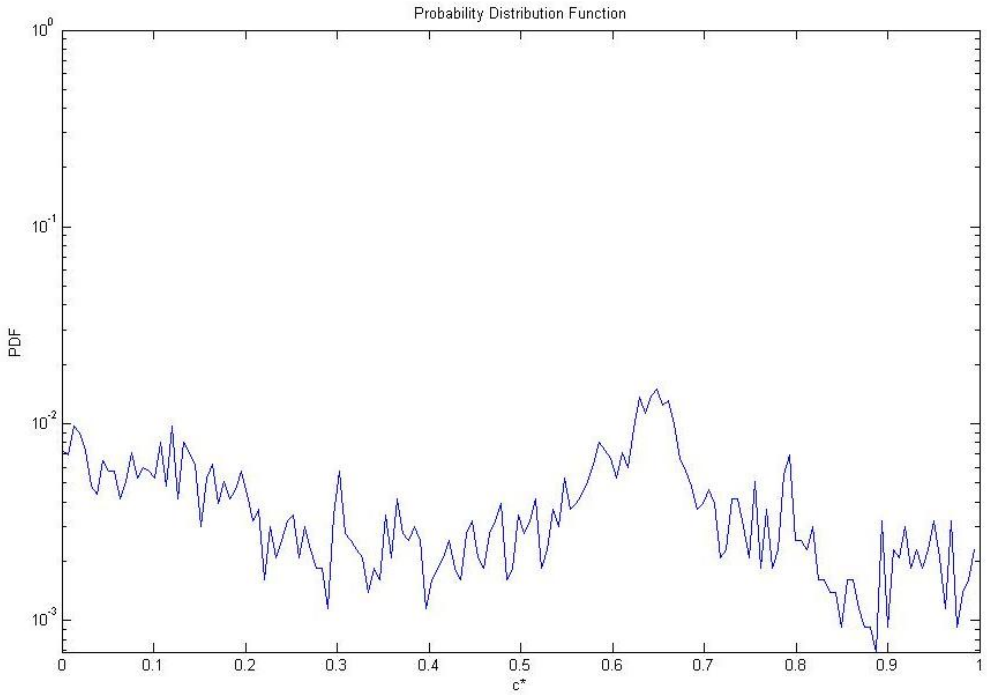

Figure 4.3 PDF in *T-micromixer* at Re = 0.083, entrance region.

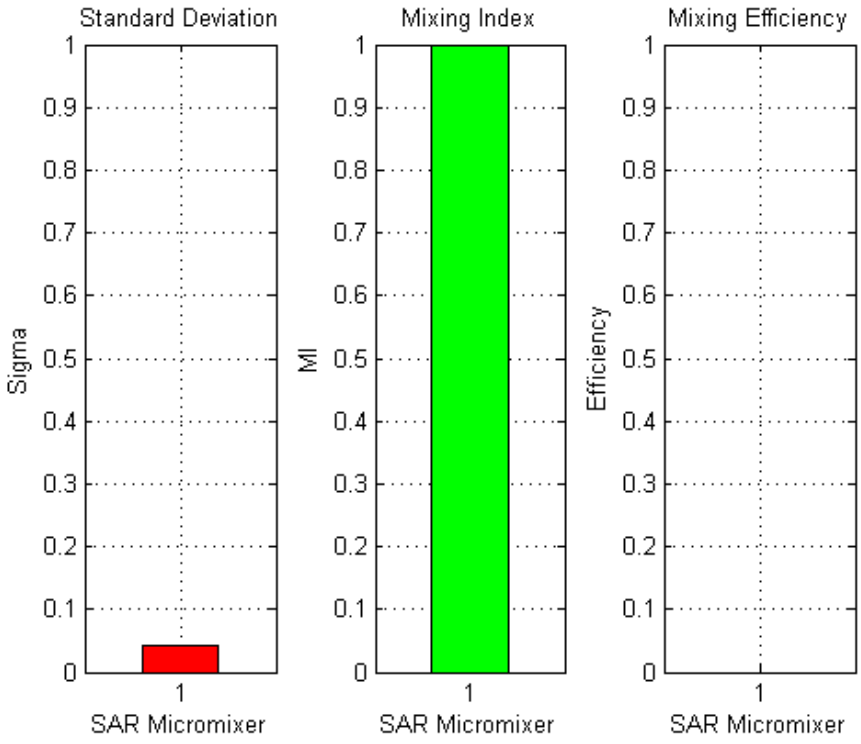

Figure 4.4 T-micromixer analysis, Re = 0.083, entrance region.

In experimentation, The experimental errors depend on the quality of the pictures and selecting the region of interest in microchannel which would be considered in the post processing step. The

maximum measurement error could be seen when the flow is far from the mixed condition. In practice this means in the entrance region or in the case of using the poor performance mixer.
Comparison of mixing efficiency during the T-microchannel is shown in figure 4.5.

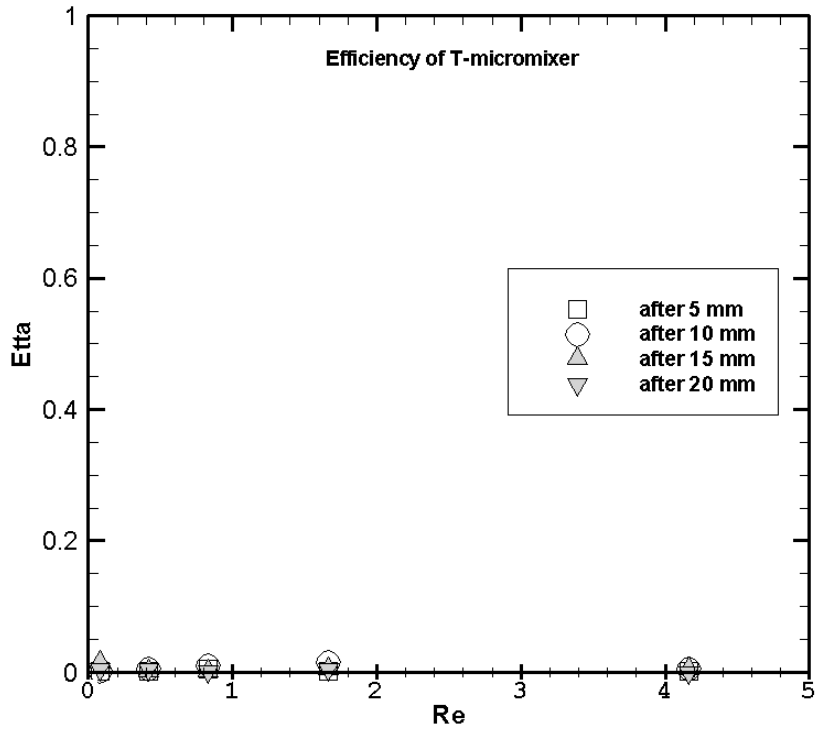

Figure 4.5 Comparison of η in terms of Re during T-micromixer.

As can be seen, in all of the regions of interest, from the entrance region to the end of microchannel at all of the tested Reynolds numbers, mixing efficiency is 0%. As mentioned before, An efficiency between 80% and 100% is acceptable for mixing process applications [1].
Refer to analyzing the T-micromixer, it has concluded that the T-mixer is not useful for application in the passive micromixing at low Reynolds number due to the mixing efficiency is 0% or very poor.

4.4 O-micromixer analyze

Figure 4.6 depicts the O-mixer [3], whose microchannel is divided into two segments: straight channel and O-segment. Like T-micromixer, O-mixer was designed and fabricated from plexiglas using a computer milling process. Results of experimental investigation of the O micromixer are presented below.

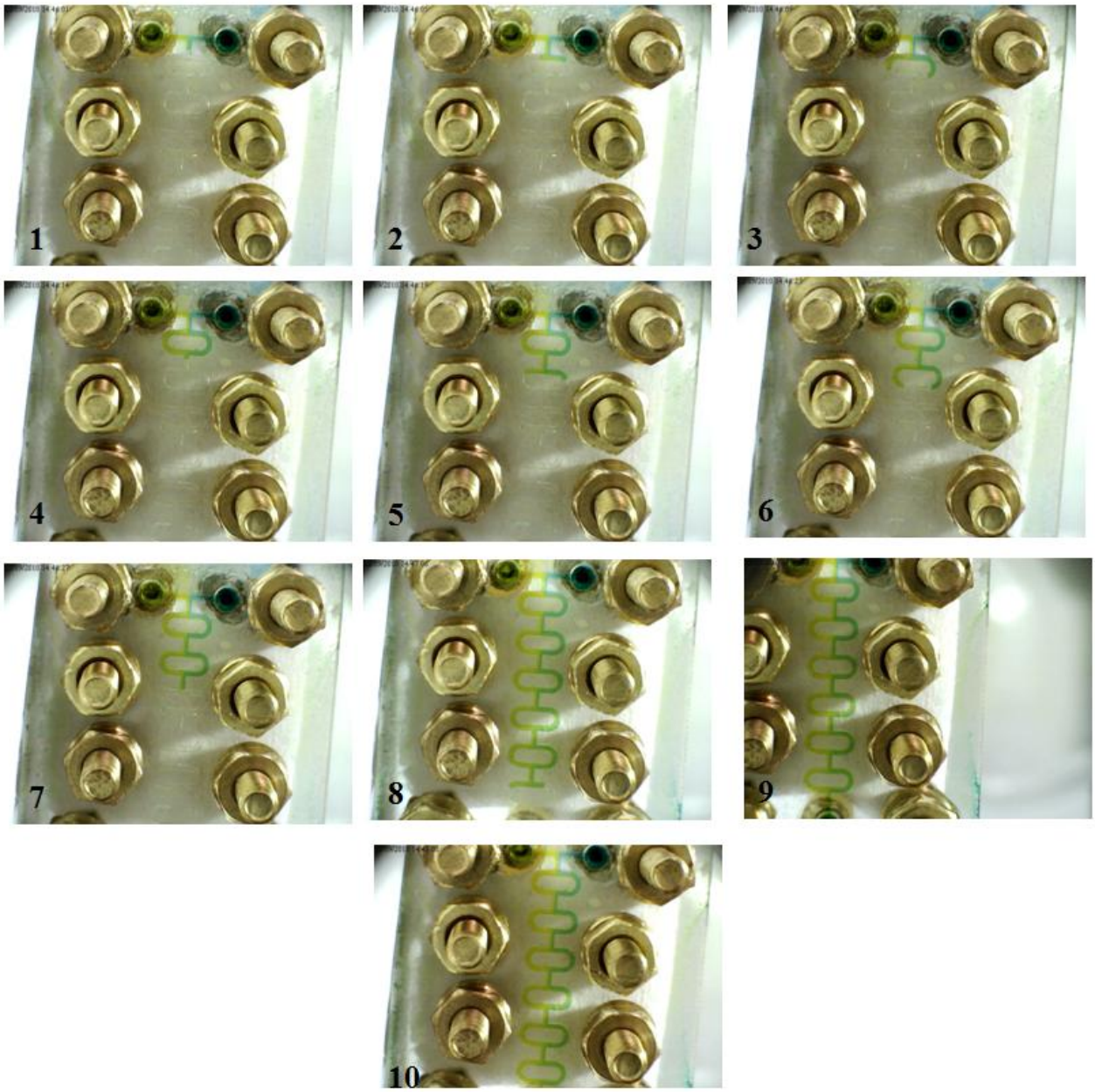

Figure 4.6 O-micromixer during the test at Re=0.416.

Again, PDF software and equations 3.4, 3.5 and 3.6 were used to calculate and plot standard deviation σ, mixing index *MI* and efficiency η at different *Re* and along the micromixer. Tables 4.4, 4.5 and 4.6 illustrate the standard deviation of concentration σ, Mixing Index (*MI*) and efficiency of mixing (η) in o-microchannel respectively.

Table 4.4 Standard deviation of concentration (σ) during experimental investigation in O-micromixer.

σ	0 mm	5 mm	10 mm	15 mm	20 mm
Q=0.001(ml/min)	0. 21	0.04	0.0424	0.388	0.40
Q=0.005	0.36	0.1213	0.12	0.1096	0.1272
Q=0.01	0.2003	0.1564	0.1769	0.1067	0.1564
Q=0.02	0.1827	0.1915	0.1944	0.1798	0.1915
Q=0.05	0.189	0.1245	0.1888	0.232	0.22

Table 4.5 Mixing index (*MI*) during experimental test in O-micromixer.

MI	0 mm	5 mm	10 mm	15 mm	20 mm
Q=0.001(ml/min)	0.9956	1	0.8757	0.983	0.88
Q=0.005	0.9985	1	0.99	0.9898	0.95
Q=0.01	0.9806	1	0.9985	0.9927	0.9985
Q=0.02	0.99	0.9985	0.98	0.99	0.9885
Q=0.05	0.99	1	0.98	0.998	0.99

Table 4.6 Mixing efficiency (η) in O-micromixer.

η	0 mm	5 mm	10 mm	15 mm	20 mm
Q=0.001(ml/min)	0.0015	0.00	0.1301	0.1702	0.22
Q=0.005	0.0015	0	0.1	0.0102	0.051
Q=0.01	0.0194	0	0.0015	0.0073	0.044
Q=0.02	0.0015	0.0015	0.0044	0.0069	0.015
Q=0.05	0.001	0.00	0.0052	0.0050	0.01

Figures 4.7 depicts the probability distribution function in terms of concentration after 10 mm from the entrance region in O-micromixer at Q=0.001 ml/min (Re=0.083). Also figure 4.8 shows the mixing efficiency in O-micromixer at the same Reynolds number. As can be seen also visually in the figure 4.6, in the outlet of the O-micromixer, there are two separate color (yellow and blue) like can be seen in T-mixer. It shows that the mixing does not occur (or very poor). Then analyzing the data show that in the O-micromixer, mixing index is near to 1 and efficiency is 0% (refer to table 4.5 and 4.6). However at Re=0.083 at the outlet region of the O-micromixer, the efficiency of mixing is 22% , but sill is not acceptable for mixing processing ($\eta<80\%$).

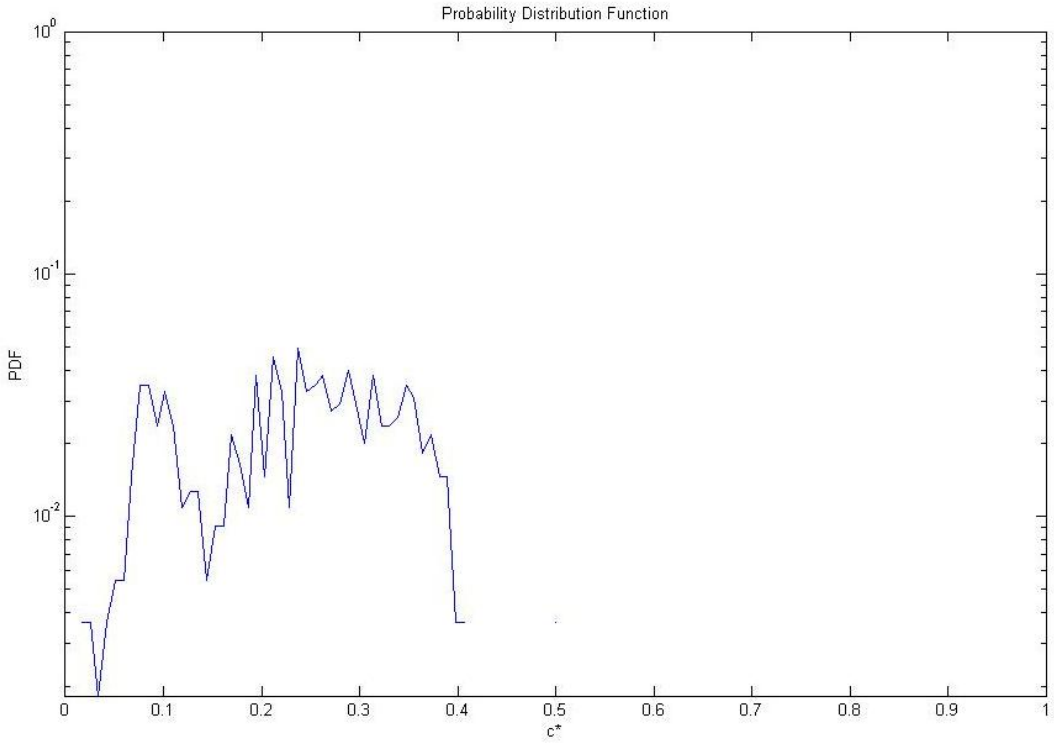

Figure 4.7 PDF in *O-micromixer* at Re = 0.083, after 10 mm.

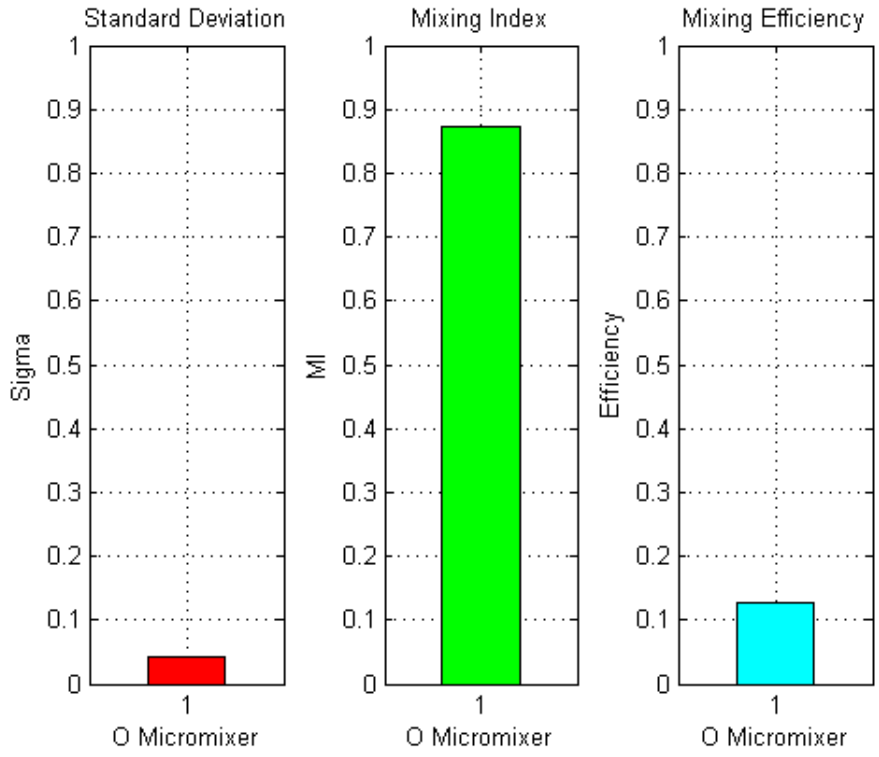

Figure 4.8 O-micromixer analysis, Re = 0.083, after 10 mm.

Comparison of mixing efficiency during the O-microchannel is depicted in figure 4.9.

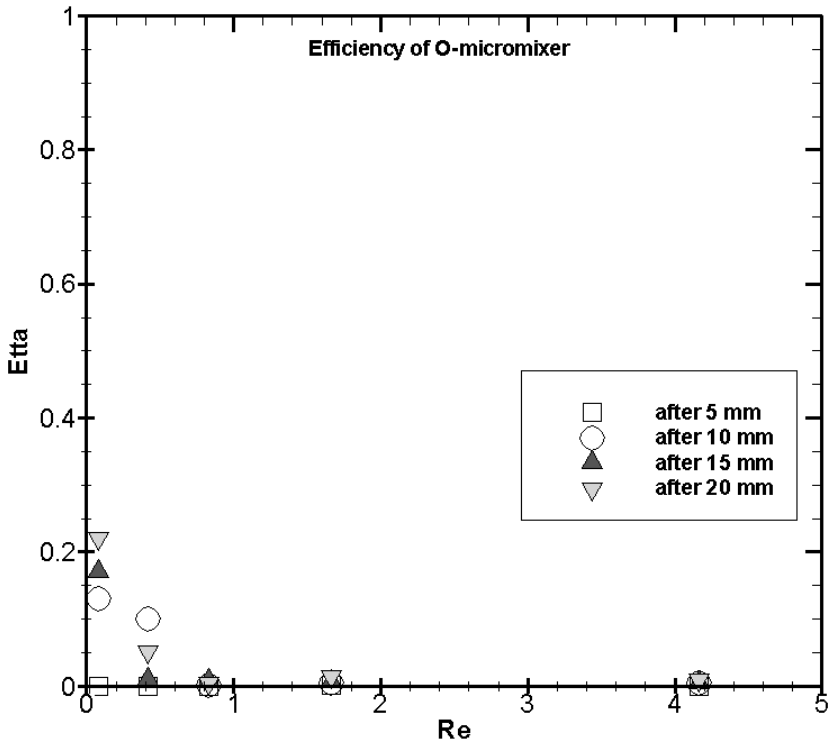

Figure 4.9 Comparison of η in terms of Re during O-micromixer.

Figure 4.9 illustrates efficiency versus Reynolds number in O-micromixer. As the diagram shows, efficiency decreases as Reynolds number increases and vice versa. Also in all of the tested Reynolds numbers, the efficiency is under 80% and are not acceptable for mixing process. Maximum value of efficiency is 22% and occurs the outlet region of O-mixer at the Re=0.083. Hence, this kind of micromixer is not useful for passive mixing processing. But O- and T-mixers are a good reference for comparison of the degree of mixing in passive micromixers.

4.5 Tear-drop micromixer analyze

On the basis of the investigation presented in [4], a split and recombination micromixer consisting of plate symmetrical modules (SAR PSM micromixer) was designed and constructed with polycarbonate using a computerized milling process. Tear-drop micromixer during he experimentation is shown in figure 4.10 at Re=0.083. Channel width and height are 0.4 mm. As can be seen from figure, the Tear-drop mixer has a two-layer structure. The modules of the upper layer and lower layer are connected by simple vertical channels. The inlet to the mixer is designed as a T-junction element (up side of figure).

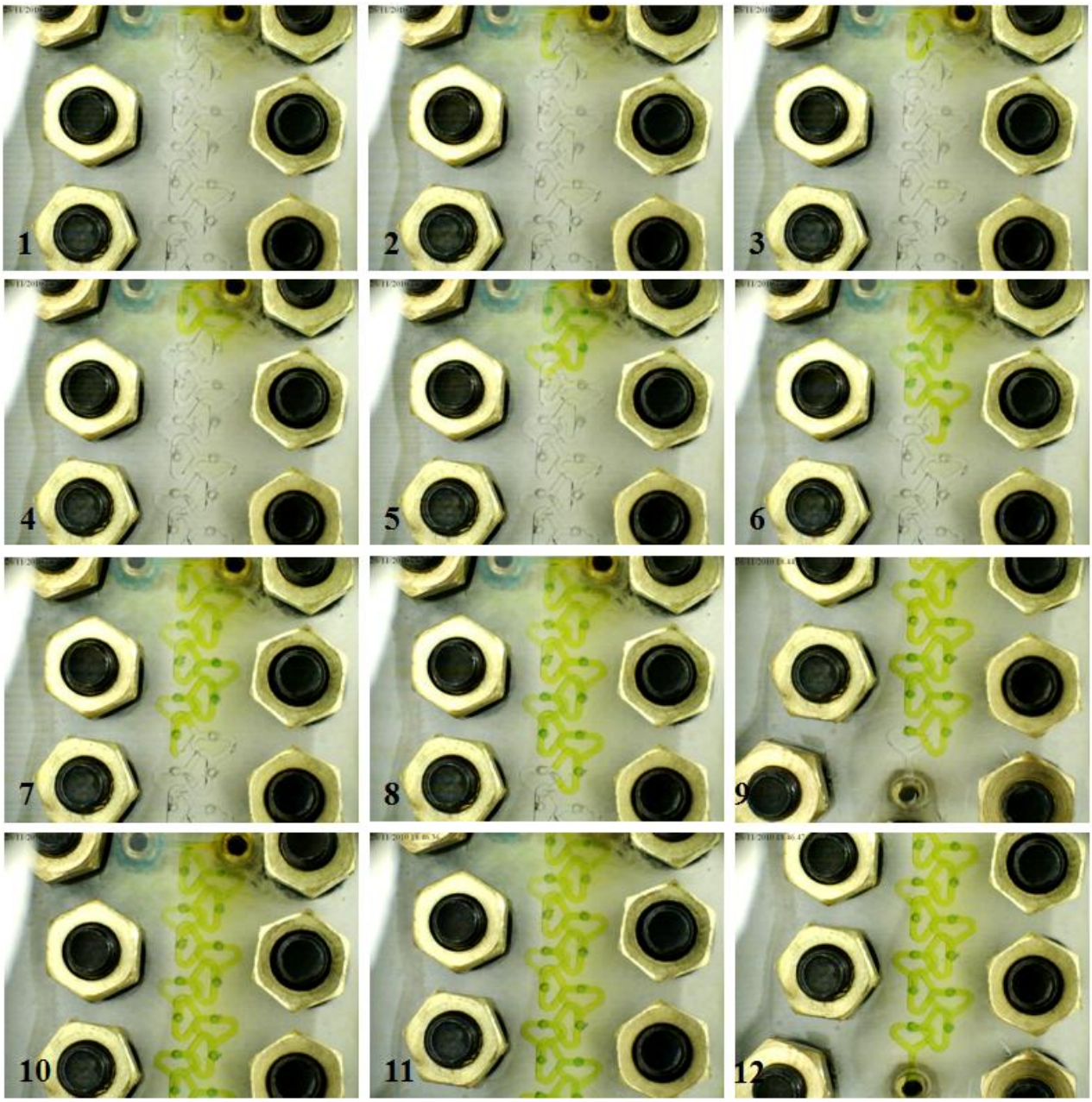

Figure 4.10 Tear- drop micromixer during the test at Re=0.083.

Results of experimental investigation of the Tear-drop micromixer are presented below. Tables 4.7, 4.8 and 4.9 illustrate the standard deviation of concentration (σ), Mixing Index (MI) and efficiency of mixing (η) in Tear-drop microchannel respectively.

Table 4.7 Standard deviation of concentration (σ) during experimental investigation in Tear-drop micromixer.

σ	0 mm	5 mm	10 mm	15 mm	20 mm
Q=0.001(ml/min)	0.4810	0.0161	0.0161	0.0132	0.0190
Q=0.005	0.04839	0.0219	0.0102	0.0190	0.0161
Q=0.01	0.4693	0.0132	0.0161	0.013	0.0219
Q=0.02	0.04927	0.016	0.0219	0.0249	0.0261
Q=0.05	0.4781	0.0453	0.0390	0.0161	0.0232

Table 4.8 Mixing index (*MI*) during experimental test in Tear-drop micromixer.

MI	0 mm	5 mm	10 mm	15 mm	20 mm
Q=0.001(ml/min)	0.09635	0.0249	0.0278	0.0219	0.0295
Q=0.005	0.9664	0.0365	0.0278	0.0365	0.0307
Q=0.01	0.9430	0.0519	0.0378	0.031	0.0365
Q=0.02	0.9839	0.0607	0.0449	0.0453	0.0349
Q=0.05	0.9518	0.0833	0.0607	0.0507	0.0365

Table 4.9 Mixing efficiency (η) in Tear-drop -micromixer.

η	0 mm	5 mm	10 mm	15 mm	20 mm
Q=0.001(ml/min)	0.0424	0.9781	0.9751	0.9785	0.9822
Q=0.005	0.0365	0.9635	0.97	0.9635	0.9722
Q=0.01	0.0629	0.9481	0.9622	0.96	0.9635
Q=0.02	0.0161	0.9393	0.9522	0.9547	0.9651
Q=0.05	0.0482	0.91	0.9393	0.94	0.9635

As a good example to show the performance of the Tear-drop mixer , figure 4.11 shown the probability distribution function at Re=4.166 in two region: (a) in the entrance region and; (b) after 5 mm from inlet region and also figure 4.12 illustrated the variance, mixing index and efficiency of mixing in two mentioned regions.

As can be seen in the figure 4.12, after 5 mm the efficiency of the mixing is 91% (over 80%) and mixing is completed. This is a particular good result for mixing process at high Reynolds number. Because with this property the length of the micromixer can reduce and also the pressure drop will be decreased (discussed in chapter 5).

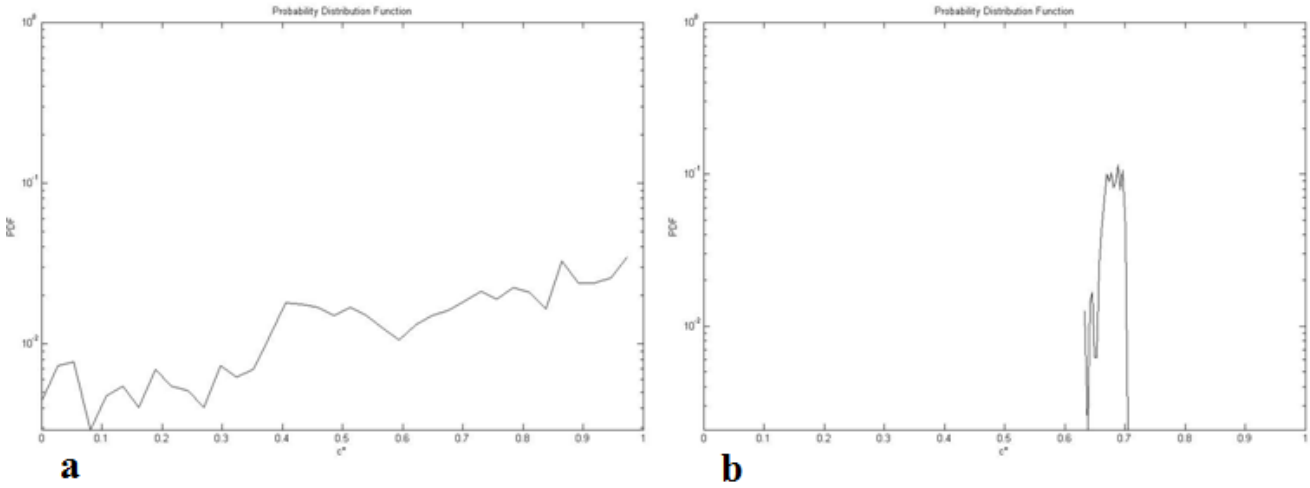

Figure 4.11 PDF in Tear-drop micromixer at Re = 4.166: (a) entrance region; (b)after 5 mm.

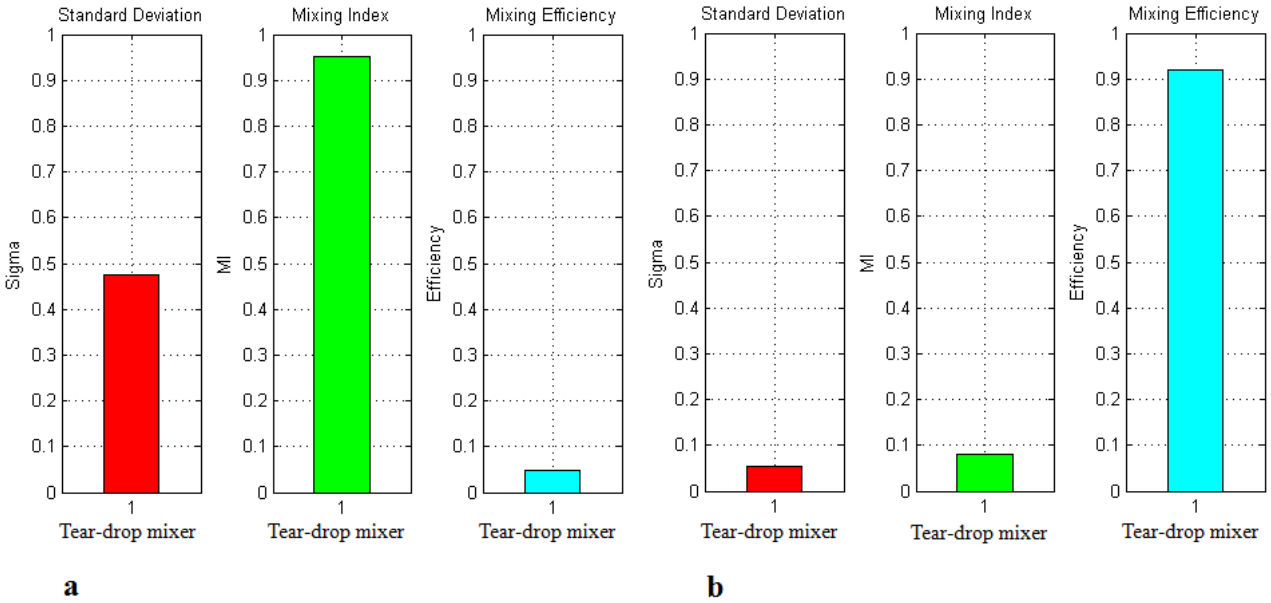

Figure 4.12 Tear-drop micromixer analysis at Re = 4.166:(a) entrance region; (b) after 5 mm.

Comparison of mixing efficiency during the Tear-drop microchannel is depicted in figure 4.13. Figure 4.13 illustrates efficiency versus Reynolds number in Tear-drop micromixer. As the diagram shows, in all of the tested Reynolds numbers, the efficiency is over 90% and are acceptable for mixing process. Also efficiency decreases as Reynolds number increases and vice versa. Minimum value of efficiency is 91% and occurs at the highest tested Reynolds number (Re=4.166) after 5 mm from inlet region and maximum value of efficiency is up to 98% and occurs at the lowest Reynolds number (Re=0.083) at the outlet of the micromixer.

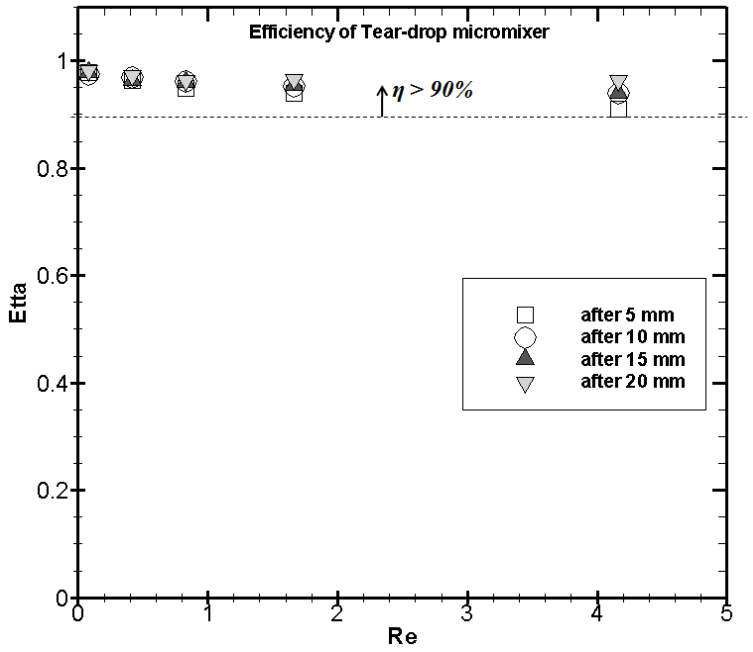

Figure 4.13 Comparison of η versus Re during Tear-drop micromixer.

Hence, this kind of micromixer is useful for passive mixing processing.

4.5.1 Comparison of Tear-drop micromixer with T- and O-micromixers

Results of experimental tests on the Tear-drop micromixer and comparison of mixing efficiency with T- and O-mixer are illustrated in this paragraph. Figure 4.14 depicts the mixing process through the microchannels in T-, O- and Tear-drop micromixers.

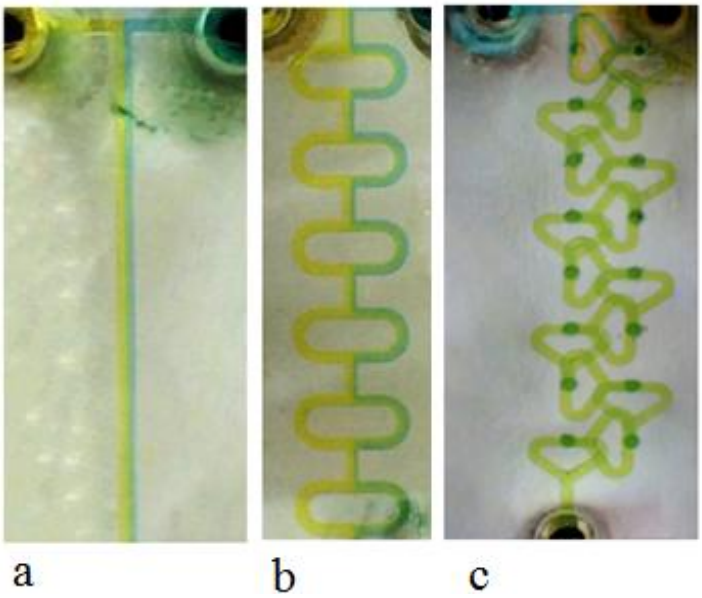

Figure 4.14 Comparison of η by visualization: (a) T- mixer; (b)O-mixer; (c) Tear-drop mixer.

After the mixing process was visualized as shown in the figure 4.14, mixing efficiencies for all micromixers were calculated and compared. As can be seen visually, the Tear-drop mixer is more efficient than the other prototypes in all regions of interest. Figure 4.15 shown the Tear-drop mixer during experimentation. It depicts visually (figure 4.15 part c), in few distance from inlet (after 5mm), mixing process is completed.

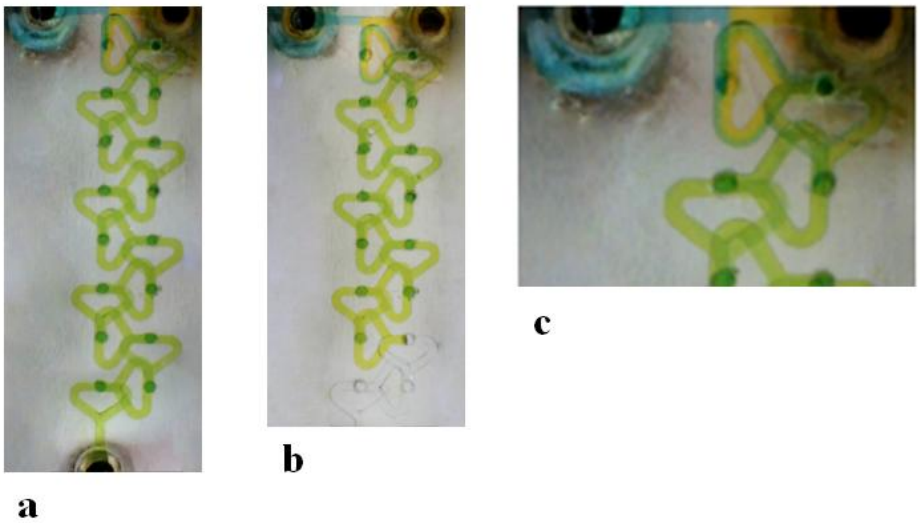

Figure 4.15 Tear-drop micromixer during test.

Also figure 4.16 shows that at Re=0.083 the T- and O-mixer's efficiency is 0% and 22% respectively, which is not acceptable for mixing processes, whereas the efficiency of the Tear-drop mixer is up to 98%.

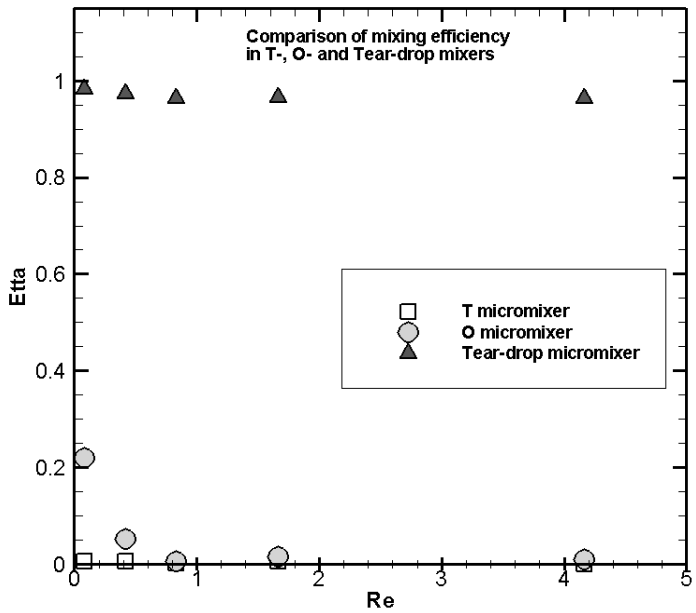

Figure 4.16 Comparison of mixing efficiency in T-, O- and Tear-drop micromixers at outlet region.

A comparison of the Tear-drop mixer's efficiency at Re=4.166 also indicates that fluids are well mixed at this Reynolds number, and that it is possible to increase the flow rate to achieve complete mixing rapidly.

This capability is significant for micromixer design, as this device requires special geometry since it cannot rely on turbulence flow to enhance mixing performance.

As the diagrams show, efficiency of the T- and O-mixers is less than 80% for $1 \leq Re \leq 4.66$, which is not acceptable for mixing processes. In the Tear-drop mixer, however, the fluids are well mixed even for $1 \leq Re \leq 4.66$. Rapid mixing is thus possible in this kind of geometry, and complete mixing as seen to take place in this prototype.

4.6 H-micromixer analyze

This type of passive micromixer is based on the SAR process meaning that the two fluids to be mixed are split and recombined to optimize the diffusion process. In this case, the H-shape makes it possible to move part of the flow near the wall, in the central zone of the channel along the axial direction and vice versa. The H-micromixer has been designed and constructed from plexiglas using a computer milling process. Design and a photograph of the prototype are shown in figure 4.17.

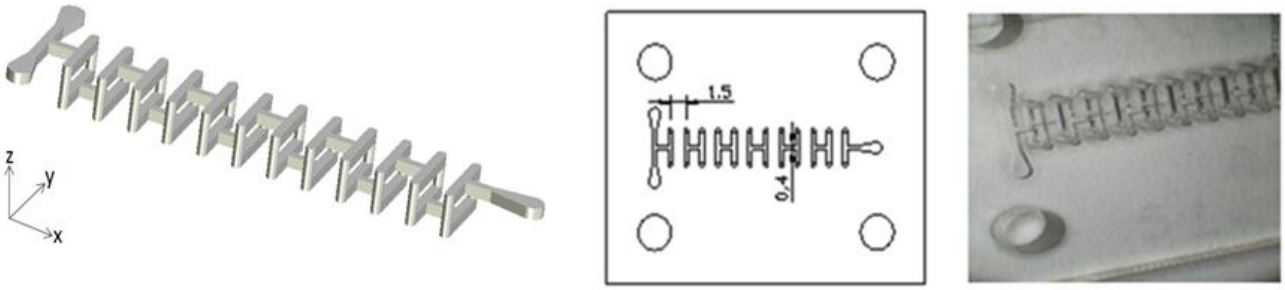

Figure 4.17 H-micromixer.

As illustrated in figure 4.17, the H-micromixer geometry consists of two parts: the straight channel and the H-segment and the flow follows a 3D path. During the mixing process, several pictures were taken with the microscope from the entrance area to the end of the channel. This was repeated for all Reynolds numbers used in this study. As an example, H-micromixer during the experimentation at Re=4.166 is shown is figure 4.18 step by step from the inlet region to the end of the microchannel. It is obvious after a few distance from inlet region, mixing is complete.

In fact, in figure 4.18 after part 4 mixing efficiency is completed and it is recognizable by visualization.

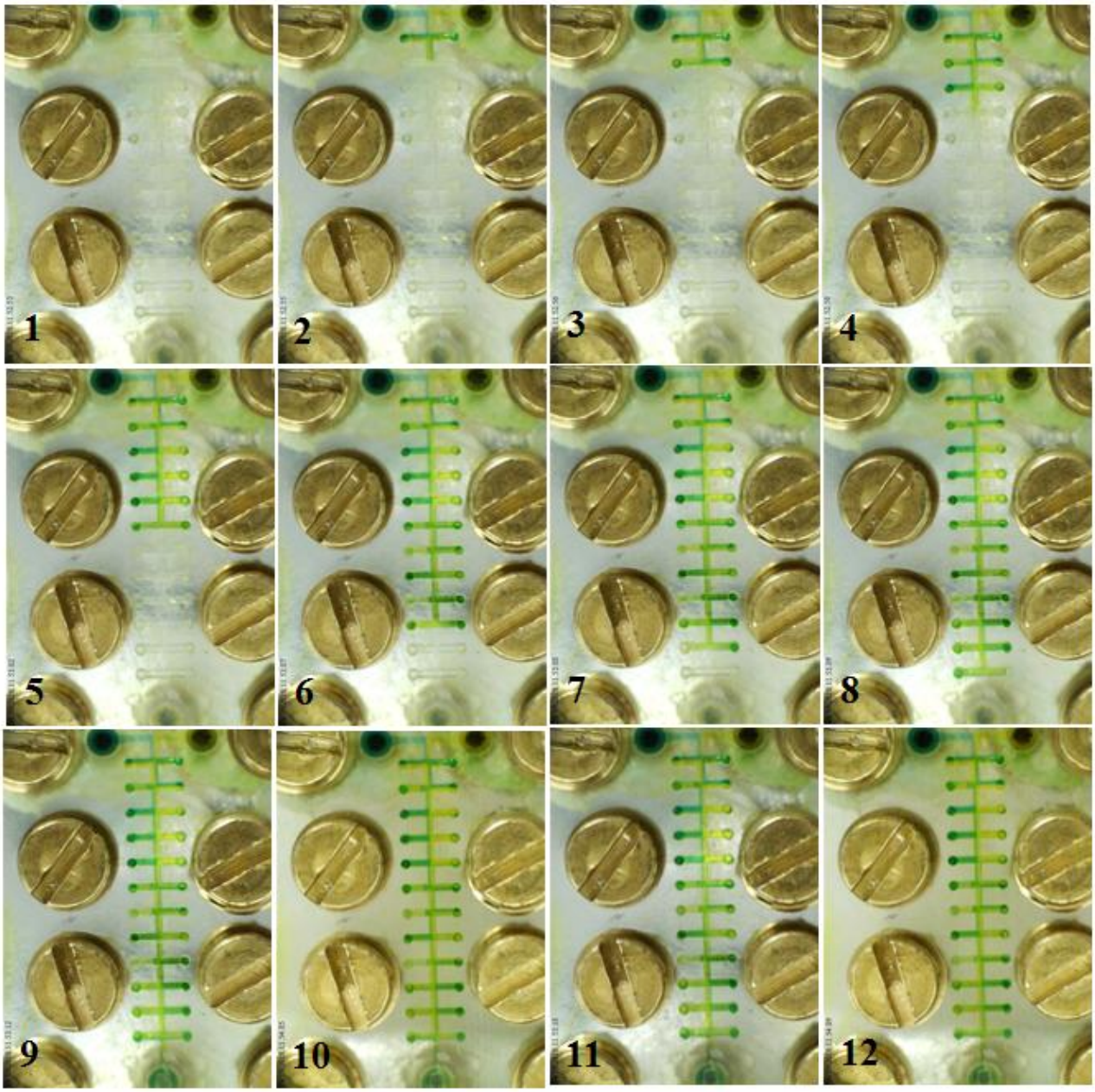

Figure 4.18 H-micromixer during the test at Re=4.166.

Results of experimental survey of the H- micromixer are presented below. Tables 4.10, 4.11 and 4.12 illustrate the standard deviation of concentration (σ), Mixing Index (MI) and efficiency of mixing (η) in H-microchannel respectively. Therefore, Image-based techniques were used to evaluate the mixing performance of the prototypes, and the gray scale value was applied for post processing.

Table 4.10 Standard deviation of concentration (σ) during experimental investigation in H-micromixer.

σ	0 mm	5 mm	10 mm	15 mm	20 mm
Q=0.001(ml/min)	0.4777	0.0044	0.0102	0.0161	0.0073
Q=0.005	0.4985	0.0307	0.0219	0.0102	0.0219
Q=0.01	0.4882	0.0599	0.0424	0.0132	0.01
Q=0.02	0.455	0.0388	0.0287	0.0336	0.0132
Q=0.05	0.46	0.0541	0.0355	0.0482	0.0424

Table 4.11 Mixing index (*MI*) during experimental test in H-micromixer.

MI	0 mm	5 mm	10 mm	15 mm	20 mm
Q=0.001(ml/min)	1	0.0102	0.0132	0.01	0.010
Q=0.005	0.9985	0.0365	0.0336	0.0132	0.02
Q=0.01	0.98	0.0892	0.0570	0.0219	0.025
Q=0.02	1	0.1	0.0736	0.0453	0.0335
Q=0.05	1	0.0863	0.0988	0.0858	0.0770

Table 4.12 Mixing efficiency (η) in H-micromixer.

η	0 mm	5 mm	10 mm	15 mm	20 mm
Q=0.001(ml/min)	0	0.9898	0.9898	0.99	0.99
Q=0.005	0.0015	0.9605	0.9664	0.9781	0.98
Q=0.01	0.0132	0.9108	0.9430	0.9751	0.97
Q=0.02	0	0.90	0.9264	0.9576	0.96
Q=0.05	0	0.91	0.9012	0.9142	0.923

Figures 4.19 illustrates the probability distribution function in terms of concentration after 5 mm from the entrance region in H-micromixer at Q=0.001 ml/min (Re=0.083). Also figure 4.20 shows the mixing efficiency in H-micromixer at the same Reynolds number. As can be seen also visually in the figure 4.18, in the outlet of the H-micromixer, there is one color (green color). It shows that the mixing process is completed in this type of microchannel. Mixing efficiency at the end of the H –shaped microchannel at Re=0.083 is up to 99% and this is a specific result for the new geometry (H-micromixer). Also the efficiency at Re=4.166 (highest Reynolds number) is 92% which shows that it could be possible to increase the Reynolds number for rapid mixing.

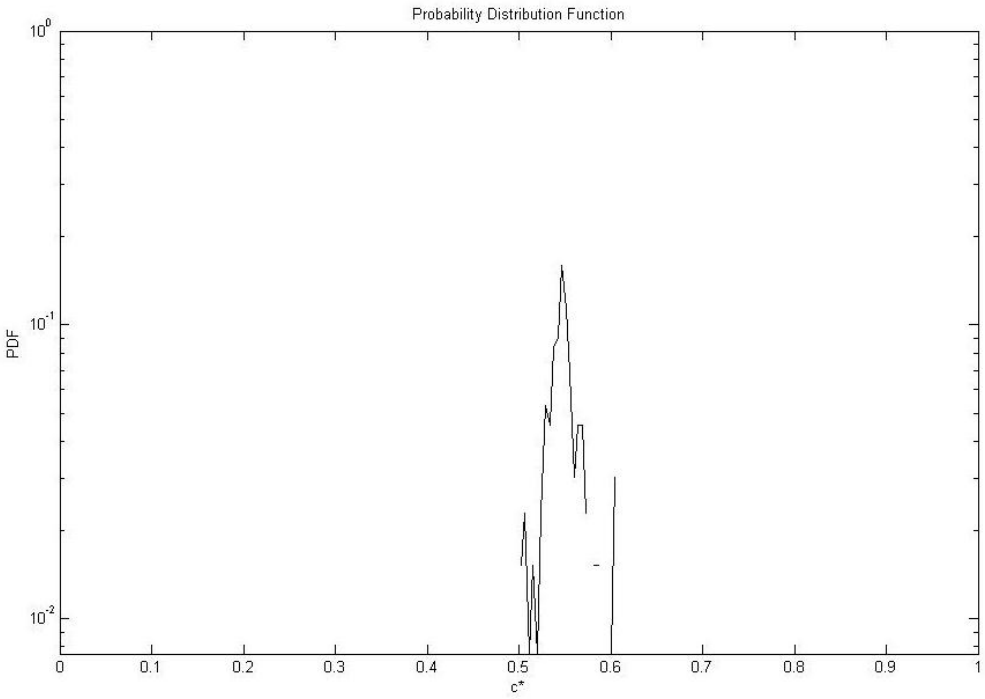

Figure 4.19 PDF in H-micromixer at Re = 0.083, after 5 mm.

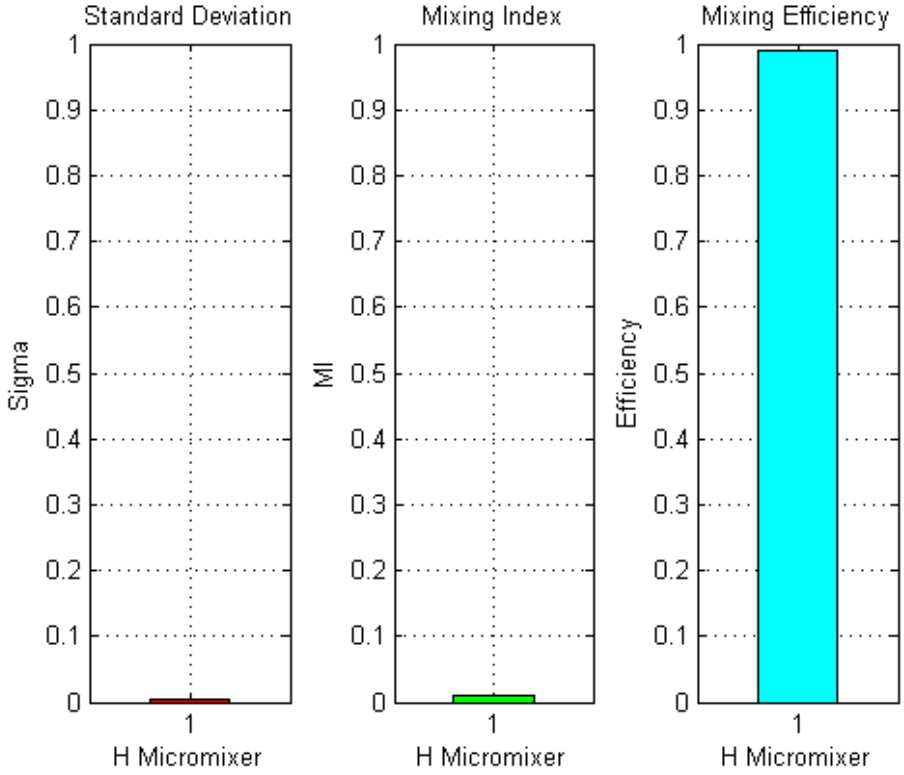

Figure 4.20 H-micromixer analysis, Re = 0.083, after 5 mm.

Comparison of mixing efficiency during the H-microchannel is depicted in figure 4.21.

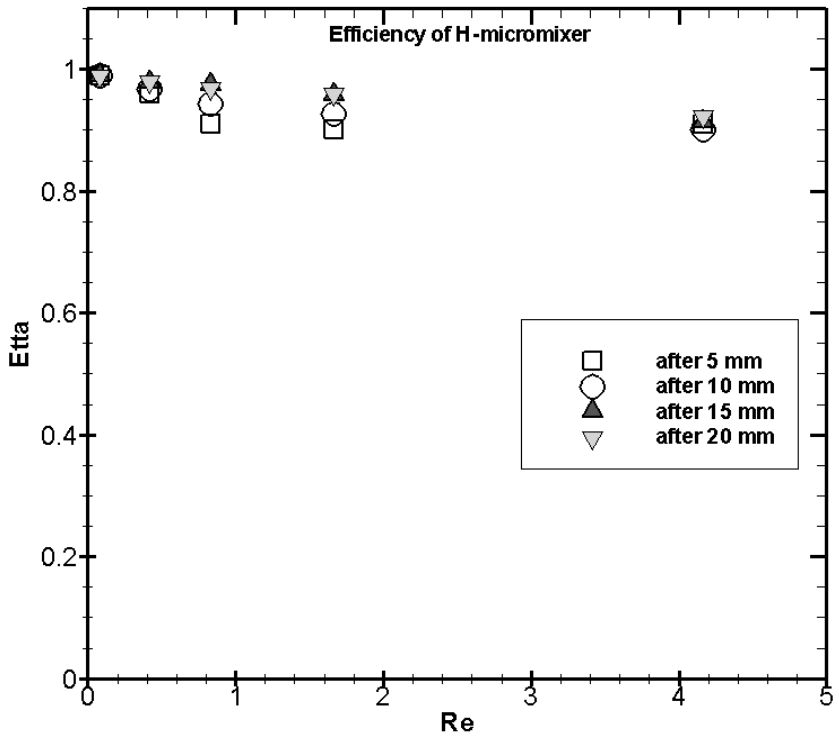

Figure 4.21 Comparison of η versus Re during H-micromixer.

Figure 4.21 illustrates efficiency versus Reynolds number in H-shaped sub-channel. As the diagram shows, in all of the tested Reynolds numbers, the efficiency is over 90% and are acceptable for mixing process. Minimum value of efficiency is 90% and occurs at the highest tested Reynolds number (Re=4.166) after 5 mm from inlet region and maximum value of efficiency is up to 99% and occurs at the lowest Reynolds number (Re=0.083) at the outlet of the micromixer. Also efficiency decreases as Reynolds number increases and vice versa.

4.6.1 Comparison of H-micromixer with T- and O-micromixers

Results of experimental tests on the H-micromixer and comparison of mixing efficiency with T- and O-mixers are illustrated in this paragraph. Figure 4.22 shows the mixing process through the microchannels in T-, O- and H-micromixers. It is obvious that in the H-shaped sub-channel there is only one color (green color) which is why the mixing process is well-done, but in the T- and O-mixers there are two separate color (yellow and blue) which shows that mixing does not occur or the degree of mixing in very low (poor mixing). Concentration based analysis is the most reputable and trustworthy method of investigating and evaluating mixing efficiency.

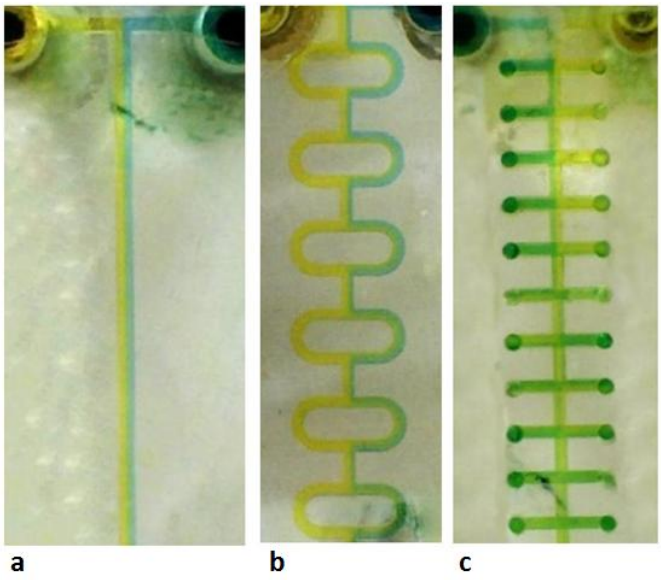

Figure 4.22 Comparison of η by visualization: (a) T- mixer; (b)O-mixer; (c) H-mixer.

By improving concentration image analysis, the detailed process taking place in the microchannel can be investigated. When flow is not in the turbulent regime, it is essential to observe changes in concentration through the channel to understand mixing performance. Figure 4.23 depicts the efficiency comparison between H-, O- and T-micromixers.

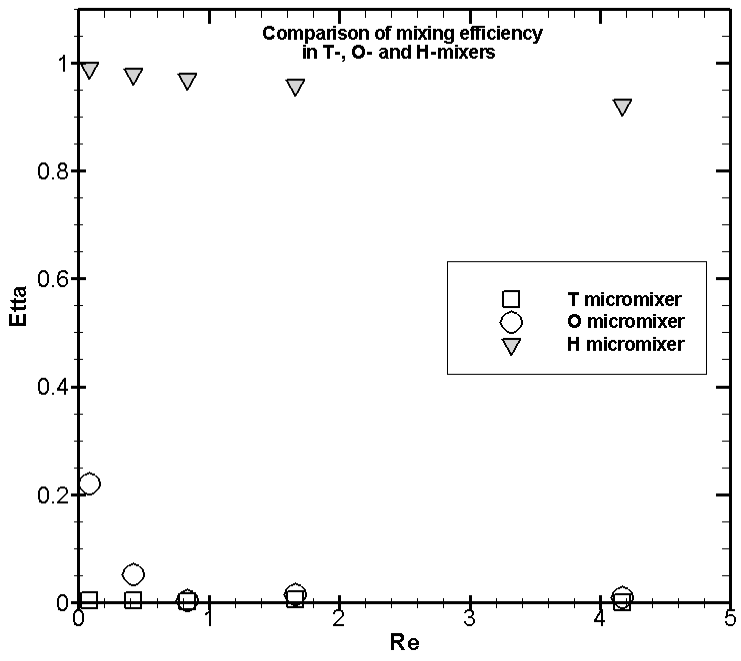

Figure 4.23 Comparison of mixing efficiency in T-, O- and H-micromixers at outlet region.

As figure 4.23 shows, H-mixer efficiency is up to 99% at *Re*= 0.083, the best result among mentioned prototypes and tested Reynolds numbers.

Also figure 4.23 shows that the H-micromixer's mixing efficiency is significantly higher than that of the T- and O-micromixers at all tested Reynolds numbers and regions. This capability is significant for micromixer design, as this device requires special geometry since it cannot rely on turbulence flow to enhance mixing performance. Figure 4.23 illustrates the optimum condition (maximum efficiency) among tested Reynolds numbers, indicating that the H-mixer's mixing efficiency is up to 99% . As the diagram shows, the O-mixer is more efficient than the T-mixer, but still the mixing efficiency is not acceptable ($\eta < 80\%$) in both O- and T-mixers. As can be seen, the H-mixer is more efficient than the O- and T-mixers at all tested *Re* numbers and the highest efficiency at *Re*=0.083 is achieved by the H-micromixer.

4.7 Chain micromixers

This study introduces a novel generation of 3D splitting and recombination (SAR) passive micromixer with microstructures placed on the top and bottom floors of microchannels called ''*Chain mixer*''. Both experimental verification and numerical analysis (discussed in chapter 5) of the flow structure of this type of passive micromixer have substantiated to evaluate the mixing performance and pressure drop (chapter 5) of the microchannel respectively. We propose here Chain micromixers of four types: Chain 1-, Chain 2-, Chain 3-, and Chain 4- and compare their mixing performance and pressure drop (discussed in chapter 5) with other micromixers, T-, o- , H- and Tear-drop micromixers. Like previous micromixers, experimental tests carried out in the laminar flow regime with a low Reynolds number range, $0.083 \leq Re \leq 4.166$, and image-based techniques are used to evaluate mixing efficiency. Also, CFD code, ANSYS FLUENT-13.0 has been used (chapter 5) to analyze the flow and pressure drop in the microchannel.

4.7.1 Chain 1-micromixer analyze

A novel generation of 3D passive micromixer concept is introduced. This type of micromixer called the ''Chain micromixer'' which is based on the SAR process, meaning that the two fluids to be mixed are split and recombined to optimize the diffusion process. The main working principle for this type of microchannel is to make 90º rotation of a flow, folding the stream and then split and recombine the flow to enhance the efficiency of the microchannel. This process is repeated during the microchannel until achieving the desired degree of mixing. First, Chain 1-micromixer was designed and fabricated from plexiglas using a computer milling process. As mentioned before, the prototypes were fabricated in I.T.D S.n.c. di Depaoli S. & C. (Turin, Italy) using CNC Milling and

Engraving Machine P20 S, KUNLMANN (Germany). As illustrated in figure 4.24 (a), the flow follows a 3D path along the microchannel.

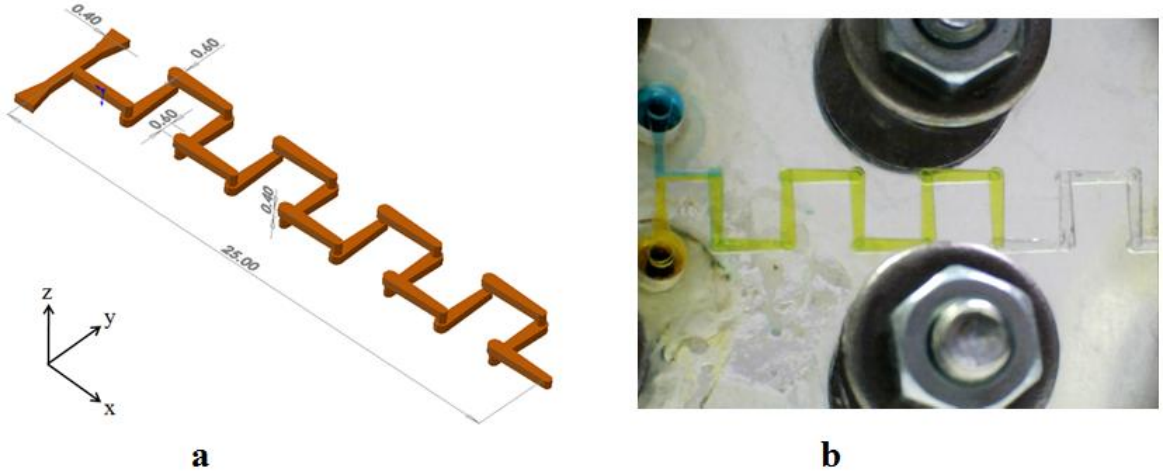

Figure 4.24 Chain 1-micromixer: (a) design of Chain1-micromixer; (b)during the experimentation.

During the mixing process, several pictures were taken with the microscope from the entrance area to the end of the channel. As a good example, figure 4.25 shows the filling of the Chain 1-mixer step by step at Re=0.832 and it can be seen the stage of filling and performance of this type of micromixer visually.

Figure 4.25 Chain 1-micromixer during the test at Re=0.832.

Results of experimental investigation of the Chain 1- micromixer are presented below. Therefore, Image-based technique was used to evaluate the mixing performance of the prototype, and the gray scale value was applied for post processing. Tables 4.13, 4.14 and 4.15 illustrate the standard deviation of concentration (σ), Mixing Index (MI) and efficiency of mixing (η) in Chain 1-microchannel respectively.

Table 4.13 Standard deviation of concentration (σ) during experimental investigation in Chain 1-micromixer.

σ	0 mm	5 mm	10 mm	15 mm	20 mm
Q=0.001(ml/min)	0.4868	0.0132	0.0132	0.0190	0.0185
Q=0.005	0.48	0.0232	0.0190	0.0179	0.0073
Q=0.01	0.4693	0.0249	0.0161	0.0190	0.0290
Q=0.02	0.4576	0.0336	0.0249	0.0102	0.0278
Q=0.05	0.4927	0.0440	0.0307	0.0120	0.0220

Table 4.14 Mixing index (MI) during experimental test in Chain 1-micromixer.

MI	0 mm	5 mm	10 mm	15 mm	20 mm
Q=0.001(ml/min)	0.9693	0.0219	0.0161	0.0295	0.0236
Q=0.005	0.9751	0.0290	0.0249	0.0278	0.0365
Q=0.01	0.9313	0.0524	0.0349	0.0307	0.0440
Q=0.02	0.9137	0.0612	0.0495	0.0361	0.0453
Q=0.05	0.9810	0.0582	0.0482	0.0361	0.0419

Table 4.15 Mixing efficiency (η) in Chain 1-micromixer.

η	0 mm	5 mm	10 mm	15 mm	20 mm
Q=0.001(ml/min)	0.0307	0.9781	0.9810	0.9793	0.9851
Q=0.005	0.0278	0.9610	0.9622	0.9693	0.9635
Q=0.01	0.0687	0.9476	0.9595	0.9690	0.9560
Q=0.02	0.0863	0.9359	0.9505	0.9612	0.9547
Q=0.05	0.0190	0.9388	0.9518	0.9606	0.9522

Figures 4.26 illustrates the probability distribution function in terms of concentration after 5 mm from the entrance region in Chain 1-micromixer at Q=0.01 (Re=0.832). Also figure 4.27 shows the mixing efficiency in Chain 1-micromixer at the same Reynolds number.

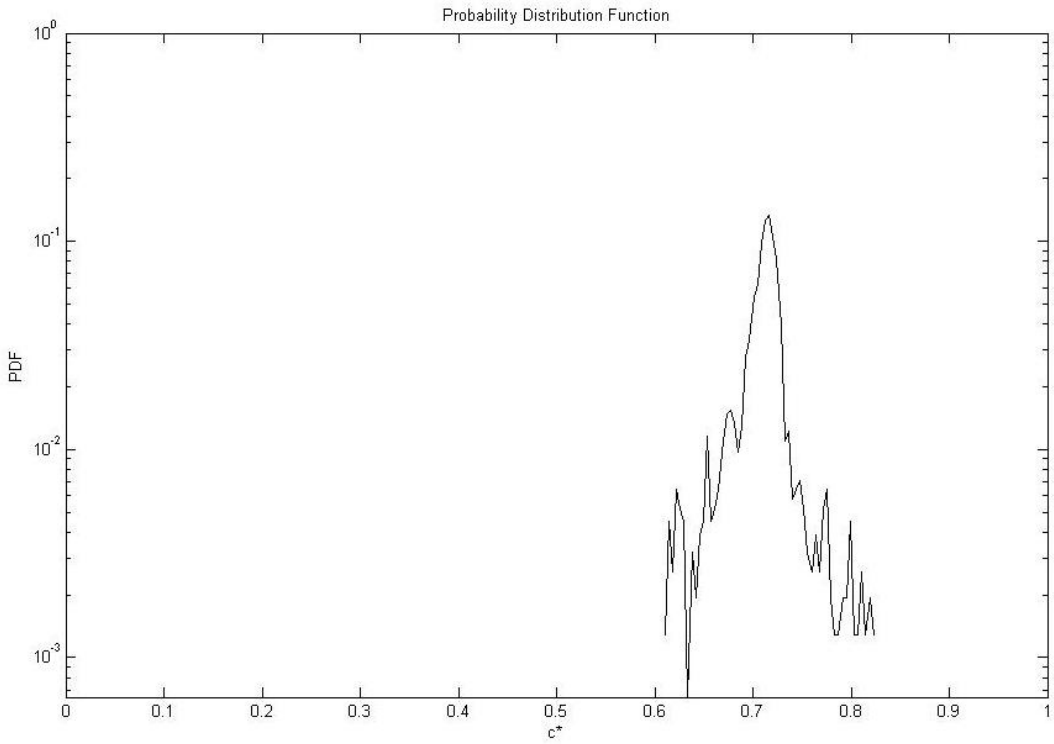

Figure 4.26 PDF in *Chain 1-micromixer* at Re = 0.832, after 5 mm.

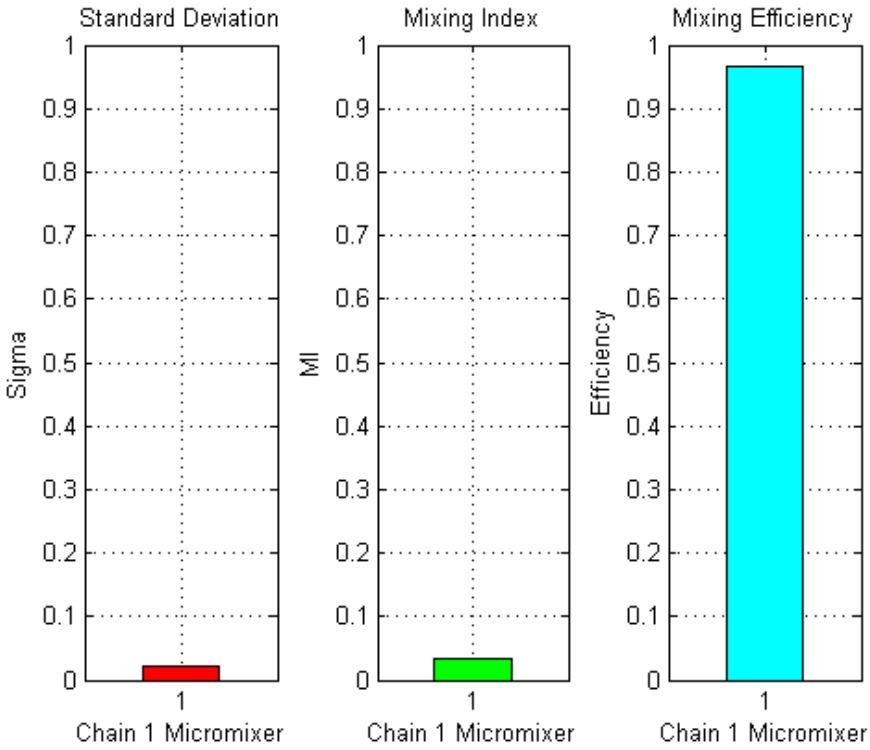

Figure 4.27 Chain 1-micromixer analysis, Re = 0.832, after 5 mm.

As can be seen also visually in the figure 4.25, after 5 mm from inlet region and also in the outlet of the Chain 1-micromixer, there is only one color (green color). It shows that the mixing is completed

in this type of microchannel. Mixing efficiency at the end of the Chain 1-microchannel at Re=0. 832 is up to 95% and this is a particular good result for the new geometry (Chain 1-micromixer) at this Reynolds number. Also the efficiency at Re=4.166 (highest Reynolds number) is 95% which shows that it could be possible to increase the Reynolds number for rapid mixing.
Comparison of mixing efficiency during the Chain 1-microchannel is depicted in figure 4.28.

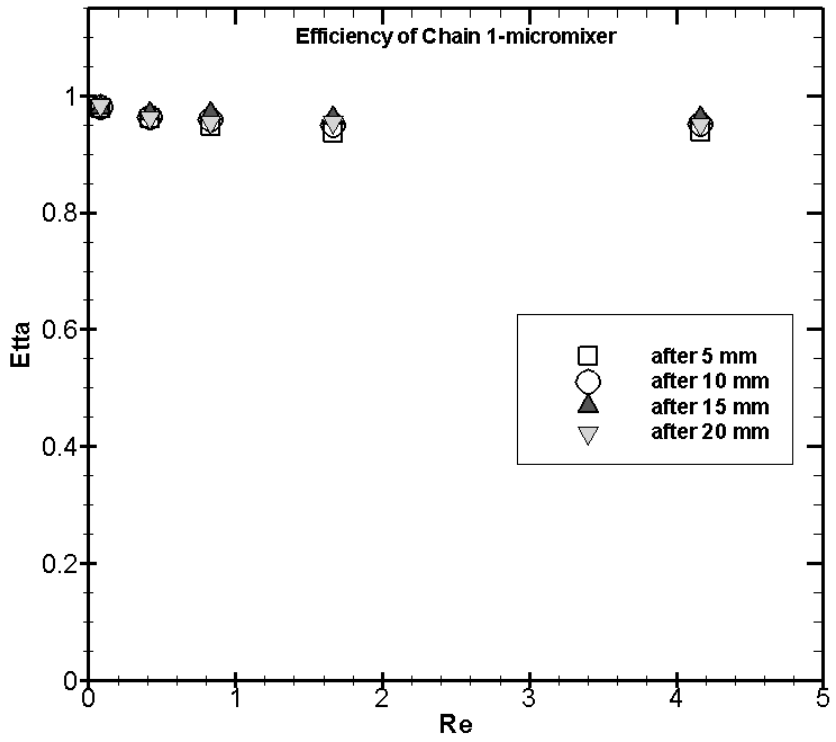

Figure 4.28 Comparison of η versus Re during Chain 1-micromixer.

Figure 4.28 illustrates efficiencies versus tested Reynolds numbers in Chain 1- mixer. As the diagram shows, in all of the tested Reynolds numbers, the efficiency is over 90% and are acceptable for mixing process. Minimum value of efficiency is 93% and occurs at the highest tested Reynolds number (Re=4.166) after 5 mm from inlet region and maximum value of efficiency is up to 98% and occurs at the lowest Reynolds number (Re=0.083) at the outlet of the micromixer. Also diagram shows the efficiency decreases as Reynolds number increases and vice versa.

4.7.2 Chain 2-micromixer analyze

Figure 4.29 illustrates the Chain 2 mixer which differs only by one parameter from the Chain 1 mixer. As shown in figure 4.29, after each vertical part (z direction), the diameter of the new section is 0.8 mm and extended 0.4 mm rather than the outlet of vertical part (0.4 mm).

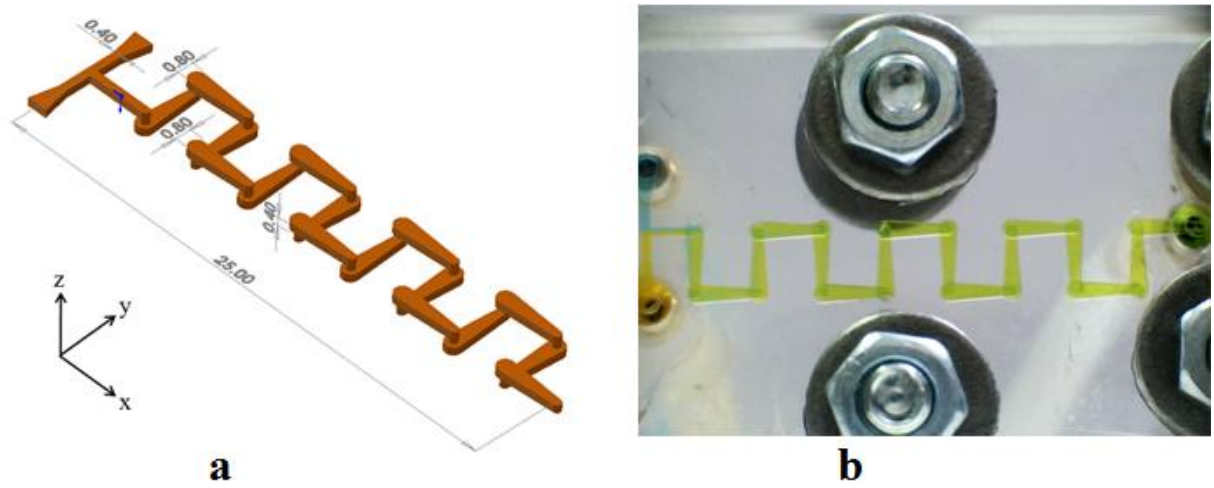

Figure 4.29 Chain 2-micromixer: (a) design of Chain2-micromixer; (b)during the experimentation.

Like Chain 1-micromixer, the main working principle for this type of microchannel is also to make 90º rotation of a flow, folding the stream and then split and recombine the flow to enhance the efficiency of the microchannel.

Figure 4.30 Chain 2-micromixer during the test at Re=0.416.

This process is repeated during the microchannel. Chain 2-micromixer was designed and fabricated from plexiglas using a computer milling process. As illustrated in figure 4.29 (a), the flow follows a 3D path along the microchannel. As an example, figure 4.30 illustrates the filling of the Chain 2-mixer step by step at Re=0.416 and it can be seen the stage of filling and performance of this type of micromixer visually. Results of experimental investigation of the Chain 2- micromixer are presented in tables 4.16, 4.17 and 4.18.

Table 4.16 Standard deviation of concentration (σ) during experimental investigation in Chain 2-micromixer.

σ	0 mm	5 mm	10 mm	15 mm	20 mm
Q=0.001(ml/min)	0.49	0.0073	0.0190	0.0102	0.0161
Q=0.005	0.48	0.0307	0.0278	0.0102	0.0132
Q=0.01	0.4768	0.0336	0.0161	0.0219	0.0190
Q=0.02	0.4710	0.0349	0.0249	0.0229	0.0249
Q=0.05	0.4985	0.0365	0.0219	0.0361	0.0278

Table 4.17 Mixing index (*MI*) during experimental test in Chain 2-micromixer.

MI	0 mm	5 mm	10 mm	15 mm	20 mm
Q=0.001(ml/min)	0.9898	0.0102	0.0336	0.0249	0.0307
Q=0.005	0.9810	0.0582	0.0482	0.0361	0.0261
Q=0.01	0.9693	0.770	0.0519	0.0424	0.0407
Q=0.02	0.9605	0.0853	0.0436	0.05	0.0512
Q=0.05	0.9985	0.09012	0.0636	0.0649	0.0553

Table 4.18 Mixing efficiency (η) in Chain 2-micromixer.

η	0 mm	5 mm	10 mm	15 mm	20 mm
Q=0.001(ml/min)	0.0102	0.9664	0.9722	0.9781	0.9898
Q=0.005	0.0219	0.9388	0.9488	0.9668	0.9768
Q=0.01	0.0307	0.9230	0.9522	0.9576	0.9590
Q=0.02	0.0365	0.9188	0.95564	0.95	0.9488
Q=0.05	0.0044	0.9001	0.9364	0.93	0.9447

Probability distribution function versus concentration is shown in figure 4.31 after 10 mm from the entrance region in Chain 2-micromixer at Q=0.005 ml/min (Re=0.416). Also figure 4.32 shows the mixing efficiency in Chain 2-micromixer at the same Reynolds number.

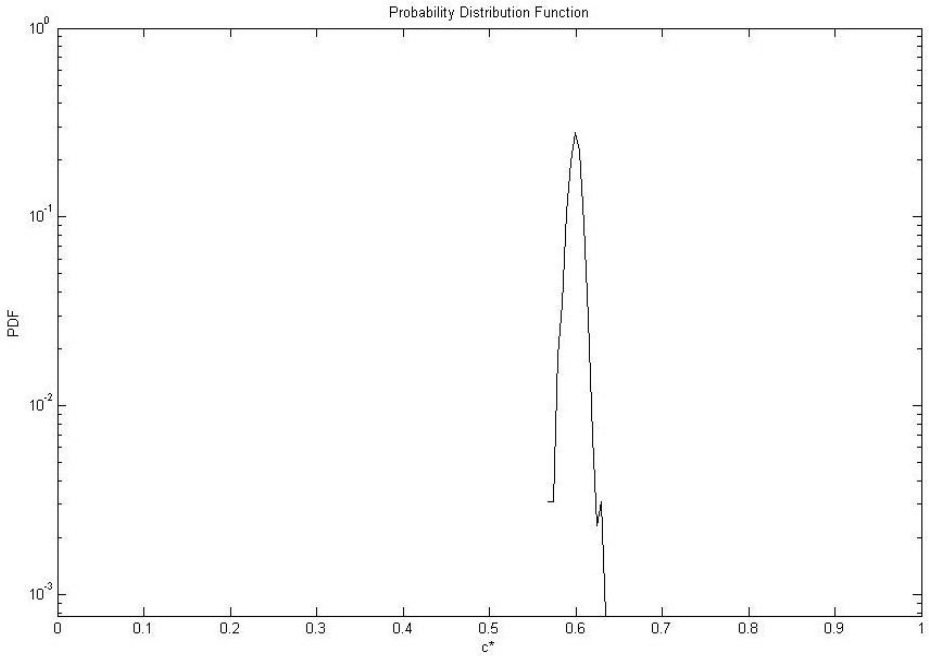

Figure 4.31 PDF in *Chain 1-micromixer* at Re = 0.832, after 5 mm.

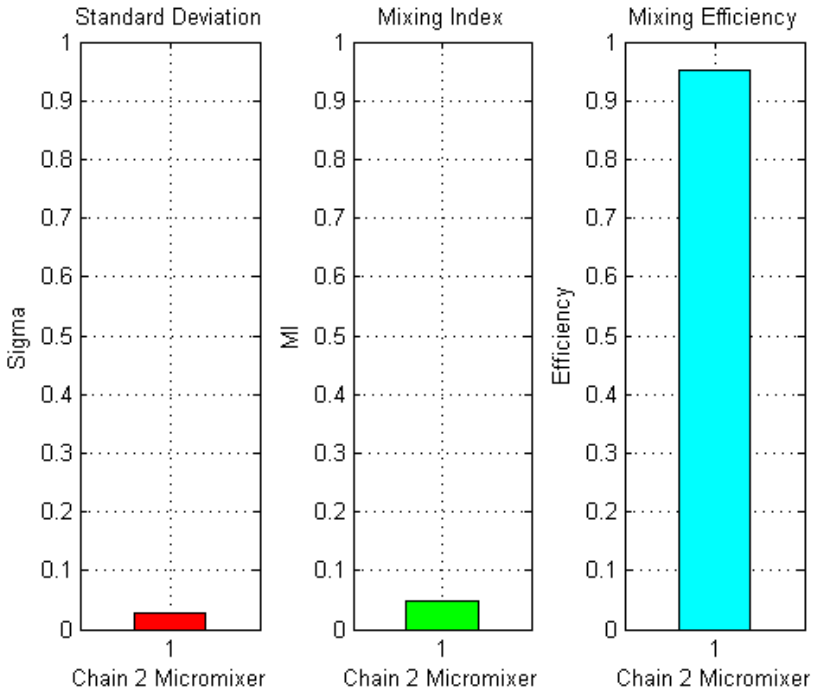

Figure 4.32 Chain 2-micromixer analysis, Re = 0.416, after 10 mm.

As can be seen visually in the figure 4.30, after 5 mm from inlet region in Chain 2-micromixer, there is only one color (green color). It shows that the mixing is completed in this type of microchannel. Mixing efficiency at the end of the Chain 2-microchannel at Re=0. 416 is up to 97% and this is a particular good result for the new geometry (Chain 2-micromixer) at this Reynolds number. Also the efficiency at Re=4.166 (highest Reynolds number) is 94% (η > 80%)which shows that it could be possible to increase the Reynolds number for rapid mixing in this prototype.
Comparison of mixing efficiency during the Chain 2-microchannel is depicted in figure 4.33.

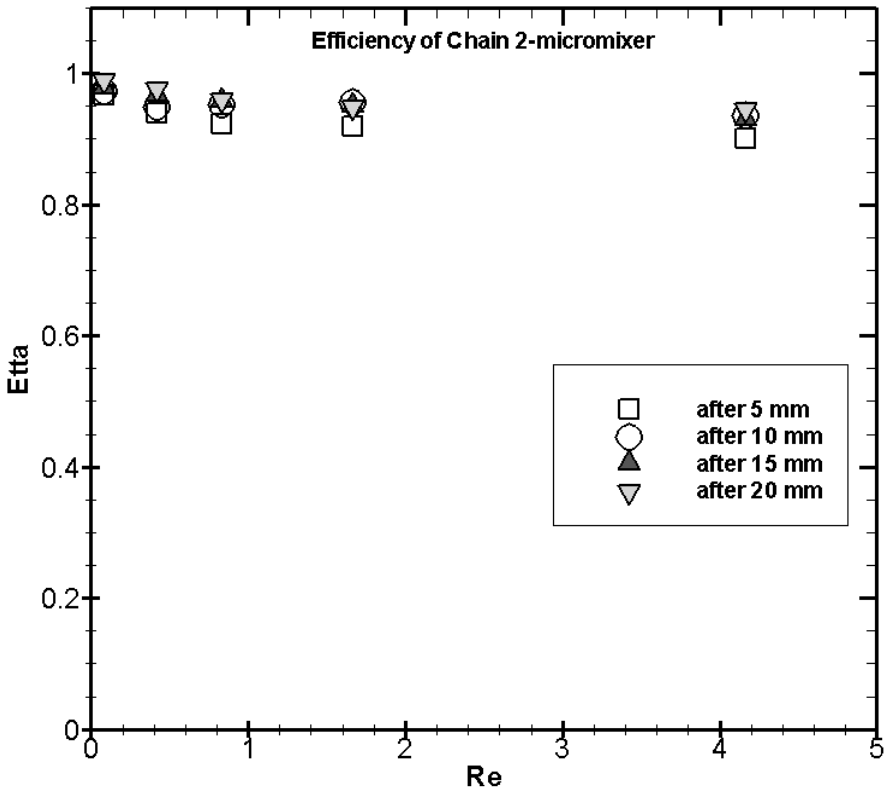

Figure 4.33 Comparison of η versus Re during Chain 2-micromixer.

As the diagram shows, in all of the tested Reynolds numbers, the efficiency is over 90% and are acceptable for mixing process. Also diagram shows the efficiency decreases as Reynolds number increases and vice versa.

4.7.3 Chain 3-micromixer analyze

To compare the effect on the number of splitting and recombination in Chain micromixers, chain 3 is designed.

As shown in figure 4.34, after each vertical part (z direction), the diameter of the new section is 0.6 mm (like Chain 1) and extended 0.2 mm rather than the outlet of vertical part (0.4 mm).

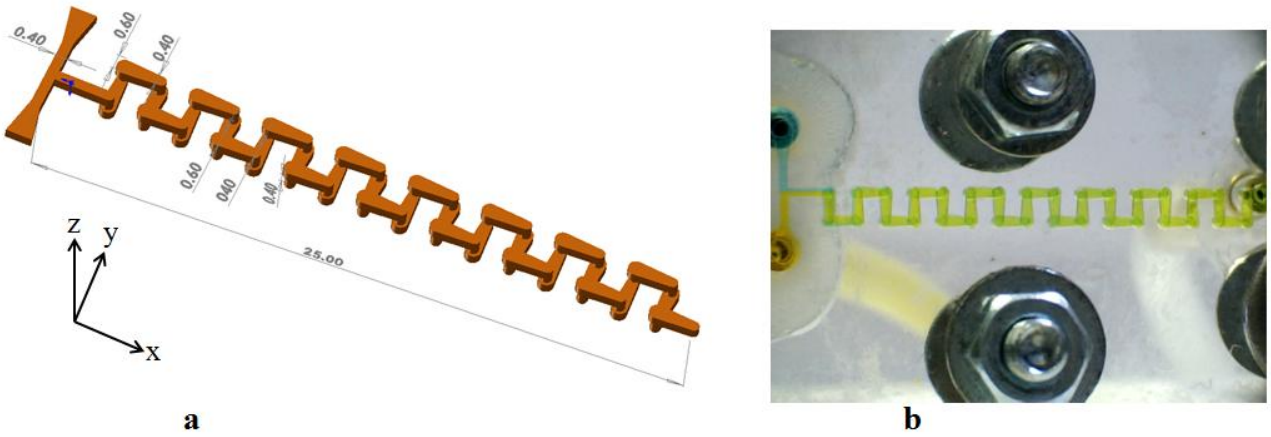

Figure 4.34 Chain 3-micromixer: (a) design of Chain3-micromixer; (b)during the experimentation.

Like Chain 1-micromixer, the main working principle for this type of microchannel is also to make

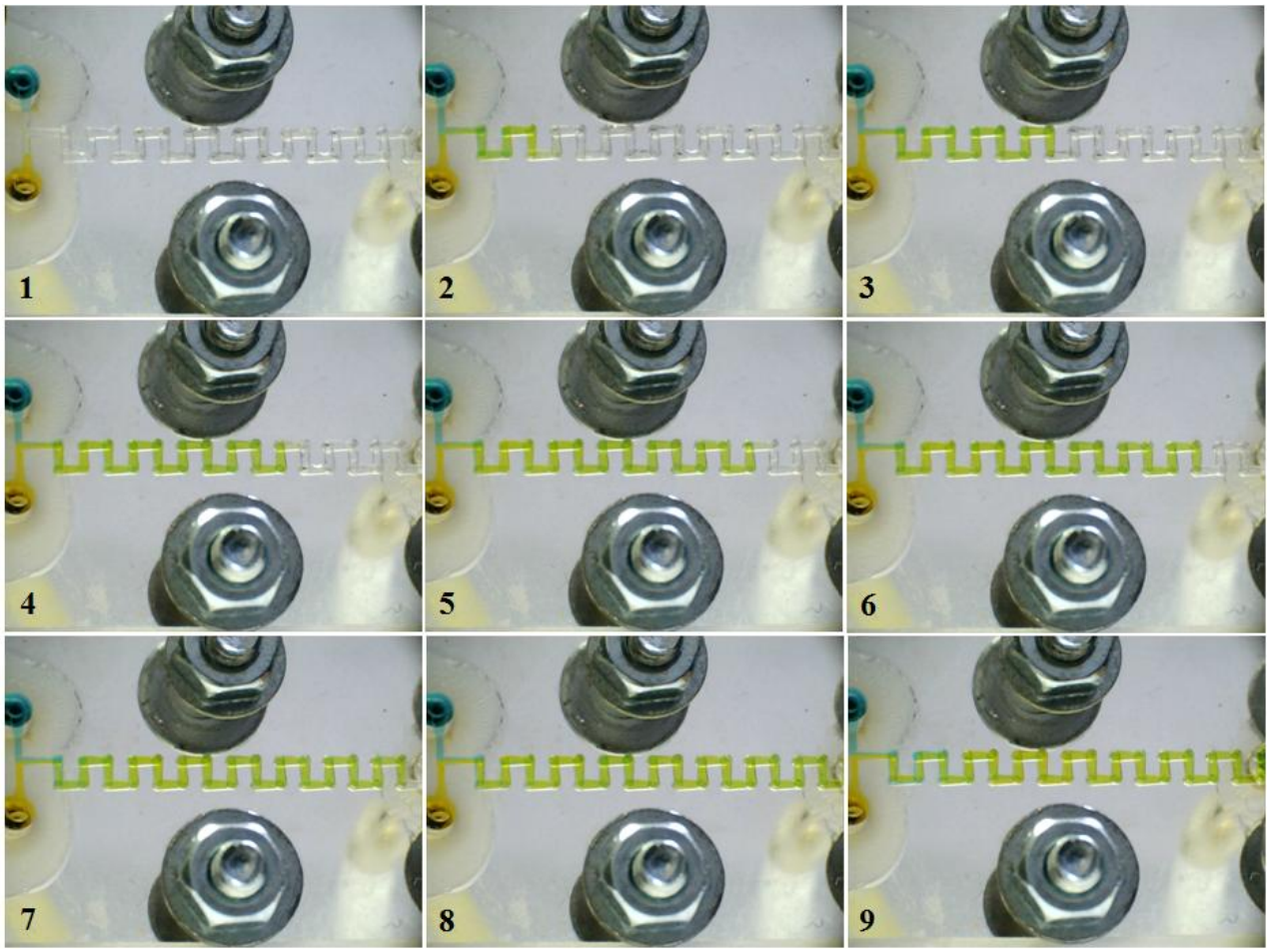

Figure 4.35 Chain 3-micromixer during the test at Re=4.166.

90º rotation of a flow, folding the stream and then split and recombine the flow to enhance the efficiency of the microchannel. This process is repeated along the microchannel length. Chain 3-micromixer is fabricated from plexiglas using a computer milling process. As illustrated in figure 4.34 (a), the flow follows a 3D path along the microchannel. As an example, figure 4.35 illustrates the filling of the Chain 3-mixer step by step at Re=4.166 and the stage of filling and performance of this type of micromixer is visually shown. Results of experimental investigation of the Chain 3-micromixer are presented in tables 4.19, 4.20 and 4.21.

Table 4.19 Standard deviation of concentration (σ) during experimental investigation in Chain 3-micromixer.

σ	0 mm	5 mm	10 mm	15 mm	20 mm
Q=0.001(ml/min)	0.4871	0.0265	0.0132	0.0219	0.0132
Q=0.005	0.4927	0.0102	0.0249	0.0161	0.0190
Q=0.01	0.4868	0.0202	0.0132	0.0073	0.0102
Q=0.02	0.4927	0.0161	0.0132	0.0102	0.0219
Q=0.05	0.4868	0.0202	0.0102	0.0144	0.0173

Table 4.20 Mixing index (*MI*) during experimental test in Chain 3-micromixer.

MI	0 mm	5 mm	10 mm	15 mm	20 mm
Q=0.001(ml/min)	0.9576	0.0329	0.0219	0.0382	0.0178
Q=0.005	0.9868	0.0132	0.0295	0.0307	0.0336
Q=0.01	0.9751	0.0461	0.0249	0.0232	0.0261
Q=0.02	0.9839	0.0407	0.0319	0.0232	0.0395
Q=0.05	0.9693	0.0332	0.0332	0.0202	0.0303

Table 4.21 Mixing efficiency (η) in Chain 3-micromixer.

η	0 mm	5 mm	10 mm	15 mm	20 mm
Q=0.001(ml/min)	0.0424	0.9671	0.9781	0.9735	0.9851
Q=0.005	0.0161	0.98	0.9764	0.9722	0.9793
Q=0.01	0.0307	0.9639	0.9722	0.9768	0.9710
Q=0.02	0.0161	0.9622	0.9710	0.9768	0.9664
Q=0.05	0.0307	0.9610	0.9698	0.9760	0.9798

Probability distribution function in terms of concentration is shown in figure 4.36 in the inlet region (4.36 a) and after 10 mm from the entrance region (4.36 b) in Chain 3-micromixer at Q=0.05 (Re=4.166). Also figure 4.37 shows the mixing efficiencies in Chain 3-micromixer at the same Reynolds number.

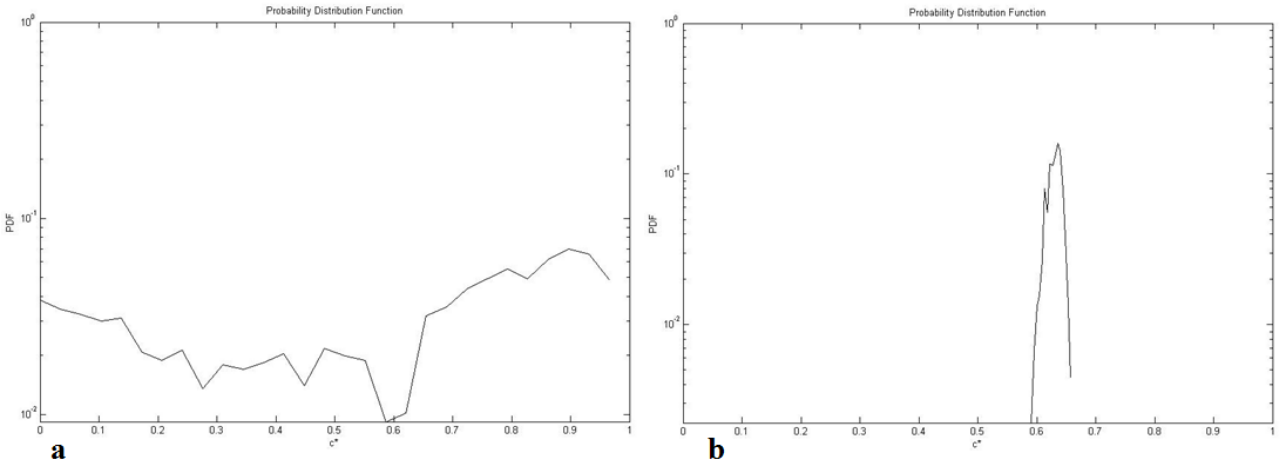

Figure 4.36 PDF in Chain 3-micromixer at Re = 4.166: (a) entrance region; (b)after 10 mm.

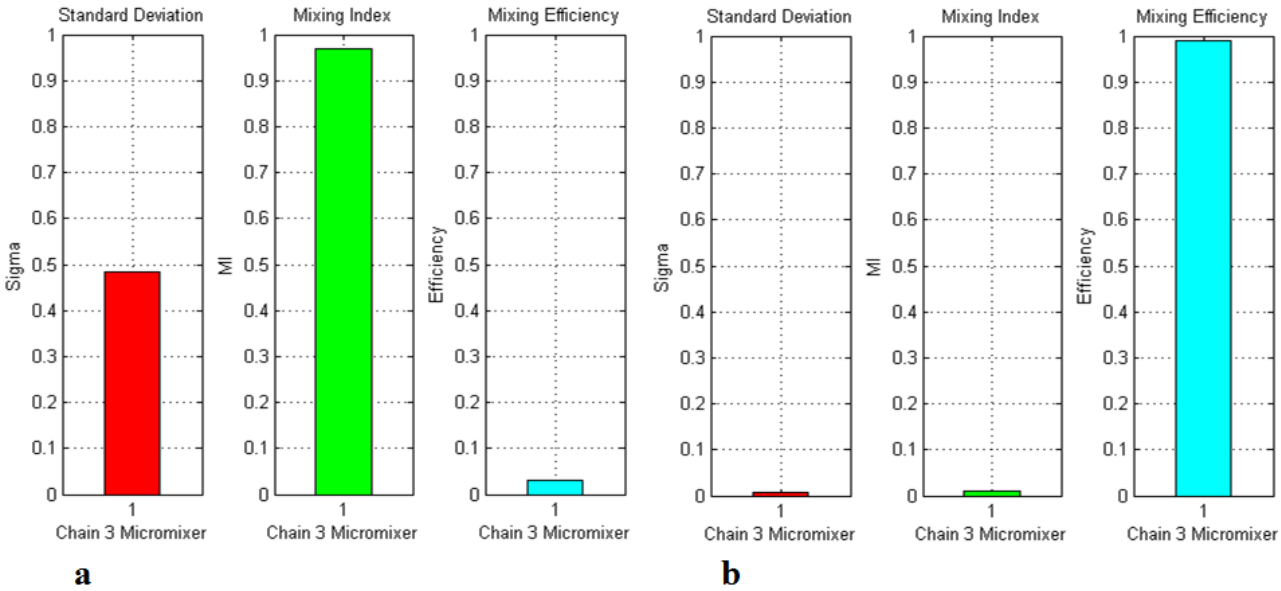

Figure 4.37 Chain 3-micromixer analysis at Re = 4.166:(a) entrance region; (b) after 10 mm.

As can be seen visually in the figure 4.35, after 5 mm from inlet region in Chain 3-micromixer, there is only one color (green color). It illustrates that the mixing performance is completed. Mixing efficiency at the end of the Chain 3-microchannel at Re=4.166 is up to 97% and this is a particular good result for the new geometry (Chain 3-micromixer) at this high Reynolds number. Hence, this

performance at the highest Reynolds number shows that it could be possible to increase the Reynolds number for rapid mixing in this prototype.

Comparison of mixing efficiency in Chain 3-microchannel is depicted in figure 4.38.

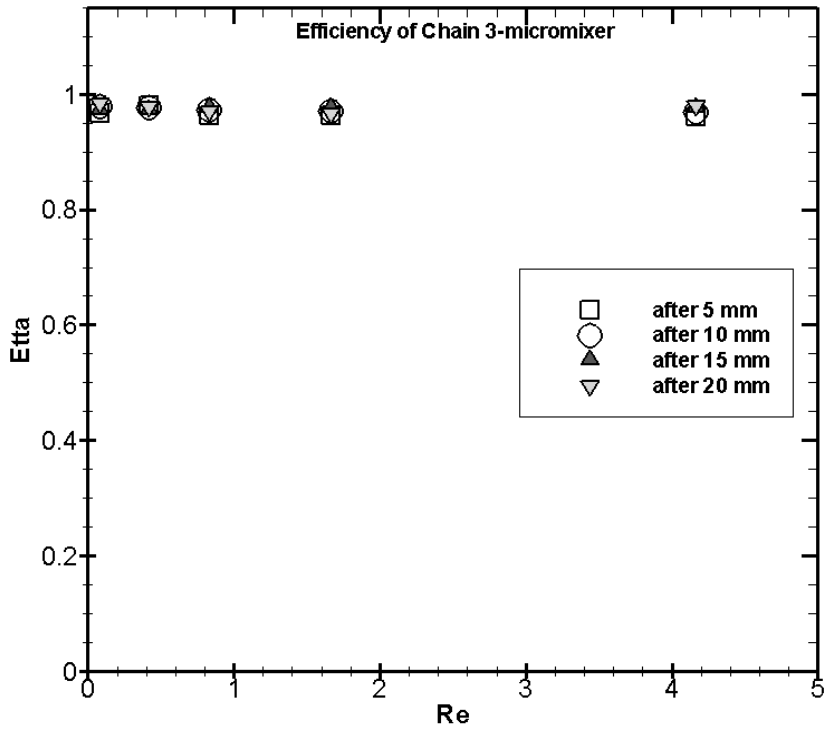

Figure 4.38 Comparison of η versus Re during Chain 3-micromixer.

As the diagram shows, in all of the tested Reynolds numbers, the efficiency is over 90% and are acceptable for mixing process.

4.7.4 Chain 4-micromixer analyze

To compare the effect of diameter and the number of splitting and recombination in Chain micromixers, chain 4 is designed. As shown in figure 4.39, after each vertical part (z direction), the diameter of the new section is 0.8 mm (like Chain 2) and extended 0.4 mm rather than the outlet of vertical part (0.4 mm). In fact, the difference between Chain 3 and Chain 4 is the extra diameter after vertical part in horizontal element which is 0.2 mm and 0.4 mm in Chain 3 and Chain 4 respectively.

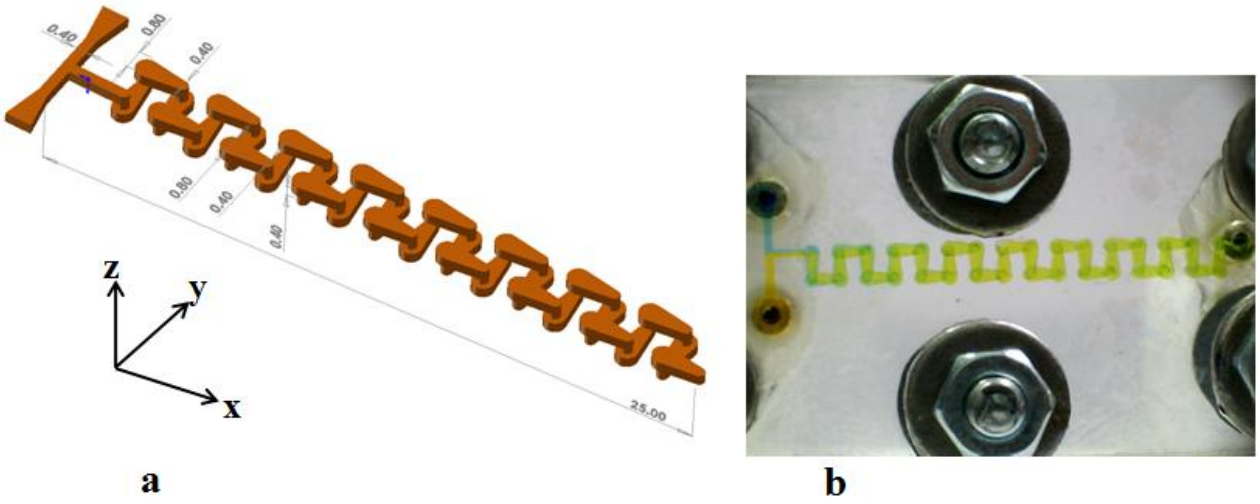

Figure 4.39 Chain 4-micromixer: (a) design of Chain4-micromixer; (b)during the experimentation.

Like Chain 2-micromixer, the main working principle for this type of microchannel is also to make 90º rotation of a flow, folding the stream and then split and recombine the flow to enhance the efficiency of the microchannel.

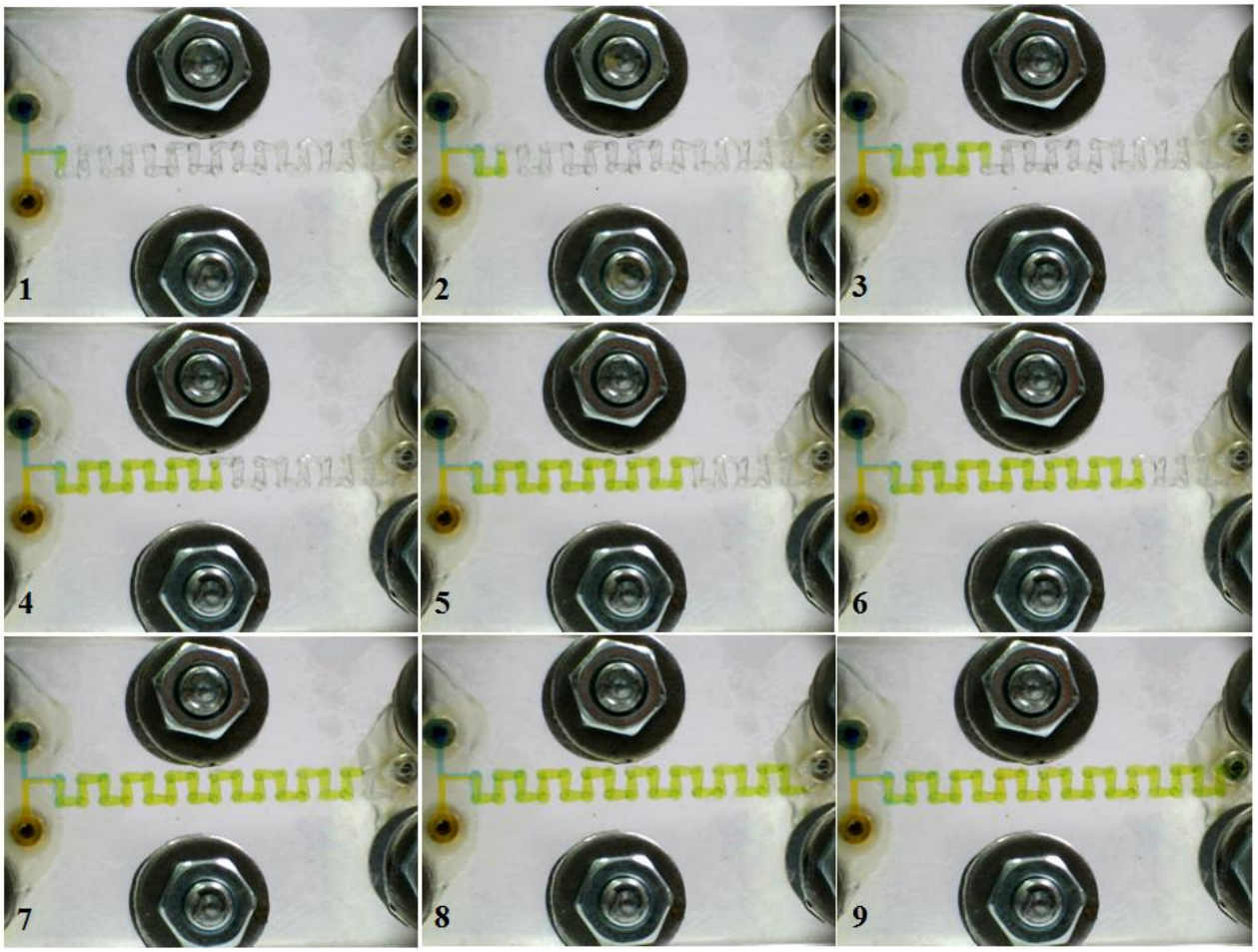

Figure 4.40 Chain 4-micromixer during the test at Re=1.666.

Chain 4-micromixer is fabricated from plexiglas using a computer milling process (like previous three chain prototypes). As depicted in figure 4.39 (a), the flow follows a 3D path along the microchannel. As an useful example, figure 4.40 shows the filling of the Chain 4-mixer step by step at Re=1.666 and performance of this type of micromixer is visually illustrated.
Tables 4.22, 4.23 and 4.24 illustrate the standard deviation of concentration (σ), Mixing Index (*MI*) and efficiency of mixing (η) in Chain 4-microchannel respectively as results of experimentation.

Table 4.22 Standard deviation of concentration (σ) during experimental investigation in Chain 4-micromixer.

$\boldsymbol{\sigma}$	0 mm	5 mm	10 mm	15 mm	20 mm
Q=0.001(ml/min)	0.4927	0.0132	0.0044	0.0132	0.0120
Q=0.005	0.4898	0.0128	0.0102	0.102	0.0073
Q=0.01	0.4722	0.0073	0.0073	0.0044	0.0044
Q=0.02	0.4781	0.0102	0.0100	0.0085	0.0132
Q=0.05	0.4635	0.0073	0.0249	0.0132	0.0140

Table 4.23 Mixing index (*MI*) during experimental test in Chain 4-micromixer.

MI	0 mm	5 mm	10 mm	15 mm	20 mm
Q=0.001(ml/min)	0.9781	0.0249	0.0102	0.0219	0.0110
Q=0.005	0.9780	0.0190	0.0161	0.0161	0.0160
Q=0.01	0.9459	0.0202	0.0102	0.0100	0.0140
Q=0.02	0.9488	0.0232	0.0261	0.0132	0.0161
Q=0.05	0.9284	0.0202	0.0424	0.0190	0.0265

Table 4.24 Mixing efficiency (η) in Chain 4-micromixer.

$\boldsymbol{\eta}$	0 mm	5 mm	10 mm	15 mm	20 mm
Q=0.001(ml/min)	0.0219	0.9751	0.9898	0.9839	0.9890
Q=0.005	0.0220	0.978	0.9868	0.9839	0.9840
Q=0.01	0.0541	0.9798	0.9898	0.9890	0.9852
Q=0.02	0.0512	0.9739	0.9781	0.9810	0.9868
Q=0.05	0.0716	0.9727	0.9635	0.98	0.9764

Probability distribution function versus concentration is shown in figure 4.41 in the inlet region (4.41 a) and after 10 mm from the entrance region (4.41 b) in Chain 4-micromixer at Q=0.02 ml/min (Re=1.666). Also figure 4.42 shows the mixing efficiencies in Chain 4-micromixer at the same Reynolds number.

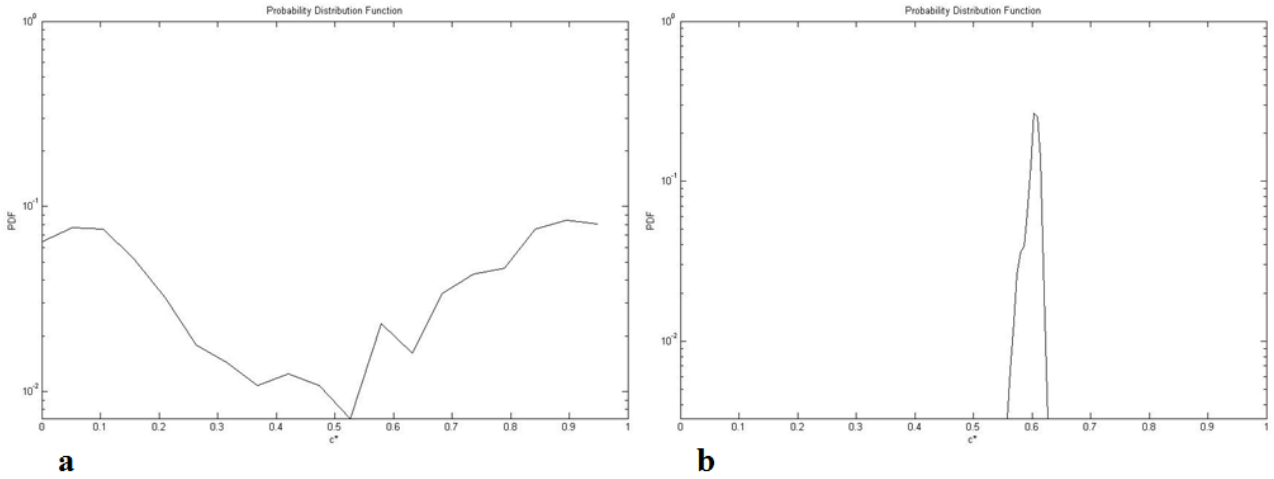

Figure 4.41 PDF in Chain 4-micromixer at Re = 1.666: (a) entrance region; (b)after 10 mm.

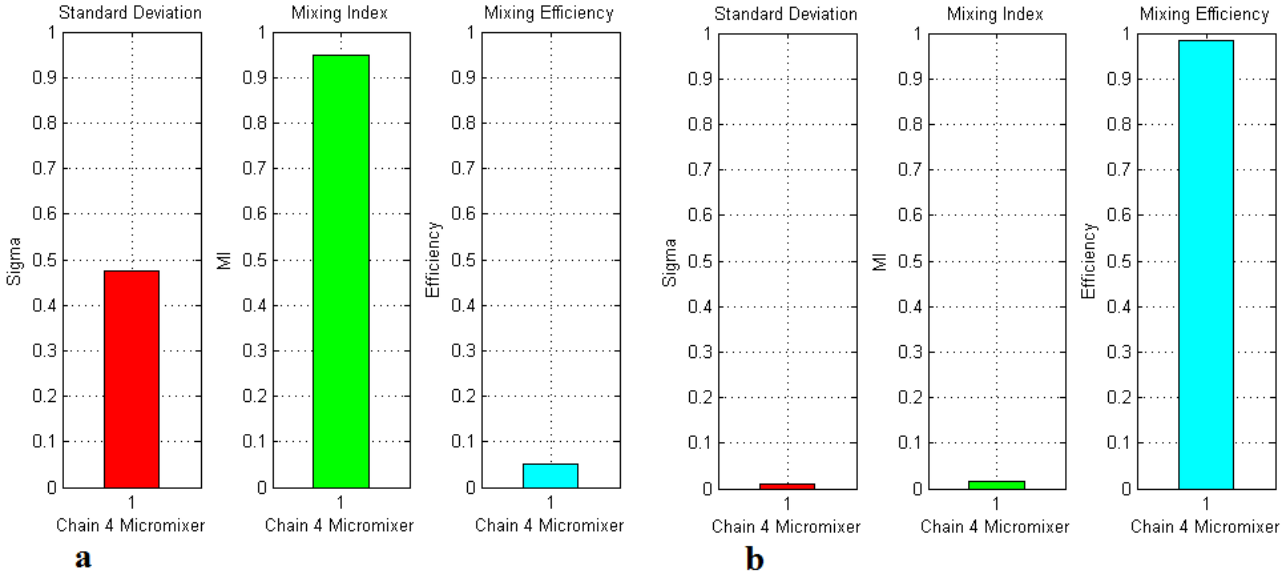

Figure 4.42 Chain 4-micromixer analysis at Re = 1.666:(a) entrance region; (b) after 10 mm.

As can be seen visually in the figure 4.40, after 5 mm from inlet region in Chain 4-micromixer, only one color (green color) could be seen. It illustrates that the mixing performance is completed. Mixing efficiency at the end of the Chain 4-microchannel at Re=1.666 is up to 98% and this is a particular good result for the new geometry (Chain 4-micromixer) at this high Reynolds number.

Also mixing efficiency at the highest Reynolds number (Re=4.166) is up to 97% and shows that it could be possible to increase the Reynolds number for rapid mixing in this prototype.

Comparison of mixing efficiency in Chain 4-microchannel is depicted in figure 4.43.

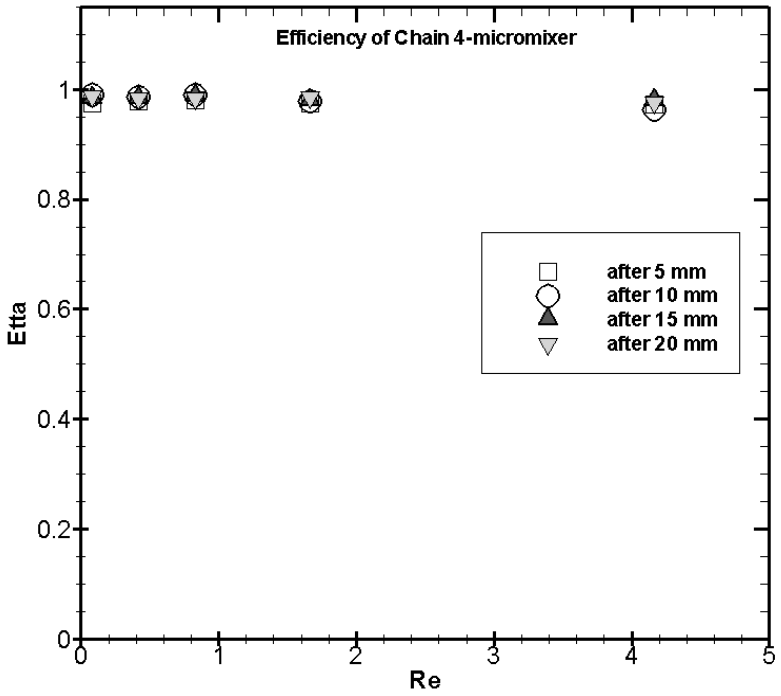

Figure 4.43 Comparison of η versus Re during Chain 4-micromixer.

As the diagram shows, in all of the tested Reynolds numbers, the efficiency is over 90% and are acceptable for mixing process.

4.8 Comparison of Chain micromixers

Results of experimental tests and comparison of mixing efficiency on the Chain micromixers are illustrated in this paragraph. Figure 4.44 depicts the mixing process through the microchannels in four types of Chain micromixers. It is obvious that in all of the four Chain prototypes, there is only one color (green color) after few distance from inlet section, which is why the mixing process is well-done, but in comparison with figures 4.14 and 4.22 it has found that in the T- and O-mixers there are two separate color (yellow and blue) which shows that mixing does not occur or the degree of mixing is very low (poor mixing). Concentration based analysis is the most reputable and trustworthy method of investigating and evaluating mixing efficiency. By improving concentration image analysis, the detailed process taking place in the microchannel can be investigated. As

mentioned before, when flow is not in the turbulent regime, it is essential to observe changes in concentration through the channel to understand mixing performance.

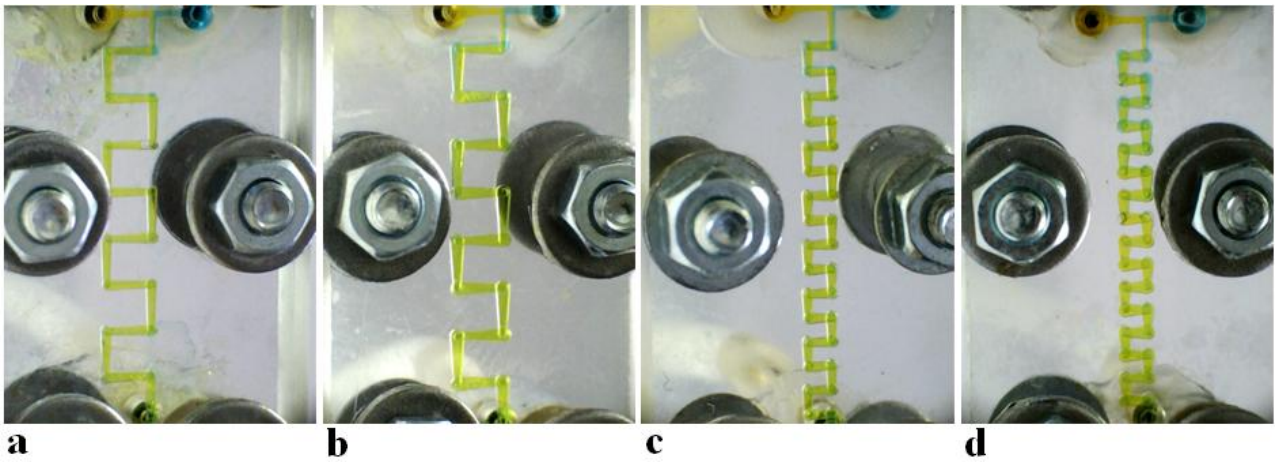

Figure 4.44 Comparison of η by visualization at Re=4.166: (a) Chain 1; (b) Chain 2; (c) Chain 3; (d) Chain 4.

Figure 4.45 depicts the efficiency comparison between four types of Chain micromixers.

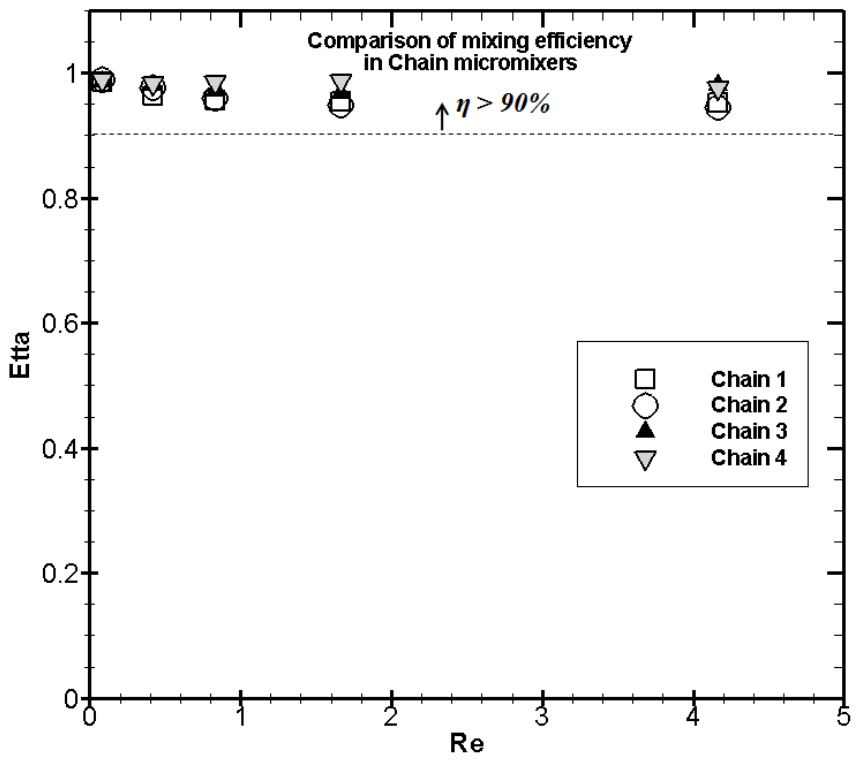

Figure 4.45 Comparison of mixing efficiency in Chain micromixers at outlet region.

As figure 4.45 shows, mixing efficiency is over 90% at all tested Reynolds numbers. Also figure 4.45 shows that the Chain micromixer's mixing efficiency is significantly high (in comparison with other micromixers). This capability is significant for micromixer design, as this device requires special geometry since it cannot rely on turbulence flow to enhance mixing performance. As alluded before, The Chain mixers have been designed with the goals of maximizing the mixing efficiency and minimizing the pressure drop associated with the energy consumption (discussed in chapter 5). The developed Chain micromixers offer major advantages by virtue of their higher fluid conductivity of the Chain mixer element in comparison with the Tear-drop and H- mixers element. Hence at this stage, this new geometry satisfies one of the targets in micromixer design which is higher mixing efficiency. For achieving the second target (lower pressure drop), numerical investigation is applied to find out the required pressure drop along side of the microchannels which explained in chapter 5.

References

[1] Nguyen N.T., 2008. Micromixers: Fundamentals, Design and Fabrication. William Andrew, Norwich, NY, USA.

[2] Ma Y.et al., 2008. An unsteady microfluidic T-form mixer perturbed by hydrodynamic pressure, J. Michromech. Microeng. 18, 045015, doi: 1088/0960-1317/18/045015.

[3] Garstecki P., Fuerstman M.J., Fischbach M.A., Sia S.K., Whitesides G.M., 2006. Mixing with bubbles: a practical technology for use with portable microfluidic devices, Lab on a Chip 6, 207-212, doi :10.1039/b510843h.

[4] Chen Z., Bown M.R., Sullivan B.O., MacInnes J.M., Allen R.W.K., Mulder M., Blom M., van't Oever R., 2009. Performance analysis of a folding flow micromixer, Microfluid Nanofluid 6:763–774, doi: 10.1007/s10404-008-0351-z.

Chapter 5
Numerical Method

5.1 Introduction

Fluid motion is governed by the Navier-Stokes equations [1], a set of coupled and nonlinear partial differential equations derived from the basic laws of conservation of mass, momentum and energy. In the micromixer analysis, the unknowns are usually the velocity and the pressure (pressure drop) alongside the microchannel [2] and some tracers like temperature. The analytical solution of these equations is practically impossible. The simplifications can take the form of geometrical simplification (the flow in rectangle or circle), and physical simplification (homogeneous density, linearity, etc...). Occasionally, it is possible to develop by using asymptotic analyses technique, and there has been considerable success in the past years, like the development of boundary layer theory. Scientist had to resort to laboratory experiments when theoretical analysis was impossible. Physical complexity can be resorted to the system. The answers delivered are usually qualitatively different since dynamic and geometric similitude are difficult to enforce simultaneously between the lab experiment and the prototype. A good example is the Reynolds number similarity [3] which if violated can turn a turbulent flow laminar. Furthermore, the design and construction of these experiments can be difficult and costly.

Computational fluid dynamics (CFD) is an additional tool in the arsenal of the scientists. In its early days CFD was often controversial, as it involved additional approximation to the governing equations and raised additional issues [4]. Nowadays CFD is an established discipline alongside theoretical and experimental methods[5-8]. This position is in large part due to the exponential growth of computer power which has allowed us to tackle ever large and more complex problems. In order to evaluate each type of micromixer, the flow and diffusion between two solutions were numerically analyzed by CFD in some research articles [9-12]. The result is a wealth of predictions for flow velocity, temperature, pressure, density, and chemical concentration for any region where flow occurs. CFD calculation is used in this research for detecting the required pressure drop in the

micromixers. Hence, CFD code, ANSYS FLUENT-13.0 has been used to analyze the flow and pressure drop in the microchannel.

5.2 Mathematical Model

At the continuum level, constitutive governing equations are described with a set of conservation equations.

1- Continuity (conservation of mass)

2- Navier-Stokes equation or Newton's second law (conservation of momentum)

Solving above equations will result in two variables : the velocity ***V*** and the pressure ***P***. These equations are formulized for a solo phase of homogenous composition. In microfluidic device, fluid convey one or more samples. Hence further equation are needed to explain the transport of species in micromixers [13].

3- Conservation of species (convection- diffusion equation)

Continuity (conservation of mass):

$$\frac{\partial \rho}{\partial t} + \nabla(\rho \overrightarrow{V}) = 0 \qquad (1)$$

Navier-Stokes equation :

$$\frac{\partial \rho \vec{V}}{\partial t} + \nabla(\rho \vec{V}\vec{V}) = -\nabla p + \nabla\left\{\mu\left[(\nabla \vec{V} + \nabla \vec{V}^{T}) - \frac{2}{3}\nabla \vec{V} I\right]\right\} \qquad (2)$$

Species convection- diffusion equation:

$$\frac{\partial C}{\partial t} + \vec{V}.\nabla C = D\nabla C \qquad (3)$$

Where ρ denotes density, μ the viscosity, p the pressure, C the species concentration and D the diffusion coefficient of the species.

Computational fluid dynamics software, ANSYS-Fluent 13.0, was used to solve the governing equations (1) and (2). In this study the value of the ρ and μ are 998 kg m^{-3} and 0.00089 kg $m^{-1}s^{-1}$ respectively. Also some assumptions such as steady-state flow, no-slip conditions and incompressible fluid are proposed. Required information for numerical calculations are as follows: solver Fluent13.0.0, Mesh nodes for 1) T =280000 hexahedral cells; 2) O =220480 tetrahedral cells, 3) Tear-drop=379670 hexahedral cells; 4) H=462563 tetrahedral cells; 5) Chain 1=218810 hexahedral cells; 6) Chain 2=259870 hexahedral cells, 7) Chain 3=251940 hexahedral cells 8) Chain 4=310180 hexahedral cells. Under Relaxation Factor: a) Pressure=0.3; b) Density=1; c) Body

Force=1 and d) Momentum=0.7, and Monitor Convergence Criteria a) Continuity= 1e-20; b) x-velocity= 1e-20; c) y-velocity= 1e-20; d) z-velocity= 1e-20. Also the boundary conditions used in this investigation are as follows: inlet 1: mass flow inlet (kg/s); inlet 2: mass flow inlet (kg/s); outlet: pressure outlet (Gauge Pressure (Pascal) is equal 0).

5.3 Numerical simulation

To analyze the flow and pressure drop in the microchannel, CFD code, ANSYS FLUENT-13.0 has been used. The Fluent solves the continuity and Navier-Stokes equations in steady condition.

To validate the approximation accuracy of the solver and assumptions which applied in this study, analytical method compared with numerical method in T mixer. To find out the pressure drop in analytical method, Darcy's law is applied.

$$\frac{dp}{dx} = \frac{-32\mu v}{d^2} \qquad (4)$$

Where μ denotes the viscosity, v the velocity, P the pressure, and d the hydraulic diameter of the microchannel. The results are presented in Table 5.1.

Table 5.1 Calculation of pressure drop in T micromixer, analytical and numerical methods.

Flow Inlet (ml/min)	Flow (kg/s)	Re	V (m/s)	Pressure Drop(Analytical) Pascal	Pressure Drop(Fluent) Pascal
0.001	$1.66*10^{-8}$	0.083	0.0001	1	0.759
0.005	$8.31*10^{-8}$	0.416	0.00052	4	3.81
0.01	$1.66*10^{-7}$	0.832	0.001	8	7.62
0.02	$3.32*10^{-7}$	1.666	0.002	15	15.3
0.05	$8.32*10^{-7}$	4.166	0.0052	39	38.7

Figure 5.1 demonstrated the differences between two mentioned method is very small and negligible.

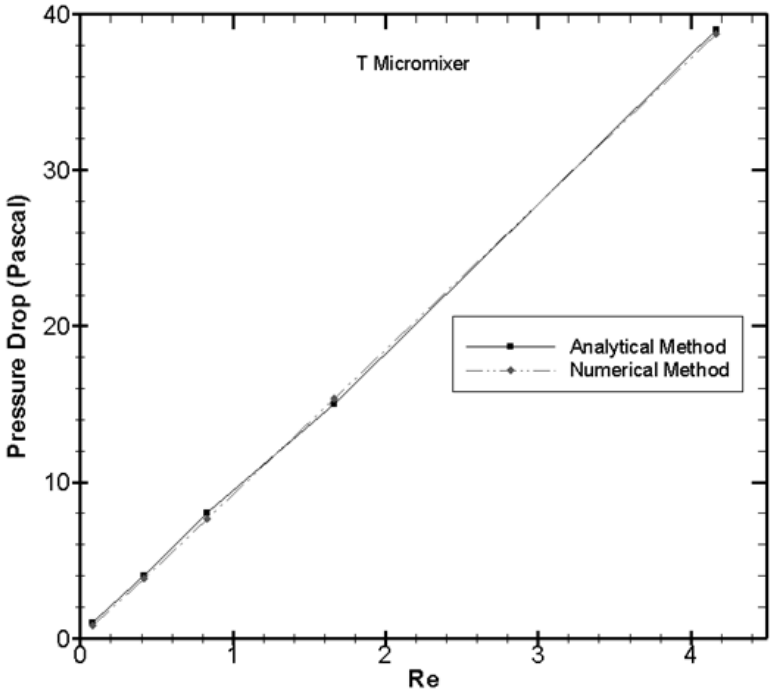

Figure 5.1 Comparison of Pressure Drop between Analytical Method and Numerical Method in T Mixer.

Also to validate the accuracy of the solver and assumptions, experimental acknowledgement has performed at *Re*=63.929 and the result compared with numerical method in T mixer

Table 5.2 Calculation of pressure drop in T micromixer at *Re*=63.929; analytical, numerical and experimental methods.

Flow Inlet (ml/min)	Flow (kg/s)	Re	V (m/s)	Pressure Drop(Analytical) Pascal	Pressure Drop(Fluent) Pascal	Pressure Drop(Experimental) Pascal
0.68 (=1.36/2)	$1.13*10^{-5}$	63.929	0.1425	**524**	**596**	720 (T mixer(=**535**) +2 tube inlet(=120)+1 tube outlet (=65))

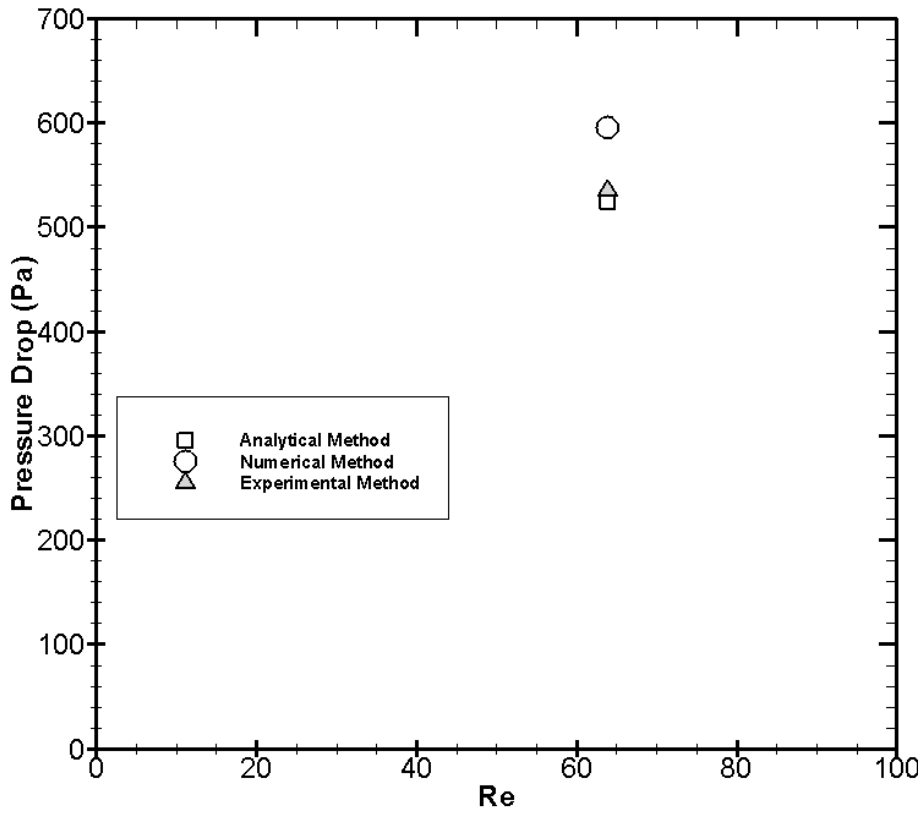

Figure 5.2 Comparison of Pressure Drop between Analytical, Numerical and Experimental methods in T Mixer at Re=63.929.

Hence, it could be found the CFD calculation with ANSYS FLUENT under the mentioned assumptions to find out the pressure drop is reliable. Therefore, numerical technique is applied to detect the pressure drop during the microchannel which was found to be accurate in comparison with analytical and experimental methods.

5.4 T-micromixer analyze

Results of numerical investigation of the T micromixer [14] are presented below. Figure 5.3 demonstrates the pressure drop distribution in T micromixer at five tested Reynolds numbers.

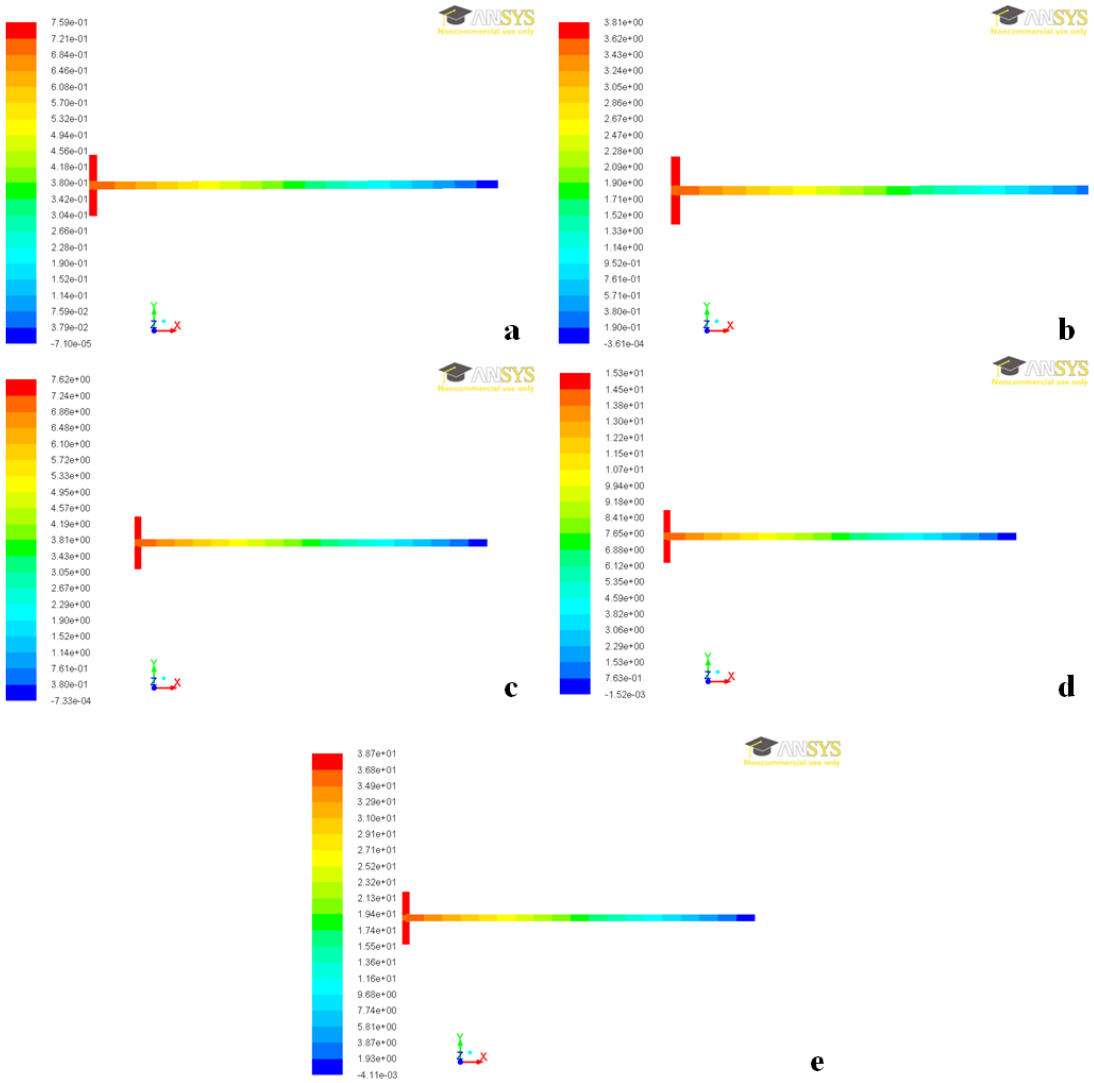

Figure 5.3 Pressure drop distribution in T micromixer:(a) Re=0.083; (b) Re=0.416; (c) Re=0.832; (d) Re=1.666; (e) Re=4.166.

Also table 5.3 illustrates the detailed explanation of pressure drop calculation in T microchannel which is calculated and plotted with ANSYS FLUENT-13.0.

Table 5.3 Detailed explanation of pressure drop Calculation in T micromixer.

Flow inlet (ml/min)	Flow (kg/s)	Re	V (m/s)	Pressure Drop(with Fluent) Pascal
0.001	$1.66*10^{-8}$	0.083	0.0001	0.759
0.005	$8.31*10^{-8}$	0.416	0.00052	3.81
0.01	$1.66*10^{-7}$	0.832	0.001	7.62
0.02	$3.32*10^{-7}$	1.666	0.002	15.3
0.05	$8.32*10^{-7}$	4.166	0.0052	38.7

Comparison of pressure drop in T-microchannel is depicted in figure 5.4.

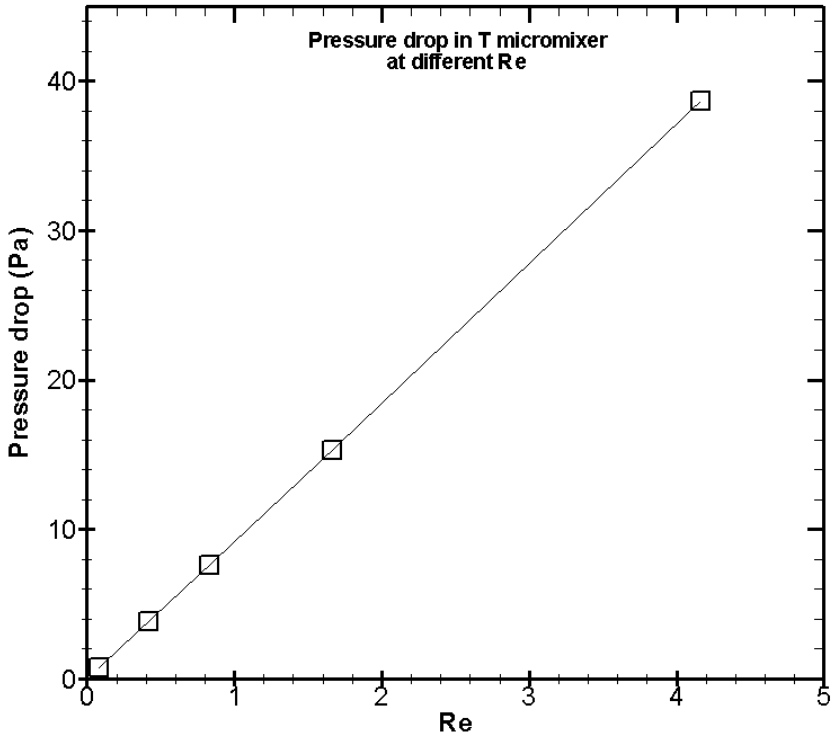

Figure 5.4 Pressure drop comparison in T micromixer.

As figure 5.4 illustrated, it could be found that in T micromixer pressure drop increases as Reynolds number increases and vice versa.

5.5 O-micromixer analyze

Results of numerical survey in O micromixer [15] are presented in this section. Figure 5.3 demonstrates the pressure drop distribution in O micromixer at different Reynolds numbers.

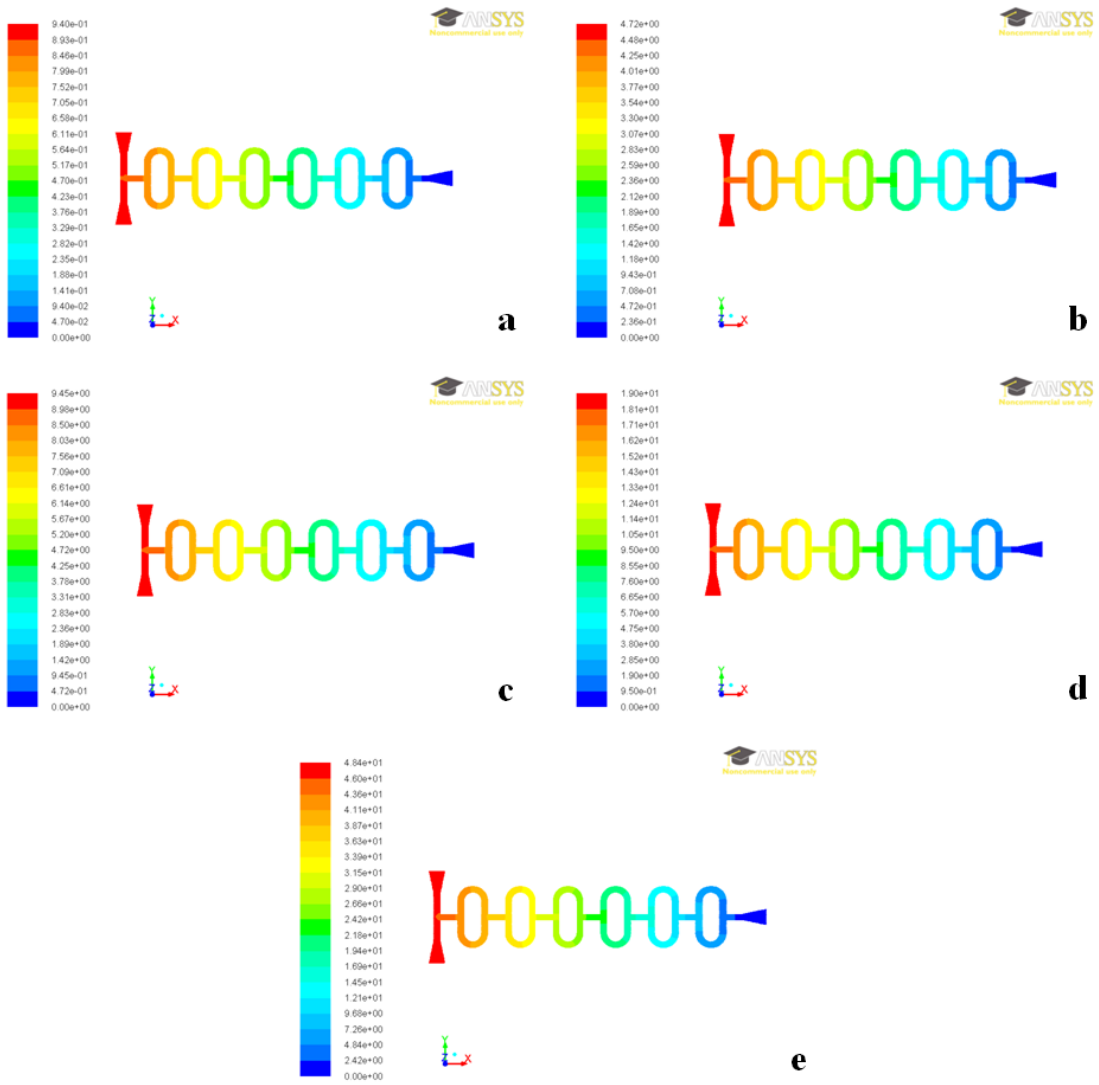

Figure 5.5 Pressure drop distribution in O micromixer:(a) Re=0.083; (b) Re=0.416; (c) Re=0.832; (d) Re=1.666; (e) Re=4.166.

Also table 5.4 illustrates the detailed explanation of pressure drop calculation in O microchannel which is estimated with ANSYS FLUENT-13.0.

Table 5.4 Detailed explanation of pressure drop Calculation in O micromixer.

Flow inlet (ml/min)	Flow (kg/s)	Re	V (m/s)	Pressure Drop(with Fluent) Pascal
0.001	$1.66*10^{-8}$	0.083	0.0001	0.94
0.005	$8.31*10^{-8}$	0.416	0.00052	4.72
0.01	$1.66*10^{-7}$	0.832	0.001	9.45
0.02	$3.32*10^{-7}$	1.666	0.002	19
0.05	$8.32*10^{-7}$	4.166	0.0052	48.4

Comparison of pressure drop in O-microchannel is depicted in figure 5.6.

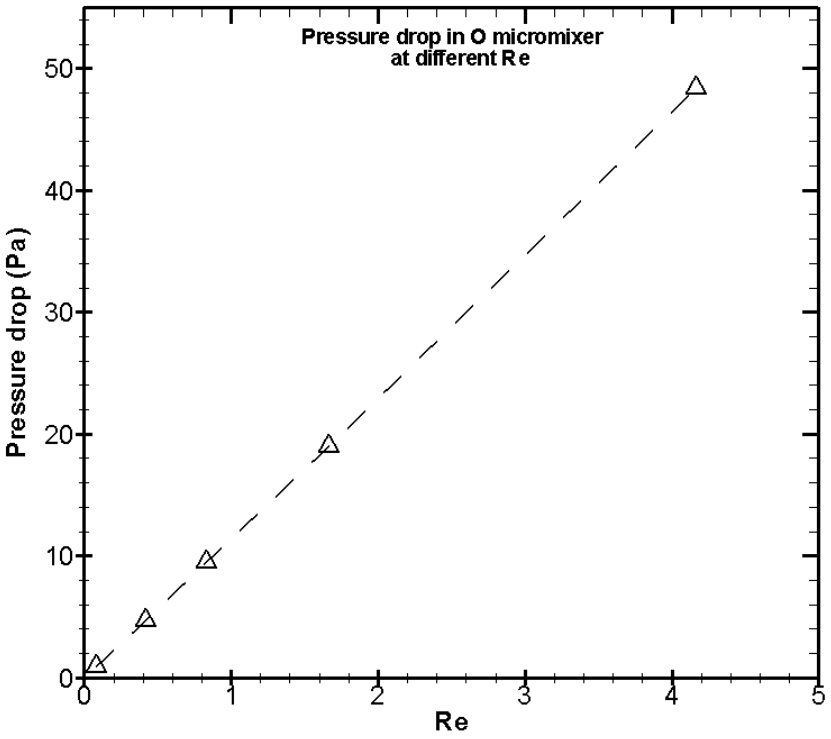

Figure 5.6 Pressure drop comparison in O micromixer.

It is concluded that like in T micromixer, in O micromixer pressure drop increases as Reynolds number increases and vice versa.

5.6 Tear-drop micromixer analyze

Results of numerical investigation of the Tear-drop micromixer [16] are presented below. Figure 5.7 demonstrates the pressure drop distribution in Tear-drop micromixer at five tested Reynolds numbers.

Also table 5.5 depicts the detailed explanation of pressure drop calculation in Tear-drop microchannel which is calculated and plotted with ANSYS FLUENT-13.0.

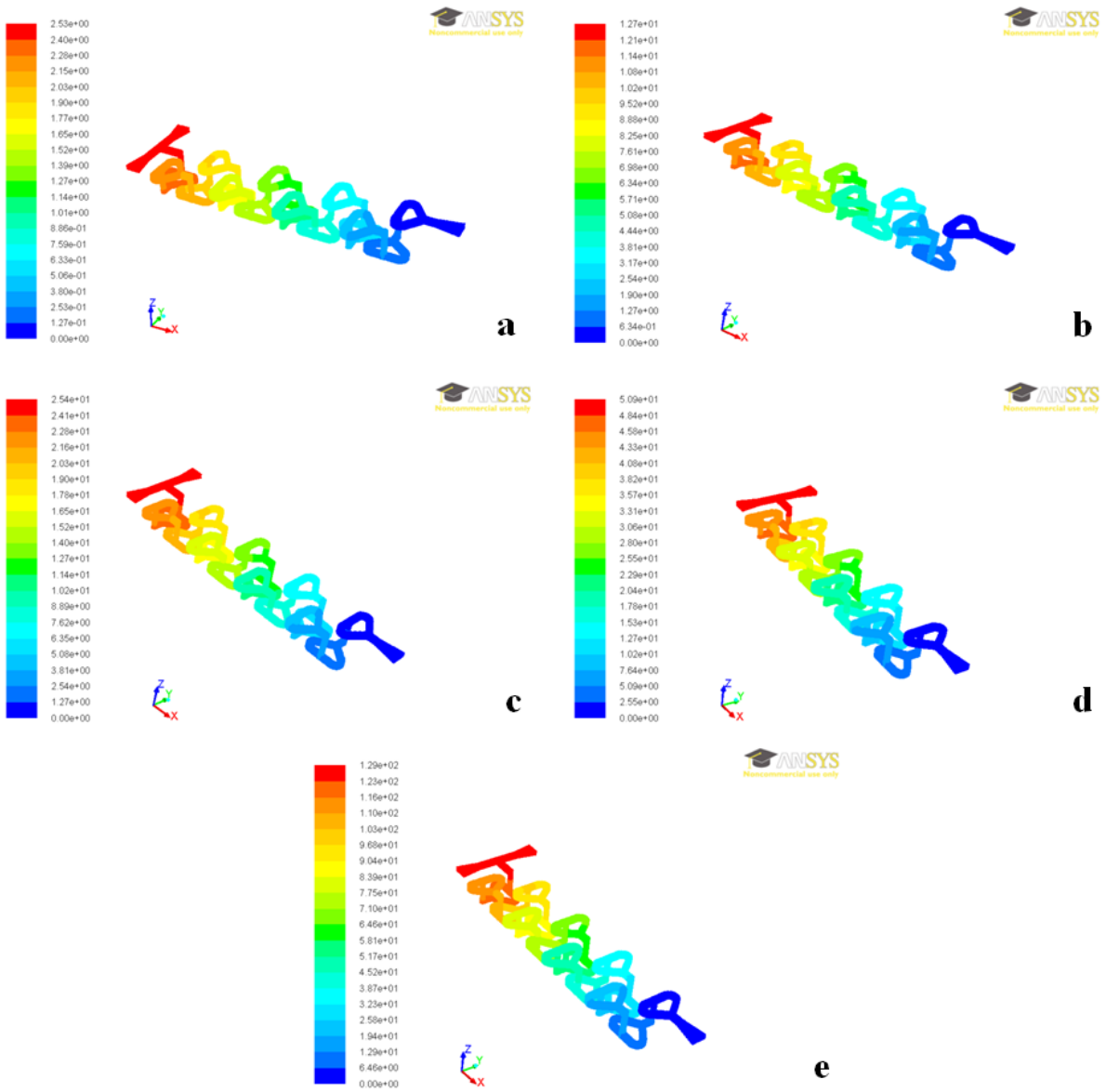

Figure 5.7 Pressure drop distribution in Tear-drop micromixer:(a) Re=0.083; (b) Re=0.416; (c) Re=0.832; (d) Re=1.666; (e) Re=4.166.

Table 5.5 Detailed explanation of pressure drop Calculation in Tear-drop micromixer.

Flow inlet (ml/min)	Flow (kg/s)	Re	V (m/s)	Pressure Drop(with Fluent) Pascal
0.001	$1.66*10^{-8}$	0.083	0.0001	2.53
0.005	$8.31*10^{-8}$	0.416	0.00052	12.7
0.01	$1.66*10^{-7}$	0.832	0.001	25.4
0.02	$3.32*10^{-7}$	1.666	0.002	50.9
0.05	$8.32*10^{-7}$	4.166	0.0052	129

Comparison of pressure drop in Tear-drop microchannel is depicted in figure 5.8.

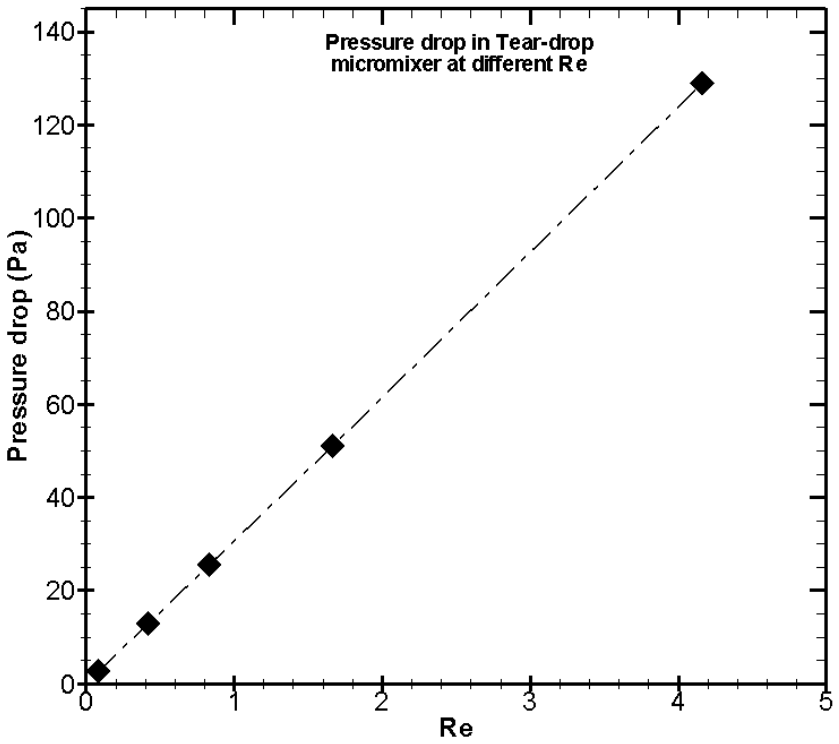

Figure 5.8 Pressure drop comparison in Tear-drop micromixer.

It could be found that pressure distribution is linear during the mixing length and also pressure drop increases as Reynolds number increases.

5.7 H-micromixer analyze

Results of numerical survey in H micromixer are presented in this section. Also this type of passive micromixer is based on the SAR process. Figure 5.9 demonstrates the pressure drop distribution in H micromixer at different Reynolds numbers.

Table 5.6 illustrates the detailed explanation of pressure drop calculation in H microchannel which is estimated with ANSYS FLUENT-13.0.

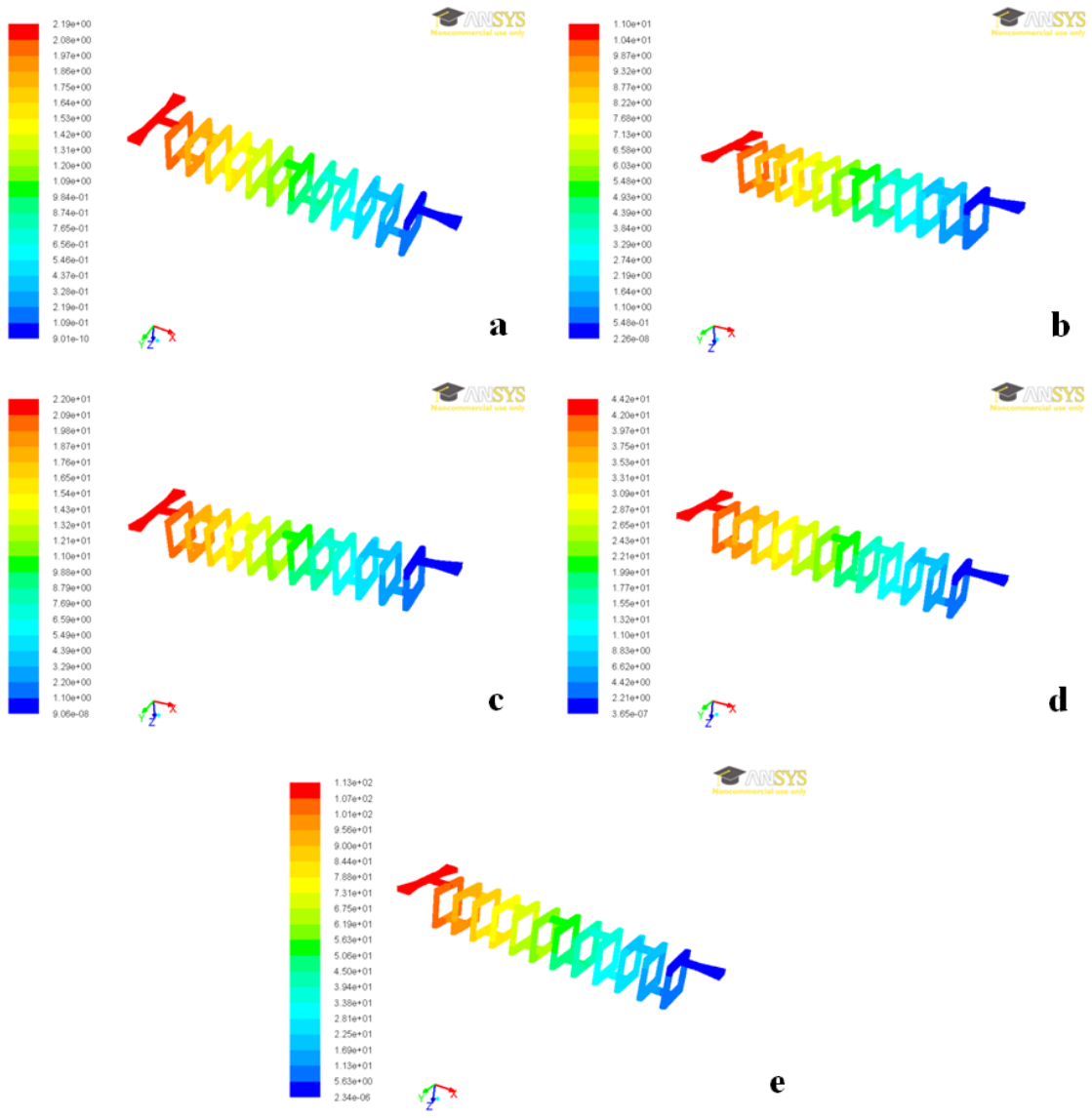

Figure 5.9 Pressure drop distribution in H micromixer:(a) Re=0.083; (b) Re=0.416; (c) Re=0.832; (d) Re=1.666; (e) Re=4.166.

Table 5.6 Detailed explanation of pressure drop Calculation in H micromixer.

Flow inlet (ml/min)	Flow (kg/s)	Re	V (m/s)	Pressure Drop(with Fluent) Pascal
0.001	$1.66*10^{-8}$	0.083	0.0001	2.19
0.005	$8.31*10^{-8}$	0.416	0.00052	11
0.01	$1.66*10^{-7}$	0.832	0.001	22
0.02	$3.32*10^{-7}$	1.666	0.002	44.2
0.05	$8.32*10^{-7}$	4.166	0.0052	113

Comparison of pressure drop in H-microchannel is depicted in figure 5.10.

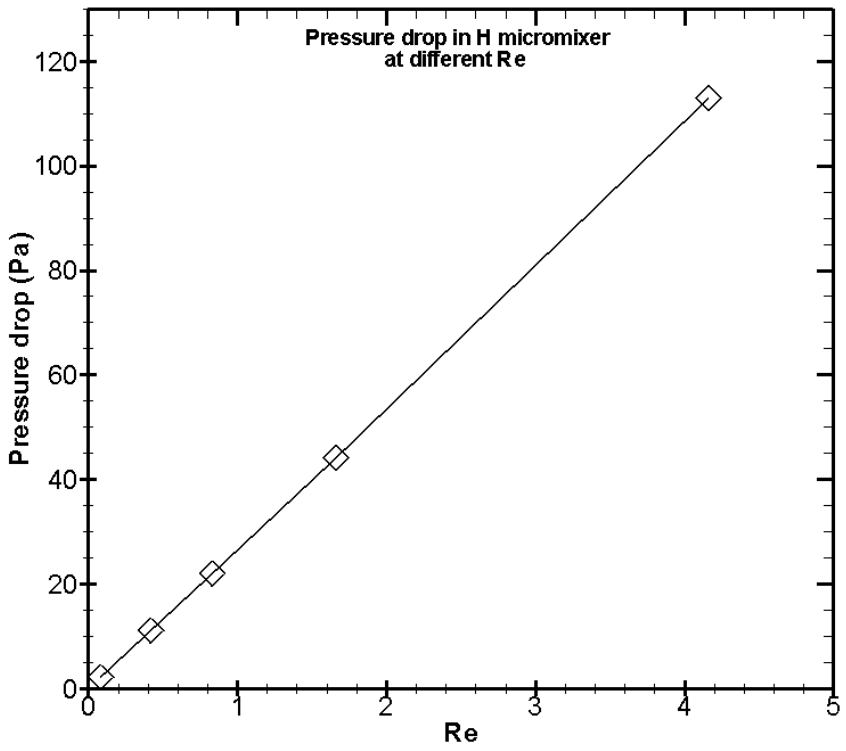

Figure 5.10 Pressure drop comparison in H micromixer.

As the diagram shows, it could be found like other tested prototypes, pressure drop is linear during the mixing length and also pressure drop increases as Reynolds number increases.

5.8 Chain micromixer analyze

As alluded before, this study introduces a novel generation of 3D splitting and recombination (SAR) passive micromixer called ‘’*Chain mixer*’’. We proposed here Chain micromixers of four types: Chain 1-, Chain 2-, Chain 3-, and Chain 4- micromixer. Mixing performance is compared in chapter 4 and in this section pressure drop is analyzed and compared with other micromixers, T-, o-, H- and Tear-drop micromixers. For this reason, CFD code, ANSYS FLUENT-13.0 has been used to analyze the flow and pressure drop in the microchannel.

5.8.1 Chain 1-micromixer analyze

Results of numerical investigation of the Chain 1 are presented in this paragraph. Figure 5.11 demonstrates the pressure drop distribution in Chain 1 mixer at different tested Reynolds numbers.

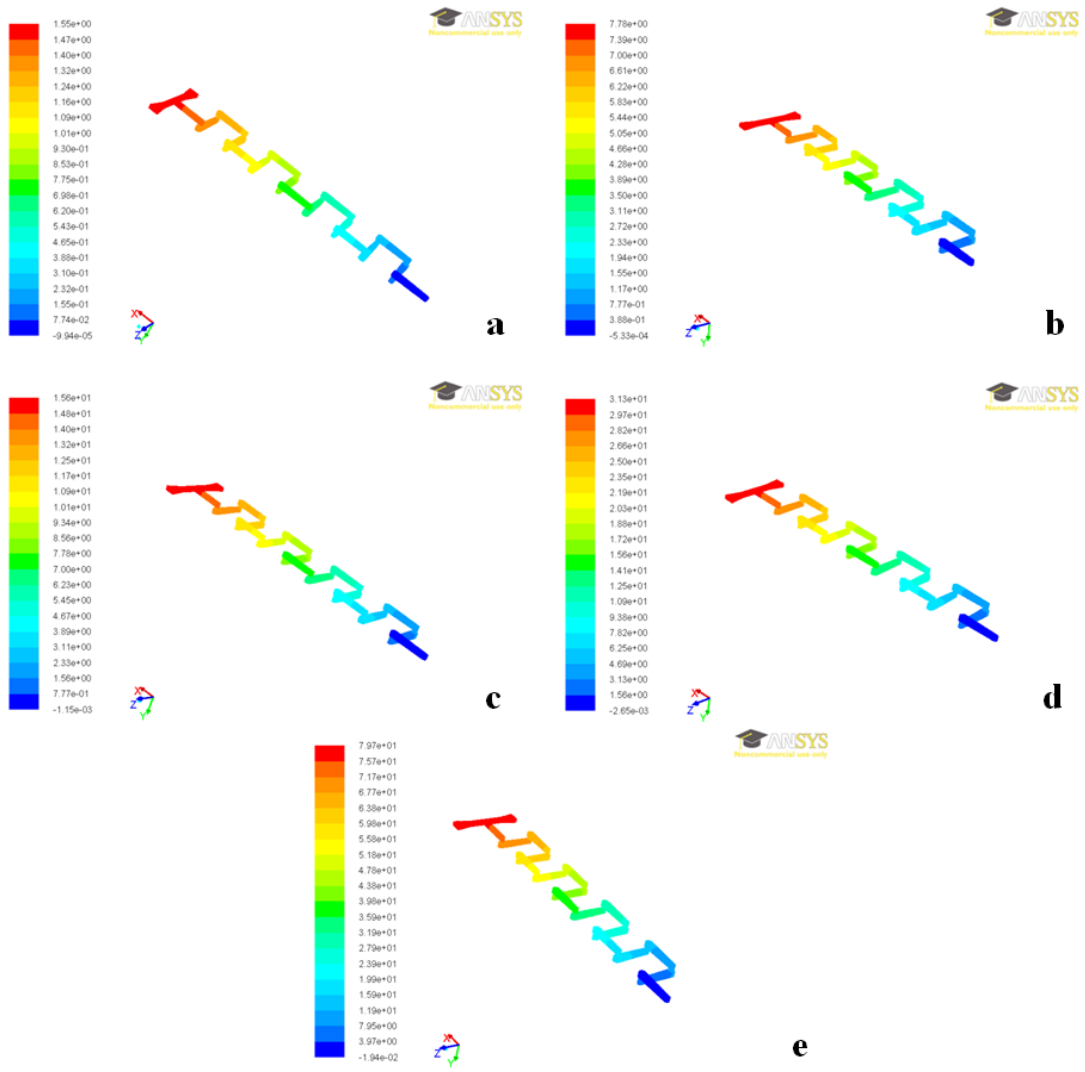

Figure 5.11 Pressure drop distribution in Chain 1 micromixer:(a) Re=0.083; (b) Re=0.416; (c) Re=0.832; (d) Re=1.666; (e) Re=4.166.

Also table 5.7 shows the detailed explanation of pressure drop calculation in Chain 1 microchannel which is calculated and plotted with ANSYS FLUENT-13.0.

Table 5.7 Detailed explanation of pressure drop Calculation in Chain 1 micromixer.

Flow inlet (ml/min)	Flow (kg/s)	Re	V (m/s)	Pressure Drop(with Fluent) Pascal
0.001	$1.66*10^{-8}$	0.083	0.0001	1.55
0.005	$8.31*10^{-8}$	0.416	0.00052	7.78
0.01	$1.66*10^{-7}$	0.832	0.001	15.6
0.02	$3.32*10^{-7}$	1.666	0.002	31.3
0.05	$8.32*10^{-7}$	4.166	0.0052	79.7

Figure 5.12 shows the pressure drop comparison in Chain 1-microchannel.

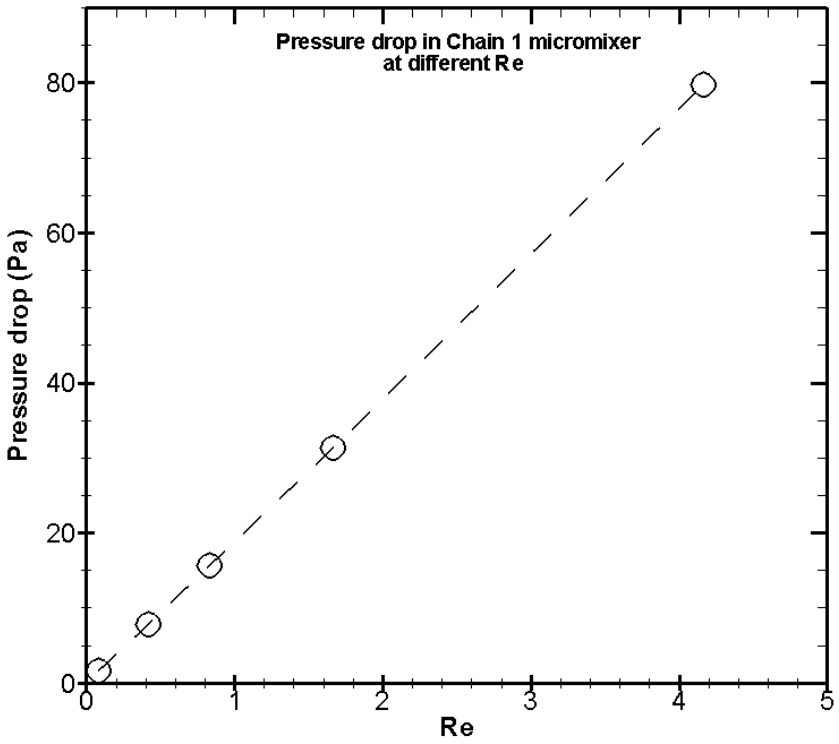

Figure 5.12 Pressure drop comparison in Chain 1 micromixer.

As the diagram 5.12 shows, it could be found like other tested prototypes, pressure drop is linear during the mixing length and also pressure drop increases as Reynolds number increases. Also it is concluded that required pressure drop decreased in comparison with H- and Tear-drop mixer.

5.8.2 Chain 2-micromixer analyze

As mentioned before, Chain 2 mixer differs only by one parameter from the Chain 1 mixer and after each vertical part (z direction), the diameter of the new section is 0.8 mm and extended 0.4 mm rather than the outlet of vertical part (0.4 mm). In this part, the effect of the extended diameter is investigated and finally the results compared with other microchannels. Also Like Chain 1-micromixer, the main working principle for this type of microchannel is also to make 90º rotation of a flow, folding the stream and then split and recombine the flow to enhance the efficiency of the microchannel. Figure 5.13 demonstrates the pressure drop distribution in Chain 2 mixer at different Reynolds numbers.

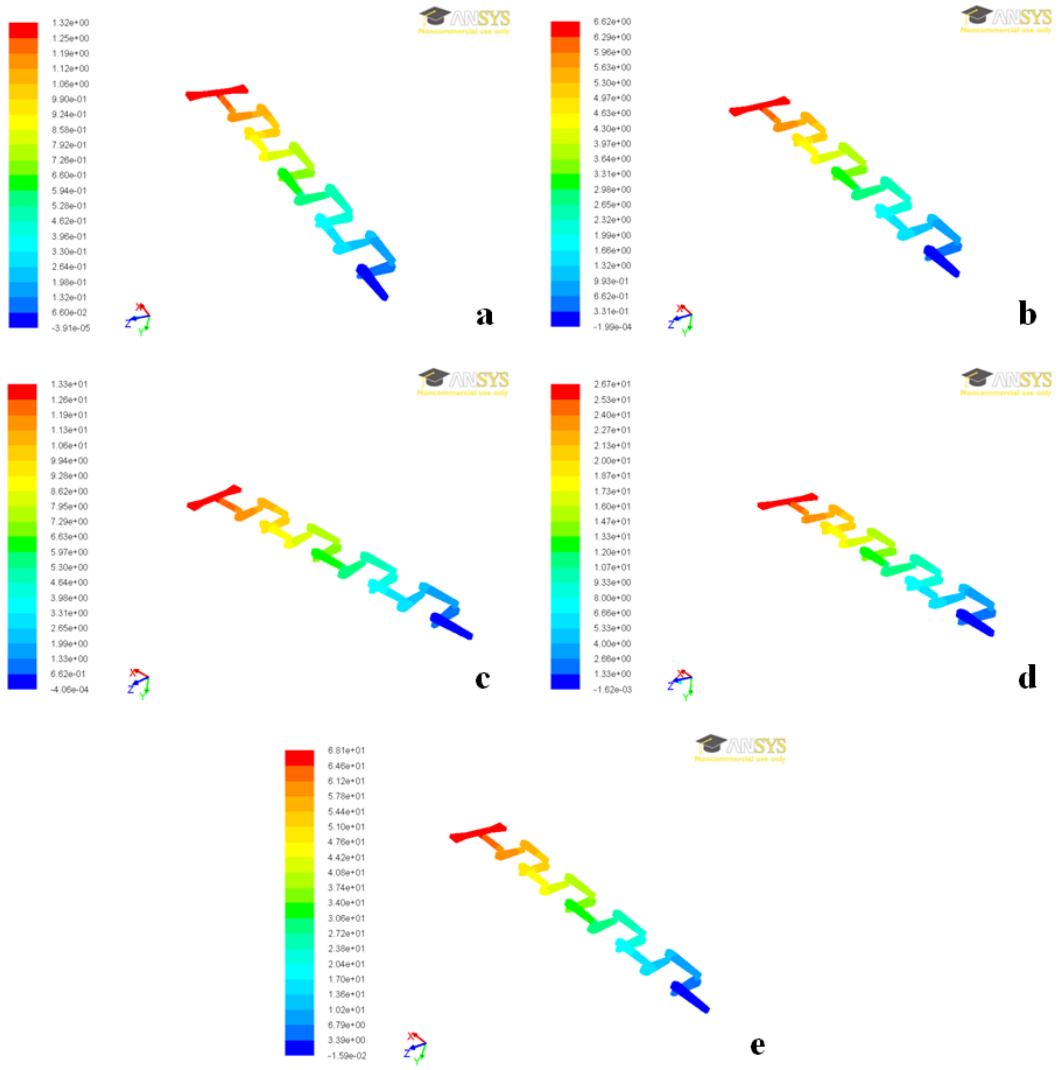

Figure 5.13 Pressure drop distribution in Chain 2 micromixer:(a) Re=0.083; (b) Re=0.416; (c) Re=0.832; (d) Re=1.666; (e) Re=4.166.

Table 5.8 shows the detailed explanation of pressure drop calculation in Chain 2 microchannel which is estimated with ANSYS FLUENT-13.0.

Table 5.8 Detailed explanation of pressure drop Calculation in Chain 2 micromixer.

Flow inlet (ml/min)	Flow (kg/s)	Re	V (m/s)	Pressure Drop(with Fluent) Pascal
0.001	$1.66*10^{-8}$	0.083	0.0001	1.32
0.005	$8.31*10^{-8}$	0.416	0.00052	6.62
0.01	$1.66*10^{-7}$	0.832	0.001	13.3
0.02	$3.32*10^{-7}$	1.666	0.002	26.7
0.05	$8.32*10^{-7}$	4.166	0.0052	68.1

Comparison of pressure drop in Chain 2-microchannel is depicted in figure 5.14.

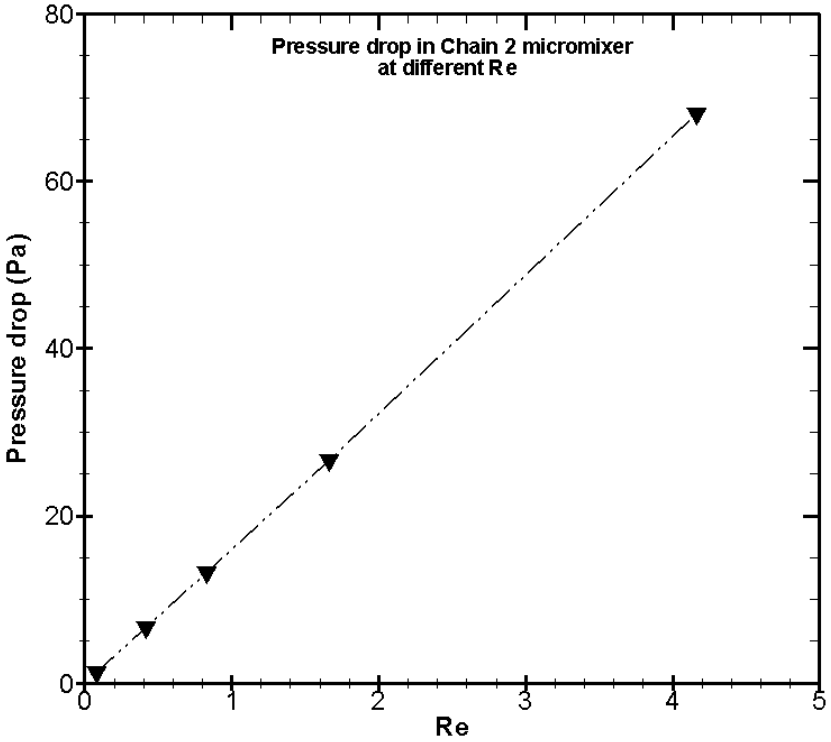

Figure 5.14 Pressure drop comparison in Chain 2 micromixer.

As the diagram 5.14 illustrated, it could be found the pressure drop is linear during the mixing length and also pressure drop increases as Reynolds number increases and vice versa. Also it is concluded that required pressure drop decreased in comparison with H-, Tear-drop and also Chain 1 mixer.

5.8.3 Chain 3-micromixer analyze

To compare the effect on the number of splitting and recombination in Chain micromixers, chain 3 is designed and constructed. As shown in figure 4.34, after each vertical part (z direction), the diameter of the new section is 0.6 mm (like Chain 1) and extended 0.2 mm rather than the outlet of vertical part (0.4 mm) and the flow follows a 3D path along the microchannel. Results of the numerical investigation of the Chain 3 are presented in this paragraph. Figure 5.15 demonstrates the pressure drop distribution in Chain 3 mixer at different tested Reynolds numbers.

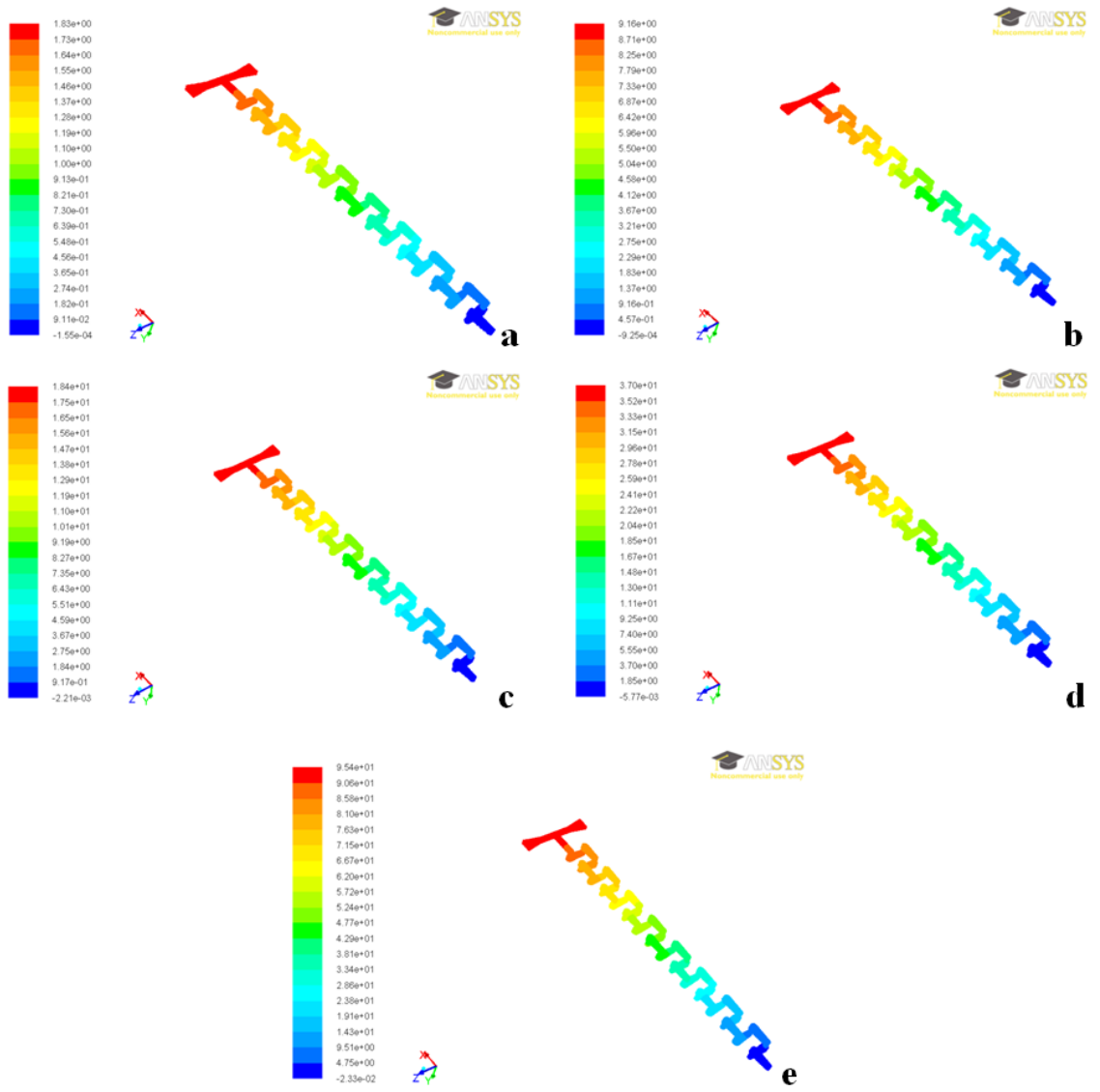

Figure 5.15 Pressure drop distribution in Chain 3 micromixer:(a) Re=0.083; (b) Re=0.416; (c) Re=0.832; (d) Re=1.666; (e) Re=4.166.

Also table 5.9 shows the detailed explanation of pressure drop calculation in Chain 3 microchannel which is calculated and plotted with ANSYS FLUENT-13.0.

Table 5.9 Detailed explanation of pressure drop Calculation in Chain 3 micromixer.

Flow inlet (ml/min)	Flow (kg/s)	Re	V (m/s)	Pressure Drop(with Fluent) Pascal
0.001	$1.66*10^{-8}$	0.083	0.0001	1.83
0.005	$8.31*10^{-8}$	0.416	0.00052	9.16

0.01	$1.66*10^{-7}$	0.832	0.001	18.4
0.02	$3.32*10^{-7}$	1.666	0.002	37
0.05	$8.32*10^{-7}$	4.166	0.0052	95.4

Figure 5.16 shows the pressure drop comparison in Chain 3-microchannel.

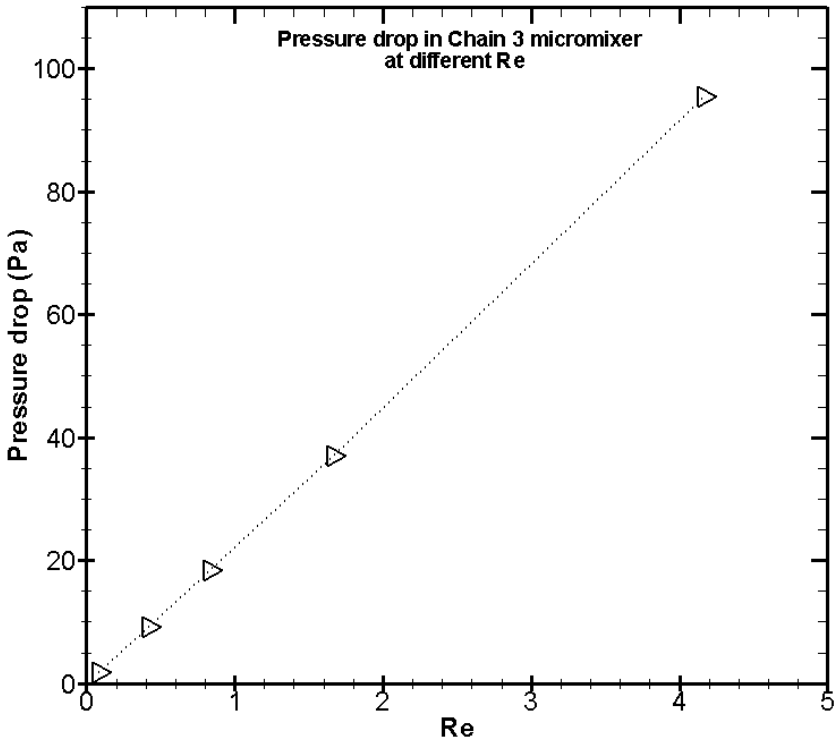

Figure 5.16 Pressure drop comparison in Chain 3 micromixer.

As the diagram 5.16 depicted, it could be found like other tested prototypes, pressure drop is linear during the mixing length and also pressure drop increases as Reynolds number increases and vice versa.

5.8.4 Chain 4-micromixer analyze

As alluded, Chain 4 mixer differs only by one parameter from the Chain 3 mixer and after each vertical part (z direction), the diameter of the new section is 0.8 mm and extended 0.4 mm rather than the outlet of vertical part (0.4 mm). In this part, the effect of the extended diameter and also number of the split and recombination are investigated and the results compared with other microchannels. Also Like other Chain micromixers, the main working principle for this type of microchannel is also to make 90º rotation of a flow, folding the stream and then split and recombine

the flow to enhance the efficiency of the microchannel. Figure 5.17 demonstrates the pressure drop distribution in Chain 4 mixer at different Reynolds numbers.

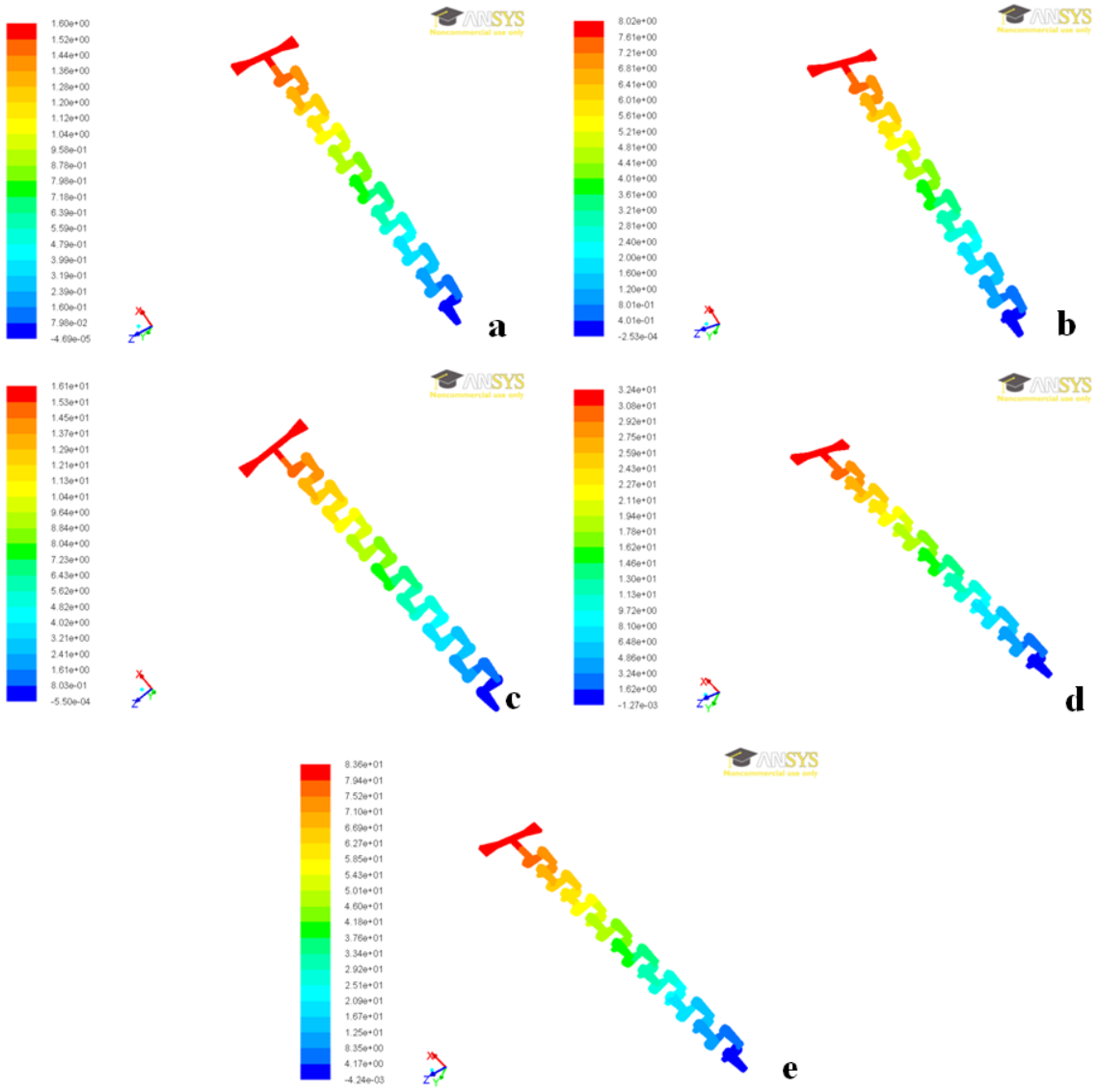

Figure 5.17 Pressure drop distribution in Chain 4 micromixer:(a) Re=0.083; (b) Re=0.416; (c) Re=0.832; (d) Re=1.666; (e) Re=4.166.

Furthermore, table 5.10 shows the detailed explanation of pressure drop calculation in Chain 4 microchannel which is estimated with ANSYS FLUENT-13.0.

Table 5.10 Detailed explanation of pressure drop Calculation in Chain 4 micromixer.

Flow inlet (ml/min)	Flow (kg/s)	Re	V (m/s)	Pressure Drop(with Fluent) Pascal
0.001	$1.66*10^{-8}$	0.083	0.0001	1.6
0.005	$8.31*10^{-8}$	0.416	0.00052	8.02
0.01	$1.66*10^{-7}$	0.832	0.001	16.1
0.02	$3.32*10^{-7}$	1.666	0.002	32.4
0.05	$8.32*10^{-7}$	4.166	0.0052	83.6

Also comparison of pressure drop in Chain 4-microchannel is depicted in figure 5.18.

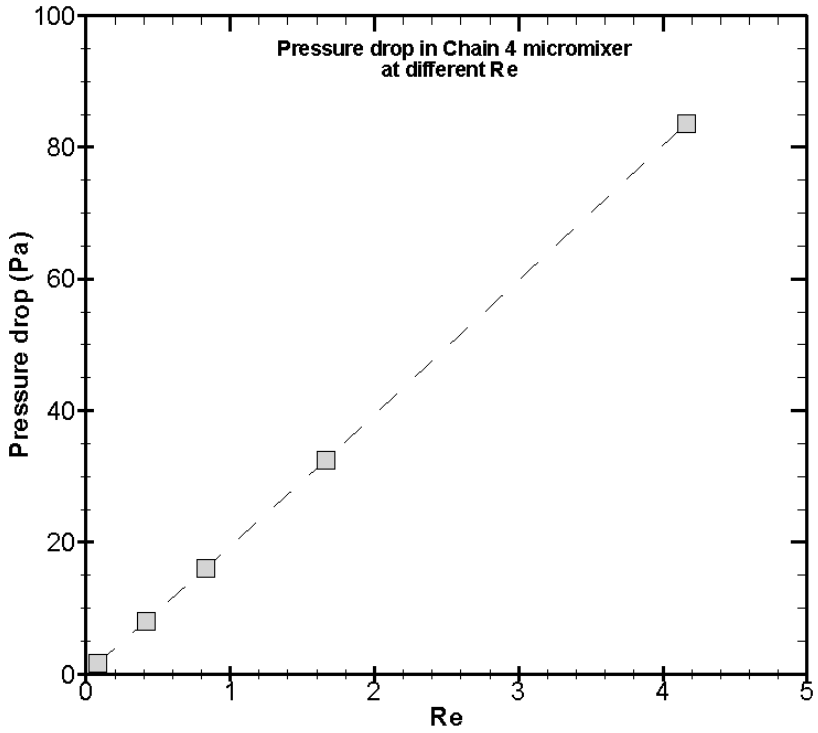

Figure 5.18 Pressure drop comparison in Chain 4 micromixer.

As the diagram 5.18 depicted, it could be found like other tested prototypes, pressure drop is linear during the mixing length and also pressure drop increases as Reynolds number increases and vice versa.

5.9 Comparison of micromixers

In this paragraph, the required pressure drop compared in all tested prototypes. Figure 5.19 demonstrates that Tear-drop micromixer's pressure drop is significantly higher than that of the Chain1-, Chain2-, Chain3-, Chain4-, T- and O-micromixers at all tested Reynolds numbers.

According to figures 5.19 and also 5.20 to 5.24, in comparison with other Reynolds number it could be found that the T- and O-mixers pressure drops are very low, but they are invalid for mixing processing because of the low degree of mixing (figures 5.20-5.24). Also it has concluded that with increasing the Reynolds number, efficiency decreases and pressure drop increases.

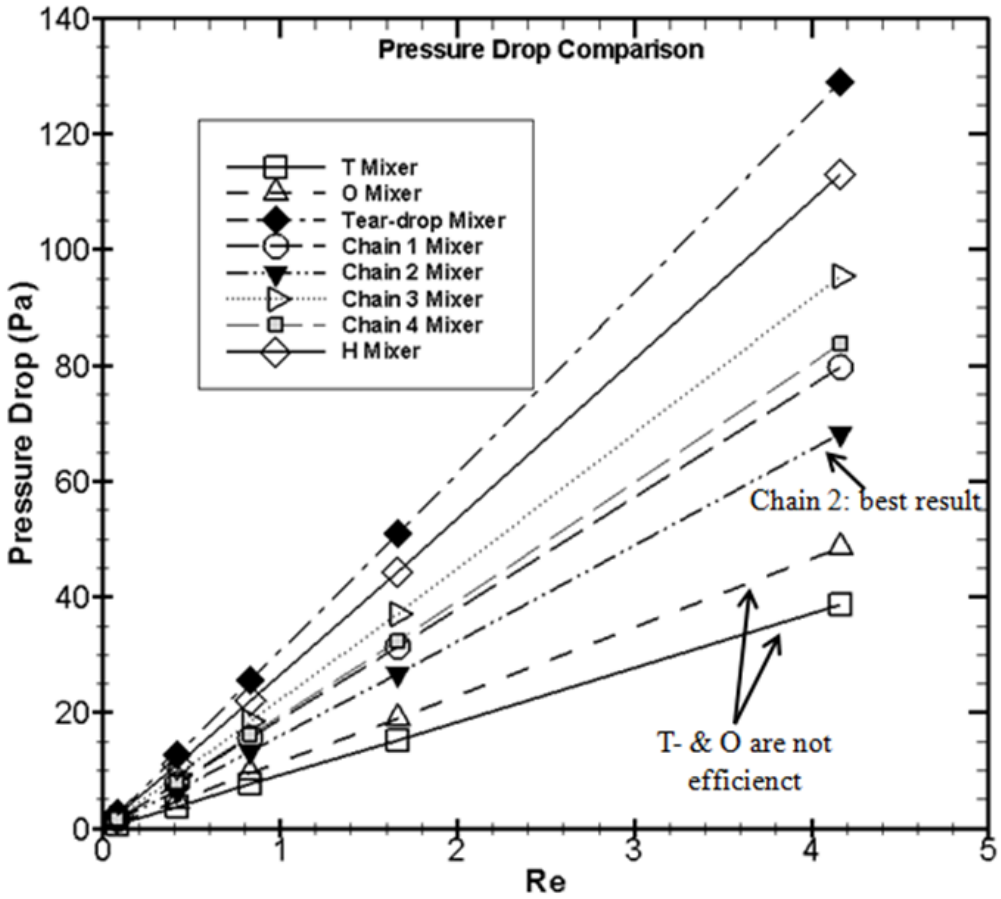

Figure 5.19 Pressure drop Vs. Re.

The Chain mixers have been designed with the goal of maximizing the mixing efficiency and minimizing the pressure drop associated with the energy consumption. As is evident from the foregoing the mixing efficiency of the Chain mixers is practically identical with those of the Tear-drop mixer while the pressure drop at the Chain mixers is approximately two times less than it is at the Tear-drop mixers. The developed Chain micromixers offer major advantages by virtue of their higher fluid conductivity of the Chain mixer element in comparison with the Tear-drop mixer

element. Also figures 5.19-5.24 depicts that in all of the Reynolds numbers range, the required pressure drop in Chain 2 is less than other efficient mixers.

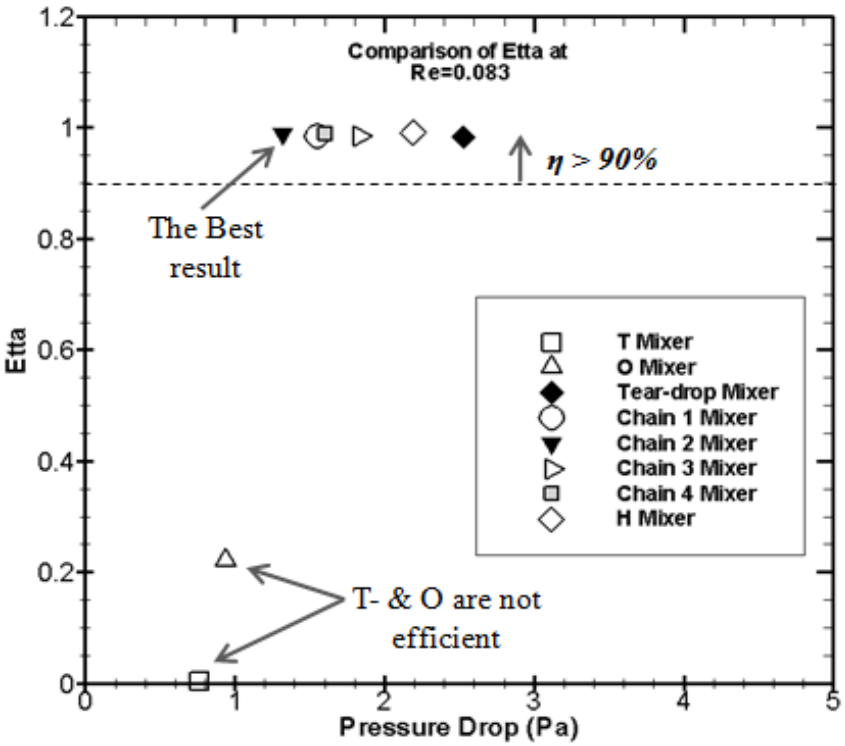

Figure 5.20 Etta Vs. pressure drop at Re=0.083.

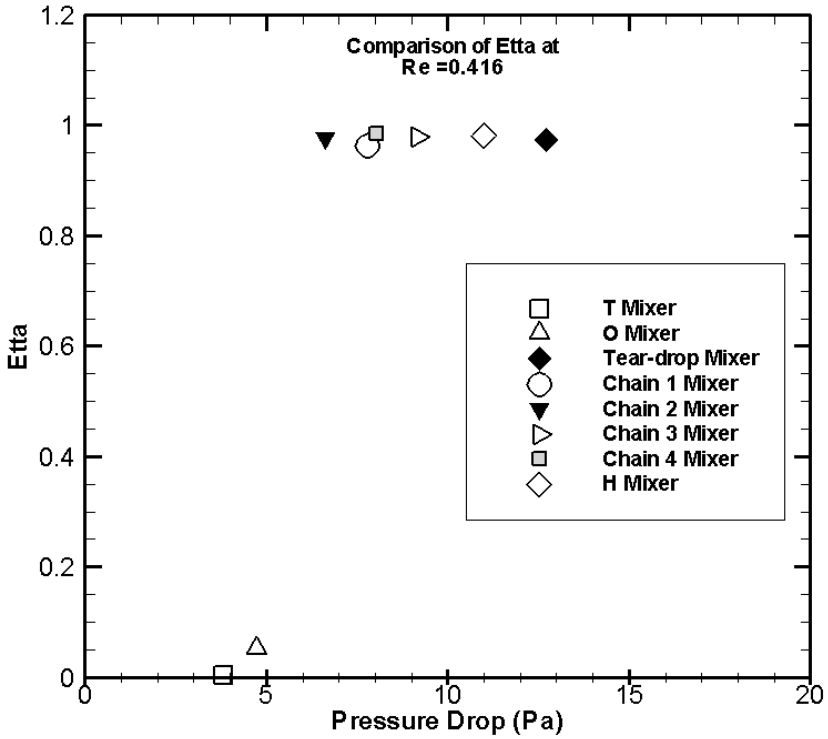

Figure 5.21 Etta Vs. pressure drop at Re=0.416.

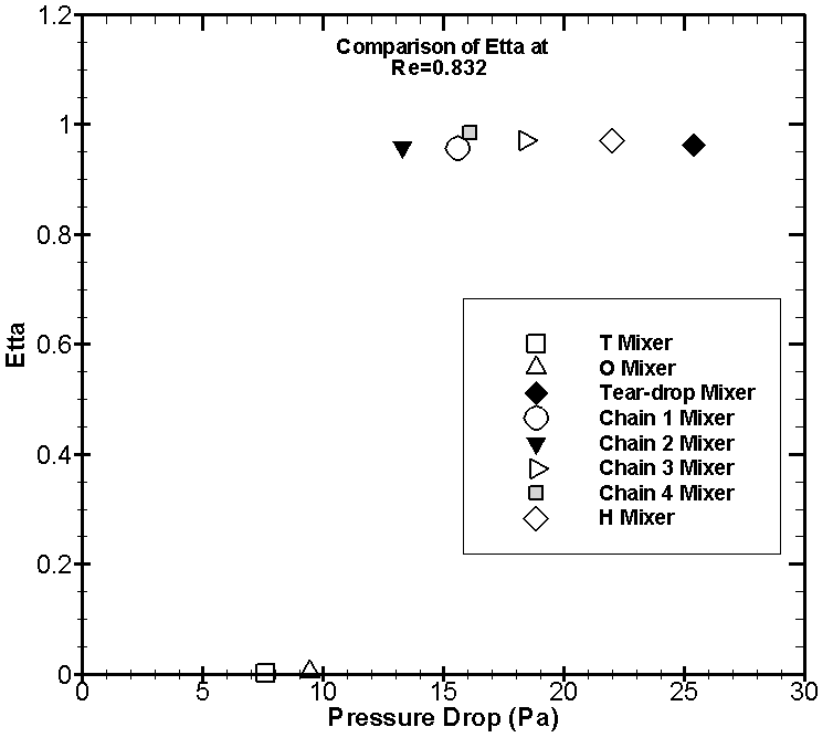

Figure 5.22 Etta Vs. pressure drop at Re=0.832.

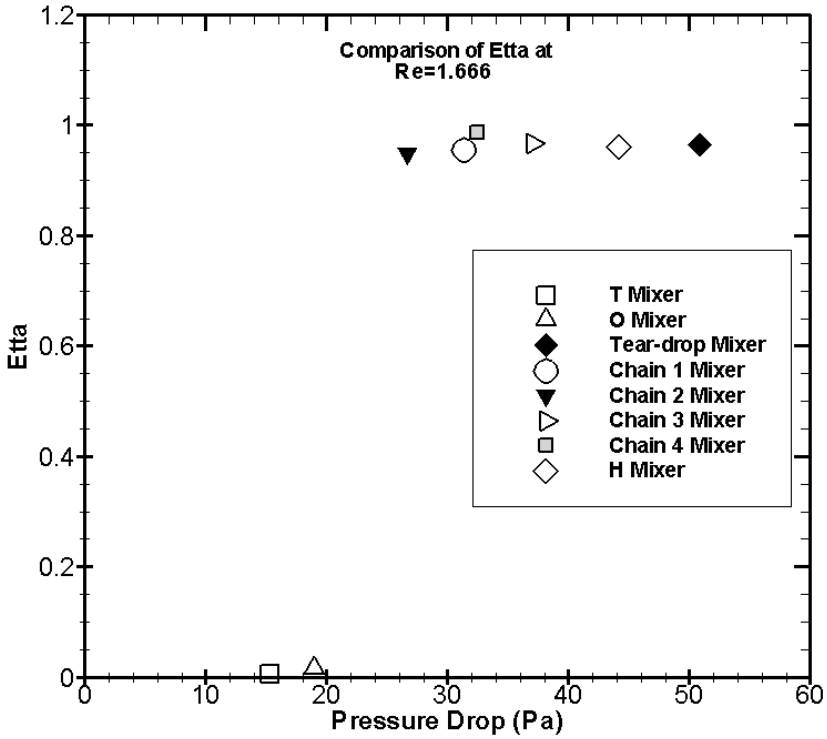

Figure 5.23 Etta Vs. pressure drop at Re=1.666.

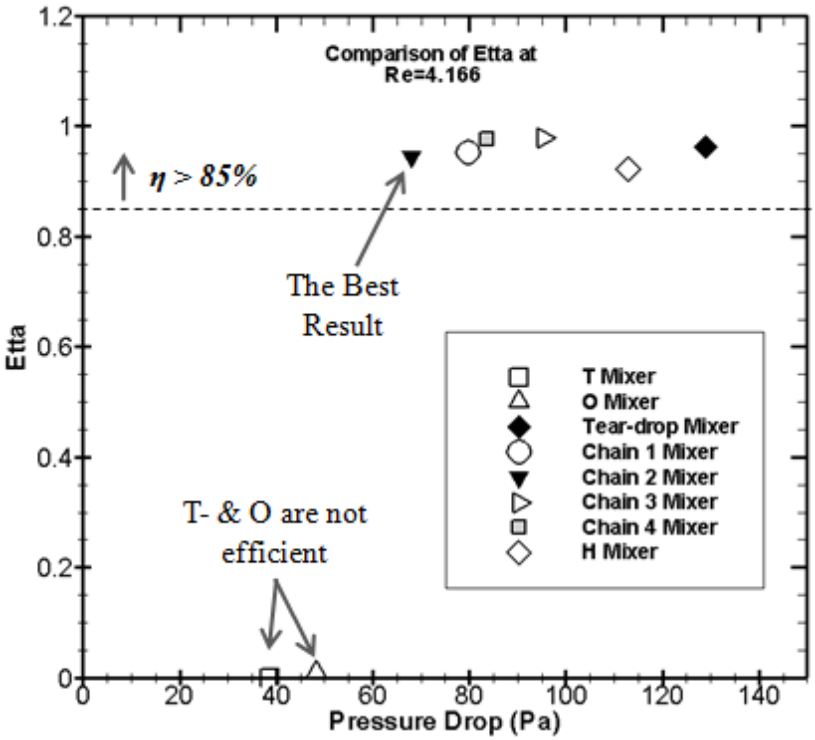

Figure 5.24 Etta Vs. pressure drop at Re=4.166.

This is a good result that with the same (or higher) efficiency the required pressure drop decreases. Hence, this new geometry satisfies both of targets in micromixer design which are higher mixing efficiency and lower pressure drop (in comparison with H- and Tear-drop mixers).

References

[1] Suh Y.K., Jayaraj S. and Kang S, 2007.A review on the Analysis and Experiment of Fluid Flow and Mixing in Micro-Channels, Journal of Mechanical Science and technology 21 536-548.

[2] Aoki N., Fukuda T., Maeda N. and Mae K., 2012. Design of confluence and bend geometry for rapid mixing in microchannels, Chemical engineering Journal. doi:10.1016/j.cej.2012.03.061.

[3] Cook K.J., Fan Y.F. and Hassan I., 2012. Experimental investigation of a scaled-up passive micromixer with uneven interdigital inlet and teardrop obstruction elements, Exp Fluids 52: 1261-1275, doi: 10.1007/s00348-011-1246-4.

[4] Chen J.J. and Shie Y.S., 2012. Interfacial configurations and mixing performances of fluids in staggered curved-channel micromixers, Microsyst Technol 18 1823-1833, doi: 10.1007/s00542-012-1489-x.

[5] Erickson D., 2005. Toward numerical prototyping of labs-on-chip: modelling for integrated microfluidic devices, Microfluidic Nanofluidic 1: 301-318, doi:10.1007/s10404-005-0041-z.

[6] Hardt S., Pennemann H. and Schonfeld F., 2006. Theoretical and experimental characterization of a low-Reynolds number split-and-recombine mixer, Microfluidic Nanofluidic 2: 237-248, doi:10.1007/s10404-005-0071-6.

[7] Mansur E.A., Mingxing Y.E., Yundong W. and Youyuan D., 2008. A State –of-the-Art Review of Mixing in Microfluidic Mixers, Chinese Journal of Chemical Engineering, 16(4) 503-516.

[8] Malecha K., Golonka L.J., Baldyga J., Jasinska M. and Sobieszuk P., 2009. Serpentine microfluidic mixer made in LTCC, Sensors and Actuators B: Chemical 143 400-413, doi:10.1016/j.snb.2009.08.010.

[9] Lee S.W. and Lee S.S, , 2007. Rotation effect in split and recombination micromixing, Sensors and Actuators B 129 364–371, doi: 10.1016/j.snb.2007.08.038.

[10] Fang W.F. and Yang J.T, 2009. A novel microreactor with 3D rotating flow to boost fluid reaction and mixing of viscous fluids, Sensors and Actuators B: Chemical 140 629-642, doi: 10.1016/j.snb.2009.05.007.

[11] Zhang Y., Hu Y. and Wu H., 2012. Design and simulation of passive micromixers based on capillary, Microfluidic Nanofluidic, doi: 10.1007/s10404-012-1002-y.

[12] Hardt S., Drese K.S., Hessel V. And Schonfeld F., 2005.Passive micromixers for applications in the microreactor and μTAS fields, Microfluidic Nanofluidic 1: 108-118, doi: 10.1007/s10404-004-0029-0.

[13] Nguyen N.T., 2008. Micromixers: Fundamentals, Design and Fabrication. William Andrew, Norwich, NY, USA.

[14] Ma Y.et al., 2008. An unsteady microfluidic T-form mixer perturbed by hydrodynamic pressure, J. Michromech. Microeng. 18, 045015, doi: 1088/0960-1317/18/045015.

[15] Garstecki P., Fuerstman M.J., Fischbach M.A., Sia S.K., Whitesides G.M., 2006. Mixing with bubbles: a practical technology for use with portable microfluidic devices, Lab on a Chip 6, 207-212, doi :10.1039/b510843h.

[16] Chen Z., Bown M.R., Sullivan B.O., MacInnes J.M., Allen R.W.K., Mulder M., Blom M., van't Oever R., 2009. Performance analysis of a folding flow micromixer, Microfluid Nanofluid 6:763–774, doi: 10.1007/s10404-008-0351-z.

Conclusion

This thesis presents a novel microfluidic device called the "H-micromixer". This type of passive micromixer is based on the SAR process, meaning that the two fluids to be mixed are split and recombined to optimize the diffusion process.

The H-micromixer was compared with other two well-known micromixers, i.e., an O-shaped micromixer and a T-junction micromixer. Experimental tests were carried out at very low *Re*, specifically in the $0.083<Re<4.166$ range. The mixing index was evaluated using blue and yellow colored water solutions and image-based techniques.

Experimental data show that the H-micromixer's mixing efficiency (η) is higher than that of the O- and T-micromixers. Specifically, H-micromixer efficiency reaches to 98% (over 80%) at *Re*=0.083. This study demonstrates that splitting and recombining the two species to be mixed (the SAR process) increases the degree of mixing (η) in micromixers at low Reynolds numbers. Consequently, we concluded that a micromixer based on the SAR process are more effective at low Reynolds numbers than devices without SAR process.

Also this investigation introduced a novel generation of 3D splitting and recombination passive micromixer called ''*Chain micromixer*''. Mixing characteristics of two species are elucidated via experimental and numerical studies with various inlet flow rates (velocities) and results compared with the previous well-known micromixers. Chain micromixers are designed and fabricated from plexiglas using a computer milling process and the flow follows a 3D path along the microchannel. It was found that mixing performance is significantly affected by the split and recombination (SAR) flows and depends on Reynolds number (inlet velocities).

Experimental results illustrate that the micromixers with SAR process like Chain and Tear-drop micromixers have outstanding mixing efficiency than those without SAR characteristic. Indeed split and recombine (SAR) structures of the flow channels result in the reduction of the diffusion distance of two fluids and after a short distance from inlet high mixing efficiency can be achieved.

In Chain micromixers, after each vertical channel, the diameter of the new section is extended 0.2 mm or 0.4 mm in Chain 1- and Chain 2 – micromixers respectively rather than the outlet of vertical part (0.4 mm). At the outlet of this part, the diameter is again 0.4 like vertical part. Indeed, after extension in the inlet, the flow getting constricted while goes across these parts and the maximum

constriction occurs at the outlet of this section and mentioned properties cause the homogeneity in the mixed layers. Therefore splitting and recombination along the Chain micromixers and repeating these processes lead to significantly improved mixing and it was obvious that the efficiency of Chain 2 is the same as Chain 1 (and also Tear-drop) mixer at each desired region. Also it could be found that with increasing the Reynolds number, efficiency decreases and pressure drop increases. As well as the efficiencies of Chain mixers and Tear-drop mixer are almost quite the same at each desired region, the required pressure drop in Chain mixers is approximately two times less than pressure drop in Tear-drop mixer. Also in chain mixers, required pressure drop in Chain 2 is less than other Chain mixers. This is a good particular result that with higher efficiency the required pressure drops decreases. Hence, this new geometries satisfies both of targets in micromixer design which have higher mixing efficiency and lower pressure drop in comparison with Tear-drop.

These results open the new operating windows for rapid mixing in the microchannel to overcome the fluid mixing which strongly limited to laminar regime with lower required pressure drop.